UNIWERSYTET MARII CURIE-SKŁODOWSKIEJ W LUBLINIE

Wydział Chemii
Instytut Nauk Chemicznych

mgr Karolina Pietrzak
nr albumu: 255441

NOWE MATERIAŁY FUNKCJONALNE W KONSTRUKCJI ELEKTROD JONOSELEKTYWNYCH ZE STAŁYM KONTAKTEM CZUŁYCH NA WYBRANE JONY NIEORGANICZNE

New functional materials in the construction of ion-selective electrodes with solid contact sensitive to selected inorganic ions

Rozprawa doktorska

wykonana w Katedrze Chemii Analitycznej

pod kierunkiem dr hab. Cecylii Wardak, prof. UMCS

Lublin 2022

SPIS TREŚCI

WYKAZ PRAC NAUKOWYCH WCHODZĄCYCH W SKŁAD CYKLU

D1   **K. Pietrzak**, C. Wardak, R. Łyszczek, *Solid contact nitrate ion-selective electrode based on cobalt(II) complex with 4,7-diphenyl-1,10-phenanthroline*, Electroanalysis. 32 (2020) 724–731. https://doi.org/10.1002/elan.201900462.

$IF_{2020} = 3{,}223$; punktacja MEiN: 70

D2   **K. Pietrzak**, C. Wardak, *Comparative study of nitrate all solid state ion-selective electrode based on multiwalled carbon nanotubes-ionic liquid nanocomposite*, Sensors and Actuators B: Chemical. 348 (2021) 130720. https://doi.org/10.1016/j.snb.2021.130720.

$IF_{2021} = 9{,}221$; punktacja MEiN: 140

D3 C. Wardak, **K. Pietrzak**, *Nitrate ion-selective electrodes – new constructions and applications in the monitoring of nitrate ions in environmental samples*, Post-conference monograph Modern Problems and Solutions in Environmental Protection, Białystok (2021) 11-28, ISBN. 978-83-7431-692-1.

punktacja MEiN: 20

D4   **K. Pietrzak**, C. Wardak, S. Malinowski, *Application of polyaniline nanofibers for the construction of nitrate all-solid-state ion-selective electrodes*, Applied Nanoscience. 11(12) (2021) 2823-2835. https://doi.org/10.1007/s13204-021-02228-1.

$IF_{2021} = 3{,}869$; punktacja MEiN: 100

D5   **K. Pietrzak**, K. Morawska, S. Malinowski, C. Wardak, *Chloride ion-selective electrode with solid-contact based on polyaniline nanofibers and multiwalled carbon nanotubes nanocomposite*, Membranes. 12 (2022) 1150.
https://doi.org/10.3390/membranes12111150.

$IF_{2021} = 4{,}562$; punktacja MEiN: 100

D6   **K. Pietrzak**, C. Wardak, B. Cristóvão, *Copper ion-selective electrodes based on newly synthesized salen-type Schiff bases and their complexes*, Ionics. 28 (2022) 2423-2435. https://doi.org/10.1007/s11581-022-04482-x.

$IF_{2021} = 2,961$; punktacja MEiN: 70

D7   C. Wardak, **K. Pietrzak**, M. Grabarczyk, *Ionic liquid-multiwalled carbon nanotubes nanocomposite based all solid state ion-selective electrode for the determination of copper in water samples*, Water. 13 (2021) 2869. https://doi.org/doi.org/10.3390/w13202869.

$IF_{2021} = 3,530$; punktacja MEiN: 100

D8   **K. Pietrzak**, N. Krstulović, D. Blažeka, J. Car, S. Malinowski, C. Wardak, *Metal oxide nanoparticles as solid contact in ion-selective electrodes sensitive to potassium ions*, Talanta. 243 (2022) 123335. https://doi.org/10.1016/j.talanta.2022.123335.

$IF_{2021} = 6,556$; punktacja MEiN: 100

D9   **K. Pietrzak**, N. Krstulović, C. Wardak, S. Malinowski, *Solid state ion-selective electrode based on silver nanoparticles*, Proceedings of the 17th International Students Conference "Modern Analytical Chemistry", Charles University, Prague (2021) 85-90, ISBN 978-80-7444-089-2.

D10   **K. Pietrzak**, C. Wardak, *Uranyl ion-selective electrode with solid contact*, Proceedings of the 16th International Students Conference "Modern Analytical Chemistry", Charles University, Prague (2020) 45-50, ISBN 978-80-7444-079-3.

SPIS SKRÓTÓW I SYMBOLI

ATR-FTIR – (z ang. *attenuated total reflection-Fourier transform infrared spectroscopy*) metoda osłabionego całkowitego wewnętrznego odbicia sprzężona ze spektroskopią w podczerwieni z transformatą Fouriera

BMImPF$_6$ – (z ang. *1-butyl-3-methylimidazolium hexafluorophosphate*) heksafluorofosforan 1-butylo-3-metyloimidazoliowy

CP – (z ang. *chronopotencjometry*) chronopotencjometria

CPs – (z ang. *conducting polymers*) polimery przewodzące

CWE – (z ang. *coated-wire electrode*) elektroda z drutu powlekanego

EIS – (z ang. *electrochemical impedance spectroscopy*) elektrochemiczna spektroskopia impedancyjna

EMF – (z ang. *electromotive force*) siła elektromotoryczna ogniwa

FIM – (z ang. *fixed interference method*) metoda roztworów mieszanych

ISE – (z ang. *ion-selective electrode*) elektroda jonoselektywna

MWCNTs – (z ang. *multiwalled carbon nanotubes*) wielościenne nanorurki węglowe

NPs – (z ang. *nanoparticles*) nanocząstki

OMImCl – (z ang. *1-methyl-3-octylimidazolium chloride*) chlorek 1-metylo-3-oktyloimidazoliowy

LAL – (z ang. *laser ablation in liquid*) ablacja laserowa w cieczy

LOD – (z ang. *limit of detection*) limit detekcji

PANINFs – (z ang. *polyaniline nanofibers*) nanowłókna polianilinowe

SC – (z ang. *solid contact*) stały kontakt

SC-ISE – (z ang. *solid contact ion-selective electrode*) elektroda jonoselektywna ze stałym kontaktem

SEM – (z ang. *scanning electron microscopy*) skaningowa mikroskopia elektronowa

SSM – (z ang. *separate solution method*) metoda roztworów rozdzielonych

SWCNTs – (z ang. *single-walled carbon nanotubes*) jednościenne nanorurki węglowe

TG-FTIR – (z ang. *thermogravimetric analysis-Fourier transform infrared spectroscopy*) analiza termograwimetryczna sprzężona ze spektroskopią w podczerwieni z transformatą Fouriera

TG-DSC – (z ang. *thermogravimetric analysis-differential scanning calorimetry*) analiza termograwimetryczna sprzężona ze skanningową kalorymetrią różnicową

THF – (z ang. *tetrahydrofuran*) tetrahydrofuran

THTDPCl – (z ang. *trihexyltetradecylphosphonium chloride*) chlorek triheksylotetradecylofosfoniowy

UV-VIS – (z ang. *ultraviolet-visible spectroscopy*) spektroskopia UV-VIS

WPISs – (z ang. *wearable potentiometric ion sensors*) nośne jonowe czujniki potencjometryczne

XPS – (z ang. *X-ray photoelectron spectroscopy*) rentgenowska spektroskopia fotoelektronowa

STRESZCZENIE I SŁOWA KLUCZOWE

W obliczu towarzyszącego nam obecnie ogromnego rozwoju technologii i związanego z tym eksploatowania przez człowieka znacznych ilości surowców, ważniejsze niż kiedykolwiek staje się monitorowanie stanu środowiska naturalnego. Zarówno katastrofy naturalne, jak również nieodpowiedzialne działania społeczeństwa mogą mieć druzgocący wpływ na jakość otaczającego nas powietrza, wód oraz gleby, często prowadząc do długotrwałego skażenia znacznych terenów. Istotna jest ciągła obserwacja i ulepszanie systemu szybkiego reagowania w sytuacjach kryzysowych, obejmujących gwałtowny wzrost stężenia substancji niebezpiecznych, a także zapobieganie możliwym do przewidzenia wyciekom i komplikacjom. Do oznaczania zawartości różnego rodzaju jonów w próbkach środowiskowych od wielu lat z powodzeniem wykorzystywane są elektrody jonoselektywne. W prosty i szybki sposób umożliwiają one uzyskanie stężenia interesujących nas jonów w obecności innych substancji bez konieczności skomplikowanego przygotowania próbki. W porównaniu do innych metod szeroki zakres stężeń, w jakim możliwe jest oznaczanie analitu, pozwala uniknąć również rozcieńczenia badanych roztworów lub często żmudnego zatężania próbki. Szereg zalet ISEs, obejmujący ich wysoką selektywność, niskie granice wykrywalności oraz dobrą stabilność potencjału łączą w sobie SCISEs, które dzięki eliminacji elektrolitu wewnętrznego dodatkowo są łatwiejsze do miniaturyzacji i modyfikacji kształtu oraz wygodniejsze w przechowywaniu i transporcie. Dalszy rozwój tego typu czujników możliwy jest dzięki wykorzystaniu nowych związków i materiałów, pozwalających na poprawę ich właściwości i parametrów.

W niniejszej rozprawie doktorskiej, obejmującej 10 publikacji naukowych, opisane zostały badania dotyczące wykorzystania nowych materiałów w konstrukcji elektrod jonoselektywnych ze stałym kontaktem. Otrzymano nowe substancje aktywne (kompleks kobaltu(II) z fenantroliną; ligandy typu zasad Schiffa oraz ich kompleksy z jonami miedzi(II)), a także szereg materiałów pełniących funkcję stałego kontaktu (nanowłókna: PANINFs-Cl i PANINFs-NO_3; nanocząstki: ZnONPs, CuONPs, Fe_2O_3NPs, AgNPs; nanokompozyty: MWCNTs:THTDPCl, PANINFs-Cl:MWCNTs, MWCNTs:BMImPF$_6$ oraz ciecz jonowa OMImCl). Materiały te zastosowano w konstrukcji czujników do oznaczania anionów (NO_3^-, Cl^-) oraz kationów (K^+, Cu^{2+} i UO_2^{2+}). W przypadku badań dotyczących nowych związków – w pierwszym etapie skupiano się na zbadaniu struktury i właściwości otrzymywanych materiałów, m.in. za pomocą analizy termicznej, skaningowej mikroskopii

elektronowej oraz metod spektrofotometrycznych i spektroskopowych. Następnie szczegółowej analizie poddawano uzyskane z ich wykorzystaniem czujniki, wykonując szereg pomiarów potencjometrycznych w celu otrzymania i porównania wartości otrzymanych dla nich parametrów analitycznych. Elektrody różniły się między sobą m.in.: rodzajem konstrukcji, składami membran jonoselektywnych oraz obecnością lub/i rodzajem stałego kontaktu. Zbadano m.in.: nachylenia krzywych kalibracyjnych, ich zakresy liniowości oraz granice wykrywalności dla poszczególnych czujników. Skupiono się również na sprawdzeniu stabilności, odwracalności i odtwarzalności potencjału elektrod. Wykonywano testy na obecność warstwy wodnej tworzącej się między materiałem elektrody a membraną jonoselektywną. Określano zakres pH, w którym potencjał badanych elektrod nie zależy od stężenia jonów wodorowych oraz badano wrażliwość czujników na zmiany czynników zewnętrznych, takich jak światło, obecność gazów w próbce czy też zmiany potencjału redox roztworu próbki. W celu określenia parametrów elektrycznych elektrod wykorzystano metodę elektrochemicznej spektroskopii impedancyjnej (EIS) oraz chronopotencjometrię (CP).

We wnikliwy i szczegółowy sposób skupiono się na badaniach dotyczących SCISEs-NO_3^-. Zaproponowano kompleks kobaltu(II) z 4,7-difenylo-1,10-fenantroliną jako nową substancję aktywną jonoczułej membrany, który pozwolił na otrzymanie czujników opartych na elektrodzie wewnętrznej Ag/AgCl charakteryzujących się bardzo dobrymi współczynnikami selektywności, znakomitą odwracalnością i stabilnością potencjału (dryft 0,09 mV/dzień) oraz szerokim zakresem pH (5,4 – 10,6). Korzystne właściwości jonoforowe kompleksu kobaltu(II) z 4,7-difenylo-1,10-fenantroliną wykorzystano następnie w innej konstrukcji czujników z GCE jako elektrodą wewnętrzną, w których wprowadzono nanokompozyt MWCNTs:THTDPCl jako dodatkowy składnik membrany, uzyskując elektrody o szerszym zakresie liniowości (10^{-6} – 10^{-1} mol L^{-1}) oraz niższej granicy wykrywalności ($5,0 \times 10^{-7}$ mol L^{-1}). W badaniach tych zastosowano nanokompozyty otrzymane z różnych rodzajów MWCNTs, co pozwoliło na zbadanie wpływu nie tylko modyfikacji membrany na pracę elektrod, ale również różnic wynikających z parametrów charakteryzujących jego składniki. Kolejnym materiałem stosowanym jako SC w grupie elektrod azotanowych, jednakże dla innego składu ISM, były PANINFs-Cl i PANINFs-NO_3. Wprowadzona modyfikacja w tym przypadku umożliwiła uzyskanie elektrod charakteryzujących się takim samym zakresem liniowości jak w poprzednim przypadku. Czujniki działały prawidłowo w zmiennych warunkach zewnętrznych (zmiana potencjału

redox próbki, oświetlenie, gazy) oraz w bardzo szerokim zakresie pH roztworów próbki (4,0 – 12,5) przez okres minimum 3 miesięcy.

Zsyntezowane PANINFs-Cl wykorzystano wraz z MWCNTs jako składniki nanokompozytu stanowiącego SC w elektrodach czułych na jony chlorkowe. Wykonano badania porównawcze właściwości elektrycznych badanych materiałów, zarówno gotowych nanokompozytów o różnym składzie, jak i pojedynczych ich składowych, zauważając przy tym znaczną poprawę parametrów elektrycznych w przypadku materiałów kompozytowych. Uzyskano czujniki o bardzo dobrej stabilności potencjału, szerokim zakresie liniowości ($5 \times 10^{-6} – 10^{-1}$ mol L^{-1}) i niskiej granicy wykrywalności ($2,3 \times 10^{-6}$ mol L^{-1}) mogące pracować w zmiennych warunkach przez okres minimum 2 miesięcy.

W celu opracowania czujników do oznaczania jonów miedzi(II) zsyntezowano i przebadano nowe związki, mogące potencjalnie pełnić funkcję jonoforu - ligandy typu zasad Schiffa i ich kompleksy z jonami miedzi(II). Na podstawie wyników badań otrzymanych dla elektrod, których membrany różniły się składem jakościowym i ilościowym, wybrano dwurdzeniowy kompleks N,N'-bis(5-bromo-2-hydroksy-3-metoksybenzylideno)2-hydroksypropyleno-1,3-diaminy z miedzią(II) (L^1Cu_2). Związek ten zastosowany jako aktywny składnik membrany pozwala uzyskać elektrody o Nernstowskim nachyleniu krzywej kalibracyjnej (29,68 mV pa^{-1}), niskiej granicy wykrywalności ($6,2 \times 10^{-7}$ mol L^{-1}) i krótkim czasie odpowiedzi (< 10 s). W ramach badań dotyczących SCISEs-Cu^{2+} otrzymano nanokompozyt MWCNTs:$BMImPF_6$, który zastosowany jako dodatek do ISM znacznie poprawił parametry analityczne i elektryczne elektrod.

W przypadku elektrod potasowych wykorzystując powszechnie znany jonofor – walinomycynę, skupiono się w głównej mierze na zbadaniu wpływu modyfikacji, jaką było wprowadzenie warstwy pośredniej SC w postaci nanocząstek srebra oraz wybranych tlenków metali. Wykorzystano w tym celu AgNPs, ZnONPs, CuONPs, Fe_2O_3NPs, które otrzymano metodą ablacji laserowej w cieczy – metody cenionej ze względu na prostotę wykonania, brak dodatkowych substratów oraz produktów ubocznych. Najlepsze rezultaty uzyskano dla elektrod otrzymanych z wykorzystaniem ZnONPs, które charakteryzowały się wyjątkowo długim czasem życia oraz znacznie lepszymi parametrami analitycznymi i elektrycznymi w porównaniu do elektrod niemodyfikowanych.

Kolejnym jonem, dla którego poczyniono starania mające na celu skonstruowanie odpowiednich SCISEs, był jon uranylowy – najbardziej stabilna forma uranu w roztworach wodnych. W elektrodach uranylowych jako aktywny składnik membrany wykorzystano

Cyanex-272 (w literaturze opisywany jako bardzo dobry ekstrahent jonów uranylowych) oraz ciecz jonową (OMImCl) jako dodatkowy jonowy składnik poprawiający jej zdolności ekstrakcyjne w stosunku do jonów uranylowych oraz zapewniający stałe stężenie jonów chlorkowych w fazie membrany. Elektroda z membraną o optymalnym składzie miała bardzo dobre parametry analityczne: nachylenie krzywej kalibracyjnej wynoszące 29,8 mV pa^{-1}, zakres liniowości $10^{-6} - 10^{-1}$ mol L^{-1} oraz niską granicę wykrywalności $7,1 \times 10^{-7}$ mol L^{-1}). Co więcej elektrody charakteryzowały się bardzo dobrymi współczynnikami selektywności (logK$^{pot}_{(UO22+)/M}$ < −4) oraz krótkim czasem odpowiedzi (< 8 s).

W części literaturowej rozprawy doktorskiej przedstawiono charakterystykę metod potencjometrycznych i elektrod jonoselektywnych oraz ich zastosowanie analityczne. Następnie opisano konstrukcje elektrod jonoselektywnych, ich poszczególne elementy, takie jak membrana jonoselektywna i materiały wykorzystywane jako stały kontakt oraz parametry analityczne gotowych czujników. W części eksperymentalnej natomiast przedstawiono cel pracy, zastosowane metody i zakres przeprowadzonych badań oraz omówienie i podsumowanie wyników badań opisanych w cyklu artykułów naukowych wchodzących w skład rozprawy.

Słowa kluczowe: elektrody jonoselektywne, stały kontakt, nanomateriały, nanokompozyty, potencjometria

ABSTRACT AND KEYWORDS

In view of the enormous development of technology currently accompanying us and associated with it exploitation of significant amounts of sources, it is more important than ever to monitor the state of the natural environment. Both natural disasters and irresponsible behaviours of society can have a devastating effect on the quality of the air, water and soil surrounding us, often leading to long-term contamination of large areas. It is important to constantly monitor and improve the rapid response system in emergencies, involving a rapid increase in the concentration of hazardous substances, as well as the prevention of foreseeable spills and complications. Ion-selective electrodes have been successfully used for many years to determine the content of various types of ions in environmental samples. In a simple and quick way, they make it possible to obtain the concentration of ions of interest in the presence of other substances without the need for complicated sample preparation. Compared to other methods, the wide range of concentration in which analyte determination is possible also avoids dilution of the tested solutions and, the often tedious, concentration process of the sample. A number of advantages of ISEs, including their high selectivity, low detection limits and good potential stability, combine SCISEs, which, thanks to the elimination of the internal electrolyte, are additionally easier to miniaturize and modify the shape, and more convenient to store and transport. The further development of this type of sensors is possible thanks to the use of new compounds and materials that allow to improve their properties and parameters.

In this doctoral dissertation, which includes 10 scientific publications, the research on the use of new materials in the construction of ion-selective electrodes with solid contact has been described. New active substances were synthesized (complex of cobalt(II) with phenanthroline; the Schiff base type ligands and their complexes with copper(II) ions), as well as number of materials for use as solid contact (nanofibers: PANINFs-Cl and PANINFs-NO$_3$; nanoparticles: ZnONPs, CuONPs, Fe$_2$O$_3$NPs, AgNPs; nanocomposites: MWCNTs-THTDPCl, PANINFs-Cl:MWCNTs; MWCNTs-BMImPF$_6$ and ionic liquid – OMImCl). These materials were used in the construction of sensors for the determination of anions (NO$_3^-$, Cl$^-$) and cations (K$^+$, Cu^{2+} and UO$_2^{2+}$). In the case of research on new compounds - the first stage was focused on examining the structure and properties of the obtained materials, including using thermal analysis, scanning electron microscopy as well as spectrophotometric and spectroscopic methods. Then, the sensors obtained with their use were subjected to a detailed analysis, performing a series of potentiometric measurements in order to obtain and

compare the values of their analytical parameters. The electrodes differed from each other, inter alia, type of structure, composition of ion-selective membranes and the presence and/or type of solid contact. Among others, the slopes of the calibration curves, their linearity ranges and the detection limits for individual electrodes were estimated. It was also focus on testing the stability, reversibility and reproducibility of the measured potential. Tests for the presence of a water layer forming between the electrode material and the ion-selective membrane were performed. The pH range in which the potential of the tested electrodes does not depend on the concentration of hydrogen ions was determined, and the sensitivity of sensors to changes in external factors, such as light, the presence of gases in the sample or changes in the redox potential of the sample solution, was tested. In order to determine the electrical parameters of the electrodes, the electrochemical impedance spectroscopy (EIS) and chronopotentiometry (CP) methods were used.

Research into SCISEs-NO_3^- has been carefully and thoroughly focused. A cobalt(II) complex with 4,7-diphenyl-1,10-phenanthroline was proposed as a new active substance of the ion-sensitive membrane, which allowed to obtain sensors based on an internal Ag/AgCl electrode characterized by very good selectivity coefficients, excellent reversibility and potential stability (drift 0.09 mV day^{-1}) and a wide pH range (5.4 – 10.6). The favorable ionophore properties of this complex were then used in another sensor design with GCE a internal electrode, in which the MWCNTs-THTDPCl nanocomposite was introduced as an additional membrane component, obtaining electrodes with a wider range of linearity (10^{-6} – 10^{-1} mol L^{-1}) and lower detection limit (5.0×10^{-7} mol L^{-1}). In these studies, nanocomposites obtained from various types of MWCNTs were used, what allowed to study the influence of not only membrane modification on the operation of the electrodes, but also the differences resulting from the parameters characterizing its components. Another material used as SC in the group of nitrate electrodes, however, for a different ISM composition, were PANINFs-Cl and PANINFs-NO_3. The modification introduced in this case made it possible to obtain electrodes with the same linearity range as in the previous case. The sensors worked properly in variable external conditions (change of the redox potential of the sample, lighting, gases) and in a very wide pH range of the sample solutions (4.0 – 12.5) for a minimum period of 3 months.

The synthesized PANINFs-Cl were used with MWCNTs as components of a nanocomposite used as SC in electrodes sensitive to chloride ions. Comparative tests of the electrical properties of the tested materials were carried out, both prepared nanocomposites of

various compositions and their individual components, noting a significant improvement in electrical parameters in the case of composite materials. Sensors with very good potential stability, a wide range of linearity ($5 \times 10^{-6} - 10^{-1}$ mol L^{-1}) and a low detection limit (2.3×10^{-6} mol L^{-1}) were obtained, which can work in variable conditions for a period of minimum 2 months.

In order to develop sensors for the determination of copper(II) ions, new compounds that could potentially act as an ionophore were synthesized and tested – Schiff base type ligands and their complexes with copper(II) ions. Based on the results obtained for the electrodes whose membranes differed in qualitative and quantitative composition, the dinuclear complex of N,N'-bis(5-bromo-2-hydroxy-3-methoxybenzylidene)2-hydroxypropylene-1,3-diamine with copper(II) was selected (L^1Cu_2). This compound, when used as an active component of the membrane, allows to obtain electrodes with a Nernstian slope of the calibration curve (29.68 mV pa^{-1}), a low detection limit (6.2×10^{-7} mol L^{-1}) and a short response time (< 10 s). As part of the research on SCISEs-Cu^{2+}, the MWCNTs-BMImPF$_6$ nanocomposite was obtained, which, when used as an additive to the ISM, significantly improved the analytical and electrical parameters of the electrodes.

In the case of potassium electrodes, using the commonly known ionophore – valinomycin, the focus was mainly on examining the influence of the modification, which was the introduction of the SC intermediate layer in the form of silver nanoparticles and selected metal oxides nanoparticles. For this purpose, AgNPs, ZnONPs, CuONPs, Fe$_2$O$_3$NPs were used, obtained by laser ablation in a liquid – a method valued for its simplicity of implementation, lack of additional substrates and by-products. The best results were obtained for electrodes using ZnONPs, which were characterized by exceptionally long life and significantly better analytical and electrical parameters compared to unmodified electrodes.

Another ion for which efforts to construct suitable SCISEs were made was the uranyl ion – the most stable form of uranium in aqueous solutions. In the uranyl electrodes, Cyanex-272 (described in the literature as a very good extractant of uranyl ions) as the active component of the membrane and the ionic liquid (OMImCl) as additional ionic component improving its extraction capacity in relation to uranyl ions and ensuring a constant concentration of chloride ions in the membrane phase, were used. The electrode with the optimal composition membrane had very good analytical parameters: the slope of the calibration curve was 29.8 mV pa^{-1}, the linearity range of $10^{-6} - 10^{-1}$ mol L^{-1} and a low

detection limit of 7.1×10^{-7} mol L^{-1}). Moreover, the electrodes were characterized by very good selectivity coefficients (log K$^{pot}_{(UO22+)/M}$ < −4) and a short response time (< 8 s).

The literature part of the dissertation presents the characteristics of potentiometric methods and ion-selective electrodes with their analytical application. Then, the construction of ion-selective electrodes, their individual components, such as the ion-selective membrane and materials used as solid contact, as well as the analytical parameters of the prepared sensors are described. In the experimental part, the purpose of the work, the used methods and the scope of the research, as well as a discussion and summary of the research results described in the series of scientific articles included in the dissertation, are presented.

Keywords: ion-selective electrodes, solid contact, nanomaterials, nanocomposites, potentiometry

CZĘŚĆ LITERATUROWA

WPROWADZENIE

Elektrody jonoselektywne stanowią obecnie grupę najpopularniejszych czujników potencjometrycznych i są obiektem badań wielu naukowców na całym świecie nieprzerwanie od wielu lat. Dzięki licznym zaletom, do których można zaliczyć między innymi prostą obsługę, krótki czas analizy, przenośność, stosunkowo niskie koszty użytkowania, niewielkie zużycie energii, niskie granice wykrywalności oraz bardzo dobrą selektywność, stanowią one ciągle atrakcyjne narzędzia analityczne [1–4]. Elektrody jonoselektywne (ISEs) mają zastosowanie w wielu dziedzinach życia człowieka. ISEs są obecnie używane do oznaczania zawartości różnego rodzaju jonów (zarówno nieorganicznych, jak i organicznych) w próbkach ciekłych, obejmującej już nawet około 100 różnych analitów [5–7]. Są wykorzystywane w kontroli procesowej, diagnostyce klinicznej [8–11], analizie DNA [12], przemyśle farmaceutycznym [13] i spożywczym [14–16] oraz rolnictwie i monitorowaniu środowiska naturalnego [17–19]. Mogą służyć do oznaczania zawartości wybranych jonów w wodach naturalnych, zarówno powierzchniowych (rzeki, jeziora, morza), jak i gruntowych, a także w wodach wodociągowych i ściekach. W przypadku próbek wód nie jest konieczne skomplikowane przygotowywanie próbek. Najczęściej ogranicza się ono jedynie do niewielkiego dodatku buforu mocy jonowej i/lub innych substancji do roztworu próbki bezpośrednio przed pomiarem i wymieszania. Czasem może być również konieczne zapewnienie odpowiedniego pH środowiska, w sytuacji gdy pH badanej próbki nie mieści się w zakresie, w którym elektrody mogą pracować bez zakłóceń. Jednak w większości przypadków zakres ten jest wystarczająco szeroki, aby możliwe było oznaczanie jonów bezpośrednio w pobranej próbce. Wielką zaletą elektrod jonoselektywnych jest możliwość badania za ich pomocą roztworów barwnych lub mętnych, gdyż zarówno zabarwienie jak i obecność cząstek stałych nie przeszkadza w oznaczeniu. Możliwość osiągnięcia bardzo szerokiego zakresu dynamicznego czujników obejmującego nawet osiem rzędów wielkości sprawia, że potencjometria wyróżnia się spośród innych metod analitycznych [7]. W związku z ich szerokim zastosowaniem wciąż dąży się do poprawy parametrów elektrod, takich jak granica wykrywalności jonów oraz selektywność, co jest szczególnie istotne w złożonych próbkach zawierających interferenty mogące zakłócać właściwy pomiar [20–22]. Inny

kierunek badań obejmuje dążenia do uzyskania zadowalającej stabilności potencjału czujników pozwalającej na wykonywanie pomiarów przez dłuższy czas (tygodnie, miesiące), bez konieczności wykonywania kalibracji [7].

Obecnie najczęściej opisywanym przez naukowców obiektem badań z zakresu potencjometrii są elektrody jonoselektywne ze stałym kontaktem (SCISEs), w których wyeliminowano obecny w elektrodach klasycznych roztwór wewnętrzny pełniący rolę łącznika pomiędzy elektrodą wyprowadzającą a membraną jonoselektywną. Dla elektrod tego typu bardzo istotne jest odpowiednie dobranie materiału, który będzie spełniał funkcję przetwornika jon-elektron, umożliwiając tym samym prawidłową pracę elektrod, dzięki zapewnieniu odpowiedniej stabilności i odtwarzalności potencjału. W przypadku opracowywania nowego rodzaju SCISEs istnieją dwie główne możliwości ich uzyskiwania. Pierwszą z nich jest zastosowanie nowej substancji aktywnej będącej składnikiem membrany odpowiedzialnym za odpowiednią selektywność czujników względem wybranego jonu głównego, natomiast drugą – wykorzystywanie nowych materiałów elektroaktywnych w roli stałego kontaktu, zapewniających prawidłowe parametry elektryczne elektrod bez roztworu wewnętrznego. W pracy doktorskiej skupiono na obydwu tych aspektach, opisując badania dotyczące syntezy nowych substancji i materiałów mogących pełnić bądź rolę jonoforu, bądź stałego kontaktu.

1 POTENCJOMETRIA

Potencjometria jest jedną z najprostszych technik analitycznych. Zasada pomiarów potencjometrycznych polega na pomiarze siły elektromotorycznej (EMF) będącej sumą wszystkich potencjałów granicznych faz ogniwa. Ogniwo to zbudowane jest z dwóch rodzajów elektrod: elektrody referencyjnej, której potencjał koniecznie musi być stały niezależnie od składu i stężenia próbki oraz elektrody wskaźnikowej (pracującej), której potencjał zmienia się w zależności od aktywności jonu głównego obecnego w roztworze próbki, na który czuła jest membrana jonoselektywna (Rys. 1).
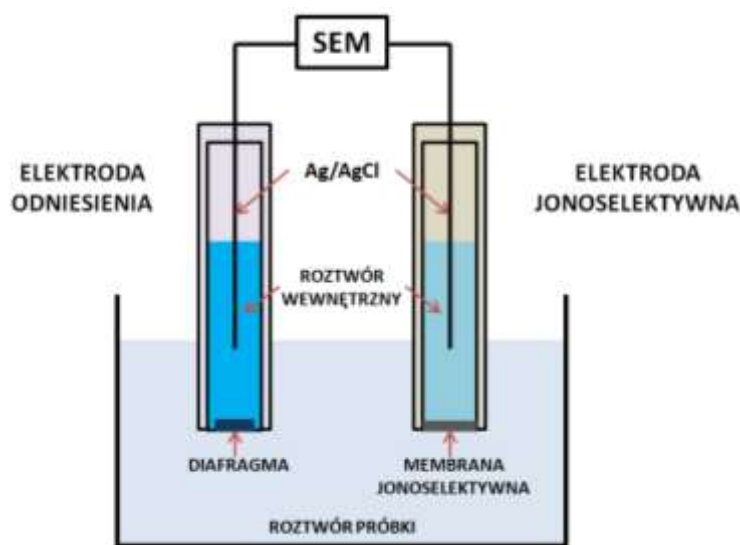

Rys. 1 Schemat układu pomiarowego stosowanego w potencjometrii z klasyczną elektrodą jonoselektywną i elektrodą referencyjną.

Uzyskuje się odpowiedź potencjometryczną, która jest zależnością zmian potencjału w czasie rzeczywistym [6]. Z racji tego, że pomiary wykonywane są przy prawie zerowym przepływie prądu, konieczne jest stosowanie woltomierza o niskim prądzie polaryzacji wejściowej i wysokiej rezystancji wejściowej [4]. Potencjometria wyróżnia się spośród technik elektrochemicznych niskim kosztem, krótkim czasem analizy, możliwością oznaczania jonów w próbkach zabarwionych lub mętnych oraz prostotą wynikającą z braku lub minimalnego wstępnego przygotowywania ich do analizy. Ponadto charakteryzuje się również wysoką selektywnością i niskimi granicami wykrywalności [23].

W przypadku uzyskiwania odpowiedzi SCISEs potwierdzono eksperymentalnie występowanie dwóch rodzajów mechanizmów z zachodzącą transdukcją jon-elektron umożliwiającą przekształcenie sygnału wejściowego (aktywności jonów) na sygnał

wyjściowy (potencjał elektryczny): mechanizm pojemnościowy redox [24] i mechanizm pojemnościowy warstwy elektrycznej [25]. Obydwa przypadki obejmują trzy granice fazowe, występujące pomiędzy materiałem elektrody wewnętrznej a warstwą stałego kontaktu (E/SC), warstwą stałego kontaktu a membraną jonoselektywną (SC/ISM) i membraną jonoselektywną a roztworem wodnym (ISM/aq) (Rys. 2). Transdukcja sygnału przebiega na granicy roztworu próbki i membrany jonoselektywnej będącej częścią elektrody [26,27].
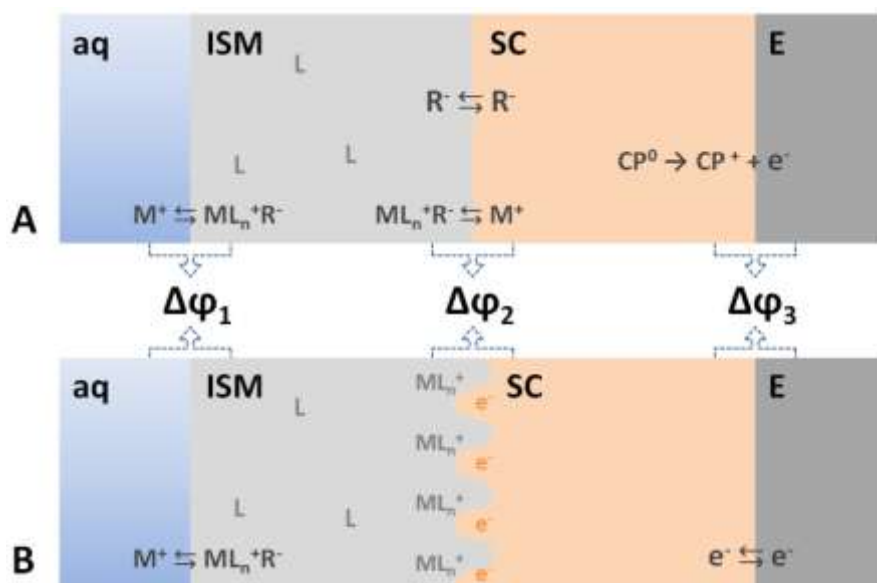
Rys. 2 Schemat przebiegu mechanizmów dla SCISEs czułych na kationy z membraną zawierającą niejonowy jonofor (L) z: (A) SC w postaci domieszkowanego polimeru przewodzącego o wysokiej pojemności redox i (B) wysokoporowatym SC o wysokiej pojemności warstwy podwójnej.

W pierwszym z tych mechanizmów materiały stosowane jako SC powinny charakteryzować się wysokim potencjałem redox. W tej roli doskonale mogą sprawdzić się polimery przewodzące, które wykazują przewodnictwo mieszane – jonowe i elektronowe. W drugim przypadku natomiast transdukcja jon-elektrod zachodzi na granicy powierzchni SC i warstwy ISM, dlatego istotne jest tutaj przewodnictwo elektryczne i wielkość powierzchni materiału SC oraz ilość ładunku i pojemność warstwy podwójnej, gdyż od tego zależy potencjał międzyfazowy. Bardzo dobrze sprawdzą się tu m.in. wysokoporowate materiały węglowe [26,27].

2 POCZĄTKI ELEKTROD JONOSELEKTYWNYCH I ICH ROZWÓJ

Do lat 60. XX wieku rozwój elektrod jonoselektywnych (ISEs) był skupiony głównie na elektrodach szklanych. W drugiej połowie dziesięciolecia Ross i Frant skonstruowali elektrodę fluorkową z membraną z monokryształu fluorku lantanu, zaś Simon otrzymał potasową elektrodę z ciekłą membraną zawierającą obojętny nośnik [28]. Pierwsze ISEs z ciekłym wymieniaczem jonowym czułe na jony wapnia zawierające naładowany jonofor fosforoorganiczny skonstruowane zostały w 1967 roku przez Rossa, natomiast pierwsze polimerowe membrany jonoselektywne z PVC– przez Bloch'a i współpracowników [20]. Konwencjonalne ISEs pomiędzy elektrodą wyprowadzającą a materiałem membrany zawierają elektrolit zapewniający odpowiedni transfer ładunku. Jednakże jego obecność wiąże się z wieloma trudnościami w obsłudze, transporcie czy przechowywaniu ISEs [29]. Obecność roztworu wewnętrznego powoduje, że są one wrażliwe na parowanie cieczy oraz zmiany temperatury próbki i ciśnienia. Wewnątrz korpusu czujników mogą również pojawiać się pęcherzyki powietrza, których obecność jest niepożądana. Sam elektrolit wewnętrzny może ponadto wyciekać do roztworu badanego, sztucznie zawyżając szacowaną wartość granicy wykrywalności w wyniku znacznego zwiększenia stężenia jonu głównego w otoczeniu membrany. W związku z tym poziom roztworu wewnętrznego również należy regularnie uzupełniać [5].

Chęć wyeliminowania roztworu wewnętrznego doprowadziła do powstania w 1971 roku *coated-wire electrodes* (CWEs) w wyniku bezpośredniego nałożenia membrany na powierzchnię elektrody stałej [30]. CWEs jednak w wyniku połączenia materiałów o innym rodzaju przewodnictwa (jonowe i elektronowe) charakteryzowały się słabą stabilnością potencjału i krótkim czasem życia, wynikającym głównie z powodu braku dobrze zdefiniowanej pary redoks, przepływu prądów resztkowych przez membranę oraz tworzenia się warstwy wody na granicy faz membrana-metal elektrody wewnętrznej [5]. Dlatego też po dwóch dekadach poczyniono kolejne próby eliminacji roztworu wewnętrznego stosując jako rozwiązanie warstwę stałego kontaktu charakteryzującego się zarówno przewodnictwem jonowym i elektronowym. W tym celu zastosowano po raz pierwszy polipirol w konstrukcji elektrody czułej na jony sodowe zbudowanej na bazie elektrody Pt [31]. Umieszczenie warstwy pośredniej polipirolu umożliwiło lepsze przenoszenie ładunku pomiędzy materiałem elektrody stałej i jonowoprzewodzącą membraną jonoselektywną, co objawiało się znaczną poprawą stabilności potencjału w porównaniu do CWE. W ten sposób powstały elektrody

jonoselektywne ze stałym kontaktem (SCISEs) [1,32] / *all solid state*. Wydarzenie to zapoczątkowało badania nad materiałami, które można zastosować jako stały kontakt w ISEs. W tym celu wykorzystano już szereg różnego rodzaju materiałów (szerzej opisane w podrozdziale „4.4 Materiały stosowane jako stały kontakt"). Istnieją dwie możliwości modyfikacji konstrukcji czujników z wykorzystaniem stałego kontaktu. Oprócz nałożenia dodatkowej warstwy w zależności od postaci, w jakiej dany materiał występuje, można go również dodawać bezpośrednio do mieszaniny membranowej i nakładać bezpośrednio na powierzchnię elektrody. W znaczny sposób ułatwia to i przyspiesza czas potrzebny do przygotowania sensorów, zwanych potocznie *single piece electrodes*.

Pojawienie się czujników typu SCISEs umożliwiło zmiany kształtu oraz znaczne zmniejszenie rozmiarów czujników, które oprócz tego, że zajmują znacznie mniej miejsca i mogą pracować w różnych pozycjach i konfiguracjach, mogą być również wykorzystywane w wieloczujnikowych platformach pomiarowych [33,34] służących m. in. do bezpośredniego oznaczania zawartości jonów w środowisku in situ bez konieczności pobierania próbek [35]. Przewaga pomiarów w środowisku in situ nad ex situ wynika głównie z możliwości szerokich badań zasobów wodnych [36].

Pomiary wykonywane w ten sposób pozwalają również na otrzymywanie wyników w krótkim czasie oraz ograniczają konieczność procesu przygotowywania próbki obejmującego na przykład filtrację czy dodawanie dodatkowych substancji chemicznych [19]. Elektrody używane w tym celu powinny charakteryzować się również bardzo dobrą stabilnością potencjału oraz odpornością na zmiany warunków pomiarowych (temperatura, nasłonecznienie, obecność gazów) [35]. SCISEs charakteryzują się wysoką wytrzymałością mechaniczną, łatwością przechowywania i transportu oraz mogą pracować w warunkach podwyższonego ciśnienia i w każdej pozycji [13]. Wydajność elektrod jonoselektywnych ze stałym kontaktem, w których wyeliminowano roztwór wewnętrzny, zależy nie tylko od właściwości membrany jonoczułej, ale także od rodzaju elektrody wewnętrznej i właściwości warstwy pośredniej (stałego kontaktu) umieszczonej między tą elektrodą a membraną [2].

Już ponad dekadę temu wzrosło zainteresowanie dotyczące zminiaturyzowanych i prostych w obsłudze czujników, które pracując w sposób zdalny w postaci złożonych układów mogłyby zbierać i przetwarzać informacje w celu monitorowania zarówno poziomu zanieczyszczeń środowiska naturalnego, jak również stanu organizmu ludzkiego [37]. W związku z rosnącym zainteresowaniem tematyką dotyczącą stanu zdrowia i ciągłą obserwacją funkcji fizjologicznych zachodzących w ciele człowieka konstruowane są czujniki

potencjometryczne nieinwazyjne, które można nosić w czasie rzeczywistym w postaci opasek, naszywek, czy elementów odzieży (tzw. *wearable potentiometric ion sensors* - WPISs) [38]. Mogą być one wykorzystywane do oznaczania zawartości jonów, które w stosunkowo wysokich stężeniach znajdują się w pocie (m.in. Na^+, K^+, Mg^{2+}, Ca^{2+}, Cl^- i NH_4^+) oraz do kontroli pH (ważne np. w procesie gojenia się ran). W przypadku występowania niektórych chorób, takich jak zaburzenia stresowe i zaburzenia pracy serca, mukowiscydoza, hipo- i hipernatremia, czy hipo- i hiperkaliemia, a nawet utrata minerałów kostnych i nadużywanie narkotyków, monitorowanie zawartości kluczowych dla określonych zaburzeń anionów i kationów pozwala na kontrolowanie przebiegu choroby [38,39]. WPISs mogą być stosowane zarówno w celu kontroli stanu zdrowia, jak również do badania wydajności organizmu podczas ćwiczeń. Zastosowanie w nich stałego kontaktu zamiast roztworu wewnętrznego umożliwia wszechstronne ich użytkowanie, zmianę kształtu i rozmiarów czujników. W tym przypadku miniaturyzacja oraz opracowywanie nowych, odpornych na uszkodzenia mechaniczne i długotrwałe użytkowanie oraz nieszkodliwych materiałów są szczególnie ważne, aby nie przeszkadzały one w codziennym funkcjonowaniu użytkownika. Ogniwo elektrochemiczne stanowią zintegrowane elektrody: wskaźnikowa i referencyjna oraz zbiornik na próbkę. W trakcie pracy urządzeń monitorowana jest w czasie rzeczywistym aktywność/stężenie jonów w płynach biologicznych (głównie w pocie) [38].

Wraz z rozwojem nauki i technologii dąży się automatyzacji jak największej liczby procesów, aby możliwe było bez udziału człowieka m.in. pobieranie próbek, ich przetwarzanie oraz zbieranie danych i ich analiza przez urządzenie. Zainteresowaniem cieszy się również możliwość zdalnej kontroli, sterowania przyrządami, zmian i modyfikacji parametrów metody oraz generowania raportów z wynikami [40]. Monitorowanie środowiska w czasie rzeczywistym umożliwia znacznie szybszą reakcję w przypadku odkrycia np. wzrostu stężenia substancji toksycznych oraz podjęcie natychmiastowych działań mających na celu ich ograniczenie lub zatrzymanie.
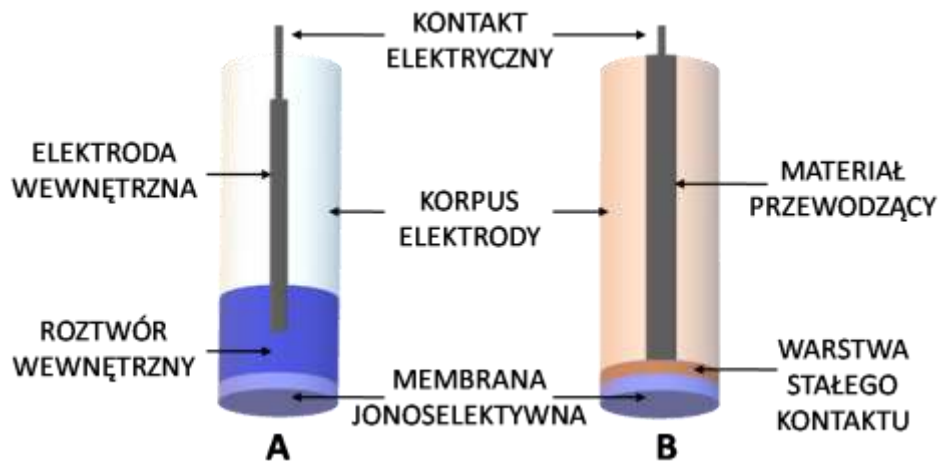
3 KONSTRUKCJA ELEKTROD JONOSELEKTYWNYCH

3.1 Klasyczna konstrukcja elektrod jonoselektywnych

W klasycznej konstrukcji ISEs, jak wspomniano wcześniej, znajduje się roztwór wewnętrzny soli jonu głównego, na który elektroda jest czuła (Rys. 3). Pełni on funkcję ciekłego kontaktu umożliwiającego odpowiedni transport/przepływ ładunku pomiędzy materiałem elektrody wyprowadzającej i membraną jonoselektywną. Elektrody te posiadają wiele zalet, m.in. charakteryzują się bardzo dobrą stabilnością potencjału, dobrą selektywnością i zwykle szerokim zakresem liniowości wynoszącym $1 \times 10^{-6} - 1 \times 10^{-1}$ mol L^{-1}. Niestety w związku z obecnością elektrolitu wewnętrznego konieczne jest ich przechowywanie i użytkowanie w pozycji pionowej, a ponadto istnieją ograniczenia związane z ich miniaturyzacją oraz modyfikacją kształtu. Istnieje również ryzyko zapowietrzenia elektrody wynikające głównie z nieprawidłowego przechowywania [41].

3.2 Czujniki potencjometryczne typu solid contact

W elektrodach ze stałym kontaktem (SCISEs) elektroda wewnętrzna ma bezpośredni kontakt z membraną jonoselektywną (Rys. 3). Ułatwia i przyspiesza to znacznie proces przygotowania elektrod oraz poprawia odporność mechaniczną, natomiast wymaga odpowiedniego doboru materiałów, które mogą zostać zastosowane w tej roli. SCISEs dzięki wyeliminowaniu roztworu wewnętrznego mogą być poddawane większej liczbie modyfikacji, obejmujących zmniejszanie ich rozmiarów (mikroelektrody) oraz zmiany ich wyglądu i kształtu, aby ułatwić ich stosowanie do konstrukcji urządzeń i czujników, które umieszczane w różnych miejscach (od platform pomiarowych do skóry pacjenta) będą mogły w wygodny i szybki sposób umożliwić uzyskanie informacji na temat badanego obiektu w czasie rzeczywistym. Dużą zaletą SCISEs może być również możliwość ich bezobsługowej pracy w warunkach podwyższonej temperatury i ciśnienia oraz w dowolnej orientacji [4]. Uzyskiwanie elektrod w rozmiarach mikro cieszy się obecnie dużym zainteresowaniem ze względu na znacznie mniejsze ilości materiałów zużywanych do ich konstrukcji oraz kompatybilność z małymi objętościami próbek niezbędnych do wykonania pomiarów [7]. Dodatkowo SCISEs są prostsze w obsłudze i transporcie, gdyż nie zachodzi ryzyko wycieku elektrolitu bądź 'zapowietrzenia' elektrod oraz charakteryzują się one znacznie lepszą odpornością na zniszczenia mechaniczne [42].

Rys. 3 Porównanie konstrukcji elektrod jonoselektywnych: (A) klasycznej z roztworem wewnętrznym, (B) ze stałym kontaktem.

3.3 Membrana jonoselektywna i jej składniki

Membrana jonoselektywna jest najważniejszym elementem elektrod jonoselektywnych, dzięki której mogą one być w ogóle wykorzystywane do oznaczania wybranych jonów (głównych) w obecności innych jonów (interferujących/przeszkadzających) w roztworze próbki. Skład membrany jest optymalizowany w celu uzyskania odpowiednich wartości parametrów analitycznych, elektrycznych i mechanicznych elektrod (Rys. 4) [42].
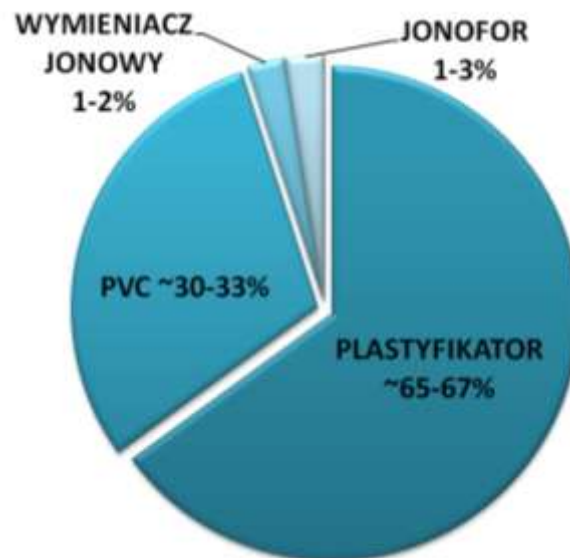
Rys. 4 Skład membrany jonoselektywnej.

Większą część (około 65 – 67% wagowych) mieszaniny membranowej stanowi plastyfikator odpowiadający za plastyczność membrany oraz polichlorek winylu (około 30 – 33% wagowych). Natomiast kluczowym składnikiem jest jonofor odpowiadający za właściwości jonoselektywne membrany, który oddziałuje w sposób selektywny z jonem, na który membrana ma być czuła. Mimo, że jest to składnik, którego w membranie jest bardzo mało, to właśnie jemu ISEs zawdzięczają swoją nazwę, gdyż nadaje on membranie wyjątkowe właściwości bez których niemożliwe byłoby wykonanie oznaczenia. W celu uzyskania lepszej pracy czujników do membrany dodaje się również inne substancje, które mają dodatkowo wzmocnić działanie głównej substancji aktywnej. Na przykład różnego rodzaju wymieniacze jonowe, których zadaniem jest przyciąganie jonów analitu do fazy membrany, gdzie następnie są one wiązane przez jonofor [74]. Odpowiednio odważone składniki membrany miesza się z rozpuszczalnikiem organicznym (najczęściej tetrahydrofuranem) i homogenizuje w celu uzyskania jednolitej mieszaniny. W elektrodach klasycznych, w których membrana ma za zadanie oddzielać roztwór wewnętrzny od roztworu próbki membranę wycina się z „dużej" membrany otrzymanej po odparowaniu rozpuszczalnika i umieszcza w obudowie czujnika na etapie przygotowania. Natomiast w przypadku SCISEs, przygotowaną mieszaninę membranową najczęściej nakrapla się bezpośrednio na przygotowaną wcześniej powierzchnię elektrody z nałożoną uprzednio warstwą stałego kontaktu i zostawia do wyschnięcia. Dostępne są również badania opisujące elektrody z membranami wielowarstwowymi, w której poszczególne warstwy różniły się między sobą składem oraz grubością w celu zapewnienia między innymi zmiennych współczynników dyfuzji jonów przez membranę oraz poprawy właściwości czujników [43,44].

3.4 Materiały stosowane jako stały kontakt

Elektrody jonoselektywne są proste w użyciu, nie wymagają stosowania skomplikowanego i drogiego sprzętu. Sama produkcja elektrod też nie jest procesem bardzo drogim, jednak koszt jest uwarunkowany rodzajem wybranych elektrod bazowych oraz ceną rynkową materiałów wykorzystywanych do konstrukcji elektrod lub też syntezy tych materiałów. Obecnie dąży się do uzyskania czujników charakteryzujących się znakomitymi parametrami analitycznymi oraz elektrycznymi. W tym celu podejmowane są próby syntezy związków chemicznych, które pełniąc funkcję substancji aktywnej w membranie jonoselektywnej będą zapewniać jej odpowiednią selektywność umożliwiającą oznaczenie wybranych jonów (głównych) w

obecności innych jonów towarzyszących znajdujących się w próbce, a także materiałów pełniących rolę stałego kontaktu, które mogą służyć do modyfikacji konstrukcji elektrod. W roli stałego kontaktu zastosowano do tej pory wiele materiałów w celu poprawy parametrów analitycznych czujników, do konstrukcji których zostały wykorzystane. W większości przypadków wpływało to głównie na parametry elektryczne elektrod, w szczególności na zwiększenie pojemności warstwy podwójnej czy zmniejszenie oporności membrany. Istotną zmianą następującą w wyniku dodatkowej modyfikacji konstrukcji elektrod jest znaczna poprawa stabilności ich potencjału w porównaniu do elektrod niemodyfikowanych [45,46]. Czasami poprawie ulegały również parametry analityczne, rozszerzeniu ulegał zakres liniowości krzywej kalibracyjnej [47,48] czy obniżeniu – granica wykrywalności [47,49]. Dobranie odpowiedniego materiału przewodzącego jest szczególnie istotne ze względu na znaczący wpływ rodzaju warstwy pośredniej również na stabilność składu membrany jonoselektywnej [50].

Nowoopracowane materiały mające pełnić funkcję stałego kontaktu powinny spełniać szereg warunków. W pierwszej kolejności muszą być to materiały o wysokiej pojemności objętościowej zapewniającej stabilność potencjału oraz stabilne chemicznie, niegenerujące żadnych reakcji ubocznych w procesie transdukcji jon-elektron. Ponadto proces zamiany pomiędzy przewodnością jonową i elektronową powinien być odwracalny. Istotna jest również wystarczająca hydrofobowość materiału, aby pomiędzy materiałem elektrody wewnętrznej a membraną jonoselektywną nie tworzyła się warstwa wodna [51]. Wybór materiału stosowanego jako SC powinien być dokonywany z uwzględnieniem wielu wymagań i parametrów, m.in. na podstawie metody i kosztu ich wytwarzania, ich odporności mechanicznej, trwałości oraz wydajności analitycznej i żywotności [6].

Na Rys. 5 przedstawiono obrazy SEM wybranych materiałów, których zastosowanie w konstrukcji SCISEs opisano w publikacjach naukowych wchodzących w skład cyklu. Stanowią one nanomateriały pochodzące z różnych grup związków wykorzystywanych jako stały kontakt, którym większą uwagę poświęcono w dalszej części rozprawy.
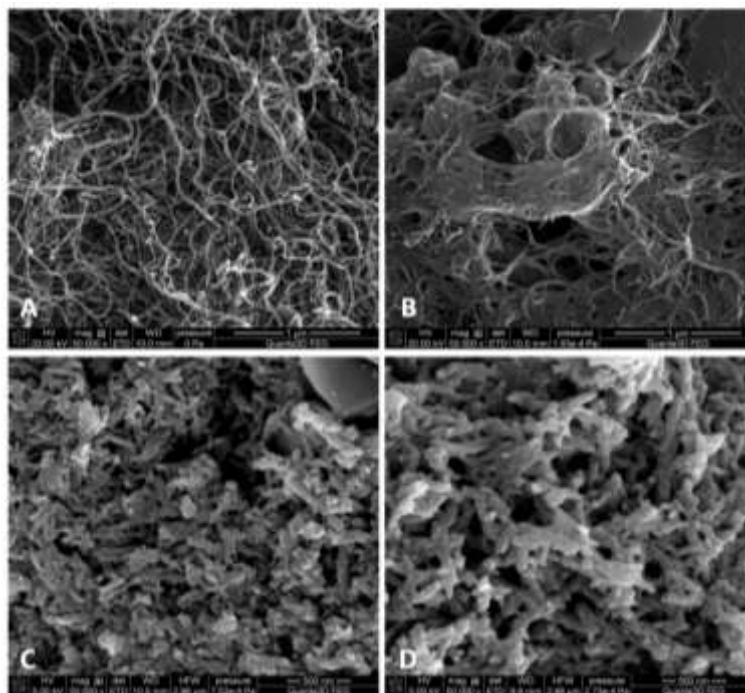
Rys. 5 Obrazy SEM: (A) MWCNTs, (B) nanokompozytu MWCNTs z PANINFs-Cl, (C) PANINFs-Cl, (D) PANINFs-NO$_3$.

3.4.1 Polimery przewodzące

Pierwszymi materiałami zastosowanymi jako stały kontakt były polimery przewodzące (CPs). Z tej grupy związków wykorzystano w tym celu już w latach 90. XX wieku polipirol (PPy) [31,52], a następnie poli(3,4-etylenodioksytiofen) (PEDOT) [53–55], poli(3-oktylotiofen) (POT) [56–58], czy polianilinę (PANI) [59,60]. Do konstrukcji czujników zastosowano również różnego rodzaju nanostrukturalne polimery przewodzące głównie na bazie polianiliny: w postaci nanorurek [61], nanowłókien [62] czy nanodrutów [63,64].

CPs można otrzymywać na wiele sposobów. Można do nich zaliczyć polimeryzację: elektrochemiczną, międzyfazową, radiolityczną, sonochemiczną, a także metody z wykorzystaniem szablonów: tzw. „twardych" (zeolity, anodowy tlenek glinu itp.) [65] i „miękkich" (surfaktanty, polielektrolity itp.) [66]. Szerokie zastosowanie CPs zawdzięczają swoim licznym zaletom: prostocie syntezy i różnorodności możliwych modyfikacji z użyciem innych materiałów, wysokiej stabilności środowiskowej, atrakcyjnej cenie oraz unikalnym strukturom chemicznym [67,68]. Związki te charakteryzują się podwójnym przewodnictwem, zarówno jonowym, jak i elektronowym, i w związku z tym mogą być z powodzeniem stosowane jako przetworniki jon-elektron umieszczone w postaci warstwy pośredniej stałego kontaktu w elektrodach jonoselektywnych, a także jako dodatkowy składnik rozpuszczony w

membranie lub w formie sfunkcjonalizowanej jako gotowe membrany [69]. Dzięki wykorzystaniu tych materiałów umożliwiono przekształcenie sygnału jonowego w sygnał elektroniczny wykorzystując opisany wcześniej mechanizm pojemnościowy redox.

Pierwsze czujniki wykorzystujące CPs miały znacznie poprawioną przewodność membrany, jednak często wykazywały wrażliwość na zmienne warunki środowiskowe (światło, obecność tlenu i dwutlenku węgla w roztworze próbki oraz zmiany pH), będącą efektem ubocznych reakcji elektrochemicznych [68]. Materiały te często nie wykazywały również wystarczająco wysokiej hydrofobowości, co skutkowało powstawaniem warstwy wodnej na granicy faz pomiędzy membraną a elektrodą wewnętrzną. Dlatego rozpoczęto poszukiwania materiałów o podobnych właściwościach, różniących się jednak metodą syntezy, budową czy składem oraz bardziej hydrofobowych, w celu poprawy adhezji membrany jonoselektywnej i ograniczenia wchłaniania przez nią wody [7].

3.4.2 Nanomateriały węglowe

Nanomateriały węglowe stanowią kolejną grupę materiałów o wyjątkowych właściwościach, które do tej pory powszechnie stosuje się w konstrukcji elektrod jonoselektywnych. Definiuje się je jako materiały o minimum jednym wymiarze mniejszym niż 100 nm [70]. Są one szczególnie popularne głównie ze względu na ich unikalne właściwości chemiczne, fizyczne i elektryczne, tj. odporność mechaniczną, hydrofobowość oraz dobre przewodnictwo elektryczne i wysoką pojemność elektryczną [1,51]. Bardzo wysoki stosunek powierzchni do objętości wynikający z małego rozmiaru nanostruktur sprzyja ich interakcji z sąsiadującymi materiałami, a ich wyjątkowe właściwości elektryczne wpływają na poprawę stabilności potencjału, co czyni je szczególnie atrakcyjnymi materiałami, które można wykorzystać jako przetworniki jon-elektron w SCISEs [23]. Właściwości syntezowanych nanomateriałów oraz ich późniejsze możliwe zastosowania zależą w dużej mierze od sposobu ich otrzymywania [71,72]. Ponadto nanomateriały te można poddawać różnego rodzaju modyfikacjom m.in. przyłączając do nich wybrane grupy funkcyjne w procesie derywatyzacji w celu zmiany ich właściwości. W ten sposób można otrzymywać nanomateriały charakteryzujące się na przykład lepszą rozpuszczalnością lub reaktywnością chemiczną w porównaniu do próbki wyjściowej [73–75]. Do najpopularniejszych nanomateriałów węglowych stosowanych w SCISEs należą nanorurki węglowe (CNTs) wynalezione przez Iijima w 1991 roku. Poświęcone są im liczne artykuły przeglądowe [76–85], w których opisano liczne sposoby otrzymywania i oczyszczania CNTs oraz ich szeroko badane właściwości, możliwe reakcje

funkcjonalizacji i wykorzystanie do syntezy nanokompozytów. Dostępne są również artykuły skupiające się na ich zastosowaniu w elektrochemii [86–89].

Naukowcy opisali już wyniki badań dotyczące wykorzystania jako stałego kontaktu w konstrukcji elektrod różnego rodzaju nanomateriałów węglowych: SWCNTs [90–93], MWCNTs [94–97], grafenu [98,99], fullerenów [100], czy też mezoporowatego węgla z nadrukiem koloidalnym (CIM) [46], węgla bezpostaciowego w postaci sadzy [101], uporządkowanego trójwymiarowo węgla mikroporowatego (3DOM) [49,102] lub chemicznie i elektrochemicznie zredukowanego tlenku grafenu (CRGO [103] i ERGO [104]).

3.4.3 Nanocząstki metali i niemetali

Obecnie coraz częściej pojawiają się badania nad różnego rodzaju nanocząstkami (z definicji materiały o co najmniej dwóch wymiarach poniżej 100nm [70]), głównie nanocząstkami metali i tlenków metali, ich właściwościami i możliwymi zastosowaniami. Do jednego z takich zastosowań należy wykorzystanie ich do poprawy parametrów analitycznych i elektrycznych czujników potencjometrycznych, co możliwe jest dzięki ich wysokiej aktywności redox i bardzo dużej powierzchni właściwej. Dotychczas wykorzystano już w tym celu nanocząstki metali: złota [105–108], srebra [109], platyny [110–112], tlenków metali: tlenku miedzi(II) [113], tlenku ceru [114], tlenku rutenu [115] i tlenku irydu [116], a także nanocząstki dwumetaliczne [117]. Oprócz typowych badań dotyczących wpływu obecności nanocząstek na bezpośrednią pracę czujników opisano również zastosowanie nanocząstek srebra o znanych właściwościach bakteriobójczych i przeciwdrobnoustrojowych [118,119] na wydłużenie żywotności elektrod stosowanych do badania złożonych próbek środowiskowych narażonych na obecność mikroorganizmów i biofilmów [120]. Ponadto nanocząstki Ag stosowane są również w elektronice, farbach, odzieży, filtrach przeciwsłonecznych, kosmetykach i wyrobach medycznych [121,122]. Natomiast nanocząstki tlenków metali, np. tlenku cynku są szeroko znane z zastosowań w materiałoznawstwie, magazynowaniu energii, monitorowaniu środowiska i naukach biomedycznych, czy też przy produkcji fotodetektorów i czujników gazowych [123]. Podobnie jak nanocząstki srebra, również nanocząstki ZnO czy TiO$_2$ mają silne działanie antybakteryjne. Ponadto nanostrukturalny tlenek cynku jest obiecującym, nietoksycznym fotokatalitycznym materiałem półprzewodnikowym o wysokiej wydajności, znacznie tańszym niż tlenek tytanu [124]. Ze względu na antybakteryjne właściwości niektórych z nanocząstek metali i tlenków metali są wykorzystywane w procesach uzdatniania wody wykorzystujących metody fotokatalizy i adsorpcji [125].

Możliwe jest również otrzymywanie nanocząstek tlenków 'mieszanych' zawierających tlenki dwóch różnych metali (np. $ZnO:Al_2O_3$ [126]).

Tlenki metali (PtO_2, IrO_2, RuO_2, OsO_2, Ta_2O_5 and TiO_2) zostały wykorzystane w konstrukcji elektrod do pomiaru pH już prawie 40 lat temu [127]. Potwierdzono, że modyfikacja czujników za pomocą nanocząstek wpływa pozytywnie na stabilność potencjału w wyniku osiągniętych niskich wartości oporności i dużych pojemności elektrycznych [114,115].

3.4.4 Nanokompozyty

Kompozyty z definicji stanowią materiały, które zostały utworzone z minimum dwóch komponentów różniących się pomiędzy sobą, w celu znacznej poprawy wybranych parametrów charakteryzujących materiał i/lub uzyskania nowych właściwości materiału. Szczególnie popularne są kompozyty powstałe z mieszaniny nanomateriałów węglowych i polimerów [128]. Dodatek m. in. nanorurek węglowych do polimerów umożliwia uzyskanie materiałów kompozytowych o ulepszonych właściwościach mechanicznych, termicznych, elektrycznych, optycznych i chemicznych [128–131]. W literaturze opisano do tej pory wiele przykładów zastosowania materiałów kompozytowych jako stałego kontaktu w ISEs: kompozytu trójwymiarowego porowatego grafenu z nanocząstkami platyny [132], nanokompozytu błękitu pruskiego z chitozanem [29], tetratiafulwalenu z grafenem [133], poli(3,4-etylenodioksytiofenu) z poliakrylanem [134], wielościennych nanorurek węglowych z pochodną poli(3-oktylotiofenu) [135] czy poli(metakrylanu metylu) z nanowłóknami grafenu [136].

4 PARAMETRY ANALITYCZNE ELEKTROD JONOSELEKTYWNYCH

Elektrody jonoselektywne powinny spełniać szereg warunków i charakteryzować się odpowiednimi wartościami określonych parametrów analitycznych, koniecznych dla ich prawidłowej pracy i rzetelności otrzymanych wyników [2]. Do szczególnie ważnych, ale i jednocześnie podstawowych parametrów, które wyznaczane są na wstępnym etapie badań należą: nachylenie charakterystyki elektrody (czułość odpowiedzi), zakres liniowości krzywej odpowiedzi (zakres, w którym zależność potencjału od ujemnego logarytmu z aktywności jonów głównych jest liniowa) i granica wykrywalności analitu LoD (najniższa aktywność jonu, jaką można wiarygodnie wykryć). Najczęściej granica wykrywalności może być wyznaczana w punkcie przecięcia ekstrapolowanych prostoliniowych odcinków krzywej kalibracyjnej (Rys. 6A). Bardziej uniwersalną metodą, szczególnie przydatną w przypadku nietypowego przebiegu krzywej kalibracyjnej, np. zmiany odpowiedzi elektrody z super-Nernstowskim nachyleniem krzywej kalibracyjnej, granicę wykrywalności wyznacza się jako aktywność jonów, dla której potencjał elektrody odbiega od prostoliniowego przebiegu krzywej kalibracyjnej o mniej niż ln1(RT/ZF) (czyli t=25°C → 18/n mV, gdzie n – wartościowość jonu głównego) (Rys. 6B) [4,137].
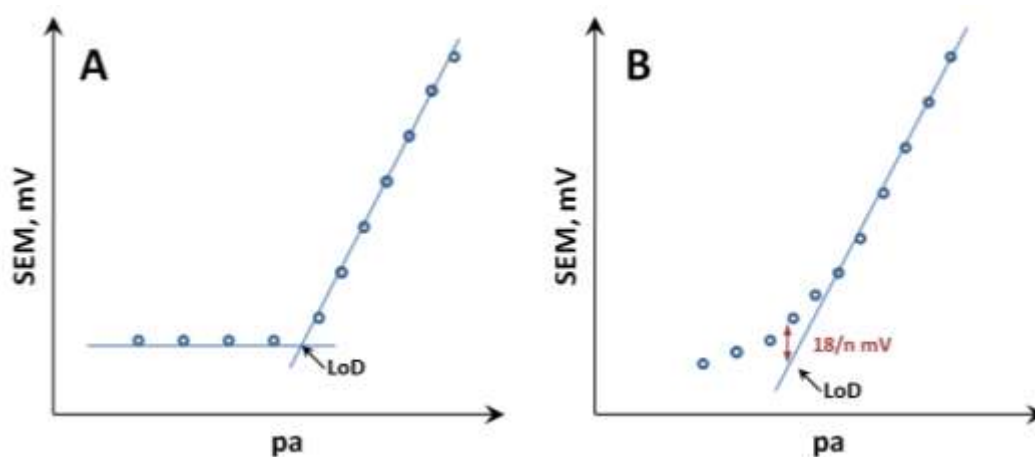
Rys. 6 Sposoby wyznaczania granicy wykrywalności elektrod na podstawie krzywych kalibracyjnych, gdzie: pa – ujemny logarytm z aktywności jonu głównego, LoD – granica wykrywalności.

Ponadto bardzo istotna jest również selektywność czujników w odniesieniu do jonów głównych względem jonów interferujących, aby można było jak najlepiej przewidzieć zachowanie czujników w próbkach rzeczywistych, a otrzymane wyniki były jak najbliższe

prawdziwej wartości stężenia analitu w roztworze. Selektywność określa zdolność do rozróżnienia jonów obecnych w próbce i jest ilościowo przedstawiana za pomocą współczynnika selektywności K_{IJ}. Współczynnik selektywności zależy m.in. od współczynników podziału jonów między fazą wodną a fazą membranową, ruchliwości jonów w membranie oraz stałych tworzenia kompleksu jonofor–jon. Do najczęściej stosowanych metod wyznaczania współczynników selektywności elektrod należą: metoda roztworów rozdzielonych (SSM) oraz metoda roztworów mieszanych (FIM) [4,138]. Dodatkowo parametry dotyczące potencjału elektrod, takie jak jego stabilność (zarówno krótkoterminowa i długoterminowa), odwracalność i odtwarzalność są kluczowe, jeśli czujniki mają być wykorzystywane z powodzeniem przez dłuższy czas. Stabilność potencjału elektrod ma duże znaczenie dla uzyskania prawidłowych wyników oznaczeń i pozwala określić, jak często konieczne jest wykonywanie kalibracji niwelujących powstawanie błędów oznaczeń powyżej określonego progu. Na stabilność potencjału może mieć wpływ szereg czynników. Dla uzyskania dobrej stabilności potencjału konieczne jest zapewnienie szybkiej, bezpośredniej i odwracalnej transdukcji jon-elektron pomiędzy membraną a elektrodą wewnętrzną oraz stabilność składu membrany jonoselektywnej [6]. Ponadto ważna jest wystarczająco wysoka pojemność redox materiału SC oraz brak reakcji ubocznych z jego udziałem [4].

Przydatność badanych czujników do oznaczania próbek rzeczywistych jest określana na podstawie dodatkowych testów. Wymienić tu należy pomiary potencjału w roztworach o zmiennym potencjale redox, zmiennej zawartości gazów (O_2, CO_2) oraz przy różnym rodzaju oświetlenia [6,55]. Określa się również zakres pH, w których potencjał elektrod w roztworze o stałej aktywności jonu głównego pozostaje bez zmian. Wszystkie tego typu pomiary mają na celu sprawdzenie wrażliwości czujników na zmienne warunki środowiskowe.

W trakcie pomiarów może dochodzić do występowania niepożądanych procesów, jakimi są: zmiana składu membrany jonoselektywnej, jak również powstawanie warstwy wodnej pomiędzy materiałem elektrody wewnętrznej a membraną jonoselektywną. Pierwszy z nich może nastąpić na skutek wymywania składników membrany do roztworu próbki czy też współekstrakcji składników lipofilowych lub przeciwjonów z roztworów próbek wykazujących wysokie stężenie soli [4,139]. Powstawanie warstwy wodnej może wpływać znacznie na dryft potencjału elektrod wynikający ze zmiany składu warstwy wodnej wraz ze zmianą składu próbki. Test umożliwiający stwierdzenie, czy taka warstwa wodna powstaje polega na kondycjonowaniu czujników w roztworze jonu głównego o wysokim stężeniu (najczęściej 0,1 mol L^{-1}) przez dobę, a następnie zmianie roztworu na zawierający jon

interferujący o tym samym stężeniu na kilka godzin. Ostatecznym etapem jest powrót do poprzedniego roztworu zawierającego jon główny i obserwowanie, w jaki sposób i jak szybko zmianie ulega potencjał badanych elektrod. Dowiedziono zarówno w sposób teoretyczny, jak i eksperymentalny, że jony interferujące znacznie łatwiej przechodzą przez membranę w porównaniu do jonów głównych [140]. Aby uniemożliwić powstawanie warstwy wodnej konieczny jest odpowiedni dobór materiału pełniącego funkcję stałego kontaktu, który powinien zapewnić wystarczającą adhezję membrany jonoselektywnej i materiału elektrody wewnętrznej [141]. Jako jeden z możliwych z sposobów zaproponowano zastosowanie lipofilowej samoorganizującej się monowarstwy na powierzchni elektrody wewnętrznej [140].

Kolejnymi parametrami są: czas odpowiedzi i czas życia elektrod [137]. W przypadku tych parametrów bardziej pożądane są czujniki reagujące szybciej na zmiany stężeń roztworów, a więc charakteryzujące się krótszym czasem odpowiedzi oraz mogące pracować przez dłuższy okres czasu bez znacznej zmiany swoich właściwości, czyli o dłuższym czasie życia [142].

W celu lepszego poznania zależności wynikających z modyfikacji elektrod poprzez wprowadzenie materiału stałego kontaktu i porównania ich z elektrodami niemodyfikowanymi określa się również parametry elektryczne elektrod. Zalicza się do nich pojemność redox warstwy przewodzącej / warstwy podwójnej (C) oraz opór elektrody i opór membrany jonoselektywnej (R). Do ich wyznaczenia wykorzystuje się metodę elektrochemicznej spektroskopii impedancyjnej i chronopotencjometrię [133,143].

Elektrochemiczna spektroskopia impedancyjna jest stosowana od dawna w badaniach układów elektrochemicznych. Technika ta pozwala na scharakteryzowanie procesów fizykochemicznych w szerokim zakresie stałych czasowych, gdzie transfer masy odpowiada niskim częstotliwościom, natomiast transfer elektronów – wysokim częstotliwościom. Fazowa odpowiedź prądowa, którą uzyskuje się podczas pomiaru, charakteryzuje składową rzeczywistą (rezystancyjną, Z'), natomiast przeciwfazowa odpowiedź prądowa – składową urojoną (pojemnościową, -Z''). EIS umożliwia badania nad systemami elektrochemicznymi, w szczególności dotyczącymi procesów elektroosadzania i korozyjnych oraz baterii i ogniw paliwowych [144]. Pozwala na oszacowanie wartości parametrów elektrycznych elektrod oraz rozdzielenie i scharakteryzowanie zachodzących poszczególnych procesów kinetycznych [145,146]. Metodę tą można wykorzystać do badania powierzchni materiałów, również tych stosowanych jako stały kontakt w ISEs oraz wpływ rodzaju SC na pracę czujników. Wyniki

otrzymane za pomocą EIS mogą być dopasowywane do różnego rodzaju obwodów elektrycznych składających się m.in. z rezystorów i kondensatorów. Złożoność tych układów zależy od kształtu i wielkości otrzymanego widma impedancyjnego [144]. Najczęściej występującym kształtem widma w przypadku ISEs jest półokrąg w zakresie wysokich częstotliwości związany z pojemnością geometryczną (C_g) i rezystancją (oporem) objętościową (R_b) membrany połączony z częścią półokręgu w zakresie niskich częstotliwości związaną z pojemnością podwójnej warstwy elektrycznej (C_{dl}) na granicy faz – membrana polimerowa/elektroda wewnętrzna i rezystancją (oporem) przenoszenia ładunku (R_{ct}) odwrotnie proporcjonalną do szybkości przenoszenia elektronów. Na początku obwodu zastępczego przedstawiony jest również opór występujący w fazie roztworu (elektrolitu) (R_s). Oprócz elementów przedstawiających opór i pojemność, w obwodzie mogą również występować elementy stałoprądowe (CPE) związane z defektami powierzchni badanego materiału oraz procesem dyfuzji. W związku z CPE występuje parametr n, którego wartość definiuje występowanie pojemności „idealnej" (n=1) bądź impedancji Warburga (n=0,5) związanej z ograniczeniami transferu masy, o której występowaniu świadczyć może linia o nachyleniu 45° widoczna na widmie impedancyjnym [144,147–149].

Na Rys. 7A przedstawiono przykładowe widma impedancyjne dla dwóch rodzajów elektrod: elektrody niemodyfikowanej z membraną o podstawowym składzie nałożoną bezpośrednio na elektrodę wewnętrzną GC oraz elektrody z warstwą pośrednią nanocząstek ZnO, do których dopasowano obwód zastępczy przedstawiony na Rys. 7B. Wprowadzenie warstwy pośredniej wpłynęło na znaczną poprawę parametrów elektrycznych elektrod w wyniku ułatwienia zachodzących procesów dyfuzji oraz transportu ładunku na granicy faz. Otrzymano wartości R_b równe 479 i 882 kΩ; R_{ct}: 22 i 180 kΩ oraz C_{dl}: 26,7 i 0,116 nF, a więc oporność uległa znacznemu zmniejszeniu, a pojemność znacznemu zwiększeniu (ponad 200-krotnie) wpływając na znaczną poprawę stabilności potencjału elektrod.
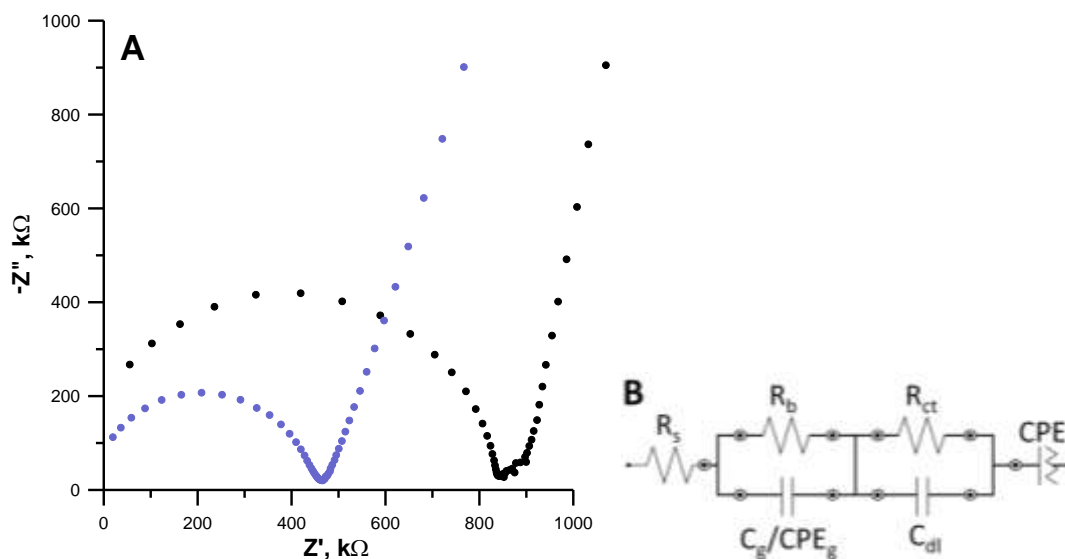
Rys. 7 (A) Przykład widma impedancyjnego dla elektrod potasowych: ISE niemodyfikowanej (⬤) i ISE z warstwą stałego kontaktu nanocząstek – ZnO (⬤) oraz (B) zastępczy obwód elektryczny R(RC/Q)(RC)Q.

W przypadku, gdy obecność analitu w roztworze wpływa na parametry obwodu i brak jest innych substancji, które również mają wpływ na zmianę tych parametrów, EIS można stosować do oznaczania analitów [144]. Naukowcy badali też, czy za pomocą tej techniki możliwe jest rozróżnienie jakim uszkodzeniom uległa membrana jonoselektywna (obejmujące uszkodzenia fizyczne, wypłukiwanie składników aktywnych lub zanieczyszczenia biologiczne) oraz czy elektrody są jeszcze zdolne do pracy czy są już niesprawne. Takie testy mogłyby być szczególnie przydatne w badaniu sprawności urządzeń wykorzystywanych m.in. do monitorowania środowiska naturalnego [148].

Standardową metodą eksperymentalną umożliwiającą szybką i wygodną ocenę rzeczywistej stabilności potencjału (ΔE/Δt) różnego rodzaju elektrod jonoselektywnych ze stałym kontaktem oraz pozwalającą na oszacowanie pojemności (C) i oporności całkowitej (R) elektrody jest chronopotencjometria [53]. Z użyciem chronopotencjometrii zmiennoprądowej można uzyskać również potencjał równowagowy badanych czujników [143]. Pomiar chronopotencjometryczny polega na polaryzowaniu elektrody za pomocą prądu stałego (naprzemiennie o dodatnim i ujemnym znaku) [26]. Na krzywych chronopotencjometrycznych przedstawiających zależność potencjału od czasu widoczny jest skok potencjału przy zmianie kierunku prądu, a następnie powolny dryft potencjału (Rys. 8) [53]. Na podstawie otrzymanego skoku za pomocą wzorów przedstawionych na Rys.8 można wyznaczyć parametry elektryczne czujników. W przypadku elektrod, których dotyczy

przedstawiony chronopotencjogram R wyniósł: 10,7 i 227 kΩ, $\Delta E/\Delta t$: 0,106 i 5,36 mV s^{-1}, a C: 1237 i 21,18 μF, odpowiednio dla ISE-2 i ISE-3. Zarówno ocena wizualna wykresu, jak również porównanie otrzymanych wartości pozwala wysnuć wnioski, że ISE-2 (w tym przypadku z dodatkiem jako stałego kontaktu do membrany jonoselektywnej nanokompozytu zawierającego MWCNTs o mniejszych rozmiarach) wykazuje znacznie lepsze parametry elektryczne w porównaniu do ISE-3 (gdzie stały kontakt stanowił nanokompozyt z MWCNTs o rozmiarach większych i mniej jednorodnej strukturze). ISE-2 charakteryzuje się bowiem ponad 20-krotnie niższą opornością, ponad 50-krotnie niższym dryftem potencjału, a przy tym prawie 60-krotnie większą pojemnością. Tego typu różnice wynikające z odmiennej struktury i właściwości materiałów uwidaczniają się również w odpowiedzi potencjometrycznej czujników oraz w wartościach innych parametrów analitycznych.
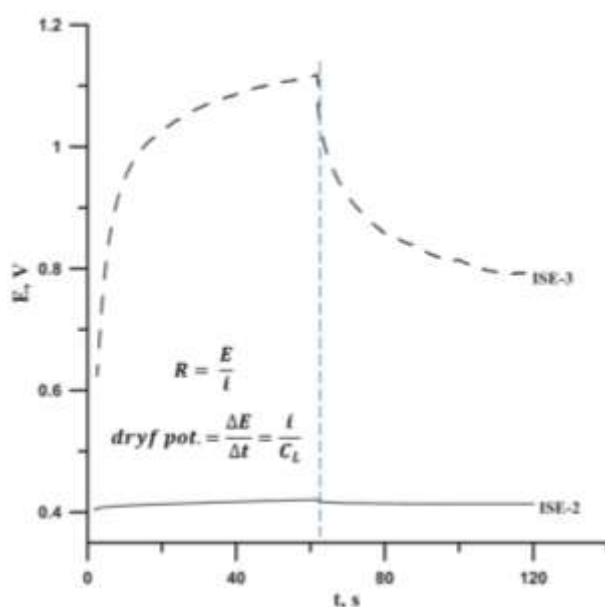
Rys. 8 Przykładowy chronopotencjogram reprezentujący elektrody azotanowe o stabilnym (——) i mniej stabilnym (- - -) potencjale (odpowiednio przykład ISE-2 i ISE-3); wzory pozwalające na wyznaczenie oporności całkowitej (R) i dryftu potencjału ($\Delta E/\Delta t$), gdzie: E – skok potencjału w wyniku zmiany kierunku prądu (i), C_L - pojemność SC.

Ograniczona pojemność redox elektrody zależy od ilości materiału o aktywności redox. Miniaturyzacja elektrod, zarówno z ciekłym, jak i stałym kontaktem, może wpłynąć na zmniejszenie pojemności i zwiększenie oporności membrany, co może spowodować pogorszenie stabilności potencjału. Trzeba to mieć również na uwadze podczas konstruowania nowych czujników [6].

CZĘŚĆ DOŚWIADCZALNA

CEL PRACY I ZAKRES BADAŃ

Czujniki potencjometryczne dzięki swoim licznym zaletom są wciąż szeroko stosowane oraz opisywane w wielu publikacjach naukowych przedstawiających badania przeprowadzane w celu uzyskania elektrod o lepszych parametrach analitycznych. Ze względu na powszechny trend do miniaturyzacji urządzeń i chęć ich stosowania w sposób bezpośredni w środowisku naturalnym konieczne jest uzyskanie czujników charakteryzujących się wystarczająco dobrymi wartościami parametrów analitycznych, a jednocześnie łatwych w obsłudze i odpornych mechanicznie. Jedynie za pomocą elektrod wykazujących określony zestaw cech można osiągnąć wiarygodne i rzetelne rezultaty pomiarów.

Głównym celem badań przeprowadzonych podczas realizacji doktoratu było opracowanie nowych elektrod jonoselektywnych ze stałym kontaktem o dobrych parametrach analitycznych czułych na wybrane jony (NO_3^-, Cl^-, K^+, Cu^{2+}, UO_2^{2+}), z wykorzystaniem nowych materiałów do ich konstrukcji.

Motywacją do wykonania badań było występowanie i zastosowanie wymienionych powyżej jonów oraz ich wpływ na organizmy żywe. Azotany(V) występują bardzo powszechnie w środowisku naturalnym, zarówno nieożywionym jak i ożywionym. Stosuje się je m.in. do produkcji materiałów wybuchowych, środków konserwujących żywność oraz nawozów stosowanych w rolnictwie. Zwiększenie stężenia azotanów(V) w wodzie na skutek działalności człowieka może mieć negatywny wpływ na życie zwierząt w zbiornikach wodnych, które w wyniku przerostu glonów mogą ulec postępującej eutrofizacji. Ponadto zbyt wysokie zawartości azotanów(V) w żywności również nie są pożądane i powinny być na bieżąco monitorowane. Jony potasowe natomiast są ważne z punktu widzenia medycyny dla prawidłowego funkcjonowania organizmów żywych. Zarówno spadek, jak i gwałtowny wzrost stężenia jonów potasowych jest niebezpieczny dla zdrowia i życia człowieka, dlatego czujniki potasowe są wykorzystywane głównie w analizie klinicznej. Stężenie jonów chlorkowych jest ważne również z punktu widzenia zdrowia człowieka i mierzone powszechnie w płynach ustrojowych. Oprócz tego badanie ich zawartości ma również zastosowanie w przemyśle spożywczym i kontroli procesów przemysłowych. W przypadku jonów miedzi(II) oraz uranylowych oznaczanie ich zawartości jest głównie istotne ze względu

na ich toksyczność w przypadku zbyt dużej ich zawartości. Pomimo, że miedź jest mikroelementem niezbędnym do funkcjonowania organizmów żywych, to przy przekroczonej dziennej dawce spożycia (wynoszącej około 2 mg) może wykazywać działanie szkodliwe. Jony uranylowe stanowiące najbardziej stabilną formę uranu w roztworach wodnych są oznaczane ze względu na wysoką toksyczność tego pierwiastka. Zanieczyszczenie środowiska powodowane jest w tym przypadku poprzez wydobycie węgla oraz rud uranu i wykorzystanie go jako paliwa atomowego.

Aby było możliwe selektywne oznaczanie wybranych jonów w złożonych próbkach zawierających inne substancje towarzyszące, konieczne jest zastosowanie elektrody jonoselektywnej otrzymanej z wykorzystaniem odpowiednich substancji aktywnych. Bez uzyskania odpowiedniego nachylenia krzywej kalibracyjnej oraz selektywności elektroda nie będzie działać prawidłowo. Bardzo ważną rolę w działaniu ISEs spełniają także materiały stosowane w roli stałego kontaktu, które mają poprawić stabilność potencjału i żywotność elektrod oraz rozszerzyć zakres zastosowań i ułatwić ich użytkowanie w różnych warunkach. Z tego względu w niniejszej pracy skupiono się zarówno na otrzymaniu nowych substancji aktywnych, jak i materiałów stałego kontaktu.

Cel główny pracy realizowano za pomocą poszczególnych celów cząstkowych:

- synteza nowej substancji aktywnej - kompleksu kobaltu(II) z 4,7-difenylo-1,10-fenantroliną i zastosowanie jej jako jonoforu w membranach elektrod do oznaczania jonów azotanowych(V) (D1);

- zastosowanie nanokompozytu wielościennych nanorurek węglowych z cieczą jonową (MWCNTs:THTDPCl) jako SC do konstrukcji elektrod azotanowych z zastosowaniem kompleksu kobaltu(II) z 4,7-difenylo-1,10-fenantroliną jako jonoforu (D2) oraz wykorzystanie otrzymanych elektrod do oznaczeń zawartości jonów azotanowych(V) w próbkach wód i warzyw (D3);

- zastosowanie nanowłókien polianilinowych domieszkowanych jonami chlorkowymi i azotanowymi(V) (PANINFs-Cl i PANINFs-NO$_3$) w ISEs wykorzystywanych do oznaczania jonów azotanowych(V) (D4);

- zastosowanie nanokompozytu nanowłókien polianilinowych domieszkowanych jonami chlorkowymi z wielościennymi nanorurkami węglowymi (PANINFs-Cl:MWCNTs) jako SC do konstrukcji elektrod czułych na jony chlorkowe (D5);

- synteza nowych substancji aktywnych - zasad Schiffa i ich kompleksów oraz wykorzystanie ich w ISEs czułych na jony miedzi(II) (D6);

- wprowadzenie nanokompozytu nanorurek węglowych z cieczą jonową (MWCNTs:BMImPF$_6$) (D7) jako SC do konstrukcji elektrod czułych na jony miedzi(II);

- zastosowanie nanocząstek tlenków metali (ZnO, CuO, Fe$_2$O$_3$) (D8) oraz metali (Ag) (D9) otrzymanych metodą ablacji laserowej w wodzie w ISEs do oznaczania jonów potasowych;

- zastosowanie cieczy jonowej (chlorku 1-oktylo-3-metyloimidazolu) w obecności substancji aktywnej Cyanex-272 (kwas bis(2,4,4-trimetylopentylo)fosfoniowy) (D10) w ISEs do oznaczania jonów uranylowych.

Wykonano i przebadano szereg czujników, których konstrukcja różniła się m.in. materiałem elektrody wewnętrznej, składem membrany jonoselektywnej (jakościowym i ilościowym) oraz rodzajem i sposobem wykorzystania materiału pełniącego funkcję stałego kontaktu (jako warstwa pośrednia lub dodatkowy składnik membrany). Zsyntezowano szereg nowych materiałów, zbadano ich właściwości za pomocą wielu różnorodnych metod analitycznych, a następnie wykorzystano do konstrukcji elektrod jonoselektywnych. Dla uzyskanych czujników wyznaczono wartości najważniejszych parametrów analitycznych i na ich podstawie określono wpływ poszczególnych modyfikacji elektrod na ich pracę. Za pomocą części z otrzymanych elektrod wykonano również analizę zawartości wybranych jonów w próbkach naturalnych sprawdzając, czy mogą one zostać wykorzystane w praktycznych oznaczeniach.

METODY BADAWCZE

Właściwości otrzymanych substancji aktywnych, nanowłókien, nanocząstek oraz nanokompozytów badano m.in. za pomocą analizy termicznej TG-DSC, TG-FTIR (D1), metod spektrofotometrycznych UV-VIS (D4, D8), spektroskopowych ATR-FTIR / XPS (D1, D4, D8) oraz skaningowej mikroskopii elektronowej SEM (D4, D5, D8). Dodatkowe badania wykorzystywano głównie w celu identyfikacji produktu otrzymanego w wyniku zajścia konkretnej reakcji chemicznej i/lub procesu fizycznego oraz lepszego poznania struktur, rozmiarów i budowy wybranych materiałów.

Natomiast parametry analityczne i elektryczne elektrod jonoselektywnych wyznaczono za pomocą potencjometrii (D1–D2, D4–D10) oraz elektrochemicznej spektroskopii impedancyjnej (D1, D2, D4, D5, D7, D8) i chronopotencjometrii (D2, D5).

Podstawowymi parametrami analitycznymi, które wyznaczano dla wszystkich otrzymanych elektrod były: nachylenie prostoliniowego odcinka krzywej kalibracyjnej elektrody, zakres liniowości i granica wykrywalności oznaczanego jonu głównego. Wykonywano również pomiary stabilności potencjału elektrod w czasie (krótkoterminowa – obejmująca kilka godzin i długoterminowa – obejmująca tygodnie lub miesiące), jego odwracalności i odtwarzalności. Czujniki poddawano również testom odporności na zmianę potencjału redox próbki (D2, D4, D5, D7), zmianę oświetlenia (D4, D5, D8) oraz obecność gazów w roztworze próbki (D4, D5, D7, D8). Sprawdzano również tendencję do powstawania warstwy wodnej pomiędzy materiałem elektrody a membraną jonoselektywną i/lub warstwą stałego kontaktu (D2, D7, D8) oraz wyznaczono zakresy pH, w których potencjał elektrody jest stały (D1–D2, D4–D7). Dla wszystkich rodzajów elektrod wykonano również badania selektywności (metodą SSM) (D1–D2, D4–D10).

Pomiary SEM wykonywano dla ogniwa składającego się z elektrody referencyjnej chlorosrebrowej Ag/AgCl z podwójnym kluczem (Metrohm 6.0750.100) oraz elektrod badanych, zanurzonego w roztworze próbki mieszanej za pomocą mieszadła magnetycznego w temperaturze pokojowej. Pomiary impedancyjne oraz chronopotencjometryczne wykonywano w roztworze jonu głównego o stężeniu 10^{-2} mol L^{-1} lub 10^{-1} mol L^{-1} w układzie trójelektrodowym: badana elektroda pracująca, elektroda referencyjna chlorosrebrowa (Metrohm 6.0733.100) oraz elektroda pomocnicza – pręt z węgla szklistego GC 2 mm/65 mm (Metrohm). Do pomiarów pH roztworów wykorzystywano elektrody szklane: ORION 81-72 BN oraz ORION 8104BN ROSS. Określone pH uzyskiwano z wykorzystaniem stężonych

roztworów kwasów i zasad zawierających jony inne, niż jony główne, na które elektrody były czułe (w zależności od rodzaju jonu głównego HCl, H_2SO_4, HNO_3, NaOH).

Aparatura pomiarowa obejmowała:

- 16-kanałowy analizator elektrochemiczny (Lawson Labs. Inc., USA) sprzężony z komputerem;

- analizator elektrochemiczny (AUTOLAB, Eco Chemie, Holandia) z oprogramowaniem NOVA 2.1;

- wielofunkcyjny miernik ELMETRON CX-741 (Zabrze Mikulczyce Polska).

Odczynniki chemiczne stosowane w badaniach pozyskiwano od producentów: Fluka, Sigma Aldrich, Merck.

DYSKUSJA WYNIKÓW

W Tabeli 1. przedstawiono zestawienie zawierające rodzaje elektrod, których opisy oraz przeprowadzone badania zawarto w poszczególnych artykułach. W trzech przypadkach były to elektrody z membraną otrzymaną metodą żelowania w oparciu o elektrodę chlorosrebrową (D1, D6, D10) - w dalszej części pracy nazywane „elektrodami żelowanymi" lub z „membraną żelowaną". Konstrukcję tą wybrano do badań dotyczących zastosowania nowych substancji aktywnych ze względu na wygodę ich przygotowania i stosowania oraz trwałość. W pozostałych artykułach natomiast (D2, D3, D4, D5, D7, D8, D9) wykorzystano konstrukcję opierającą się na elektrodach wewnętrznych z węgla szklistego, na powierzchnię których nadkładano warstwę membrany jonoselektywnej lub warstwy pośrednie stałego kontaktu.

Tabela 1. Rodzaje badanych elektrod ze stałym kontaktem.

Jon główny	Rodzaj SC	Jonofor	Praca
NO_3^-	Ag/AgCl/Cl$^-$	Co(Bphen)$_2$(NO$_3$)$_2$	D1
NO_3^-	MWCNTs:THTDPCl nanokompozyt (2% membrany)	Co(Bphen)$_2$(NO$_3$)$_2$	D2, D3
NO_3^-	PANINFs-Cl (0,5-2% membrany) PANINFs-Cl (warstwa) PANINFs-NO$_3$ (0,5-2% membrany) PANINFs-NO$_3$ (warstwa)	TDMANO$_3$	D4
Cl^-	PANINFs-Cl:MWCNTs nanokompozyt (warstwa)	jonofor III chlorkowy	D5
Cu^{2+}	Ag/AgCl/Cl$^-$	L^{1}Cu$_2$	D6
Cu^{2+}	MWCNTs:BMImPF$_6$ nanokompozyt (2-8% membrany)	jonofor IV miedzi(II)	D7
K^+	ZnONPs (warstwa) CuONPs (warstwa) Fe$_2$O$_3$NPs (warstwa)	walinomycyna	D8
K^+	AgNPs (warstwa)	walinomycyna	D9
UO_2^{2+}	Ag/AgCl/Cl$^-$	Cyanex-272	D10

Konstrukcja elektrody żelowanej składała się z wewnętrznej elektrody chlorosrebrowej Ag/AgCl (otrzymanej w wyniku procesu elektrolizy anodowej w roztworze kwasu chlorowodorowego z wykorzystaniem drucika srebrnego jako anody) umieszczonej w

teflonowym korpusie i pokrytej odpowietrzoną wcześniej mieszaniną membranową. Żelową konsystencję membrany uzyskiwano w wyniku ogrzewania tak przygotowanych korpusów w suszarce w temperaturze około $100^{o}C$ w czasie kilku minut. Przed rozpoczęciem pomiaru tego typu elektrody kondycjonowano w odpowiednim roztworze jonu głównego (stężenie 10^{-3} mol L^{-1}) przez godzinę. Natomiast, w drugim rodzaju konstrukcji wykonanie czujnika polegało na nakropleniu określonej objętości koktajlu membranowego (mieszanina membranowa rozpuszczona lub zdyspergowana w THF) na odpowiednio przygotowaną powierzchnię elektrody stałej (tutaj GCE). Oczyszczenie elektrody wewnętrznej polegało na usunięciu pozostałości poprzedniej membrany lub stałego kontaktu, następnie wypolerowaniu powierzchni za pomocą papieru ściernego oraz zwilżonego wodą destylowaną Al_2O_3 (Ø 0,3 µm), a następnie usunięciu cząstek stałych z użyciem łaźni ultradźwiękowej, dokładnym opłukaniu wodą destylowaną i odtłuszczeniu poprzez zanurzenie w THF. W przypadku dodatkowej modyfikacji obejmującej zastosowanie warstwy stałego kontaktu, na powierzchnię elektrody wprowadzano stały kontakt, a dopiero w kolejnym etapie nakraplano membranę. Warstwa membranowa czujnika była nakładana 3-krotnie, za każdym razem w odstępie czasowym umożliwiającym odparowanie rozpuszczalnika (około 30 minut). Jako roztwory kondycjonujące stosowano roztwory jonu głównego o stężeniu 10^{-3} mol L^{-1}. Na Rys. 9 przedstawiono porównanie konstrukcji elektrod, które wykorzystywano w badaniach.
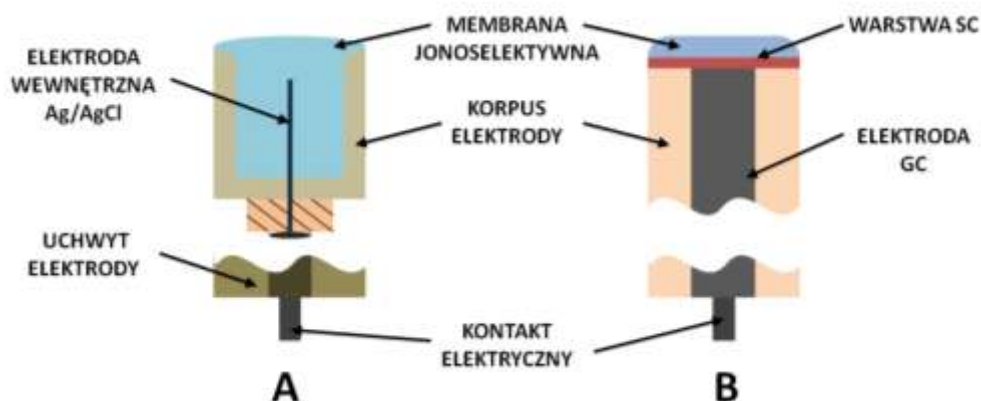
Rys. 9 Porównanie konstrukcji elektrod jonoselektywnych ze stałym kontaktem: (A) żelowanej z elektrodą wewnętrzną chlorosrebrową, (B) dyskowej z elektrodą wewnętrzną z węgla szklistego.

W przypadku wprowadzania do membrany jonoselektywnej nowej substancji aktywnej przeprowadzono jakościową i ilościową optymalizację składu mieszaniny membranowej (D1, D6, D10). Proces optymalizacji składu ISM był przeprowadzany również dla elektrod, w których materiał pełniący funkcję stałego kontaktu dodawano bezpośrednio do

membrany (D2, D4, D7). W pozostałych przypadkach natomiast, gdy głównym celem badań było określenie wpływu obecności i rodzaju stałego kontaktu jako warstwy pośredniej, skład ISM był stały, natomiast sporządzane elektrody różniły się materiałem SC i w niektórych przypadkach jego grubością (D8, D9).

W pracach D2 i D4 badano elektrody różniące się umiejscowieniem stałego kontaktu oraz związanym z tym sposobem przygotowania czujników. Wykorzystywano dwie możliwości konstrukcyjne (Rys. 10). W pierwszej z nich materiał SC tworzył warstwę pośrednią między powierzchnią GCE i ISM. Natomiast w drugiej – materiał ten dodawany był bezpośrednio do mieszanki membranowej, która następnie była nakładana bezpośrednio na powierzchnię elektrody wewnętrznej. Dodatkowo we wszystkich badaniach jako punkt odniesienia wykorzystywano elektrody niemodyfikowane – o prostej konstrukcji, z membraną o podstawowym składzie, umieszczoną bezpośrednio na podłożu elektrody wewnętrznej z GC (D2, D4, D5, D7, D8, D9).
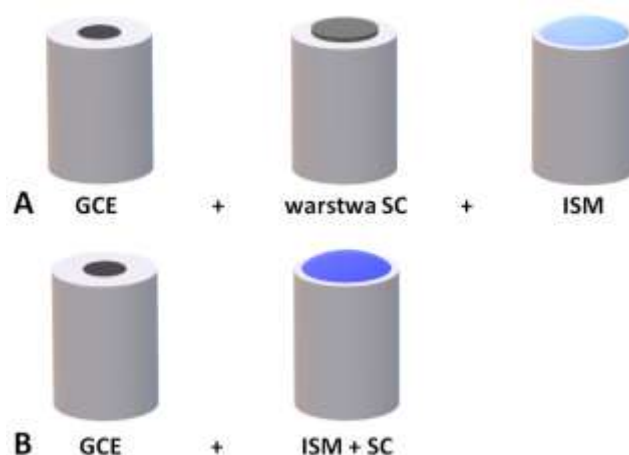
Rys. 10 Schemat wykonania SCISEs: (A) 2-etapowy obejmujący nałożenie warstwy SC, a następnie pokrycie jej warstwą ISM; (B) 1-etapowy – bezpośrednie nałożenie ISM wzbogaconej dodatkiem SC.

Dla wszystkich rodzajów czujników wykonywano systematyczne pomiary potencjału dla uzyskania krzywych kalibracyjnych, a tym samym wyznaczenia nachylenia ich prostoliniowego odcinka, granicy wykrywalności, zakresu liniowości oraz stabilności długoterminowej. W kolejnych etapach skupiano się na odwracalności potencjału i jego stabilności w czasie. Za pomocą metody roztworów rozdzielonych (SSM) wyznaczano również współczynniki selektywności membrany jonoselektywnej, szczególnie istotne w przypadku zastosowania nowych substancji aktywnych wpływających bezpośrednio na selektywność czujnika.

Badano również typowo praktyczne właściwości elektrod poprzez testy sprawdzające ich odporność na zmiany warunków pomiarowych. Potencjał elektrod w czasie był monitorowany w przypadku m.in. zmiany potencjału redox roztworów próbki (D2, D4, D5, D7), zmiany oświetlenia (D4, D5, D8) oraz obecności gazów w roztworze próbki (D4, D5, D7, D8). Określano ponadto zakres pH, w którym potencjał czujników jest stały (D1–D2, D4-D6, D10) oraz wykonywano testy na obecność warstwy wodnej (D2, D7, D8). Wyznaczono również parametry elektryczne ISEs wykorzystując metody: EIS (D1, D2, D4, D5, D7, D8) oraz CP (D2, D5).

NO_3^--ISEs

W badaniach dotyczących elektrod jonoselektywnych czułych na jony azotanowe(V) po raz pierwszy jako składnik aktywny membrany zastosowano nowozsyntezowany kompleks kobaltu(II) z 4,7-difenylo-1,10-fenantroliną o wzorze sumarycznym $Co(Bphen)_2(NO_3)_2(H_2O)_2)$ (D1). Wykonano badania spektroskopowe (ATR-FTIR) i termograwimetryczne metodami TG-DSC, TG-FTIR mające na celu określenie składu i struktury kompleksu oraz poznanie jego właściwości termicznych. W związku z tym, że obecnie komercyjnie dostępnych jest niewiele jonoforów azotanowych, podjęto działania mające na celu uzyskanie nowej substancji aktywnej, którą można wykorzystać do konstrukcji ISEs-NO_3. Obecnie jedynie jonofor VI oraz wymieniacze jonowe: $TOANO_3$ (azotan tetraoktyloamoniowy) i $TDMANO_3$ (azotan tridodecylometyloamoniowy) są dostępne w sprzedaży jako składniki aktywne membran czułych na jony NO_3^-. Jonofory II, III i V zostały wycofane z obiegu (Sigma Aldrich). Dla rekomendowanego przez producenta składu membrany jonoselektywnej zawierającej 5,2% wag. jonoforu VI, 0,6% wag. TOACl (chlorek tetraoktyloamoniowy), 47,1% DBP (ftalan dibutylu) i 47,1% PVC (poli(chlorek winylu)) o wysokiej masie cząsteczkowej zgodnie z dostępnym raportem można osiągnąć granicę wykrywalności niższą od $3{,}2 \times 10^{-6}$ mol L^{-1}. Jednocześnie zadeklarowano współczynniki selektywności wynoszące $-1{,}1$; $-1{,}2$; $-2{,}5$; $-3{,}2$; $-4{,}4$ i $-4{,}5$ odpowiednio dla jonów: Br^-, NO_2^-, Cl^-, HCO_3^-, HPO_4^{2-} i SO_4^{2-} [150]. W kolejnej propozycji mieszanki membranowej zawierającej 6,0% $TDMANO_3$, 65% NPOE i 29% PVC w informacji dotyczącej produktu umieszczono możliwą do osiągnięcia granicę wykrywalności wynoszącą $2{,}0 \times 10^{-5}$ mol L^{-1} oraz współczynniki selektywności 3,0; 1,7; 1,3; $-0{,}7$; $-2{,}1$; $-3{,}1$; $-3{,}2$; $-3{,}2$ i $-3{,}4$ odpowiednio dla jonów: ClO_4^-, SCN^-, I^-, Br^-, Cl^-, HCO_3^-, SO_4^{2-}, CH_3COO^- i HPO_4^{2-} [151]. W związku z tym zaproponowany w artykule D1 kompleks Bphen stanowi obiecujące rozwiązanie, gdyż

zaledwie 1% dodatek do membrany składającej się ponadto z 1% THTDPCl, 33% PVC i 65% NPOE pozwolił na uzyskanie korzystniejszych wartości współczynników selektywności: 3.3; 2.1; –1.0; –2.1; –2.6; –4.4; –4.6; –4.8; –4.9 i –5.1; dla ClO_4^-, SCN^-, Br^-, NO_2^-, Cl^-, CH_3COO^-, F^-, SO_4^{2-}, CO_3^{2-}, $H_2PO_4^-$. Do badań wstępnych mających na celu optymalizację składu mieszanki membranowej wybrano konstrukcję elektrod żelowanych z teflonowymi korpusami, które opisano wcześniej (Rys. 8). Wykonane elektrody różniły się zawartością kompleksu w mieszance membranowej (0, 1 i 2% wag.) oraz rodzajem dodatku jonowego (TOACl lub THTDPCl). Na podstawie pomiarów potencjometrycznych ustalono, że dla najlepszego składu (podanego powyżej) uzyskano nachylenie równe –56,3 mV pa^{-1} i zakres liniowości krzywej kalibracyjnej $1 \times 10^{-5} – 1 \times 10^{-1}$ mol L^{-1}. Elektrody te charakteryzowały się bardzo dobrą odwracalnością i stabilnością potencjału oraz zakresem pH 5,4 – 10,6. Ponadto wykazały się one bardzo dobrą trwałością (działały poprawnie po ponad 5 miesiącach użytkowania).

Opracowany w pracy D1 jonofor zastosowano w kolejnych badaniach, w których do konstrukcji elektrod tym razem zastosowano GCE jako elektrodę wewnętrzną. Badania polegały na modyfikacji membrany poprzez wprowadzenie dodatkowego składnika pełniącego funkcję stałego kontaktu – nanokompozytu MWCNTs:THTDPCl. Jak wiadomo, zarówno MWCNTs, jak i ciecze jonowe wykazują właściwości hydrofobowe i przewodzące, a otrzymany z nich nanokompozyt może wykazywać jeszcze lepsze właściwości niż jego składniki. Poza tym obecność cieczy jonowej zapewnia osiągnięcie stabilizacji elektrostatycznej i sterycznej oraz umożliwia powstanie jednorodnego materiału nanokompozytowego łatwiej dyspergującego się w materiale membrany. W badaniach stosowano nanokompozyty otrzymane z wykorzystaniem czterech rodzajów nanorurek węglowych różniących się rozmiarami (długością oraz średnicą). Jako układ porównawczy badano elektrody niemodyfikowane (membrana jonoselektywna bez dodatku nanokompozytu) oraz ze stałym kontaktem w postaci warstwy pośredniej MWCNTs. Na podstawie uzyskanych wyników stwierdzono, że rodzaj nanorurek wchodzących w skład nanokompozytu miał istotny wpływ na parametry uzyskanych elektrod. Szczególnie zauważalne było to w przypadku III-MWCNTs o największych rozmiarach, które najgorzej sprawdziły się w roli stałego kontaktu. Najlepsze wyniki uzyskano dla nanokompozytu z II-MWCNTs, które były najkrótsze i najbardziej jednorodne spośród wszystkich pozostałych. Efektem tego było otrzymanie najbardziej homogenicznej membrany. W pomiarach CP dla elektrody z nanokompozytem II-MWCNTs/IL otrzymano najniższą wartość oporności

elektrody (ponad 20-krotnie niższą niż dla elektrody z nanokompozytem III-MWCNTs/IL) oraz najwyższą pojemność (ponad 250-krotnie wyższą niż dla elektrody z III-MWCNTs/IL). Podobne zależności zaobserwowano na podstawie wyników otrzymanych metodą EIS, a występujące różnice można było zaobserwować już na etapie analizy widm impedancyjnych. W porównaniu do czujników niemodyfikowanych, elektrody zawierające nanokompozyt w membranie charakteryzowały się zakresem liniowości szerszym o rząd wielkości (1×10^{-6} – 1×10^{-1} mol L^{-1}) i niższą granicą wykrywalności – 5×10^{-7} mol L^{-1} oraz wyższym nachyleniem krzywej kalibracyjnej: –57,1 mV pa^{-1} (dla II-MWCNTs). W przypadku selektywności jedynie dla jonów bromkowych otrzymano logK wyższy od –2. Przeprowadzony test warstwy wodnej wykazał, że przy zmianie roztworów jonów dryft potencjału elektrod modyfikowanych był mniejszy niż w przypadku elektrody niemodyfikowanej. Wykazano również, że zastosowanie nanorurek w postaci nanokompozytu jako składnika ISM jest efektywniejsze niż wykorzystanie ich jako warstwy pośredniej pomiędzy membraną i GCE. Dodatkowym atutem zastosowania nanokompozytu był prostszy jednoetapowy sposób przygotowania elektrod.

W ostatniej pracy dotyczącej elektrod azotanowych(V) jako stały kontakt zaproponowano PANINFs-Cl i PANINFs-NO$_3$ (D4). Nanowłókna umieszczono zarówno jako dodatkową warstwę między materiałem elektrody wewnętrznej a membraną jonoselektywną, jak również jako składnik membrany o różnej zawartości (0,5; 1,0 i 2,0%). Zsyntezowany materiał zbadano za pomocą spektrofotometrii UV-VIS i FTIR oraz SEM. Reakcja polimeryzacji międzyfazowej prowadzona w obecności jonów NO$_3^-$ pozwoliła na syntezę dłuższych i lepiej uformowanych nanowłókien, natomiast nanowłókna otrzymane w obecności jonów Cl- były znacznie mniejsze i bardziej jednorodne, co wpłynęło na ich wyższą skuteczność w poprawie parametrów elektrod (niższe granice wykrywalności, lepsza stabilność i odwracalność potencjału). Nachylenia krzywych kalibracyjnych oszacowane dla wszystkich elektrod modyfikowanych mieściły się w zakresie 56 – 58 mV pa^{-1}. W przypadku tych czujników szczegółowo zbadano ich wrażliwość na zmianę czynników zewnętrznych (światło, gazy, potencjał redox) udowadniając, że mogą one pracować bez istotnych zmian potencjału w zmiennych warunkach. Stanowi to ważny aspekt w pomiarach próbek środowiskowych oraz w przypadku wykonywania pomiarów w środowisku in situ. Ponadto oszacowany zakres pH pracy elektrod był bardzo szeroki (dla elektrod z PANINFs-Cl nawet 4,0 – 12,5). Dodatkowo pomiary wykonane metodą EIS pozwoliły stwierdzić, że wraz ze wzrostem zawartości nanowłókien w membranie – oporność membrany spada, natomiast

pojemność rośnie. Dla elektrod z oddzielną warstwą stałego kontaktu wzrost pojemności jest największy w porównaniu do elektrod niemodyfikowanych oraz wciąż kilkukrotnie wyższy w porównaniu do pozostałych elektrod modyfikowanych. W celu potwierdzenia możliwości oznaczania jonów azotanowych w roztworach naturalnych, zawierających bardziej złożoną matrycę i inne jony poza jonem głównym, wykonano oznaczenie jonów azotanowych(V) w wodzie pitnej, rzecznej i gruntowej, a otrzymane wyniki porównano z wynikami otrzymanymi metodą spektrofotometryczną.

W literaturze dostępnych jest wiele artykułów naukowych opisujących różnego typu elektrody do oznaczania jonów azotanowych(V). W Tabeli 2. zestawiono podstawowe parametry elektrod azotanowych i porównano je z innymi SCISEs opisanymi w literaturze oraz dostępnymi na rynku. Można zauważyć, że w przypadku czujników komercyjnych (nie tylko czułych na jony azotanowe(V) – również Tabele 3, 4, 5, 6) dostępnych jest niewiele informacji dotyczących parametrów analitycznych. Najczęściej są one ograniczone jedynie do podania zakresów niezbędnych z punktu widzenia samego poprawnego wykonania oznaczeń: liniowości czujników oraz zakresu pH. Rzadko podawane są informacje dotyczące nachylenia charakterystyki elektrody czy selektywności, a granice wykrywalności oraz stabilność potencjału nie są podawane praktycznie w ogóle. Natomiast w przypadku opisów badań zamieszczonych w artykułach naukowych charakterystyka elektrod jest znacznie bardziej wyczerpująca, co znacznie ułatwia porównanie różnego rodzaju sensorów.

W zakresie badań wykonanych w ramach rozprawy doktorskiej otrzymano elektrody azotanowe o niskich granicach wykrywalności, pracujące w szerokim zakresie pH próbki (wystarczającym dla nieinwazyjnych pomiarów próbek wód naturalnych). Wprowadzony nowy jonofor wykazywał bardzo dobrą selektywność względem jonów interferujących, a dodatkowe modyfikacje przyspieszyły i ułatwiły przygotowanie czujników oraz poprawiły ich parametry analityczne. W przypadku elektrod z elektrodą wewnętrzną z GC [D2] dodatek do membrany nanokompozytu II-MWCNTs:THTDPCl znacznie poprawił stabilność względem niemodyfikowanych czujników (z 0,625 $\mu V\ s^{-1}$ na 0,042 $\mu V\ s^{-1}$) oraz spowodował wzrost nachylenia krzywej kalibracyjnej (o 5 mV pa^{-1}) i rozszerzenie zakresu liniowego o rząd wielkości. Natomiast dodatek PANINFs spowodował znaczną poprawę stabilności potencjału (nawet prawie 10-krotna w porównaniu elektrody niemodyfikowanej i elektrody z warstwą PANINFs-Cl) w wyniku wzrostu pojemności elektrod (z 0,85 μF do 11 μF). Modyfikacja elektrod w sposób znaczący wpłynęła również na obniżenie granic wykrywalności.

Tabela 2. Zestawienie parametrów analitycznych dla opracowanych elektrod jonoselektywnych i elektrod opisanych w literaturze oraz dostępnych komercyjnie, czułych na jony azotanowe(V).

Jonofor	Rodzaj kontaktu	Nachylenie, mV pa^{-1}	LOD, mol L^{-1}	Zakres liniowości, mol L^{-1}	Zakres pH	Stabilność potencjału	Jony interferujące, K$^{pot} \geq 1\times10^{-2}$	Praca
Co(Bphen)$_2$(NO$_3$)$_2$	Ag/AgCl/Cl$^-$	-56,3	$4,0\times10^{-6}$	$1,0\times10^{-5} – 1,0\times10^{-1}$	5,4 – 10,6	np	ClO$_4^-$, SCN$^-$, Br$^-$	D1
Co(Bphen)$_2$(NO$_3$)$_2$	MWCNTs:THTDPCl	-57,1	$5,0\times10^{-7}$	$1,0\times10^{-6} – 1,0\times10^{-1}$	4,2 – 10,8	0,106 mV s^{-1} (i=±100 nA) 0,042 µV s^{-1} (i=0)	Br$^-$	D2 D3
TDMANO$_3$	PANINFs-Cl (1% membrany)	-56,7	$3,4\times10^{-7}$	$1,0\times10^{-6} – 1,0\times10^{-1}$	4,0 – 12,5	1,02 mV h^{-1} (i=0)	Br$^-$	D4
	PANINFs-Cl (warstwa)	-56,8	$3,2\times10^{-7}$	$1,0\times10^{-6} – 1,0\times10^{-1}$	4,0 – 12,5	0,53 mV h^{-1} (i=0)	NO$_2^-$, Cl$^-$, Br$^-$	
	PANINFs-NO$_3$ (1% membrany)	-57,2	$1,4\times10^{-6}$	$5,0\times10^{-6} – 1,0\times10^{-1}$	4,0 – 11,5	1,12 mV h^{-1} (i=0)	–	
	PANINFs-NO$_3$ (warstwa)	-57,8	$1,1\times10^{-6}$	$5,0\times10^{-5} – 1,0\times10^{-1}$	4,0 – 11,5	0,84 mV h^{-1} (i=0)	–	
TDMANO$_3$	laserowo indukowany grafen	-54,8	$2,1\times10^{-5}$	$5,0\times10^{-5} – 1,0\times10^{-1}$	–	-5,3 µV h^{-1} (i=0)	np	[152]
TDMANO$_3$	MWCNTs	-57,7	$2,5\times10^{-6}$	$3,2\times10^{-6} – 1,0\times10^{-1}$	–	40 µV h^{-1} (i=0)	NO$_2^-$, ClO$_4^-$, SCN$^-$, Cl$^-$	[153]
TDMANO$_3$	grafit	-57,9	$3,0\times10^{-5}$	$5,0\times10^{-5} – 1,0\times10^{-1}$	–	np	Cl$^-$	[154]
TDMANO$_3$	PtNPs-CB	-58,6	$5,0\times10^{-7}$	$1,0\times10^{-6} – 1,0\times10^{-1}$	3,0 – 9,0	6,3 µV h^{-1} (i=0)	NO$_2^-$, ClO$_4^-$, salicylany	[155]
TDMANO$_3$	POT:MoS$_2$	-64,0	$9,2\times10^{-5}$	$7,1\times10^{-4} – 1,0\times10^{-1}$	–	np	PO$_4^{3-}$, SO$_4^{2-}$, HCO$_3^-$, NO$_2^-$, Cl$^-$	[156]
Ppy(NO$_3^-$)	AuNPs	-50,4	$5,3\times10^{-5}$	$5,3\times10^{-5} – 1,0\times10^{-1}$	–	np	Cl$^-$, Br$^-$	[108]
Ppy(NO$_3^-$)	sproszkowany grafit	-57,1	$5,4\times10^{-5}$	$1,5\times10^{-4} – 1,0\times10^{-1}$	4,3 – 7,4	np	ClO$_4^-$, SCN$^-$, Br$^-$, I$^-$, CN$^-$	[157]
THTDPCl	Ag/AgCl/Cl$^-$	-60,1	$2,8\times10^{-6}$	$1,0\times10^{-5} – 1,0\times10^{-1}$	3,0 – 10,0	5,9 µV h^{-1} (i=0)	NO$_2^-$, ClO$_4^-$, SCN$^-$, Br$^-$	[158]
jonofor V azotanu(V)	TTF-TCNQ	-58,5	$3,2\times10^{-6}$	$1,0\times10^{-5} – 1,0\times10^{-1}$	–	16,7 µV s^{-1} (i=±10 nA)	NO$_2^-$	[159]
DX262 NO$_3$ (Mettler Toledo)		–	–	$3,0\times10^{-5} – 1,0\times10^{0}$	2,0 – 12,0	np	np	[160]
ISE-NO$_3$ (Pasco)		–	–	$1,6\times10^{-5} – 1,0\times10^{0}$	2,5 – 11,0	np	np	[161]
ISE-NO$_3$ Hanna HI 4013 (Hanna Instruments)		-56,0	–	$1,0\times10^{-5} – 1,0\times10^{0}$	3,0 – 8,0	np	np	[162]
ISE-NO$_3$ Go Direct® GDX-NO$_3$ (Vernier)		-55,0	–	$1,6\times10^{-5} – 2\times10^{-1}$	2,0 – 11,0	np	np	[163]
ISE-NO$_3$ Mini 4,6 (Ntsensors)		-54,5	–	$1,0\times10^{-5} – 5\times10^{-1}$	2,0 – 11,0	np	OH$^-$, NO$_2^-$, Br$^-$	[164]

Co(Bphen)$_2$(NO$_3$)$_2$ – kompleks kobaltu(II) z 4,7-difenylo-1,10-fenantroliną; Ag/AgCl/Cl$^-$ – elektroda chlorosrebrowa; MWCNTs:THTDPCl – nanokompozyt wielościennych nanorurek węglowych z chlorkiem triheksylotetradecylofosfoniowym; TDMANO$_3$ – azotan tridodecylometyloaminy; PANINFs-Cl – nanowłókna polianiliny domieszkowane jonami chlorkowymi; MWCNTs – wielościenne nanorurki węglowe; PtNPs-CB – sadza domieszkowana nanocząstkami platyny; POT-MoS$_2$ – nanokompozyt poli(3-oktylotiofenu) i siarczku molibdenu(IV); Ppy(NO$_3^-$) – polipyrol domieszkowany azotanem; AuNPs – nanocząstki złota; THTDPCl – chlorek triheksylotetradecylofosfoniowy; TTF-TCNQ – tetratiafulwaleno-tetracyjanochinodimetan; np – nie podano.

Cl⁻-ISEs

W pracy D5 opisano elektrody jonoselektywne czułe na jony chlorkowe, w których jako SC wykorzystano nanokompozyt otrzymany z MWCNTs oraz PANINFs-Cl. Wykonane zostały wstępne pomiary impedancyjne i chronopotencjometryczne parametrów elektrycznych elektrod modyfikowanych warstwą pośrednią składającą się z nanokompozytów o różnym stosunku masowym składników oraz warstwą zawierającą tylko MWCNTs lub PANINFs-Cl. Potwierdzono, że nanokompozyty wykazywały lepsze parametry elektryczne (niższa oporność, wyższa pojemność) niż ich składniki oddzielnie. Najlepsze spośród badanych elektrod okazały się czujniki z warstwą pośrednią nanokompozytu PANINFs-Cl:MWCNTs w stosunku wagowym 2:1. Porównując już same warstwy SC, te zawierające (2:1) PANINFs-Cl:MWCNTs wykazywały pojemność prawie 4-krotnie wyższą niż PANINFs i ponad 10-krotnie wyższą niż MWCNTs. W przypadku gotowych czujników elektrody z tą warstwą nanokompozytu charakteryzowały się natomiast prawie 4-krotnie niższą opornością membrany i ponad 200-krotnie niższym oporem przenoszenia ładunku przy jednoczesnym niemal 200-krotnym wzroście pojemności warstwy podwójnej w wyniku znacznie szybszych procesów dyfuzji i transportu ładunku na granicy membrana/GCE. Ponadto elektrody z warstwą pośrednią nanokompozytu (2:1) PANINFs-Cl:MWCNTs wykazywały nachylenie charakterystyki równe –61,3 mV pa⁻¹, zakres liniowości krzywej kalibracyjnej $5 \times 10^{-6} - 1 \times 10^{-1}$ mol L⁻¹ oraz najniższą granicę wykrywalności ($2,3 \times 10^{-6}$ mol L⁻¹) i najlepszą stabilność potencjału (0,03 mV h⁻¹) w porównaniu do pozostałych elektrod modyfikowanych oraz elektrody niemodyfikowanej. Wszystkie czujniki bez wyjątku były odporne na zmiany warunków zewnętrznych oraz zachowywały stały potencjał w zakresie pH 4 – 9. Porównanie parametrów najlepszej opracowanej elektrody z innymi opisanymi w literaturze i dostępnymi komercyjnie umieszczono w Tabeli 3. Dane w Tabeli 3. pokazują, że opracowana w pracy D5 elektroda wykazuje niższą granicę wykrywalności niż elektrody oferowane komercyjnie i większość elektrod opisanych dotychczas w literaturze. Jedynie elektrody przedstawione w pracach [165] i [166] charakteryzowały się niższą granicą wykrywalności. Nie ma natomiast danych odnośnie ich stabilności potencjału oraz trwałości w czasie.

Tabela 3. Zestawienie parametrów analitycznych dla opracowanych elektrod jonoselektywnych i elektrod opisanych w literaturze oraz dostępnych komercyjnie, czułych na jony chlorkowe.

Jonofor	Rodzaj kontaktu	Nachylenie, mV pa^{-1}	LOD, mol L^{-1}	Zakres liniowości, mol L^{-1}	Zakres pH	Stabilność potencjału	Jony interferujące, $K^{pot} \geq 1 \times 10^{-2}$	Praca
jonofor chlorkowy III	nanokompozyt PANINFs-Cl:MWCNTs	-61,3	$2,3 \times 10^{-6}$	$5,0 \times 10^{-6} - 1,0 \times 10^{-1}$	4,0 – 9,0	0,03 mV h^{-1} (i=0)	Br$^-$	D5
HIPM	ciekły	-59,8	$1,0 \times 10^{-8}$	$5,0 \times 10^{-8} - 1,0 \times 10^{-1}$	6,5 – 8,0	–	–	[165]
nanokompozyt g-C$_3$N$_4$/AgCl	pasta grafitowa	-55,4	$4,0 \times 10^{-7}$	$1,0 \times 10^{-6} - 1,0 \times 10^{-1}$	2,0 – 7,0	np	CN-, Br$^-$, I-,	[166]
TDMACl	Ag/AgCl	-58,7	–	$1,0 \times 10^{-4} - 1,0 \times 10^{-1}$	2,0 – 12,0	0,9 mV h^{-1} (i=0)	–	[167]
TDMACl	ciekły	-55,0	$1,0 \times 10^{-6}$	$1,0 \times 10^{-3} - 5,0 \times 10^{-1}$	–	–	ClO$_4^-$, HCO$_3^-$, SCN$^-$, Cl-, Br$^-$, CH$_3$COO$^-$, mleczany, cytryniany, salicylany	[168]
TDMACl	ciekły	-48,4	–	–	3,0 – 5,5	np	np	[169]
In(OEP)Cl	pył grafitowy	-87,5	–	$1,0 \times 10^{-5} - 5,0 \times 10^{-2}$	–	–	NO$_3^-$, NO$_2^-$, ClO$_4^-$, SCN$^-$, F$^-$, Cl$^-$, Br$^-$, I$^-$, CH$_3$COO$^-$, salicylany	[170]
NH$_4$Cl	ciekły	-59,0	–	$1,0 \times 10^{-5} - 1,0$	4,0 – 10,0	–	NO$_3^-$, ClO$_4^-$, ClO$_3^-$, HCO$_3^-$, SCN$^-$, F$^-$, Br$^-$, I$^-$, H$_2$PO$_4^-$, S$_2^-$, CH$_3$COO$^-$, HCOO$^-$, C$_2$O$_4^{2-}$	[171]
Elektroda chlorkowa ECl-01 polikrystaliczna (ELMETRON)		-56±3	–	$5,0 \times 10^{-5} - 1$	2,0 – 11,0	–	Br$^-$, S$_2$O$_3^{2-}$, I$^-$, S^{2-}	[172]
ISE Hanna HI 4107 (MERA)		–	–	$1,0 \times 10^{-5} - 1$	2,0 – 11,0	–	–	[173]
ISE-Cl$^-$ (VERNIER)		-56±3	–	$3,0 \times 10^{-5} - 1$	2,0 – 12,0	–	OH$^-$, CN$^-$, Br$^-$, I$^-$, S$^-$, NH$_3$	[174]
Orion™ ISE-Cl$^-$ 9417SC (THERMOFISHER)		–	–	$1,0 \times 10^{-5} - 1$	–	–	–	[175]

nanokompozyt PANINFs-Cl:MWCNTs – nanokompozyt TDMACl – chlorek tridodecylometyloamoniowy; In(OEP)Cl – ind(III) oktaetylo-porfiryna; HIPM – 2-(1-H-imidazo[4,5-f][1,10]fenantrolin-2-ylo)-6metoksyfenol; nanokompozyt g-C$_3$N$_4$/AgCl – grafitowy azotek węgla zakotwiczony w AgCl; np – nie podano.

Cu^{2+}-ISEs

W ramach badań do pracy doktorskiej zbadano również możliwości zastosowania nowych substancji aktywnych do konstrukcji elektrod jonoselektywnych dedykowanych do oznaczania jonów miedzi(II) (D6). Podobnie jak w przypadku nowego jonoforu do oznaczania jonów azotanowych(V) wykorzystano konstrukcję elektrody z membraną żelowaną i chlorosrebrową elektrodą wewnętrzną. Przebadano związki z grupy zasad Schiffa, obejmujące ligandy oraz ich kompleksy z jonami miedzi(II). W toku badań przygotowano kilkanaście składów mieszanek membranowych różniących się rodzajem jonoforu i jego zawartością w membranie, rodzajem plastyfikatora oraz soli lipofilowej. Wyznaczono parametry analityczne dla jak największej liczby kombinacji składu membrany w celu wyłonienia membrany jonoselektywnej o najlepszym składzie. Spośród badanych związków najlepszym okazał się dwurdzeniowy kompleks N,N'-bis(5-bromo-2-hydroksy-3-metoksybenzylideno)-2-hydroksy-propyleno-1,3-diaminy z miedzią (L$_1$Cu$_2$). Elektroda z membraną zawierającą 1% tego kompleksu, 0,34% KTpClPB, 65,66% NPOE i 33,00% PVC osiągnęła nachylenie 29,68 mV pa^{-1} w zakresie stężeń $1,0 \times 10^{-6} - 1,0 \times 10^{-1}$ mol L^{-1}, a otrzymana granica wykrywalności wyniosła $6,2 \times 10^{-7}$ mol L^{-1}. Wyznaczone zostały współczynniki selektywności elektrod, a te otrzymane dla wybranego najlepszego czujnika porównano z innymi dostępnymi w literaturze. W przypadku opracowanych czujników wartości współczynników selektywności w stosunku do wszystkich badanych jonów z wyjątkiem ołowiu i kadmu były mniejsze niż 0,01. Elektrody wykazywały dobrą stabilność i odwracalność potencjału oraz działały bez znaczących zmian parametrów przez okres minimum dwóch miesięcy. W tym czasie zakres liniowości badanych czujników nie uległ zmianie, zmniejszyło się nieznacznie nachylenie krzywych kalibracyjnych do wartości ~28 mV pa^{-1}.

W kolejnej publikacji dotyczącej elektrod miedziowych skupiono się na wpływie rodzaju stałego kontaktu na pracę czujników (D7). Głównym obiektem zainteresowania był w tych badaniach nanokompozyt MWCNTs:IL (IL – heksafluorofosforan 1-butylo-3-metyloimidazoliowy). Składniki wymieszano w stosunku wagowym 1:5. Rolę substancji aktywnej w membranie pełnił wycofany już ze sprzedaży jonofor IV miedzi(II). Jedynym dostępnym obecnie jonoforem na stronie producenta jest jonofor I miedzi(II), co tym bardziej motywuje do działań mających na celu syntezę nowych substancji przydatnych w konstrukcji elektrod do oznaczaniu jonów Cu(II). Otrzymano czujniki o zawartości nanokompozytu w membranie równej 0; 2; 4; 6 i 8% wag. Modyfikowane elektrody charakteryzowały się

wyższym nachyleniem i niższymi granicami wykrywalności w porównaniu do elektrody niemodyfikowanej oraz elektrody o konstrukcji klasycznej (z ciekłym kontaktem). Najlepszy w tym przypadku okazał się dodatek 6% nanokompozytu. Jego wpływ najbardziej zauważalny był na przykładzie odpowiedzi dynamicznej czujników. Czas odpowiedzi elektrody po modyfikacji był krótszy, a ponadto odwracalność i stabilność potencjału okazała się znacznie lepsza. Dryft potencjału zmalał bowiem z 0,16 do 0,046 mV min^{-1}. W porównaniu do elektrody niemodyfikowanej zakres pH również uległ poszerzeniu (do 2,5 – 6,0 z 5,0 – 6,0), a współczynniki selektywności dla wszystkich badanych jonów interferujących znacznie się poprawiły (szczególnie w przypadku jonów dwuwartościowych – Co^{2+}, Cd^{2+} czy Pb^{2+}). Dodatkowo wykonano test warstwy wodnej oraz badania stałości potencjału zależnie od zmiany potencjału redox czy obecności gazów. Po trzech miesiącach użytkowania nachylenie krzywej kalibracyjnej nieznacznie zmalało (z 29,8 na 28,6 mV pa^{-1}). Modyfikacja membrany dodatkiem nanokompozytu zaowocowała poprawą parametrów analitycznych. Wyznaczona oporność membrany czujników zmalała ponad 10-krotnie (z 309 do 0,36 kΩ), a pojemność w zakresie niskich częstotliwości wzrosła ponad 35-krotnie (z 1,29 do 45,7 μF).

W Tabeli 4. zamieszczono porównanie parametrów otrzymanych elektrod z parametrami wybranych elektrod, opisanych w literaturze naukowej bądź dostępnymi na rynku. Istnieje mnóstwo artykułów, w których streszczone są starania badaczy dotyczące prób uzyskania substancji aktywnych nadających czujnikom bardzo dobrą selektywność. Jak można jednak zauważyć na podstawie danych, nadal należy to do niełatwych wyzwań.

Tabela 4. Zestawienie parametrów analitycznych dla opracowanych elektrod jonoselektywnych i elektrod opisanych w literaturze oraz dostępnych komercyjnie, czułych na jony miedzi(II).

Jonofor	Rodzaj kontaktu	Nachylenie, mV pa^{-1}	LOD, mol L^{-1}	Zakres liniowości, mol L^{-1}	Zakres pH	Stabilność potencjału	Jony interferujące, $K^{pot} \geq 1\times10^{-2}$	Praca
L^{1}Cu$_2$	Ag/AgCl/Cl$^-$	29,7	6,2×10^{-7}	1,0×10^{-6} –1,0×10^{-1}	2,4 – 5,5	0,017 mV min^{-1}	Cd^{2+}, Pb^{2+}	D6
jonofor IV miedzi(II)	MWCNTs:BMImPF$_6$ nanokompozyt	29,8	3,3×10^{-8}	1,0×10^{-7} –1,0×10^{-2}	2,5 – 6,0	46 μV min^{-1} (i=0)	–	D7
o-XBDiBDTC	grafit	31,3	4,9×10^{-7}	1,0×10^{-6} –1,0×10^{-1}	3,5 – 6,0	np	–	[176]
S$_2$	elektroda grafitowa	30,6	2,3×10^{-7}	6,0×10^{-7} –1,0×10^{-1}	3,0 – 7,5	np	Pb^{2+}	[177]
Me$_4$Bzo$_2$[14]aneN$_4$	ciekły	30,2	–	3,0×10^{-5} –1,0×10^{-1}	2,6 – 5,5	np	Li$^+$, Na$^+$, K$^+$, NH$_4^+$, Tl$^+$, Ag$^+$, Cs$^+$, Ni^{2+}	[178]
etambutol-miedź(II) kompleks	ciekły	29,9	–	7,9×10^{-6} –1,0×10^{-1}	2,1 – 6,3	np	Li$^+$, Na$^+$, K$^+$, Cs$^+$, Ag$^+$, NH$_4^+$, Ca^{2+}, Ba^{2+}, Sr^{2+}, Cd^{2+}, Co^{2+}, Pb^{2+}, Hg^{2+}, Zn^{2+}, Ni^{2+}, Al^{3+}, Ce^{3+}, Fe^{3+}, Bi^{2+}, Cr^{3+}	[179]
B	–	29,6	3,0×10^{-7}	5,0×10^{-6} –1,0×10^{-1}	1,9 – 5,2	np	Na$^+$, K$^+$, Cs$^+$, Ag$^+$, Ca^{2+}, Ba^{2+}, Sr^{2+}, Cd^{2+}, Co^{2+}, Hg^{2+}, Zn^{2+}, Ni^{2+}, Ce^{3+}, Fe^{3+}, Tl$^+$, Mg^{2+}	[180]
BHNHDA	MWCNTs	29,5	3,0×10^{-8}	5,0×10^{-8} –1,0×10^{-1}	2,0 – 5,0	np	Fe^{3+}	[96]
AMTOT	Ag/AgCl/Cl$^-$	29,3	6,2×10^{-8}	1,0×10^{-6}–1,0×10^{-2}	2,5 – 7,0	np	–	[181]
jonofor IV miedzi(II)	Ag/AgCl/Cl$^-$	28,9	3,2×10^{-8}	1,0×10^{-7} –1,0×10^{-2}	2,5 – 6,0	np	–	[182]
SUCC	kompozyt przewodzący	25,4	7,3×10^{-6}	1,0×10^{-4} –1,0×10^{-2}	2,0 – 6,0	np	Ca^{2+}, Co^{2+}, Ni^{2+}, Zn^{2+}, Pb^{2+}	[183]
NHS		37,5	4,4×10^{-6}	1,0×10^{-4} –1,0×10^{-2}	2,0 – 6,0		Ni^{2+}, Pb^{2+}	
DX264-Cu ISE half-cell electrode (Mettler Toledo)	–	–	–	1,0×10^{-5} – 1	2,0 – 8,0	np	np	[184]
ISE-Cu Mini 4,6 (Ntsensors)		25,0	–	1,0×10^{-6} – 5×10^{-2}	2,0 – 7,0	np	np	[185]

L$_1$Cu$_2$ – dwujądrowy kompleks N,N'-bis(5-bromo-2-hydroksy-3-metoksybenzylideno)2-hydroksypropyleno-1,3-diaminy z miedzią(II); o-XBDiBDTC – o-ksylilenobis(N,N-diizobutyditiokarbaminian); S$_2$ – 2-(indol-3-ilo)winylo)-1,3,4-tiadiazolo-2-tiol; Me$_4$Bzo$_2$[14]anN$_4$ –
5,7,12,14-tetrametylodibenzo[b,i]-1,4,8,11-tetraazacyklotetradekan; B – kompleks zasady Schiffa pochodzący z 2,3-diaminopirydyny i o-waniliny; BHNHDA – bis(2-hydroksynaftaldehydeno)-1,6-heksanodiamina; AMTOT – 4-amino-6-metylo-1,2,4-triazyno-5-on-3-tion; SUCC – sukcynoimid; NHS – N-hydroksysukcynoimid; np – nie podano.

K⁺-ISEs

Zaprojektowane zostały również badania ISEs czułych na jony potasowe. W tym przypadku najważniejszym celem było wykorzystanie jako SC nanocząstek tlenków metali (ZnO, CuO, Fe$_2$O$_3$) (D8) oraz metali (Ag) (D9), dlatego zastosowano ISM o sprawdzonym składzie zawierającą walinomycynę w roli jonoforu (3% walinomycyna, 1% KTPClPB, 32% PVC, 64% DOS). Walinomycyna stanowi najpopularniejszą substancję aktywną stosowaną w czujnikach potasowych (Tabela 5.). Zapewnia ona bardzo dobrą selektywność czujników oraz umożliwia osiągnięcie nachylenia krzywych kalibracyjnych zbliżonego do wartości teoretycznej.

Nanocząstki wykorzystane do konstrukcji czujników uzyskano metodą ablacji laserowej w cieczy (LAL). Jest to metoda szybka i stosunkowo prosta, umożliwiająca otrzymanie nanocząstek o bardzo wysokiej czystości bez konieczności stosowania dodatkowych substancji oraz bez produktów ubocznych [186–188]. LAL od lat jest stosowana do syntezy nanocząstek [188–195]. Celem tej części pracy było zbadanie, jaki wpływ na parametry elektrod miał zarówno rodzaj i grubość warstwy NPs stosowanych jako stały kontakt. Wszystkie NPs zbadano wykorzystując m.in. SEM, spektroskopię UV-VIS i XPS (D8). We wszystkich przypadkach elektrodę wewnętrzną stanowiła GCE, a nanocząstki były nakraplane w postaci zawiesiny wodnej o odpowiedniej objętości (100 i 500 µl) i po odparowaniu wody pokrywane ISM. Wszystkie elektrody z warstwą SC (z wyjątkiem elektrody z grubszą warstwą Fe$_2$O$_3$NPs) wykazywały lepszą stabilność i odwracalność potencjału oraz działały poprawnie przez okres > 5 miesięcy (z wyjątkiem elektrod z grubszą warstwą CuONPs i Fe$_2$O$_3$NPs). Jest to czas życia znacznie dłuższy, niż otrzymany dla elektrody niemodyfikowanej oraz dłuższy również niż podawany najczęściej w publikacjach dotyczących elektrod jonoselektywnych. Poprawa stabilności elektrod w wyniku wprowadzenia warstwy pośredniej nanocząstek metali przejściowych wynikała z wykazywanych przez nie doskonałych właściwości fizycznych i elektrochemicznych w porównaniu z ich odpowiednikami masowymi, wysokim stosunkiem powierzchni do objętości oraz właściwości półprzewodnikowych. Dzięki obecności warstwy NPs pole powierzchni elektroaktywnej jest większe, a transfer elektronów między ISM a elektrodą wewnętrzną - znacznie efektywniejszy.

Najlepszymi parametrami spośród otrzymanych czujników wyróżniały się elektrody z ZnONPs. Powodem tego stanu rzeczy mogła być najlepsza homogeniczność tego rodzaju nanocząstek, potwierdzona za pomocą obrazowania SEM. To również te elektrody wypadły

najlepiej w teście na obecność warstwy wodnej. Wykazywały one nachylenie –56,07 mV pa^{-1}, zakres liniowości $1 \times 10^{-5} - 1 \times 10^{-1}$ mol L^{-1} i granicę wykrywalności $3,66 \times 10^{-6}$ mol L^{-1} (dla cieńszej warstwy NPs). Wielu cennych informacji dostarczyły pomiary EIS. Wszystkie uzyskane widma impedancyjne miały podobny kształt, półkole w zakresie wysokich częstotliwości i jego fragment – w zakresie niskich częstotliwości. Dopasowano do nich obwody zastępcze, które pozwoliły na wyznaczenie parametrów elektrycznych elektrod.

Oporność ISM (R_b) zmniejszyła się znacznie z 882 kΩ dla ISE(c) do 78,1, 391 i 479 kΩ dla odpowiednio ISE-CuO(a), ISE-Fe$_2$O$_3$(a) i ISE-ZnO(a). Podobną zmianę zaobserwowano dla oporności przeniesienia ładunku R_{ct}, która również zmalała ze 180 kΩ dla ISE(c) do 9,34, 70,0 i 22,0 kΩ dla ISE-CuO(a), ISE-Fe$_2$O$_3$(a) i ISE-ZnO(a). Jednocześnie w wyniku modyfikacji znacznie wzrosła pojemność warstwy podwójnej (C_{dl}) – z 0,116 nF do 104, 10,3 i 27,7 nF dla ISE-CuO(a), ISE-Fe$_2$O$_3$(a), ISE-ZnO(a). Wyniki te wskazują, że zastosowanie NPs tlenków metali jako warstwy przewodzącej znacznie ułatwia procesy dyfuzji i transportu ładunków na granicy faz, co skutkuje poprawą stabilności potencjału elektrod. Zaproponowane nanocząstki tlenków metali, zwłaszcza nanocząstki ZnO, stanowią tańszą alternatywę dla nanomateriałów węglowych jako materiału stałego kontaktu.

Elektrody z AgNPs również charakteryzowały się bardzo dobrymi parametrami analitycznymi. Uzyskano nachylenie 56,16 mV pa^{-1} w zakresie stężeń $1 \times 10^{-5} - 1 \times 10^{-1}$ mol L^{-1}. Stabilność czujników była znacznie lepsza w porównaniu do prostych GCE/ISM. Stabilność krótkoterminowa poprawiła się z 5,17 mV h^{-1} dla elektrody niemodyfikowanej do 1,85 i 0,32 mV h^{-1} dla grubszej i cieńszej warstwy nanocząstek. Podobnie jak w przypadku uprzednio opisanych czujników, również te zawierające AgNPs działały poprawnie przez okres minimum 5 miesięcy.

Porównanie wybranych parametrów dla badanych elektrod, z parametrami elektrod opisanych w literaturze i dostępnych komercyjnie zamieszczono w Tabeli 5. Jak już wspomniano wcześniej najpopularniejszym jonoforem potasowym wciąż jest walinomycyna, natomiast stosowane są różnego rodzaju materiały w roli stałego kontaktu. Uzyskiwana liniowość najczęściej mieściła się w zakresie $1 \times 10^{-5} - 1 \times 10^{-1}$ mol L^{-1}, a granice wykrywalności – w zakresie $10^{-6} - 10^{-7}$ mol L^{-1}.

Tabela 5. Zestawienie parametrów analitycznych dla opracowanych elektrod jonoselektywnych i elektrod opisanych w literaturze oraz dostępnych komercyjnie, czułych na jony potasowe.

Jonofor	Rodzaj SC	Nachylenie, mV pa^{-1}	LOD, mol L^{-1}	Zakres liniowości, mol L^{-1}	Zakres pH	Stabilność potencjału	Jony interferujące, K^{pot} ≥ 1×10^{-2}	Praca
walinomycyna	ZnONPs (a)	56,2	5,3×10^{-6}	1,0×10^{-5} – 1,0×10^{-1}	–	0,32 mV h^{-1}	–	D8
	ZnONPs (b)	56,1	3,7×10^{-6}	1,0×10^{-5} – 1,0×10^{-1}		0,16 mV h^{-1}		
walinomycyna	AgNPs (a)	55,5	5,4×10^{-6}	1,0×10^{-5} – 1,0×10^{-1}	–	1,85 mV h^{-1}	–	D9
	AgNPs (b)	56,2	5,2×10^{-6}	1,0×10^{-5} – 1,0×10^{-1}		0,32 mV h^{-1}		
walinomycyna	hCeO$_2$	55,3		1,0×10^{-5} – 1,0×10^{-1}	2,0 – 11,5	86 µV h^{-1} (i=0), 6,0 mV s^{-1} (i=10 nA)	np	[114]
	hCeO$_2$+NTs	58,9	–	1,0×10^{-6} – 1,0×10^{-1}		95 µV h^{-1} (i=0), 2,3 mV s^{-1} (i=100 nA)		
	hCeO$_2$+POT	58,2		1,0×10^{-6} – 1,0×10^{-1}		240 µV h^{-1} (i=0), 2,7 mV s^{-1} (i=100 nA)		
walinomycyna	RuO$_2$	59,4	1,6×10^{-5}	3,2×10^{-6} – 1,0×10^{-1}	–	42 µV h^{-1} (i=0), 0,53 mV s^{-1} (i=100 nA)	np	[115]
	RuO$_2$×H$_2$O	57,4	1,0×10^{-6}	1,0×10^{-6} – 1,0×10^{-1}		1,5 µV h^{-1} (i=0), 0,081 mV s^{-1} (i=100 nA)		
walinomycyna	IrO$_2$×2H$_2$O	59,3	6,3×10^{-7}	1,0×10^{-6} – 1,0×10^{-1}	2,0 – 10,5	97 µV h^{-1} (i=0), -0,11 mV s^{-1} (i=100 nA)	np	[116]
walinomycyna	grafit	44,0	4,0×10^{-5}	5,0×10^{-5} – 1,0×10^{-1}	5,0 – 9,0	np	–	[196]
walinomycyna	MWCNTs	57,7	–	1,0×10^{-6} – 1,0×10^{-1}	–	12 µV s^{-1} (i=1 nA)	NH$_4^+$	[197]
walinomycyna	PPy/H-ZSM-5	54,2	7,1×10^{-6}	1,0×10^{-5} – 1,0×10^{-2}	–	130 µV h^{-1} (i=0)	np	[198]
walinomycyna	MoO$_2$	55,0	3,2×10^{-6}	1,0×10^{-5} – 1,0×10^{-3}	–	np	np	[199]
walinomycyna	all-solid-state	51,6	–	1,0×10^{-5} – 1,0×10^{-1}	2,0 – 6,0	np	–	[57]
walinomycyna	MPCs	57,4	7,9×10^{-7}	1,0×10^{-5} – 1,0×10^{-1}	–	31 µV s^{-1} (i=1 nA)	–	[200]
walinomycyna	PANI	60,5	1,6×10^{-6}	1,0×10^{-5} – 1,0×10^{-1}	–	1,17 µV s^{-1} (i=0)	NH$_4^+$	[201]
walinomycyna	PEDOT-HQ	60,9	2,0×10^{-7}	1,0×10^{-6} – 1,0×10^{-1}	–	0,1 mV h^{-1} (i=0)	NH$_4^+$	[202]
walinomycyna	PANINFs	58,8	–	1,0×10^{-4} – 1,0×10^{-1}	4,0 – 7,0	np	np	[203]
dbdb-18-6	PANI	58,2	1,6×10^{-6}	1,0×10^{-5} – 1,0×10^{-1}	4,0 – 9,0	np	–	[204]
DX239-K ISE half-cell electrode (Mettler Toledo)		–	–	1,0×10^{-6} – 1	2,0 – 12,0	np	np	[205]
ISE-K (Vernier)		56,0	–	2,5×10^{-5} – 1	2,0 – 12,0	np	np	[206]
ISE-K PS-3520 (Pasco)		56,0	–	2,5×10^{-5} – 1	2,0 – 12,0	np	np	[207]
ISE-K mini 4.6 (Ntsensors)		54,0	–	1,0×10^{-5} – 1×10^{-1}	1,0 – 9,0	np	–	[208]

(a) – grubsza warstwa SC; (b) – cieńsza warstwa SC; hCeO$_2$ – uwodnione nanocząstki tlenku ceru; RuO$_2$ –nanocząstki tlenku rutenu; RuO$_2$×H$_2$O – uwodnione nanocząstki tlenku rutenu; PPy/H-ZSM-5 – kompozyt polipirol/zeolit; MoO$_2$ – mikrosfery MoO$_2$; MPCs – klastery; PEDOT-HQ – sprzężony polimer redoks z grupami hydrochinonowymi kowalencyjnie przyłączonymi do szkieletu poli(3,4-etylenodioksytiofenu); dbdb-18-6 – 4',4"(5")-di-tert-butylodibenzo-18-korona-6-eter; ; np – nie podano.

UO$_2^{2+}$-ISEs

Opracowano również elektrody czułe na kationy uranylowe (UO$_2^{2+}$), w których jako jonofor zastosowano Cyanex-272 (kwas bis(2,4,4-trimetylopentylo)fosfoniowy) (D10). Modyfikacja składu ISM polegała na dodatku cieczy jonowej OMImCl (chlorek 1-oktylo-3-metyloimidazolu), której zadaniem było utrzymanie stałego stężenia jonów chlorkowych w membranie w celu zapewnienia stałości potencjału elektrody wewnętrznej Ag/AgCl. Elektroda z membraną bez jonoforu zawierającą 5 % cieczy jonowej wykazywała odpowiedź na jony uranylowe, która po wprowadzeniu jonoforu znacznie się poprawiła. Dla elektrody ISE-3 (1% Cyanexu-272) otrzymano nachylenie bliskie teoretycznemu (29,8 mV pa^{-1}) oraz niską granicę wykrywalności (7,1 × 10^{-7} mol L^{-1}). Zakres liniowości uległ poszerzeniu (z 5 × 10^{-5} – 1 × 10^{-1} mol L^{-1} do 1 × 10^{-6} – 1 × 10^{-1} mol L^{-1}) i znacznie obniżyła się granica wykrywalności czujników (z 2,5 × 10^{-5} mol L^{-1} do 7,1 × 10^{-7} mol L^{-1}). Są to znacznie lepsze osiągi niż opisywane w literaturze dla elektrody klasycznej z tym samym jonoforem [209]. Opracowane w pracy czujniki wykazywały również krótki czas odpowiedzi (< 8 s) oraz bardzo dobrą selektywność (logK$^{pot}_{UO22+/M}$ < –4 dla wszystkich badanych jonów). Uzyskano ponadto bardzo dobrą odwracalność potencjału ISEs i stabilność długookresową (30 dni). W porównaniu do elektrod opisanych w literaturze opracowane elektrody charakteryzowały się również szerokim zakresem pH, wynoszącym 2,5 – 6,0 (Tabela 6.). Warto zauważyć, że w większości przypadków inne elektrody pracowały poprawnie w zakresie pH nie szerszym niż 1,5 jednostki, natomiast w przypadku otrzymanych elektrod zakres ten jest ponad 2-krotnie szerszy. Co więcej, znaczna większość opisanych elektrod uranylowych obejmuje konstrukcję klasyczną, tj. z elektrolitem wewnętrznym, co może wynikać z faktu, że część tych badań została wykonana dekady temu, podczas gdy pierwsze artykuły opisujące elektrody czułe na jony uranylowe pojawiły się już w latach 70. [210]. Natomiast wiele z późniejszych badań również wykorzystuje tą konstrukcję, co może być spowodowane położeniem głównego nacisku na przebadanie nowych substancji aktywnych i różnych składów ISM. Zauważalna jest ogromna różnorodność związków, które do tej pory przebadano jako potencjalne jonofory na jony uranylowe z różnym skutkiem (Tabela 6). Od rodzaju i właściwości zastosowanych związków w dużym stopniu zależała selektywność elektrod, która jest szczególnie istotna w oznaczaniu jonów wykazujących działanie toksyczne już w bardzo niskich stężeniach, często znacznie niższych niż stężenia innych jonów obecnych w próbkach rzeczywistych.

Tabela 6. Zestawienie parametrów analitycznych dla opracowanych elektrod jonoselektywnych i elektrod opisanych w literaturze oraz dostępnych komercyjnie, czułych na jony uranylowe.

Jonofor	Rodzaj kontaktu	Nachylenie, mV pa^{-1}	LOD, mol L^{-1}	Zakres liniowości, mol L^{-1}	Zakres pH	Jony interferujące, $K^{pot} \geq 1\times10^{-2}$	Praca
Cyanex-272	Ag/AgCl/Cl$^-$	29,8	$7,1\times10^{-7}$	$1,0\times10^{-6} - 1,0\times10^{-1}$	2,4 – 6,0	–	D10
Cyanex-272		29,4	$8,3\times10^{-5}$	$5,3\times10^{-4} - 1,0\times10^{-1}$	2,1 – 3,7	Th^{4+}	
Cyanex-302	ciekły	28,0	$3,0\times10^{-5}$	$5,5\times10^{-5} - 1,0\times10^{-1}$	2,1 – 3,7	Th^{4+}, Fe^{3+}	[209]
Cyanex-301		29,3	$3,3\times10^{-6}$	$5,0\times10^{-6} - 1,0\times10^{-1}$	2,2 – 3,7	Th^{4+}	
L$_2$	ciekły	30,1	$8,0\times10^{-7}$	$1,0\times10^{-6} - 1,0\times10^{-1}$	2,9 – 3,7	Hg^{2+}, Ag^{2+}	[211]
	CGE	27,8	$7,3\times10^{-8}$	$1,0\times10^{-7} - 1,0\times10^{-1}$			
TTPTP	ciekły	30,0	$1,0\times10^{-5}$	$2,0\times10^{-5} - 1,0\times10^{-1}$	2,0 – 3,5	–	[212]
L	ciekły	27,7	$8,3\times10^{-7}$	$1,0\times10^{-6} - 1,0\times10^{-1}$	2,5 – 4,0	Ag^{2+}	[213]
	CGE	29,9	$7,5\times10^{-8}$	$1,0\times10^{-7} - 1,0\times10^{-1}$			
BHAED	CGE	29,3	$2,0\times10^{-6}$	$5,0\times10^{-6} - 5,0\times10^{-2}$	3,0 – 4,5	Ag^{2+}, Zn^{2+}, Fe^{3+}, Cu^{2+}, K$^+$	[214]
Kryptofix 22DD	grafit	29,6	$1,2\times10^{-5}$	$1,0\times10^{-4} - 1,0\times10^{-1}$	1,5 – 4,0	K$^+$, NH$_4^+$, Mg^{2+}, Ca^{2+}	[215]
DMSO	ciekły	30,0	$8,9\times10^{-8}$	$1,0\times10^{-7} - 1,0\times10^{-1}$	1,5 – 4,0	–	[216]
TPTU	ciekły	27,5	$5,0\times10^{-5}$	$5,0\times10^{-5} - 1,0\times10^{-1}$	2,5 – 3,5	Fe^{3+}, Th^{4+}, Y^{3+}	[217]
UO$_2$-CBT	ciekły	28,0	$4,0\times10^{-6}$	$3,0\times10^{-5} - 6,0\times10^{-2}$	4,0 – 10,0	Cr^{3+}, La^{3+}, Ba^{2+}, Ca^{2+}, Cu^{2+} ?	[218]
IIP	ciekły	28,1	$3,0\times10^{-6}$	$3,0\times10^{-5} - 6,0\times10^{-2}$	4,3 – 10,5	Cr^{3+}, La^{3+}, Ba^{2+}, Ca^{2+}, Cu^{2+}, Na$^+$, K$^+$?	[219]
	grafit	23,6	$5,0\times10^{-6}$	$1,0\times10^{-5} - 5,0\times10^{-2}$			
HL	grafit kompozyt	74 – 83	$2,0\times10^{-5}$	$4,0\times10^{-5} - 1,0\times10^{-2}$	2,5 – 4,0	Fe^{3+}, Cu^{2+}, Mn^{2+}, Zn^{2+}, Co^{2+}, Ni^{2+}, Ba^{2+}	[220]
UO$_2$L$_2$		25 – 31	$3,0\times10^{-6}$	$7,9\times10^{-4} - 2,5\times10^{-2}$		Fe^{3+}, Mn^{2+}	
Ph	ciekły	29,0	–	$1,0\times10^{-4} - 1,0\times10^{-1}$	< 4	Fe^{2+}, Cr^{3+}, Ce^{3+}, Ni^{2+}, U^{4+}	[221]
kaliksaren	ciekły	27,0	$4,0\times10^{-5}$	$1,0\times10^{-5} - 1,0\times10^{-1}$	5,5 – 8,5	np	[222]
DBBP	ciekły	28,6	$3,0\times10^{-6}$	$5,0\times10^{-6} - 1,0\times10^{-1}$	2,1 – 3,4	Th^{4+}	[223]

Cyanex-272 – kwas bis(2,4,4-trimetylopentylo)fosfoniowy; L$_2$ – makrocykliczny diamid, 6,7,9,10,12,13,15,16,24,25,26,27-dodekahydro-22-H-dibenzo[n,w][1,4,7,10,13,17,21]pentaoksa-diazacyklotetrakozyno-22,27(23H)-dion; CGE – powlekany grafit; TTPTP – 5,6,7,8-tetrahydro-8-tioksopirydo[4',3',4,5]tieno[2,3-d]pirymidyno-4(3H)on; L – 5-(9-antracenylometylo)-5-aza-2,8-ditia[9],(2,9)-1,10-fenantrolinofan; BHAED – bis(2-hydroksyacetofenon)etyleno-diimina, Kryptofix 22DD – 4,13-dodecylo-1,7,10,16-tetraoksa-4,13-diazacyklooktadekan; Cyanex-272 – kwas bis(2,4,4-trimetylopentylo)fosfinowy; Cyanex-302 – kwas bis(2,4,4-trimetylopentylo)monotiofosfonowy; Cyanex-301 – kwas bis(2,4,4-trimetylopentylo)ditiofosforowy; DMSO – dimetylosulfotlenek; TPTU –heksafluorofosforan O-(1,2-dihydro-2-okso-1-pirydylo)-N,N,N',N'-bis(tetra-metyleno)uroniowy; IIP – polimer z nadrukiem jonowym; UO$_2$-CBT – kompleks uranylu z karboksybenzotriazolem; HL – dwufunkcyjny środek chelatujący, tlenek O-metylodiheksylofosfiny kwas O'-heksylo-2-etylofosforowy; UO$_2$L$_2$ – kompleks uranylu z HL; Ph – fosforan(III) tris(chloroetylu lub propylu); kaliksaren – funkcjonalizowany 5,11,17,23-tetra-tert-butylo-25,27-bis(hydroksy)-26-(etoksykarbonylometoksy)-28-(dietylokarbamoilometoksy)kaliks[4]aren; DBBP – fosfonian dibutylobutylu; np – nie podano.

ZASTOSOWANIE OPRACOWANYCH ELEKTROD DO OZNACZEŃ WYBRANYCH JONÓW W PRÓBKACH RZECZYWISTYCH

Wybrane elektrody zastosowano do oznaczeń zawartości poszczególnych jonów w próbkach rzeczywistych, w szczególności w różnego rodzaju wodach (wodociągowa, mineralna, rzeczna, studzienna) [D1, D3, D4, D5, D7], a także w próbkach żywności (sałata masłowa, szpinak, rzodkiewka, ogórek, kapusta, pomidor) [D3]. W celu weryfikacji poprawności uzyskanych wyników wykorzystano badanie odzysku [D1, D3, D7], oznaczenie w certyfikowanym materiale odniesienia [D7] lub zastosowanie metod porównawczych (spektrofotometria UV-VIS [D4], miareczkowanie klasyczne metodą Mohre'a [D5]. W każdym przypadku otrzymano zadowalające wyniki.

Dla potwierdzenia efektywności wykorzystania otrzymanych elektrod azotanowych do badania próbek środowiskowych przeprowadzono badania próbek wód. W artykule D1 wartości odzysku otrzymane dla próbek wód mieściły się w zakresie 100,89 – 95,77% w zależności od rodzaju wody i złożoności matrycy próbki. Wyniki oznaczenia jonów azotanowych(V) wykonane za pomocą elektrod z nanokompozytem MWCNTs:IL opisano w pracy [D3]. W tym przypadku poza wodą rzeczną i wodą z jeziora analizie poddano również próbki warzyw. Próbek wodnych nie poddawano żadnemu przygotowaniu wstępnemu, natomiast w przypadku roślin – rozdrobnione próbki warzyw o masie 5 g mieszano z wodą dejonizowaną i ogrzewano w temperaturze $80^{\circ}C$ przez 30 minut, a następnie przesączano i rozcieńczano do objętości 500 mL. Dla próbek wód, sałaty i kapusty uzyskano najlepsze wartości odzysku (w zakresie 100±1%), natomiast w pozostałych przypadkach odzysk mieścił się w zakresie 100±5%. Również elektrody azotanowe ze stałym kontaktem w postaci PANINFs [D4] zostały wykorzystane w analizie wód, a otrzymane wyniki porównano z wynikami otrzymanymi metodą spektrofotometrii UV-VIS. Przygotowanie próbek do pomiaru ograniczało się do dodatku roztworu soli Na_2SO_4 do roztworu próbki. Zgodność wyników uzyskanych obiema metodami była zadowalająca, co potwierdza, że otrzymane czujniki z powodzeniem mogą być stosowane do monitorowania zawartości jonów azotanowych(V) w próbkach rzeczywistych.

Próbki wód (wodociągowej, mineralnej i rzecznej) badano również na obecność jonów chlorkowych (D5). Dla porównania uzyskanych wyników zastosowano argentometryczne oznaczanie chlorków metodą Mohra (miareczkowanie bezpośrednie, klasyczna analiza ilościowa). Jedyną czynnością na etapie przygotowania próbki był dodatek octanu sodu

pełniącego rolę buforu mocy jonowej. Mając na uwadze liczbę niezbędnych czynności, których wykonanie jest konieczne w celu przeprowadzenia oznaczenia metodą klasyczną, instrumentalne pomiary potencjometryczne są znacznie szybsze i bardziej obiektywne oraz dzięki szerokiemu zakresowi stężeń, w jakim można oznaczać zawartość analitu (w tym przypadku liniowość krzywej kalibracyjnej $5,0 \times 10^{-6} - 1,0 \times 10^{-1}$ mol L^{-1}) nie byłoby również konieczne rozcieńczanie/zatężanie próbki. Za pomocą obu metod otrzymano porównywalne wyniki – potencjometrycznie: $0,737 \pm 0,016$; $0,311 \pm 0,018$ i $1,07 \pm 0,026$ mmol L^{-1} i klasycznie: 0,745; 0,302 i 1,01 mmol L^{-1} (odpowiednio dla wody wodociągowej, mineralnej i rzecznej).

W pracy D7 opisano oznaczenie zawartości miedzi za pomocą opracowanej elektrody ze stałym kontaktem w certyfikowanym materiale odniesienia SPS-WW1 (ścieki) (rozcieńczonym 2-krotnie i z dodatkiem NaOH w celu zapewnienia odpowiedniego pH próbki). Otrzymano wartość stężenia jonów miedzi(II) zbliżoną do wartości certyfikowanej (CRM 400 ± 2 µg L^{-1}; wynik oznaczenia 412 ± 14 µg L^{-1}). Zbadano również próbkę wody rzecznej, którą badano po zakwaszeniu w celu uzyskania pH około 4,5. Oszacowany odzysk mieścił się w zakresie 97,7 – 101,5%, co również jest potwierdzeniem poprawnego działania opracowanej elektrody.

PODSUMOWANIE I WNIOSKI

Na podstawie uzyskanych wyników, które zostały opisane szczegółowo w cyklu prac badawczych stanowiących podstawę niniejszej rozprawy doktorskiej można stwierdzić, że:

- badane w pracy nowozsyntezowane związki organiczne (kompleks Co(II) z 4,7-difenylo-1,10-fenantroliną oraz dwurdzeniowy kompleks Cu(II) z N,N'-bis(5-bromo-2-hydroksy-3-metoksybenzylideno)-2-hydroksypropyleno-1,3-diaminą) z powodzeniem zastosowano jako jonofory w membranach jonoselektywnych czułych odpowiednio na jony NO_3^- oraz Cu^{2+};

-zastosowane w konstrukcji elektrod materiały: nanokompozyty wielościennych nanorurek węglowych i cieczy jonowych oraz nanowłókien polianiliny, a także modyfikowane nanowłókna polianiliny, nanocząstki tlenków metali, nanocząstki srebra efektywnie spełniały funkcję stałego kontaktu elektrod poprawiając ich parametry analityczne, metrologiczne oraz elektryczne;

- w każdym przypadku modyfikacja elektrod poprzez wprowadzenie materiału stałego kontaktu powodowała poprawę ich parametrów elektrycznych (obniżenie oporności membrany, zwiększenie pojemności warstwy podwójnej oraz obniżenie oporności przeniesienia ładunku), co w efekcie przyniosło polepszenie stabilności i odwracalności potencjału elektrod;

- zastosowanie nanokompozytów wielościennych nanorurek węglowych oraz cieczy jonowych (MWCNTs:THTDPCl oraz MWCNTs:BMImPF$_6$) jako składnika jonoczułej membrany spowodowało obniżenie granic wykrywalności elektrod, a w przypadku nanokompozytu MWCNTs-BMImPF$_6$ również poprawę selektywności i uzyskanie szerszego optymalnego zakresu pH;

- zastosowanie nanowłókien polianiliny (PANINFs-Cl i PANINFs-NO$_3$) jako stałego kontaktu zarówno jako składnika membrany oraz jako warstwy pośredniej spowodowało rozszerzenie zakresu liniowości krzywych kalibracyjnych oraz obniżenie granic wykrywalności czujników;

- wykorzystanie nanokompozytu nanowłókien polianiliny z wielościennymi nanorurkami węglowymi (PANINFs-Cl:MWCNTs) umożliwiło otrzymanie czujników o bardzo dobrych parametrach elektrycznych i odpornych na zmiany czynników zewnętrznych;

- w wyniku wykorzystania nanocząstek metali i tlenków metali (w szczególności ZnONPs) jako warstwy pośredniej powstały elektrody charakteryzujące się zwiększoną trwałością (czas życia > 5 miesięcy) i odpornością mechaniczną oraz niewrażliwością na powstawanie niepożądanej warstwy wodnej;

- dodatek cieczy jonowej chlorku 1-oktylo-3-metyloimidazolu do membrany jonoselektywnej zawierającej substancję aktywną (Cyanex-272) pozwolił uzyskać elektrody uranylowe o niskiej granicy wykrywalności, szerokim zakresie liniowości krzywej kalibracyjnej i krótkim czasie odpowiedzi;

- w przypadku wszystkich skonstruowanych elektrod, wybranych po procesie optymalizacji, otrzymano nachylenia krzywych kalibracyjnych bliskie teoretycznym oraz niskie granice wykrywalności;

- efektywność działania materiału jako stałego kontaktu zależy od jego struktury i jest większa dla materiałów o mniejszych rozmiarach cząstek i jednorodnej strukturze;

- uzyskano elektrody o dobrej stabilności i odwracalności potencjału, które są szczególnie istotne w stosowaniu elektrod do badań próbek środowiskowych;

- obniżenie oporności membrany pozwoliło na uzyskanie elektrod o krótkich czasach odpowiedzi i niewielkim dryfcie potencjału;

- nie zaobserwowano wrażliwości skonstruowanych czujników na zmiany środowiskowe obejmujące zmienne oświetlenie, obecność gazów lub zmiany potencjału redox roztworów próbki, co ma ogromne znaczenie w trakcie analizy próbek rzeczywistych;

- opracowane czujniki nie wykazywały tendencji do powstawania niepożądanej warstwy wodnej pomiędzy materiałem elektrody wewnętrznej a warstwą stałego kontaktu/modyfikowanej membrany jonoselektywnej;

- skonstruowane elektrody z powodzeniem zastosowano do oznaczania jonów NO_3^-, Cl^- oraz Cu^2 w próbkach rzeczywistych (próbki wód, warzyw).

SPIS TABEL

SPIS RYSUNKÓW

Rys. 1 Schemat układu pomiarowego stosowanego w potencjometrii z klasyczną elektrodą jonoselektywną i elektrodą referencyjną.

Rys. 2 Schemat przebiegu mechanizmów dla SCISEs czułych na kationy z membraną zawierającą niejonowy jonofor (L) z: (A) SC w postaci domieszkowanego polimeru przewodzącego o wysokiej pojemności redox i (B) wysokoporowatym SC o wysokiej pojemności warstwy podwójnej.

Rys. 3 Porównanie konstrukcji elektrod jonoselektywnych: (A) klasycznej z roztworem wewnętrznym, (B) ze stałym kontaktem.

Rys. 4 Skład membrany jonoselektywnej.

Rys. 5 Obrazy SEM: (A) MWCNTs, (B) nanokompozytu MWCNTs z PANINFs-Cl, (C) PANINFs-Cl, (D) PANINFs-NO$_3$.

Rys. 6 Sposoby wyznaczania granicy wykrywalności elektrod na podstawie krzywych kalibracyjnych, gdzie: pa – ujemny logarytm z aktywności jonu głównego, LoD – granica wykrywalności.

Rys. 7 (A) Przykład widma impedancyjnego dla elektrod potasowych: ISE niemodyfikowanej (●) i ISE z warstwą stałego kontaktu nanocząstek – ZnO (●) (B) oraz zastępczy obwód elektryczny R(RC/Q)(RC)Q.

Rys. 8 Przykładowy chronopotencjogram reprezentujący elektrody azotanowe o stabilnym (——) i mniej stabilnym (- - -) potencjale (odpowiednio przykład ISE-2 i ISE-3); wzory pozwalające na wyznaczenie oporności całkowitej (R) i dryftu potencjału ($\Delta E/\Delta t$), gdzie: E – skok potencjału w wyniku zmiany kierunku prądu (i), C$_L$ - pojemność SC.

Rys. 9 Porównanie konstrukcji elektrod jonoselektywnych ze stałym kontaktem: (A) żelowanej z elektrodą wewnętrzną chlorosrebrową, (B) dyskowej z elektrodą wewnętrzną z węgla szklistego.

Rys. 10 Schemat wykonania SCISEs: (A) 2-etapowy obejmujący nałożenie warstwy SC, a następnie pokrycie jej warstwą ISM; (B) 1-etapowy – bezpośrednie nałożenie ISM wzbogaconej dodatkiem SC.

BIBLIOGRAFIA

[1]   R. Liang, T. Yin, W. Qin, Analytica Chimica Acta 853 (2015) 291–296.

[2]   E. Lindner, R.E. Gyurcsányi, Journal of Solid State Electrochemistry 13 (2009) 51–68.

[3]   J. Sutter, A. Radu, S. Peper, E. Bakker, E. Pretsch, Analytica Chimica Acta 523 (2004) 53–59.

[4]   C. Bieg, K. Fuchsberger, M. Stelzle, Analytical and Bioanalytical Chemistry 409 (2017) 45–61.

[5]   J. Hu, A. Stein, P. Bühlmann, Trends in Analytical Chemistry 76 (2016) 102–114.

[6]   J. Bobacka, A. Ivaska, A. Lewenstam, Chemical Reviews 108 (2008) 329–351.

[7]   C. Zuliani, D. Diamond, Electrochimica Acta 84 (2012) 29–34.

[8]   R. Koncki, Analytica Chimica Acta 599 (2007) 7–15.

[9]   L. van de Velde, E. d'Angremont, W. Olthuis, Talanta 160 (2016) 56–65.

[10]   D. Morris, S. Coyle, Y. Wu, K.T. Lau, G. Wallace, D. Diamond, Sensors and Actuators, B: Chemical 139 (2009) 231–236.

[11]   A. Lewenstam, Comprehensive Analytical Chemistry 49 (2007) 5–24.

[12]   A. Numnuam, K.Y. Chumbimuni-Torres, Y. Xiang, R. Bash, P. Thavarungkul, P. Kanatharana, E. Pretsch, J. Wang, E. Bakker, Journal of the American Chemical Society 130 (2008) 410–411.

[13]   M.K. Abd El-Rahman, M.Y. Salem, Sensors and Actuators B: Chemical 220 (2015) 255–262.

[14]   B.R. Chapman, I.R. Goldsmith, The Analyst 107 (1982) 1014–1018.

[15]   P.K.T. Lin, A.N. Araujo, M.C.B.S.M. Montenegro, R. Pérez-Olmos, Journal of Agricultural and Food Chemistry 53 (2005) 211–215.

[16]   Y. Fan, C. Xu, R. Wang, G. Hu, J. Miao, K. Hai, C. Lin, Journal of Food Composition and Analysis 62 (2017) 63–68.

[17]   V.I. Slaveykova, K.J. Wilkinson, A. Ceresa, E. Pretsch, Environmental Science and Technology 37 (2003) 1114–1121.

[18]   R. De Marco, G. Clarke, B. Pejcic, Electroanalysis 19 (2007) 1987–2001.

[19]   G.A. Crespo, Electrochimica Acta 245 (2017) 1023–1034.

[20]   E. Pretsch, Trends in Analytical Chemistry 26 (2007) 46–51.

[21]   E. Bakker, E. Pretsch, Trends in Analytical Chemistry 27 (2008) 612–618.

[22]   E. Bakker, E. Pretsch, Trends in Analytical Chemistry 24 (2005) 199–207.

[23]   A. Düzgün, G.A. Zelada-Guillén, G.A. Crespo, S. Macho, J. Riu, F.X. Rius, Analytical and Bioanalytical Chemistry 399 (2010) 171–181.

[24]   J.P. Veder, R. De Marco, K. Patel, P. Si, E. Grygolowicz-Pawlak, M. James, M.T. Alam, M. Sohail, J. Lee, E. Pretsch, E. Bakker, Analytical Chemistry 85 (2013) 10495–10502.

[25]   M. Cuartero, J. Bishop, R. Walker, R.G. Acres, E. Bakker, R. De Marco, G.A. Crespo, Chemical Communications 52 (2016) 9703–9706.

[26]   J. Hu, A. Stein, P. Bühlmann, Trends in Analytical Chemistry 76 (2016) 102–114.

[27]   Y. Lyu, S. Gan, Y. Bao, L. Zhong, J. Xu, W. Wang, Z. Liu, Y. Ma, G. Yang, L. Niu, Membranes 10 (2020) 1–24.

[28]   K.N. Mikhelson, Ion-Selective Electrodes, 2018.

[29]   T. Ghosh, H.J. Chung, J. Rieger, Sensors (Switzerland) 17 (2017) 2536.

[30] R.W. Cattrall, H. Freiser, Analytical Chemistry 43 (1971) 1905–1906.

[31] A. Cadogan, Z. Gao, A. Lewenstam, A. Ivaska, D. Diamond, A. Lewenstam, Z. Gao, Analytical Chemistry 64 (1992) 2496–2501.

[32] A. Michalska, Electroanalysis 24 (2012) 1253–1265.

[33] Z. Mousavi, K. Granholm, T. Sokalski, A. Lewenstam, Sensors and Actuators, B: Chemical 207 (2015) 895–899.

[34] S. Anastasova-Ivanova, U. Mattinen, A. Radu, J. Bobacka, A. Lewenstam, J. Migdalski, M. Danielewski, D. Diamond, Sensors and Actuators B: Chemical 146 (2010) 199–205.

[35] M. Cuartero, G.A. Crespo, Current Opinion in Electrochemistry 10 (2018) 98–106.

[36] M. Cuartero, E. Bakker, Current Opinion in Electrochemistry 3 (2017) 97–105.

[37] D. Diamond, S. Coyle, S. Scarmagnani, J. Hayes, Chemical Reviews 108 (2008) 652–679.

[38] M. Parrilla, M. Cuartero, G.A. Crespo, Trends in Analytical Chemistry 110 (2019) 303–320.

[39] S. Roy, M. David-Pur, Y. Hanein, ACS Applied Materials and Interfaces 9 (2017) 35169–35177.

[40] D. Diamond, K.T. Lau, S. Brady, J. Cleary, Talanta 75 (2008) 606–612.

[41] A. Michalska, K. Maksymiuk, Wiadomości Chemiczne 69 (2015) 9–10.

[42] K. Maksymiuk, A. Michalska, Chemik 69 (2015) 373–382.

[43] A. Kisiel, A. Michalska, K. Maksymiuk, Journal of Electroanalytical Chemistry 766 (2016) 128–134.

[44] A. Kisiel, E. Woźnica, M. Wojciechowski, E. Bulska, K. Maksymiuk, A. Michalska, Sensors and Actuators, B: Chemical 207 (2015) 995–1003.

[45] J.M. Jarvis, M. Guzinski, B.D. Pendley, E. Lindner, Journal of Solid State Electrochemistry 20 (2016) 3033–3041.

[46] J. Hu, X.U. Zou, A. Stein, P. Bühlmann, Analytical Chemistry 86 (2014) 7111–7118.

[47] Z. Jiang, X. Xi, S. Qiu, D. Wu, W. Tang, X. Guo, Y. Su, R. Liu, Journal of Materials Science 54 (2019) 13674–13684.

[48] F. Criscuolo, I. Taurino, F. Stradolini, S. Carrara, G. De Micheli, Analytica Chimica Acta 1027 (2018) 22–32.

[49] C.Z. Lai, M.M. Joyer, M.A. Fierke, N.D. Petkovich, A. Stein, P. Bühlmann, Journal of Solid State Electrochemistry 13 (2009) 123–128.

[50] B. Paczosa-Bator, R. Piech, L. Cabaj, Electrochimica Acta 85 (2012) 104–109.

[51] T. Yin, W. Qin, Trends in Analytical Chemistry 51 (2013) 79–86.

[52] J. Sutter, E. Lindner, R.E. Gyurcsányi, E. Pretsch, Analytical and Bioanalytical Chemistry 380 (2004) 7–14.

[53] J. Bobacka, Analytical Chemistry 71 (1999) 4932–4937.

[54] M. Vázquez, J. Bobacka, A. Ivaska, A. Lewenstam, Sensors and Actuators, B: Chemical 82 (2002) 7–13.

[55] T. Lindfors, Journal of Solid State Electrochemistry 13 (2009) 77–89.

[56] J. Bobacka, M. McCarrick, A. Lewenstam, A. Ivaska, Analyst 119 (1994) 1985–1991.

[57] J. Bobacka, A. Ivaska, A. Lewenstam, Analytica Chimica Acta 385 (1999) 195–202.

[58] K.Y. Chumbimuni-Torres, N. Rubinova, A. Radu, T. Lauro, E. Bakker, Analytical Chemistry 78 (2006) 1318–1322.

[59] J. Bobacka, T. Lindfore, M. Mccarrick, A. Ivaska, A. Lewenstam, Analytical Chemistry 67 (1995) 3819–

3823.

[60] Y. Huang, J. Li, T. Yin, J. Jia, Q. Ding, H. Zheng, C.T.A. Chen, Y. Ye, Journal of Electroanalytical Chemistry 741 (2015) 87–92.

[61] P. Das, S. Mondal, S. Malik, Journal of Energy Storage 39 (2021).

[62] Y. Zhang, Y. Tao, K. Wang, S. Zhao, J. Zhu, H. Cheng, J. Appl. Polym. Sci. 138 (2021) 1–12.

[63] T. Zhang, H. Yue, X. Gao, F. Yao, H. Chen, X. Lu, Y. Wang, X. Guo, Ionics (Kiel) 26 (2020) 2063–2070.

[64] X. Zeng, Y. Liu, X. Jiang, G.I.N. Waterhouse, Z. Zhang, L. Yu, Electrochim. Acta 384 (2021) 138414.

[65] D. Zhang, Y. Wang, Mater. Sci. Eng. B Solid-State Mater. Adv. Technol. 134 (2006) 9–19.

[66] X. Zhang, S.K. Manohar, Chem. Commun. (2004) 2360–2361.

[67] Y. Jiang, Z. Liu, G. Zeng, Y. Liu, B. Shao, Z. Li, Y. Liu, W. Zhang, Q. He, Environ. Sci. Pollut. Res. 25 (2018) 6158–6174.

[68] H. Mei-Rong, G.U. Guo-Li, D. Yong-Bo, F.U. Xiao-Tian, L. Rong-Gui, Chinese Journal of Analytical Chemistry 40 (2012) 1454–1460.

[69] J. Bobacka, Electroanalysis 18 (2006) 7–18.

[70] S.J. Klaine, P.J.J. Alvarez, G.E. Batley, T.F. Fernandes, R.D. Handy, D.Y. Lyon, S. Mahendra, M.M. J., J.R. Lead, Environmental Toxicology and Chemistry 27 (2008) 1825–1851.

[71] K. Balasubramanian, M. Burghard, Small 1 (2005) 180–192.

[72] S. Xie, W. Li, Z. Pan, B. Chang, S. Lianfeng, Journal of Physics and Chemistry of Solids 61 (2000) 1153–1158.

[73] A. Hirsch, Angewandte Chemie - International Edition 41 (2002) 1853–1859.

[74] V. Datsyuk, M. Kalyva, K. Papagelis, J. Parthenios, D. Tasis, A. Siokou, I. Kallitsis, C. Galiotis, Carbon 46 (2008) 833–840.

[75] H. Dai, Accounts of Chemical Research 35 (2002) 1035–1044.

[76] A. Merkoçi, Microchimica Acta 152 (2006) 157–174.

[77] Y. Liu, Y. Zhao, B. Sun, C. Chen, Accounts of Chemical Research 46 (2013) 702–713.

[78] M. Pumera, Chemistry - A European Journal 15 (2009) 4970–4978.

[79] S.B. Sinnott, R. Andrews, Critical Reviews in Solid State and Materials Sciences 26 (2001) 145–249.

[80] M.M. Titirici, R.J. White, N. Brun, V.L. Budarin, D.S. Su, F. Del Monte, J.H. Clark, M.J. MacLachlan, Chemical Society Reviews 44 (2015) 250–290.

[81] I. Dumitrescu, P.R. Unwin, J. V. MacPherson, Chemical Communications 7345 (2009) 6886–6901.

[82] J. Prasek, J. Drbohlavova, J. Chomoucka, J. Hubalek, O. Jasek, V. Adam, R. Kizek, Journal of Materials Chemistry 21 (2011) 15872.

[83] V. Sgobba, D.M. Guldi, Chemical Society Reviews 38 (2009) 165–184.

[84] D. Tasis, N. Tagmatarchis, A. Bianco, M. Prato, Chemical Reviews 106 (2006) 1105–1136.

[85] C. Herrero-Latorre, J. Álvarez-Méndez, J. Barciela-García, S. García-Martín, R.M. Peña-Crecente, Analytica Chimica Acta 853 (2015) 77–94.

[86] P. Yáñez-Sedeño, J. Riu, J.M. Pingarrón, F.X. Rius, Trends in Analytical Chemistry 29 (2010) 939–953.

[87] A. Merkoçi, M. Pumera, X. Llopis, B. Pérez, M. Del Valle, S. Alegret, Trends in Analytical Chemistry 24 (2005) 826–838.

[88]   J.M. Schnorr, T.M. Swager, Chemistry of Materials 23 (2011) 646–657.

[89]   V. Schroeder, S. Savagatrup, M. He, S. Lin, T.M. Swager, Chemical Reviews 119 (2019) 599–663.

[90]   R. Liang, T. Yin, W. Qin, Analytica Chimica Acta 853 (2015) 291–296.

[91]   M. Najafi, L. Maleki, A.A. Rafati, Journal of Molecular Liquids 159 (2011) 226–229.

[92]   G.A. Crespo, S. Macho, F.X. Rius, Analytical Chemistry 80 (2008) 1316–1322.

[93]   J. Ampurdanés, G.A. Crespo, A. Maroto, M.A. Sarmentero, P. Ballester, F.X. Rius, Biosensors and Bioelectronics 25 (2009) 344–349.

[94]   E.J. Parra, G.A. Crespo, J. Riu, A. Ruiz, F.X. Rius, Analyst 134 (2009) 1905–1910.

[95]   G.A. Crespo, D. Gugsa, S. MacHo, F.X. Rius, Analytical and Bioanalytical Chemistry 395 (2009) 2371–2376.

[96]   M. Ghaedi, M. Montazerozohori, R. Sahraei, Journal of Industrial and Engineering Chemistry 19 (2013) 1356–1364.

[97]   S.S.M. Hassan, A.G. Eldin, A.E.G.E. Amr, M.A. Al-Omar, A.H. Kamel, N.M. Khalifa, Sensors 19 (2019) 3891.

[98]   F. Li, J. Ye, M. Zhou, S. Gan, Q. Zhang, D. Han, L. Niu, Analyst 137 (2012) 618–623.

[99]   Z.A. Boeva, T. Lindfors, Sensors and Actuators B: Chemical 224 (2016) 624–631.

[100]   M. Fouskaki, N. Chaniotakis, Analyst 133 (2008) 1072–1075.

[101]   B. Paczosa-Bator, Talanta 93 (2012) 424–427.

[102]   M.A. Fierke, C.Z. Lai, P. Bühlmann, A. Stein, Analytical Chemistry 82 (2010) 680–688.

[103]   J. Ping, Y. Wang, J. Wu, Y. Ying, Electrochemistry Communications 13 (2011) 1529–1532.

[104]   J. Ping, Y. Wang, Y. Ying, J. Wu, Analytical Chemistry 84 (2012) 3473–3479.

[105]   E. Woźnica, M.M. Wójcik, M. Wojciechowski, J. Mieczkowski, E. Bulska, K. Maksymiuk, A. Michalska, Analytical Chemistry 84 (2012) 4437–4442.

[106]   M. Chen, M. Zhang, X. Wang, Q. Yang, M. Wang, G. Liu, L. Yao, Sensors (Switzerland) 20 (2020) 2270.

[107]   E. Jaworska, M. Wójcik, A. Kisiel, J. Mieczkowski, A. Michalska, Talanta 85 (2011) 1986–1989.

[108]   L. Zhang, Z. Wei, P. Liu, PLoS ONE 15 (2020) 1–14.

[109]   T. Yin, T. Han, C. Li, W. Qin, J. Bobacka, Analytica Chimica Acta 1101 (2020) 50–57.

[110]   B. Paczosa-Bator, L. Cabaj, R. Piech, K. Skupień, Analyst 137 (2012) 5272–5277.

[111]   B. Paczosa-Bator, R. Piech, C. Wardak, L. Cabaj, Ionics 24 (2018) 2455–2464.

[112]   E. Jaworska, A. Kisiel, K. Maksymiuk, A. Michalska, Analytical Chemistry 83 (2011) 438–445.

[113]   K. Khun, Z.H. Ibupoto, M. Willander, Electroanalysis 25 (2013) 1425–1432.

[114]   N. Lenar, R. Piech, B. Paczosa-Bator, Membranes 12 (2022).

[115]   N. Lenar, B. Paczosa-Bator, R. Piech, Membranes 10 (2020) 1–18.

[116]   N. Lenar, R. Piech, J. Wyrwa, B. Paczosa-Bator, Membranes 11 (2021).

[117]   Y. Liu, Y. Liu, R. Yan, Y. Gao, P. Wang, Electrochimica Acta 331 (2020) 135370.

[118]   J.R. Morones, J.L. Elechiguerra, A. Camacho, K. Holt, J.B. Kouri, J.T. Ramirez, M.J. Yacaman, Nanotechnology 16 (2005) 2346–2353.

[119]   J.S. Kim, E. Kuk, N. Yu, J. Kim, S.J. Park, J. Lee, H. Kim, Y.K. Park, H. Park, C. Hwang, Y. Kim, Y. Lee, D.H. Jeong, M. Cho, Nanotechnology, Biology, And 3 (2007) 95–101.

[120] L. Qi, T. Jiang, R. Liang, W. Qin, Sensors and Actuators B: Chemical 328 (2021) 129014.

[121] M. Ahamed, M.S. Alsalhi, M.K.J. Siddiqui, Clinica Chimica Acta 411 (2010) 1841–1848.

[122] X. Zhang, Z.-G. Liu, W. Shen, S. Gurunathan, International Journal of Molecular Sciences 17 (2016) 1534.

[123] N. Krstulović, K. Salamon, O. Budimlija, J. Kovač, J. Dasović, P. Umek, I. Capan, Applied Surface Science 440 (2018) 916–925.

[124] D. Blažeka, J. Car, N. Klobučar, A. Jurov, J. Zavašnik, A. Jagodar, E. Kovačević, N. Krstulović, Materials 13 (2020) 4357.

[125] U. Qumar, J.Z. Hassan, R.A. Bhatti, A. Raza, G. Nazir, W. Nabgan, M. Ikram, Journal of Materials Science and Technology 131 (2022) 122–166.

[126] N. Krstulović, P. Umek, K. Salamon, I. Capan, Materials Research Express 4 (2017) 105003.

[127] A. Fog, R.P. Buck, Sensors and Actuators 5 (1984) 137–146.

[128] J.N. Coleman, U. Khan, W.J. Blau, Y.K. Gun'ko, Carbon 44 (2006) 1624–1652.

[129] M. Omidi, D.T. Hossein Rokni, A.S. Milani, R.J. Seethaler, R. Arasteh, Carbon 48 (2010) 3218–3228.

[130] E.M. Jackson, P.E. Laibinis, W.E. Collins, A. Ueda, C.D. Wingard, B. Penn, Composites Part B: Engineering 89 (2016) 362–373.

[131] Z. Spitalsky, D. Tasis, K. Papagelis, C. Galiotis, Progress in Polymer Science 35 (2010) 357–401.

[132] J. Li, T. Yin, W. Qin, Sensors and Actuators B: Chemical 239 (2017) 438–446.

[133] M. Pięk, R. Piech, B. Paczosa-Bator, Electrochimica Acta 210 (2016) 407–414.

[134] A. Rzewuska, M. Wojciechowski, E. Bulska, E.A.H. Hall, K. Maksymiuk, A. Michalska, Analytical Chemistry 80 (2008) 321–327.

[135] D. Kałuza, E. Jaworska, M. Mazur, K. Maksymiuk, A. Michalska, Analytical Chemistry 91 (2019) 9010–9017.

[136] G.D. O'Neil, R. Buiculescu, S.P. Kounaves, N.A. Chaniotakis, Analytical Chemistry 83 (2011) 5749–5753.

[137] R.P. Buck, E. Lindner, Pure and Applied Chemistry 66 (1994) 2527–2536.

[138] E. Bakker, E. Pretsch, P. Bühlmann, Analytical Chemistry 72 (2000) 1127–1133.

[139] J. Veder, R. De Marco, G. Clarke, R. Chester, A. Nelson, K. Prince, E. Pretsch, E. Bakker, Anal Chem 80 (2008) 6731–6740.

[140] M. Fibbioli, W.E. Morf, M. Badertscher, N.F. De Rooij, E. Pretsch, Electroanalysis 12 (2000) 1286–1292.

[141] Z. Pławińska, A. Michalska, K. Maksymiuk, Electrochimica Acta 187 (2016) 397–405.

[142] E. Bakker, E. Pretsch, Trends in Analytical Chemistry 24 (2005) 199–207.

[143] J. Bobacka, A. Lewenstam, A. Ivaska, Journal of Electroanalytical Chemistry 509 (2001) 27–30.

[144] I.I. Suni, Trends in Analytical Chemistry 27 (2008) 604–611.

[145] F. Zaïbi, I. Slama, C. Okolie, J. Deshmukh, L. Hawco, M. Mastouri, C. Bennett, M. Mkandawire, R. Chtourou, Colloids and Surfaces A: Physicochemical and Engineering Aspects 589 (2020) 124450.

[146] L. Guagneli, Z. Mousavi, T. Sokalski, I. Leito, J. Bobacka, Journal of Electroanalytical Chemistry 923 (2022) 116785.

[147] E. Barsoukov, J.R. Macdonald, Impedance Spectroscopy. Theory, Experiment, and Applications, 2005.

[148] A. Radu, S. Anastasova-Ivanova, B. Paczosa-Bator, M. Danielewski, J. Bobacka, A. Lewenstam, D. Diamond, Analytical Methods 2 (2010) 1490–1498.

[149] K. Tóth, E. Gráf, G. Horvai, E. Pungor, R.P. Buck, Analytical Chemistry 58 (1986) 2741–2744.

[150] https://www.sigmaaldrich.com/PL/pl/product/sial/07295 (01.12.2022).

[151] https://www.sigmaaldrich.com/deepweb/assets/sigmaaldrich/product/documents/984/221/91664.pdf (01.12.2022).

[152] N.T. Garland, E.S. McLamore, N.D. Cavallaro, D. Mendivelso-Perez, E.A. Smith, D. Jing, J.C. Claussen, ACS Applied Materials and Interfaces 10 (2018) 39124–39133.

[153] D. Yuan, A.H.C. Anthis, M. Ghahraman Afshar, N. Pankratova, M. Cuartero, G.A. Crespo, E. Bakker, Analytical Chemistry 87 (2015) 8640–8645.

[154] W. Tang, J. Ping, K. Fan, Y. Wang, X. Luo, Y. Ying, J. Wu, Q. Zhou, Electrochimica Acta 81 (2012) 186–190.

[155] B. Paczosa-Bator, L. Cabaj, R. Piech, K. Skupień, Analytical Chemistry 85 (2013) 10255–10261.

[156] M.A. Ali, X. Wang, Y. Chen, Y. Jiao, N.K. Mahal, S. Moru, M.J. Castellano, J.C. Schnable, P.S. Schnable, L. Dong, ACS Applied Materials and Interfaces 11 (2019) 29195–29206.

[157] G.A. Álvarez-Romero, M.E. Palomar-Pardavé, M.T. Ramírez-Silva, Analytical and Bioanalytical Chemistry 387 (2007) 1533–1541.

[158] C. Wardak, Electroanalysis 26 (2014) 864–872.

[159] M. Pięk, R. Piech, B. Paczosa-Bator, Journal of the Electrochemical Society 165 (2018) B60–B65.

[160] https://www.mt.com/pl/pl/home/products/Laboratory_Analytics_Browse/pH-meter/sensor/ion-selective-electrode/DX262-NO3-Half-Cell.html (03.12.2022).

[161] https://www.conatex.pl/catalog/cyfrowe_wykonywanie_doswiadczen/czujniki/czujniki_chemia_klimat_pogoda/product-elektroda_jonoselektywna_azotanowa/sku-1184013#.Yx7sBHZBxPY (03.12.2022).

[162] https://www.hanna-polska.com/jonoselektywnosc/3925-elektroda-pojedyncza-azotanowa.html (03.12.2022).

[163] https://www.vernier.com/manuals/gdx-no3/ (03.12.2022).

[164] https://www.ntsensors.com/product/ise-nitrate-electrode/ (03.12.2022).

[165] V.K. Gupta, R.N. Goyal, R.A. Sharma, Electrochimica Acta 54 (2009) 4216–4222.

[166] T. Alizadeh, F. Rafiei, M. Akhoundian, Talanta 237 (2022) 122895.

[167] V.A. Nazarov, M.G. Taryba, E.A. Zdrachek, K.A. Andronchyk, V. V. Egorov, S. V. Lamaka, Journal of Electroanalytical Chemistry 706 (2013) 13–24.

[168] W. Kim, D.D. Sung, G.S. Cha, S.B. Park, Analyst 123 (1998) 379–382.

[169] A. Legin, S. Makarychev-Mikhailov, D. Kirsanov, J. Mortensen, Y. Vlasov, Analytica Chimica Acta 514 (2004) 107–113.

[170] A.M. Pimenta, A.N. Araújo, M.C.B.S.M. Montenegro, C. Pasquini, J.J.R. Rohwedder, I.M. Raimundo, Journal of Pharmaceutical and Biomedical Analysis 36 (2004) 49–55.

[171] S. Oka, Y. Sibazaki, S. Tahara, Analytical Chemistry 53 (1981) 588–593.

[172] https://www.elmetron.com.pl/ECl-01-eng.html (04.12.2022).

[173] https://www.hannainst.com/hi4107-chloride-combination-ion-selective-electrode.html (04.12.2022).

[174]   https://www.vernier.com/product/chloride-ion-selective-electrode/ (04.12.2022).

[175]   https://www.thermofisher.com/order/catalog/product/9417SC (04.12.2022).

[176]   A. Birinci, H. Eren, F. Coldur, E. Coskun, M. Andac, Journal of Food and Drug Analysis 24 (2016) 485–492.

[177]   K.R. Bandi, A.K. Singh, A. Upadhyay, Materials Science and Engineering C 34 (2014) 149–157.

[178]   V.K. Gupta, R. Prasad, A. Kumar, Journal of Applied Electrochemistry 33 (2003) 381–386.

[179]   V.K. Gupta, R. Prasad, A. Kumar, Talanta 60 (2003) 149–160.

[180]   L.P. Singh, J.M. Bhatnagar, Talanta 64 (2004) 313–319.

[181]   H.A. Zamani, G. Rajabzadeh, A. Firouz, A.A. Ariaii-Rad, Journal of the Brazilian Chemical Society 16 (2005) 1061–1067.

[182]   C. Wardak, J. Lenik, Sensors and Actuators B: Chemical 189 (2013) 52–59.

[183]   M.D. Tutulea-Anastasiu, D. Wilson, M. del Valle, C.M. Schreiner, I. Cretescu, Sensors (Switzerland) 13 (2013) 4367–4377.

[184]   https://www.mt.com/pl/pl/home/products/Laboratory_Analytics_Browse/pH-meter/sensor/ion-selective-electrode/DX264-Cu-Half-Cell.html (04.12.2022).

[185]   https://www.ntsensors.com/product/ise-copper-electrode/ (04.12.2022).

[186]   Y. V. Petrov, V.A. Khokhlov, V. V. Zhakhovsky, N.A. Inogamov, Journal of Physics: Conference Series 1556 (2020) 012002.

[187]   Y. Monsa, G. Gal, N. Lerner, I. Bar, Nanotechnology 31 (2020) 235601.

[188]   V. Amendola, M. Meneghetti, Physical Chemistry Chemical Physics 11 (2009) 3805–3821.

[189]   M.F. Becker, J.R. Brock, H. Cai, D.E. Henneke, J.W. Keto, J. Lee, W.T. Nichols, H.D. Glicksman, Nanostructured Materials 10 (1998) 853–863.

[190]   F. Mafuné, J.Y. Kohno, Y. Takeda, T. Kondow, H. Sawabe, Journal of Physical Chemistry B 104 (2000) 9111–9117.

[191]   F. Mafune, J. Kohno, Y. Takeda, T. Kondow, Journal of Physical Chemistry B 105 (2001) 5114–5120.

[192]   F. Mafuné, J.Y. Kohno, Y. Takeda, T. Kondow, Journal of Physical Chemistry B 107 (2003) 4218–4223.

[193]   A.J. Mulder, R.D. Tilbury, P.J. Wright, T. Becker, M. Massi, M.A. Buntine, Australian Journal of Chemistry 70 (2017) 1212–1218.

[194]   A.A. Hadi, B.A. Badr, R.O. Mahdi, K.S. Khashan, Optik 219 (2020) 165019.

[195]   A. V. Simakin, I. V. Baimler, O. V. Uvarov, I.I. Rakov, S. V. Gudkov, IOP Conference Series: Materials Science and Engineering 921 (2020) 012024.

[196]   G. Vardar, M. Altikatoı̇lu, D. Ortaç, M. Cemek, I. Işildak, Biotechnology and Applied Biochemistry 62 (2015) 663–668.

[197]   Z. Mousavi, J. Bobacka, A. Lewenstam, A. Ivaska, Journal of Electroanalytical Chemistry 633 (2009) 246–252.

[198]   K. Yu, N. He, N. Kumar, N.X. Wang, J. Bobacka, A. Ivaska, Electrochimica Acta 228 (2017) 66–75.

[199]   X. Zeng, W. Qin, Analytica Chimica Acta 982 (2017) 72–77.

[200]   Q. An, L. Jiao, F. Jia, J. Ye, F. Li, S. Gan, Q. Zhang, A. Ivaska, L. Niu, Journal of Electroanalytical Chemistry 781 (2016) 272–277.

[201]   T.N.T. Tran, S. Qiu, H.J. Chung, IEEE Sensors Journal 18 (2018) 9081–9087.

[202] I. Ivanko, T. Lindfors, R. Emanuelsson, M. Sjödin, Sensors and Actuators B: Chemical 329 (2021) 129231.

[203] T. Lindfors, H. Aarnio, A. Ivaska, Analytical Chemistry 79 (2007) 8571–8577.

[204] W.S. Han, Y.H. Lee, K.J. Jung, S.Y. Ly, T.K. Hong, M.H. Kim, Journal of Analytical Chemistry 63 (2008) 987–993.

[205]

https://www.mt.com/gb/en/home/products/Laboratory_Analytics_Browse/Product_Family_Browse_titrators_main/Product_Family_Titration_Sensors/Titration_Ion_Selective_sensors_Fami/Potassium_Electrode.html (05.12.2022).

[206] https://www.vernier.com/product/potassium-ion-selective-electrode/ (05.12.2022).

[207] https://www.pasco.com/products/sensors/wireless/ps-3520 (05.12.2022).

[208] https://www.ntsensors.com/product/ise-potassium-electrode/ (05.12.2022).

[209] I.H.A. Badr, W.I. Zidan, Z.F. Akl, Talanta 118 (2014) 147–155.

[210] D.L. Manning, J.R. Stokely, D.W. Magouyrk, Analytical Chemistry 46 (1974) 1116–1119.

[211] M. Shamsipur, F. Mizani, M.F. Mousavi, N. Alizadeh, K. Alizadeh, H. Eshghi, H. Karami, Analytica Chimica Acta 589 (2007) 22–32.

[212] M.B. Saleh, S.S.M. Hassan, A.A. Abdel, N.A. Abdel, Sensors and Actuators B 94 (2003) 140–144.

[213] M. Shamsipur, F. Mizani, K. Alizadeh, M.F. Mousavi, V. Lippolis, A. Garau, C. Caltagirone, Sensors and Actuators B: Chemical 130 (2008) 300–309.

[214] A. Shokrollahi, M. Ghaedi, M. Montazerozohori, N. Khanjari, M. Najibzadeh, Journal of the Chinese Chemical Society 56 (2009) 812–821.

[215] M. Ghanbari, G.H. Rounaghi, N. Ashraf, International Journal of Environmental Analytical Chemistry 97 (2017) 189–200.

[216] M.B. Saleh, E.M. Soliman, A.A.A. Gaber, S.A. Ahmed, Sensors and Actuators B 114 (2006) 199–205.

[217] S.S.M. Hassan, M.M. Ali, A.M.Y. Attawiya, Talanta 54 (2001) 1153–1161.

[218] M.A. Abu-Dalo, N.A.F. Al-Rawashdeh, I.R. Al-Mheidat, N.S. Nassory, IOP Conference Series: Materials Science and Engineering 92 (2015).

[219] M.A. Abu-Dalo, N.A.F. Al-Rawashdeh, I.R. Al-Mheidat, N.S. Nassory, Sensors and Actuators, B: Chemical 227 (2016) 336–345.

[220] A. Florido, I. Casas, J. García-Raurich, R. Arad-Yellin, A. Warshawsky, Analytical Chemistry 72 (2000) 1604–1610.

[221] I. Goldberg, D. Meyerstein, Analytical Chemistry 52 (1980) 2105–2108.

[222] D.M. Duncan, J.S. Cockayne, Sensors and Actuators, B: Chemical 73 (2001) 228–235.

[223] W.I. Zidan, I.H.A. Badr, Z.F. Akl, Journal of Radioanalytical and Nuclear Chemistry 303 (2015) 469–477.

D1

SOLID CONTACT NITRATE ION-SELECTIVE ELECTRODE BASED ON COBALT(II) COMPLEX WITH 4,7-DIPHENYL-1,10-PHENANTHROLINE

Solid Contact Nitrate Ion-selective Electrode Based on Cobalt(II) Complex with 4,7-Diphenyl-1,10-phenanthroline

Karolina Pietrzak,[a] Cecylia Wardak,*[a] and Renata Łyszczek[b]

Abstract: Nitrates are a group of compounds widely distributed in the natural environment with many applications in various industries. Due to their ambiguous impact on the human body and suspicions of their carcinogenic activity, they have been very popular for decades and are the subject of research by many scientists in the field of medicine, biology and chemistry. Due to the need to monitor their content in environmental and food samples, various methods for their determination are developed. This paper proposes the use of a nitrate ion-sensitive ion selective electrode with a membrane containing as the active ingredient a new cobalt(II) complex with 4,7-diphenyl-1,10-phenanthroline (Bphen) of the formula $Co(Bphen)_2(NO_3)_2(H_2O)_2$. The obtained sensor showed the theoretical slope of the characteristic curve, a wide measuring range, as well as short response time and very good potential stability. It was successfully used for the determination of nitrates in real samples: in mineral water, tap water and river water from eastern Poland.

Keywords: cobalt(II) complex with 4,7-diphenyl-1,10-phenanthroline · nitrates · solid contact · ion-selective · potentiometry

1 Introduction

Nitrates are widely distributed in nature, found in both surface and underground waters as well as in many plant species. They are used, inter alia, as preservatives in the production of food, for the production of glass and explosives and as inorganic fertilizers in agriculture [1]. Interestingly, the content of nitrates in plants grown outside, where they have direct access to natural sunlight, is much lower than in plants grown in greenhouses in cooler temperate zones [1]. Vegetables rich in nitrates include, root vegetables (celery, beets) and green vegetables (lettuce, spinach, arugula) [2]. The sources of human exposure to nitrates are rather exogenous. It results mainly from the consumption of raw vegetables (about 80 %) and drinking water (about 20 %). The rest is made up of cereals and animal products [3]. It is estimated that the consumption of nitrates in Europe ranges from 31 to 185 mg/day, while in the United States from about 40 to 100 mg/day, and their bioavailability in the diet is 100 % [4].

Unfortunately, many species are susceptible to nitrate poisoning, which can be reduced to much more toxic nitrites and ammonia [1]. Nitrites oxidizing iron ions in hemoglobin cause the formation of methemoglobin - unable to transport oxygen, causing hypoxia of the whole organism and the occurrence of cyanosis [1,5]. In the 1940s, it was found that infantile methaemoglobinaemia is caused by feeding infants with food, for the preparation of which was used water from local wells rich in nitrates. Later, it was examined that this disease is associated with water with a high content of nitrates contaminated by bacteria. Bacteria contamination contributes to an increased reduction of nitrates to nitrites [1]. In addition, it was found that nitrites have the potential to form nitros-

amines in the stomach, which can lead to gastric cancer [6]. Although the conducted epidemiological studies conducted on humans did not confirm these assumptions [1], in the case of animal studies, it has been clearly stated that nitrosamines cause cancer in animals. The adverse health effects attributed to nitrates and nitrites are probably due to many factors, such as their amount consumed with food along with the components of the food matrix [2]. Due to the concerns of the government and the population related to nitrates and their impact on the environment and living organisms, for decades it has been aimed at reducing the concentration of these compounds in food and water [1]. Therefore, it is important to control the nitrate concentration in drinking water and food.

Due to ambiguous views on the influence of nitrates and nitrites on the human body, for several decades there has been a lot of research on living organisms, including humans, to better understand the metabolism of nitrates, nitrates and their metabolites on the body [7], content in food products [8–10] and human consumption in various places around the world. In the literature there are also many reviews on this topic [1,2,4]. Nitrates in food

[a] K. Pietrzak, C. Wardak
Maria Curie-Sklodowska University, Faculty of Chemistry, Department of Analytical Chemistry and Instrumental Analysis, Marie Curie-Sklodowska Square 3, 20-031 Lublin, Poland
E-mail: cecylia.wardak@poczta.umcs.lublin.pl
[b] R. Łyszczek
Maria Curie-Sklodowska University, Faculty of Chemistry, Department of General and Coordination Chemistry, Marie Curie-Sklodowska Square 2, 20-031 Lublin, Poland

str. 75

products and environmental samples have so far been measured using a variety of methods: capillary electrophoresis [11,12], chemiluminescence [13], colorimetric method [14], electrochemical methods [15–19], ion chromatographic method [20], high performance liquid chromatography [21], spectrophotometric methods [22,23], spectrofluorometric metod [24], electrothermal atomic absorption spectrometry [25].

Among the electrochemical methods, potentiometric methods using ion-selective electrodes are a popular method of determining the nitrate content in samples. Potentiometry owes its popularity to, among other things, short times and low costs of analysis as well as convenient and simple equipment. In addition, it is not a destructive method, nor does it require a complicated process of preparing a test sample [15]. Ion-selective electrodes are cheap and simple analytical devices that have been successfully used to monitor many ionic types in aqueous solutions [26]. They can be used both in laboratory conditions and directly in field conditions. In environmental on-line measurements, ion-selective electrodes with solid contact are particularly useful, which are more mechanically resistant than their classic antecedents containing internal electrolyte and there is a greater possibility of modifying the shape and miniaturization of sensors. In addition, they can operate in any position and configuration, are easy to store and transport [27].

The presented article describes the process of production and testing of the properties of a new nitrate sensitive ion-selective electrode based on the use of the newly obtained cobalt(II) complex with 4,7-diphenyl-1,10-phenanthroline (Bphen) of the formula $Co(Bphen)_2(NO_3)_2$ $(H_2O)_2$ as the active ingredient of the membrane. The ISEs were produced in solid contact mode using, Ag/AgCl electrode as inner electrode and ammonium or phosphonium chlorides as transducer media and ionic additives. They were characterized, among others, by the theoretical inclination of the calibration curve of the sensor, a wide measuring range, as well as very good potential stability and short response time. Their usefulness and effectiveness were verified in the direct determination of the nitrate content in real samples: in mineral water, tap water and river water from eastern Poland.

2 Experimental

2.1 Reagents

The main reagents and suppliers were: Cobal(II) nitrate hexahydrate, 4,7-diphenyl-1,10-phenanthroline(Bphen), and tetraoctylamonium chloride (TOACl) were purchased from Sigma-Aldrich, trihexyltetradecylphosphonium chloride (THTDPCl) Aldrich (Canada), 2-nitrophenyl octyl ether (NPOE) Fluka (Switzerland), polyvinyl chloride (PVC) Aldrich (Milwaukee, WI, USA. Other reagents were purchased from Fluka (Switzerland). The aqueous solutions were prepared using freshly deionized

water and pure pro-analysis salts of the highest purity available.

2.2 Active Complex- Synthesis and Methods its Characterization

The complex of the general formula $Co(Bphen)_2(NO_3)_2$ $(H_2O)_2$ was obtained in the reaction of the aqueous solution of cobalt(II) nitrate (1 mmol) with 4,7-diphenyl-1,10-phenanthroline (3 mmol) dissolved in 20 mL of ethanol. Obtained solution was stirred and heated at 70 °C during 2 h and then slowly cooled to room temperature. Precipitated compound was filtered off, washed with small amount of water and dried in air.

Thermal analysis of the obtained complex was carried out by the TG and DSC methods using the SETSYS 16/18 analyser (Setaram). The sample (7 mg) was heated in alumina crucible up to 1000 °C at a heating rate of $10 °C min^{-1}$ in dynamic air atmosphere ($v = 0.75 dm^3 h^{-1}$). The TG-FTIR measurement was performed on the Q5000 (TA Instruments) apparatus coupled with the Nicolet 6700 (Thermo Scientific) spectrophotometer. The sample of 30 mg was heated in platinum crucible up to 700 °C at a heating rate $20 °C min^{-1}$ in flowing nitrogen atmosphere ($25 cm^3 min^{-1}$).

The composition and thermal stability of $Co(Bphen)_2$ $(NO_3)_2(H_2O)_2$ complex were determined by the thermogravimetry (TG) and differential scanning calorimetry (DSC) methods in air atmosphere. Volatile products of thermal decomposition of complex were investigated by coupled TG-FTIR (Thermogravimetric analysis-Fourier Transform Infrared Spectroscopy) method.

The Attenuated Total Reflection-Fourier Transform Infrared Spectroscopy (ATR-FTIR) spectra of free 4,7-diphenyl-1,10-phenanthroline and its cobalt(II) complex were recorded over the range $4000–600 cm^{-1}$ using a Nicolette 6700 spectrophotometer equipped with an universal ATR attachment with a diamond crystal.

2.3 ISE Membrane Composition

Quantitative and qualitative composition of electrode membrane is as follows, for ISE-1, 1 % complex, 33 % PVC, 66 % NPOE; for ISE-2, 1 % complex, 1 % THTDPCl, 33 % PVC, 65 % NPOE; for ISE-3, 1 % complex, 1 % TOACl, 33 % PVC, 65 % NPOE; for ISE-4, 2 % complex, 1 % THTDPCl, 33 % PVC, 64 % NPOE; for ISE-5, 2 % complex, 2 % THTDPCl, 33 % PVC, 63 % NPOE; for ISE-6, 1 % THTDPCl, 33 % PVC, 66 % NPOE; for ISE-7, 33 % PVC, 67 % NPOE.

2.4 Preparation of the Electrode

An internal Ag/AgCl electrode was prepared in the following manner: a clean silver wire skimmed with acetone was anodized electrochemically for 2 min in $4 mol L^{-1}$ HCl using voltage source of 5 V (KABiD-PRESS, Poland) forming an Ag/AgCl electrode. The next

str. 76

step was to rinse the electrode with water and dry it with tissue paper. Subsequently the electrode was immersed in the solution of sodium chloride overnight. Next day it was mounted in a previously prepared Teflon holder. The components of the membrane mixture were weighed, mixed thoroughly and homogenized using an ultrasonic bath and deaerated using a vacuum pump. Then the Teflon holder was filled with the membrane mixture so that the silver–silver chloride electrode was immersed in it. The sensor casing thus prepared was then gelled at 90 °C for about 5 minutes. Every time before measurements the electrode was conditioned in appropriate solution, which was the 1×10^{-3} mol L^{-1} NaNO$_3$ solution for an hour.

2.5 Electrochemical Measurements

2.5.1 The Measurement of the Electromotive Force

Potentiometric measurements of electromotive force (EMF) were performed in an electrochemical cell with an ion-selective electrode sensitive to nitrate ions (NO$_3$- SCISE) as an electrode working against a silver-chloride electrode (Metrohm 6.0750.100) as a reference electrode in solutions mixed with a magnetic stirrer at room temperature using a 16-channel data acquisition system (Lawson Labs. USA) coupled with a computer. An Orion 81-72 glass electrode and a multifunction computer meter CX-741 (Zabrze Mikulczyce Poland) were used for pH measurement.

2.5.2 Electrochemical Impedance Spectroscopy Measurements

Electrochemical impedance spectroscopy measurements (EIS) were carried out using an AUTOLAB electrochemical analyzer (Eco Chemie, Netherlands) controlled by NOVA software. The conventional three-electrode system was used where, the studied electrode was connected as the working electrode, Ag/AgCl (3 M KCl) was the reference electrode and the auxiliary electrode was a platinum wire. The impedance spectra were recorded in the frequency range 0.1–100 kHz et the open circuit potential with an amplitude 10 mV.

3 Results and Discussion

In this study, for the first time a new cobalt(II) complex with 4,7-diphenyl-1,10-phenanthroline (Bphen) as organic ligand was used as an active substance in an ion-selective PVC membrane sensitive to nitrate ions. The obtained electrodes have been widely studied. Many measurements were made, among others: slope and linearity range of the electrode characteristic curve as well as the limit of detection. The pH range in which the potential of the electrode does not depend on pH and potential stability, reversibility and reproducibility were also determined.

3.1 Study of Active Complex Structure

3.1.1 Infrared Analysis

The ATR-FTIR spectra of free ligand and cobalt(II) complex were recorded due to confirmation of coordination process by organic ligand as well as confirmation of nitrate moieties presence as counter ions in the structure of complex.

Both infrared spectra exhibit characteristic double bands at about 3050 and 3040 cm^{-1} assigned to stretching vibrations of CH groups from aromatic rings. ATR-FTIR spectra of ligand and complex show bands at 1608, 1571, 1507, 1488 and 1412 cm^{-1} due to $v(CC)$ and $v(CN)$ ring modes. The bands at about 1555 cm^{-1} can be ascribed to the phenyl substituents [28]. It is worth to mention that in the spectrum of complex besides vibration at 1607 cm^{-1} also bands at 1610 and 1604 cm^{-1} are observed most probably due to coordination of metal centre. The ATR-FTIR spectrum of complex exhibits also broad band with maximum at 1292 cm^{-1}, weak band at 830 cm^{-1} and those at 738 cm^{-1} characteristic for bidentate or bridging nitrate groups [29,30].

3.1.2 Thermal Analysis TG-DSC and TG-FTIR

The investigated complex is thermally stable up to 40 °C. Further heating leads to the weight loss of 3.95 % due to releases of two water molecules (calc. mass loss of 4.07 %). Dehydration process takes place in the temperature range 40–135 °C. An anhydrous form of complex is stable up to 264 °C. Next mass loss of 11.42 % occurs in the temperature range 265–340 °C and corresponds to the oxidizing process of nitrate ions as can be assumed based on the exothermic effect observed on the DSC curve. The next distinct mass loss observed on the TG curve is associated with breaking of the Co–N bonds, partially sublimation and combustion of 4,7-diphenyl-1,10-phenanthroline ligands. These reactions occur in the temperature range 345–605 °C and very strong exothermic effects at DSC curve accompany them. The solid residue of cobalt complex heating in air is Co$_3$O$_4$ oxide which is formed at 620 °C.

In order to confirm composition of the obtained complex, thermogravimetric analysis (TG) coupled with Fourier transform infrared spectroscopy (FTIR) was also applied. TG-FTIR method allowed identifying volatile products of complex heating in nitrogen atmosphere. The FTIR spectra recorded up to about 150 °C show characteristic bands in the wavenumber ranges: 4000–3500 and 1800–1250 cm^{-1} assigned to the stretching and deformation vibrations of hydroxyl groups $v(O–H)$ from evolved water molecules (Figure 1).

The FTIR spectra recorded above 280 °C exhibit bands derived from gaseous products of thermal decomposition of complex as the consequence of disruption of cobalt-ligands bonds and decomposition of outer sphere ions. The characteristic bands in the region 2370–2300 cm^{-1} and those in the range 750–600 cm^{-1} are due to stretching and
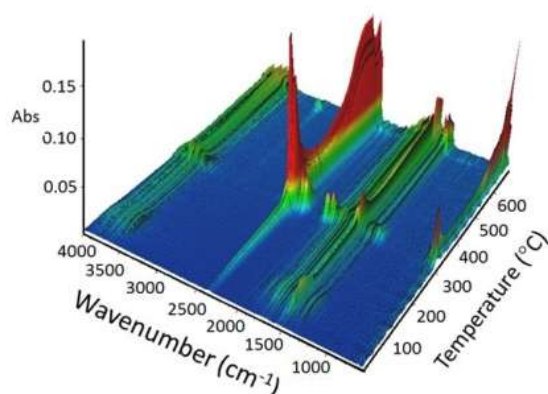
str. 77

Fig. 1. Stacked plot of the FTIR spectra of the evolved gases for $Co(Bphen)_2(NO_3)_2(H_2O)_2$.

deformation vibrations of carbon dioxide molecules [31]. Decomposition of nitrate ions in nitrogen atmosphere led to the evolution of dinitrogen molecules which give characteristic double bands at 2238, 2203 cm^{-1} and those at 1313, 1266 cm^{-1}. Besides N_2O molecules also NO is formed due to nitrate ions degradation. It gives bands at 1923 and 1843 cm^{-1} [32]. Above 600 °C decomposition of solid residue occurs. Among gaseous products of complex, carbon monoxide, some hydrocarbons and ammonia molecules are released as products of 4,7-diphenyl-1,10-phenanthroline degradation. Vibrations of CO molecules give double-band in the range 2250–2050 cm^{-1}. The absorption peaks in the range 3150–3000 cm^{-1} and those at 1569 cm^{-1} are indicative for stretching C–H and C–C vibrations of some aromatic hydrocarbons. Ammonia molecules derived from decomposition of phenanthroline moieties give characteristic double-bands at 965 and 930 cm^{-1} [31].

3.1.3 Proposed Structure of Complex

Active complex of the formula $Co(Bphen)_2(NO_3)_2(H_2O)_2$ was prepared in the reaction of cobalt(II) nitrate and 4,7-diphenyl-1,10-phenanthroline (Bphen). Because compound was obtained in the form of unsuitable for single crystal X-ray measurements, its structure was proposed based on the spectroscopic and thermal investigations. The 4,7-diphenyl-1,10-phenanthroline used to forms with divalent transition metals mononuclear complexes with octahedral coordination environments of central atom [33]. Each Bphen ligand binds metal center through both nitrogen atoms. When three phenanthroline molecules are coordinated by central atom, all sites around metal are occupied by nitrogen atoms from ligands. When only two phenanthroline molecules are bonded, two remaining sites in coordination environment of Co(II) ion can be filled by solvent molecules or counterion ligands. Pro-

posed by us structure of obtained complex was given in Figure 2. We have taken into account coordination abilities of nitrate ions which can also forms coordination bonds with metal centers [29,30,32]. Presence of water molecules in the structure of complex was confirmed by TG-DSC and TG-FTIR methods. Release of water molecules at low temperature is indicative for weak bonding of solvent molecules. This fact denotes that H_2O molecules appear in outer coordination sphere of Co(II) ion. Other structures of active complex are also possible.

3.2 Potentiometric Response

The potentiometric response of the tested electrode was determined in $NaNO_3$ solutions with a concentration of $1 \times 10^{-1}–1 \times 10^{-6}$ mol L^{-1} by measuring the EMF of the cell made of the tested ion-selective electrode and the reference electrode. All fabricated sensors exhibited sensitivity to nitrate ions but the slope of calibration curves were different for particular electrodes. The ISE-1 with the simplest composition of membrane (only 1 % Co $(Bphen)_2(NO_3)_2(H_2O)_2$ complex, plasticizer and PVC) gave a linear response in the activity range $5 \times 10^{-5}–1 \times 10^{-1}$ mol L^{-1} with the slope of −49.1 mV/decade. This indicates that presence of active complex in the polymeric membrane brings its nitrate sensitivity. Enhanced response was observed for electrodes containing additionally ion-exchanger in the membrane. ISE-2 and ISE-3 whose membranes were doped with THTDPCl and TOACl, respectively, exhibited a linear response in the activity range $1 \times 10^{-5}–1 \times 10^{-1}$ mol L^{-1}. The slopes of the calibration curves in that range were −56.3 and −54.7 mV/decade for ISE-2 and ISE-3, respectively. A further increase of the content of active complex and THTDPCl in the membrane did not cause change in the electrode response. For ISE-4 containing 2 % (w/w) of active complex and 1 % (w/w) THTDPCl similar response to those exhibited by ISE-2 was observed. The same situation was in the case of ISE-5 having 2 % (w/w) both components. It is worth to note that ISE-6 which membrane contained only 1 % THTDPCl and without
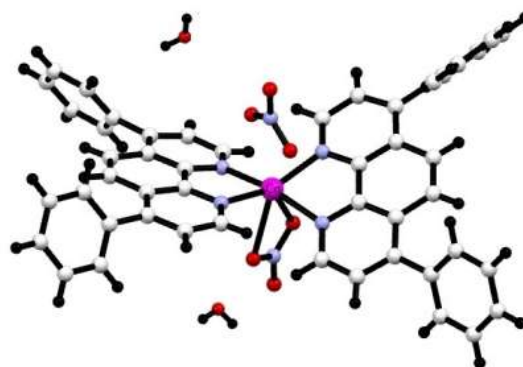

Fig. 2. Possible structure of $Co(Bphen)_2(NO_3)_2(H_2O)_2$ complex.

str. 78

active complex exhibited the poorest anionic response. Calibration curve obtained for this electrode was linear in the activity range $1 \times 10^{-4} - 1 \times 10^{-1}$ mol L^{-1} with the slope of -44.2 mV/decade. Different behaviour shoved ISE-7 with blank membrane without active complex and ionic additive. The potentiometric response of this electrode determined in NaNO$_3$ solution exhibited poor cationic sensitivity (slope was 25 mV/decade). Mentioned above facts confirm primary function of active complex in the membrane potential formation which resulted in nitrate sensitivity. Thus on the basis of the obtained results ISE-2 which exhibited good response and is the cheapest due to lower content of the active complex and ionic additive was chosen for further studies. The calibration curve obtained for this electrode is shown in Figure 3 and its analytical parameters are listed in Table 1.

3.3 Dependence of EMF on pH

Working pH range, in which the potential of the electrodes does not depend on the pH of the sample solution was determined in the pH range of 2.5–11.0 in 1×10^{-3} mol L^{-1} NaNO$_3$ solution, to which H$_2$SO$_4$ and NaOH solution was added in portions. The dependence of the potential of the tested electrodes on the pH of the sample is shown in Figure 4 where it can be seen that optimal pH range for potential measurements is 5.4–10.6. Beyond this range gradual potential change was observed. Probably it was caused by active complex decomposition in lower pH values.

3.4 Potential Stability and Reproducibility

The electrode potential stability and reproducibility was tested for four the same sensors over a period of 3 months in a 0.1 mol L^{-1} nitrate solution. The potential values were read after one hour of soaking the electrodes with the solution. The results of these measurements are shown in Figure 5. During the examined period (90 days), the potential values did not change much and electrodes worked properly. The determined potential drift value was approximately 0.09 mV/day. The reproducibility of the electrode potential was also tested in the concentration range from 1×10^{-6} mol L^{-1} to 1×10^{-1} mol L^{-1} NaNO$_3$. The standard deviation in the potential measurements for the same four ISE-2 was 2.1 mV in the solution 1×10^{-6} mol L^{-1} and 1.0 mV in the solution 1×10^{-5} mol L^{-1}. In higher concentrations it was smaller and ranged from 0.38 to 0.30 mV.

Fig. 3. Calibration curve of proposed NO$_3$-SCISE (ISE-2) after 60 min. conditioning in 1×10^{-3} mol L^{-1} NaNO$_3$ solution.

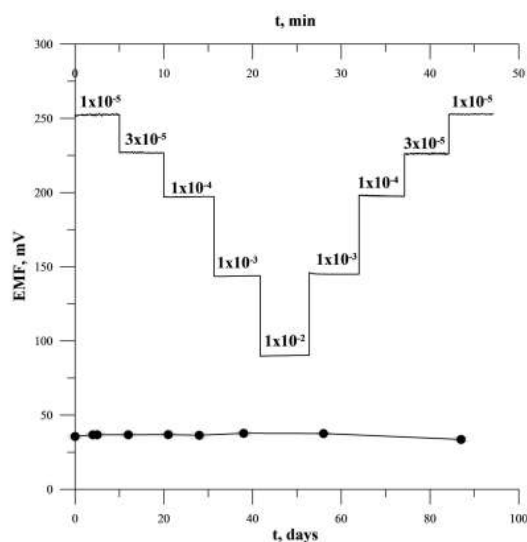Fig. 4. Effect of pH on the electrode response.

Fig. 5. Potential stability and reversibility.

str. 79

3.5 Reversibility of the Electrode Potential

In order to determine the reversibility of the electrode potential, measurements were made at various concentrations of nitrate ions with increasing concentrations (1×10^{-5}, 3×10^{-5}, 1×10^{-4}, 1×10^{-3} and 1×10^{-2} mol L^{-1}), followed by a decrease in concentrations. The results obtained are shown in Figure 5 where it can be seen that the electrode potential was fully reversible.

3.6 Electrochemical Impedance Spectroscopy

The impedance measurements allowed to determine electrical parameters of studied electrode. They were carried out in 1×10^{-2} mol L^{-1} NaNO$_3$ solution for fully conditioned electrode. The exemplary impedance spectrum of ISE-2 is presented in Figure 6. As it can be seen it showed high-frequency semicircle related to the bulk membrane resistance (R_b) and its geometric capacitance (C_g) and low frequency part connected to the diffusion processes in the polymeric membrane as well as to the interfacial charge transfer from the inner electrode/ion-selective membrane interface and from the polymeric membrane/solution interface. The bulk membrane resistance and geometric capacitance determined rom the analysis of high-frequency semicircle were 38 kΩ and 4.8 pF, respectively. In the range of low frequencies, the dependence $Z'' = f(Z')$ becomes rectilinear with the slope close to 45°. It is associated with Warburg impedance and indicates that impedance response is controlled by diffusion processes [34]. The low frequency branch of impedance spectrum is relatively low so it seems that charge transfer between membrane and inner electrode is not blocked. It is in good agreement with observed high potential stability and reproducibility of the electrode.
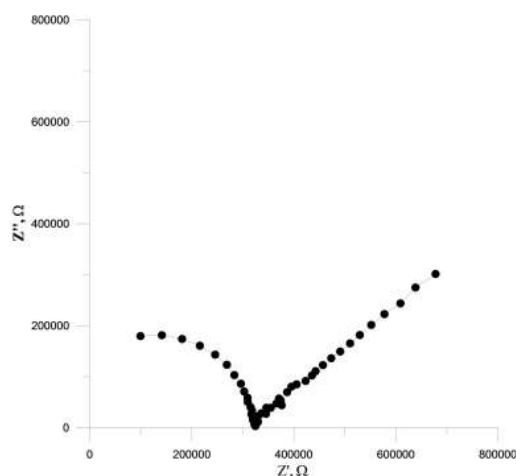
Fig. 6. Impedance spectrum of ISE-2 determined in 0.01 mol L^{-1} NaNO$_3$. The spectrum was recorded at the open circuit potential in the frequency range 0.1 Hz–100 kHz.

3.7 Selectivity

The selectivity of the tested electrodes was estimated by determining the selectivity coefficients in relation to the interfering ions. Selectivity coefficients were determined by means of separate solutions (extrapolating the response curves to $a_i = a_j = 1$ mol L^{-1}). The values of selectivity coefficients obtained for ISE-2 and ISE-6 are listed in Table 2. The proposed ISE-2 was very selective to nitrate ions over majority interfering ions. In comparison with the ISE-6 which membrane does not contain active complex ISE-2 exhibited improved selectivity in relation to almost all interfering ions. Such selectivity improvement was obtained due to the presence of active cobalt complex in the membrane of ISE-2. In the all cases the most interfering ions were perchlorate and thiocyanate. These ions are highly lipophilic and they exhibit high

Table 1. Analytical parameters of proposed NO$_3$-SCISE.

Parameter	ISE-2
Slope of the characteristic mV/pa$_{NO3-}$	−56.34
Limit of detection, mol L^{-1}	3.98×10^{-6}
Measurement range, mol L^{-1}	1.0×10^{-5}–1.0×10^{-1}
pH range, pH	5.4–10.6
Potential drift, mV/day	0.09

Table 2. Comparison of the selectivity coefficients values determined by SSM method for ISE-2 and ISE-6, respectively.

Ion	log K ISE-2	ISE-6
H$_2$PO$_4^-$	−5.1	−4.6
SO$_4^-$	−4.8	−4.5
CO$_3^-$	−4.9	−3.5
CH$_3$COO$^-$	−4.4	−3.1
F$^-$	−4.6	−3.5
Cl$^-$	−2.6	−2.0
NO$_2^-$	−2.1	−1.4
Br$^-$	−1.0	−0.7
SCN$^-$	2.1	2.3
ClO$_4^-$	3.3	3.5

Table 3. Determination of nitrates in various water samples (unspiked and spiked).

Sample	Nitrate found by NO$_3$-SCISE, mg L^{-1}[a]	Recovery, %
Tap water	9.11 ± 0.11	–
Tap water +49,60 mg L^{-1} NO$_3^-$	59.16 ± 0.64	100.89
Mineral water	1.49 ± 0.04	–
Mineral water +49,60 mg L^{-1} NO$_3^-$	50.04 ± 0.48	97.86
River water	11.89 ± 0.38	–
River water +49,60 mg L^{-1} NO$_3^-$	59.40 ± 1.80	95.77

[a] Results are based on five measurements.

str. 80

Table 4. Comparison of the proposed sensor with the recently developed nitrate solid contact electrodes and a commercial electrode with inner liquid contact.

Reference	Type of solid contact	Active membrane ingredient	Detection limit, mol L^{-1}	Linear range, mol L^{-1}	Slope, mV/decade	Working pH range, pH	Interfering ion with $K^{pot} \geq 1 \times 10^{-2}$
[36]	graphite powder	Ppy(NO_3^-)	5.4×10^{-5}	1.5×10^{-4}–1.0×10^{-1}	−57.1	4.3–7.4	ClO_4^-, SCN^-, Br^-, I^-, CN^-
[40]	graphite	TDMAN	3.0×10^{-5}	5.0×10^{-5}–1.0×10^{-1}	−57.9	nr	Cl^- (ClO_4^-, SCN^- Br^--nr)
[37]	MWCNTs	TDMAN	2.5×10^{-6}	3.2×10^{-6}–1.0×10^{-1}	−57.7		ClO_4^-, SCN^-, NO_2^-, Cl^-
[39]	TTF–TCNQ	Nitrate ionophore V	3.2×10^{-6}	1.0×10^{-5}–1.0×10^{-1}	−58.5	nr	NO_2^- (ClO_4^-, SCN^- Br^--nr)
[41]	Laser induced graphene	TDMAN	2.1×10^{-5}	5.0×10^{-5}–1.0×10^{-1}	−54.8	nr	nr
[42]	POT–MoS_2 nanocomposite	TDMAN	9.2×10^{-5}	7.1×10^{-4}–1.0×10^{-1}	−64.0	nr	nr
[35,43]	DX262 NO_3-ISE		3.0×10^{-5}	3.0×10^{-5}–1.0	−57.0	2–12	ClO_4^-, SCN^-, Br^-, I^-, CN^-, BF_4^-, salicylate
this work	Ag/AgCl/Cl^-	Co(Bphen)$_2$(NO_3)$_2$	3.98×10^{-6}	1.0×10^{-5}–1.0×10^{-1}	−56.3	5.4–10.6	ClO_4^-, SCN^-, Br^-

TTF–TCNQ – tetrathiafulvalene–tetracyanoquinodimethane; MWCNTs – miltiwalled carbon nanotubes; Ppy(NO_3^-) – polypyrolle doped with nitrate; TDMAN – tridodecylmethylaminium nitrate; DX262 NO_3-ISE – conventionalnitrate ISE offered by METTLER TOLEDO nr – not reported.

affinity to the polymeric membrane. Other nitrate ISEs both commercially available [35] and previously described in the literature [36–38] were also sensitive to these ions. Fortunately they are usually absent in the sample in which nitrate are determined including, natural waters, vegetables.

4 Determination of Nitrates in Real Samples

In order to check the suitability of the tested electrode for the determination of nitrates in real samples, measurements were made in tap water, mineral water and river water. Recovery was also examined. In the case of river water samples, the measurements were taken without mixing the sample during the measurement. The results obtained are presented below in Table 3 where it can be seen that good recoveries were obtained in all samples, what confirms the practical usefulness of proposed NO_3-SCISE.

5 Conclusion

As a result of the conducted research, an ion-selective nitrate electrode with good analytical parameters, simple in construction and operation, was obtained. A satisfactory slope of the electrode calibration curve was obtained, with a wide linear range of the calibration curve and low detection limit. The tested electrode is also characterized by a wide pH range and very good potential reproducibility and stability over time. In addition, the tested sensor has been successfully used to determine nitrate concentrations in various water samples. In Table 4 proposed electrode was compared with other previously reported nitrate ISEs with different solid contact as well a

commercially available electrode with internal electrolyte. As it can be seen the proposed electrode is superior to most of other sensors in relation to detection limit and linear range of calibration curve. Only the MWCNTs-based electrode [37] showed a slightly lower detection limit and wider measuring range while the TTF-TCN-based sensor [39] had these parameters similar to those of the proposed electrode. The advantage of the tested electrode is its very simple construction without an additional intermediate layer.

References

[1] G. M. McKnight, C. W. Duncan, C. Leifert, M. H. Golden, *Br. J. Nutr.* **2009**, *81*, 349.

[2] R. From, A. Ahluwalia, M. Gladwin, G. D. Coleman, N. Hord, G. Howard, D. B. Kim-shapiro, M. Lajous, F. J. Larsen, D. J. Lefer, *J. Am. Hear. Assoc.* **2016**, *5*, 1–10.

[3] G. Colla, H. Kim, M. C. Kyriacou, Y. Rouphael, *Sci. Hortic. (Amsterdam).* **2018**, *237*, 221–238.

[4] N. S. Bryan, J. L. Ivy, *Nutr. Res.* **2015**, *35*, 643–654.

[5] W. Bedale, J. J. Sindelar, A. L. Milkowski, *MESC.* **2016**, *120*, 85–92.

[6] N. S. Bryan, D. D. Alexander, J. R. Coughlin, A. L. Milkowski, P. Boffetta, *Food Chem. Toxicol.* **2012**, *50*, 3646–3665.

[7] A. S. Pannala, A. R. Mani, J. P. E. Spencer, V. Skinner, K. R. Bruckdorfer, K. P. Moore, C. A. Rice-Evans, *Free Radical Biol. Med.* **2003**, *34*, 576–584.

[8] M. Correia, Â. Barroso, M. F. Barroso, D. Soares, M. B. P. P. Oliveira, C. Delerue-Matos, *Food Chem.* **2010**, *120*, 960–966.

[9] Z. Ding, S. D. Johanningsmeier, R. Price, R. Reynolds, V. Truong, S. Conley, F. Breidt, *Food Control.* **2018**, *90*, 304–311.

[10] L. Chiesa, F. Arioli, R. Pavlovic, R. Villa, S. Panseri, *Food Chem.* **2019**, *288*, 361–367.

str. 81

[11] Y. Tanaka, N. Naruishi, H. Fukuya, J. Sakata, K. Saito, S. Wakida, *J. Chromatogr. A.* **2004**, *1051*, 193–197.

[12] N. Oztekin, M. S. Nutku, F. B. Erim, O. Nevin, *Food Chem.* **2002**, *76*, 103–106.

[13] D. He, Z. Zhang, Y. Huang, Y. Hu, *Food Chem.* **2007**, *101*, 667–672.

[14] D. C. Woollard, H. E. Indyk, *Int. Dairy J.* **2014**, *35*, 88–94.

[15] C. Wardak, M. Grabarczyk, *J. Environ. Sci. Heal. - Part B Pestic. Food Contam. Agric. Wastes.* **2016**, DOI: 10.1080/03601234.2016.1170545.

[16] J. Choosang, A. Numnuam, P. Thavarungkul, P. Kanatharana, T. Radu, S. Ullah, A. Radu, *Sensors (Switzerland).* **2018**, *18*, DOI: 10.3390/s18103555.

[17] E. Bomar, G. Owens, G. Murray, *Chemosensors.* **2017**, *5*, 2.

[18] F. Manea, A. Remes, C. Radovan, R. Pode, S. Picken, J. Schoonman, *Talanta.* **2010**, *83*, 66–71.

[19] F. Can, S. K. Ozoner, P. Ergenekon, E. Erhan, *Mater. Sci. Eng. C.* **2012**, *32*, 18–23.

[20] M. I. H. Helaleh, T. Korenaga, *J. Chromatogr. B Biomed. Sci. Appl.* **2000**, *744*, 433–437.

[21] V. Jedlickova, *J. Chromatogr. B.* **2002**, *780*, 193–197.

[22] R. Gürkan, N. Altunay, *J. Food Compos. Anal.* **2018**, *69*, 129–139.

[23] X. Yue, Z. Zhang, H. Yan, *Talanta.* **2004**, *62*, 97–101.

[24] S. Biswas, B. Chowdhury, B. C. Ray, *Talanta.* **2004**, *64*, 308–312.

[25] R. Roohparvar, T. Shamspur, A. Mostafavi, H. Bagheri, *Microchem. J.* **2018**, *142*, 135–139.

[26] E. Bakker, E. Pretsch, *TrAC Trends Anal. Chem.* **2005**, *24*, 199–207.

[27] K. Maksymiuk, A. Michalska, *Chemik.* **2015**, *69*, 373–382.

[28] N. Y. Mudasir, I. Hidenari, *Transit. Met. Chem.* **1999**, *24*, 210–217.

[29] M. R. Rosenthal, *J. Chem. Educ.* **1973**, *50*, 331–335.

[30] B. Cristóvão, J. Kłak, B. Miroslaw, *J. Coord. Chem.* **2014**, *67*, 2728–2746.

[31] R. Łyszczek, A. Bartyzel, H. Głuchowska, L. Mazur, M. Sztanke, K. Sztanke, *J. Anal. Appl. Pyrolysis.* **2018**, *135*, 141–151.

[32] B. Cristóvão, B. Miroslaw, A. Bartyzel, *Inorganica Chim. Acta.* **2017**, *466*, 160–165.

[33] F. H. Allen, *Acta Crystallogr.* **2002**, *B58*, 380–388.

[34] J. Bobacka, A. Lewenstam, A. Ivaska, *J. Electroanal. Chem.* **2000**, *489*, 17–27.

[35] Metter Toledo, Ion-Selective Electrodes.

[36] G. A. Álvarez-Romero, M. E. Palomar-Pardavé, M. T. Ramírez-Silva, *Anal. Bioanal. Chem.* **2007**, *387*, 1533–1541.

[37] D. Yuan, A. H. C. Anthis, M. G. Afshar, N. Pankratova, M. Cuartero, G. A. Crespo, E. Bakker, *Anal. Chem.* **2015**, *87*, 8640–8645.

[38] S. Yang, M. E. Meyerhoff, *Electroanalysis.* **2013**, *25*, 2579–2585.

[39] M. Piek, R. Piech, B. Paczosa-Bator, *J. Electrochem. Soc.* **2018**, *Vol.165*, B60–B65.

[40] W. Tang, J. Ping, K. Fan, Y. Wang, X. Luo, Y. Ying, J. Wu, Q. Zhou, *Electrochim. Acta.* **2012**, *81*, 186–190.

[41] N. T. Garland, E. S. McLamore, N. D. Cavallaro, D. Mendivelso-Perez, E. A. Smith, D. Jing, J. C. Claussen, *ACS Appl. Mater. Interfaces.* **2018**, *10*, 39124–39133.

[42] M. A. Ali, X. Wang, Y. Chen, Y. Jiao, N. K. Mahal, S. Moru, M. J. Castellano, J. C. Schnable, P. S. Schnable, L. Dong, *ACS Appl. Mater. Interfaces.* **2019**, DOI: 10.1021/acsami.9b07120.

[43] https://www.mt.com/pl/pl/home/products/Laboratory', access 16.09.2019.

str. 82

D2

COMPARATIVE STUDY OF NITRATE ALL SOLID STATE ION-SELECTIVE ELECTRODE BASED ON MULTIWALLED CARBON NANOTUBES-IONIC LIQUID NANOCOMPOSITE

Comparative study of nitrate all solid state ion-selective electrode based on multiwalled carbon nanotubes-ionic liquid nanocomposite

Karolina Pietrzak, Cecylia Wardak*

Maria Curie-Skłodowska University, Faculty of Chemistry, Institute of Chemical Sciences, Department of Analytical Chemistry, Marie Curie-Skłodowska Square 3, 20-031 Lublin, Poland

ABSTRACT

Carbon nanotubes have enjoyed unflagging popularity in recent years. They are successfully used in many fields of science, including potentiometry for the construction of ion selective electrodes with solid contact. A new type of SC-ISEs sensitive to nitrate(V) ions using multiwalled carbon nanotubes-ionic liquid nanocomposite was prepared. The effect of the kind of carbon nanotubes on the parameters of SC-ISEs was investigated. The study compares, among others, detection limits, sensitivity and linearity ranges of characteristic curves, and stability of the potential measured for the tested electrodes. Electrochemical impedance spectroscopy and chronopotentiometric techniques were also used as research methods. It was found that the type of carbon nanotubes included in the nanocomposite influences both the metrological and electrical parameters of the obtained solid contact nitrate ion-selective electrode.

1. Introduction

Ion-selective electrodes (ISEs) belong to the group of the most popular potentiometric sensors, which, thanks to the use of solid contact (SC-ISEs) and getting rid of the internal electrolyte, have become easier to prepare, store, transport and miniaturize, which is very important from the point of view of practical applications. Various types of nanoparticles and nanomaterials are often used as solid contact. To date, many carbon nanomaterials have been successfully used to construct SC-ISEs, such as: graphene [1], fullerenes [2], chemically and electrochemically reduced graphene oxide (CRGO [3] and ERGO [4]) or three-dimensional ordered microporous carbon (3DOM) [5]. Among them, carbon nanotubes are still the most popular and so far they have been used so far in both cation-sensitive (Ca^{2+} [6,7], Cd^{2+} [8], Pb^{2+} [9, 10]) and anion-sensitive SC-ISEs (ClO_4^- [11], NO_3^- [12]). In addition, dozens of reviews are available to collect the most current and most important properties and applications of these materials in chemical analysis [13,14].

There are two types of nanotubes: single-walled (SWCNTs) and multi-walled carbon nanotubes (MWCNTs). SWCNTs are hybridized sp^2 carbon in a hexagonal honeycomb structure that is coiled into a hollow tube morphology. MWCNTs consist of many concentric tubes surrounding each other, separated from each other by a granite interlayer distance of 0.34 nm [15,16]. Depending on whether CNTs consist of one or more layers, their diameter can be in the range of 1–3 nm (for SWCNT), up to 5 to 100–200 nm (for MWCNT). However, their lengths can range from several hundred nanometers to several microns [17].

Although CNTs have many similar properties to other types of carbon, they also have better electronic properties, a large ratio of edge plane to base plane and fast electrode kinetics, which translates into faster electron transfer kinetics and a lower detection limit for sensors containing CNTs compared to normal carbon electrodes. They show high electrical conductivity, chemical stability and mechanical strength [16]. The unique electronic properties of SWCNTs can depend on both radius and chirality, carbon hybridization, their cylindrical symmetry and quasi-one-dimensional nature, as well as other factors that include their detailed curvature and local environment [15,18]. CNTs show very good chemical and thermal stability, CNTs with an area not exceeding 1500 m^2 g^{-1} are thermally stable up to a temperature of up to temperature 1000 °C, have a thermal conductivity twice as high as diamond and are lighter than aluminum. In addition, they have exceptional tensile strength, 10 times stronger than Kevlar and even 100 times stronger than steel [19].

Since their discovery in 1991 by Iijim carbon nanotubes have enjoyed unflagging interest from scientists from around the world in various fields of science, both in chemical analysis, medicine,

* Corresponding author.
E-mail address: cecylia.wardak@poczta.umcs.lublin.pl (C. Wardak).

biotechnology and technical sciences (electronics, optoelectronics, photovoltaics).

Researchers and inventors are constantly striving to obtain new materials with better properties and are looking for new applications for them. Based on carbon nanotubes, lightweight nanocomposite materials are currently being constructed that have improved thermal properties compared to the nanotubes themselves, which allows their range of potential applications to be expanded [20]. The first nanocomposites in history resulting from the combination of polymer and CNTs were used as early as in 1994. Since then, scientists have sought, in addition to the effective dispersion of CNTs in the matrix, to achieve strong chemical affinity between CNTs and the polymer, which is enabled by properly implemented surface functionalization of carbon nanomaterials [21]. For the construction of SC-ISEs, CNTs can be used in the form of a nanocomposite, produced e.g. by dispersion of MWCNTs in poly (3-octylthiophene-2,5-diyl) (POT), which acts as a dispersing agent. This not only eliminates the surfactant usually used to stabilize dispersion, but also the immobilization of conductive polymer on MWCNTs as a result of its oxidation allows satisfactory sensors with very good potential stability to be obtained [22].

The CNT surface can also be functionalized with various functional groups (oxides, amides, thiols or different groups) to change the properties of nanomaterials [16]. The process of CNTs chemical functionalization opens up many possibilities of their use enabling the obtaining of materials characterized by better solubility and processability and allows the combination of the unique properties of CNTs and other compounds [23,24]. In addition, CNTs are used to produce field-effect transistors, batteries and capacitors, while in optoelectronics, photocatalysis or fuel cells, heterogeneous catalysis, mechanically reinforced composites and chemical and electrochemical sensors [25,26].

To fully enjoy the possibilities that CNTs give us in most cases it is necessary to disperse them in some solvent. To this end, many methods are used, including oxidation, sonication and centrifugation or by using ultrasonication in combination with dispersing agents, and even by attaching to their surface by means of covalent bonds of various functional groups [17]. Due to the fact that CNTs are hydrophobic, they do not disperse easily in water. The sonication technique can be used, but without the addition of a surfactant (which it is currently trying to avoid), the resulting suspension quickly splits. For CNTs dispersion, which is usually only a few micrograms per milliliter of solvent, organic solvents (toluene, acetone or ethanol) are commonly used, but there is no universal standard method [27].

One of the most popular applications of CNTs is currently to use them as a solid contact in ion-selective electrodes for the determination of various types of inorganic and organic ions. It has also been found that SC-ISEs based on carbon nanotubes are effective in both hydrophilic ion and biomolecule determination [28]. Therefore, carbon nanotubes are also increasingly used in biosensors with improved analytical properties for the determination of various organic substances, which include specific proteins and biomarkers, DNA as well as neurotransmitters and neurochemical substances such as dopamine, serotonin or ascorbic acid [29,30]. Lipophilic polyhedral carbon nanotubes have been successfully used as an internal electron transfer layer in the construction of all-solid-state selective electrodes sensitive to inorganic anions (carbonate, nitrate, nitrite and dihydrogen phosphate). Carbon nanotubes dispersed in an organic solvent are dropped onto the electrode material as an intermediate layer, to which the membrane mixture is then applied [31,32]. There is also a second way to use MWCNTs in the design of ion selective electrodes with solid contact, in which nanotubes are added directly to the membrane mixture. This one-step method is simpler and faster, but you need to take into account adequate homogenization of the membrane material [8].

The use of carbon nanotubes in the construction of potentiometric sensors has many advantages. They are used, among others to reduce the overpotential and resistance of the ion-selective membrane and to increase the electrode capacity. In addition, they are used to improve the sensitivity and stability of the sensor potential and reduce detection limits [12,16]. ISEs based on carbon nanotubes are resistant to light and changes in redox potential of solutions and are not sensitive to the presence of oxygen and carbon dioxide, and are characterized by long-term stability of potential [32]. Electrode performance may depend on many factors, including the method of nanotube synthesis and the method of surface modification as well as the method of attaching the electrode or the addition of electron mediators [16]. alone and in combination with ionic liquids.

As a component of the ion-sensitive membrane, they were successfully used alone and in combination with ionic liquids [8]. Ionic liquids (ILs) are a group of chemical substances that are composed of ions with a melting point below 100 °C and have many beneficial properties. They are characterized by, among others low volatility, which is caused by their low vapor pressure and high viscosity. ILs are highly chemically and thermally stable and show high conductivity and good solvation and dissolution properties for a wide range of chemical compounds [33–37]. The unusual properties of these compounds allow their use in many areas, which may also include analytical chemistry.

Recently we prepared cobalt(II) complex with 4,7-diphenyl-1,10-phenanthroline and successfully used this compound as active membrane component of nitrate ion-selective electrode [38]. Further studies using this complex are presented in this paper. We have developed a new all solid state ion-selective electrode sensitive to nitrate ions using as a new additional membrane component a multiwalled carbon nanotubes-ionic liquid trihexyltetradecylphosphonium chloride (THTDPCl) nanocomposite. Nanocomposite combines the valuable properties of both components and plays an important role in the electrode operation and contribute to the improvement of its analytical and electrical parameters. The MWCNTs-THTDPCl nanocomposite effectively acts as ion-to electron transducer facilitating the charge transfer between the membrane and the internal electrode. On the other hand it also acts as an ion-exchanger and ionic membrane component decreasing the membrane resistance. Therefore additional lipophilic salt was no needed. The nanocomposite was obtained by simple and fast way just by the sonication mixture of ionic liquid THTDPCl and appropriate MWCNTs. Addition of nanocomposite to the membrane results in obtaining homogenous and stable membrane cocktail. In our research we studied four kind of MWCNTs. According to our best knowledge, this is the first use of MWCNTs-ionic liquid nanocomposite in the construction of all solid state ion-selective electrodes. Although there are many studies describing the use of MWCNTs in the construction of ion-selective electrodes, there are no comparative studies for different types of nanotubes.

The nanocomposite was obtained from the sonication mixture of ionic liquid – trihexyltetradecylphosphonium chloride (THTDPCl) and various types of multi-walled carbon nanotubes (MWCNTs). Addition of MWCNTs to the membrane mixture in the form of nanocomposite with THTDPCl results in obtaining homogenous and stable membrane cocktail. Moreover the MWCNTs-THTDPCl nanocomposite effectively acts as an ion-exchanger and ionic membrane component decreasing the membrane resistance. Therefore additional lipophilic salt was no needed. Proposed method of electrode preparation is simple and fast.

2. Material and methods

2.1. Reagents

The main reagents used in the studies and their suppliers were as follows:

The active ingredient of the ion-selective membrane was cobalt(II) complex with 4,7-diphenyl-1,10-phenanthroline (Bphen) of the formula $Co(Bphen)_2(NO_3)_2(H_2O)_2$. The most important compounds used in the process of obtaining the complex were cobalt(II) nitrate hexahydrate and 4,7-diphenyl-1,10-phenanthroline (Bphen), which were purchased from Sigma-Aldrich. The method of obtaining the complex and a
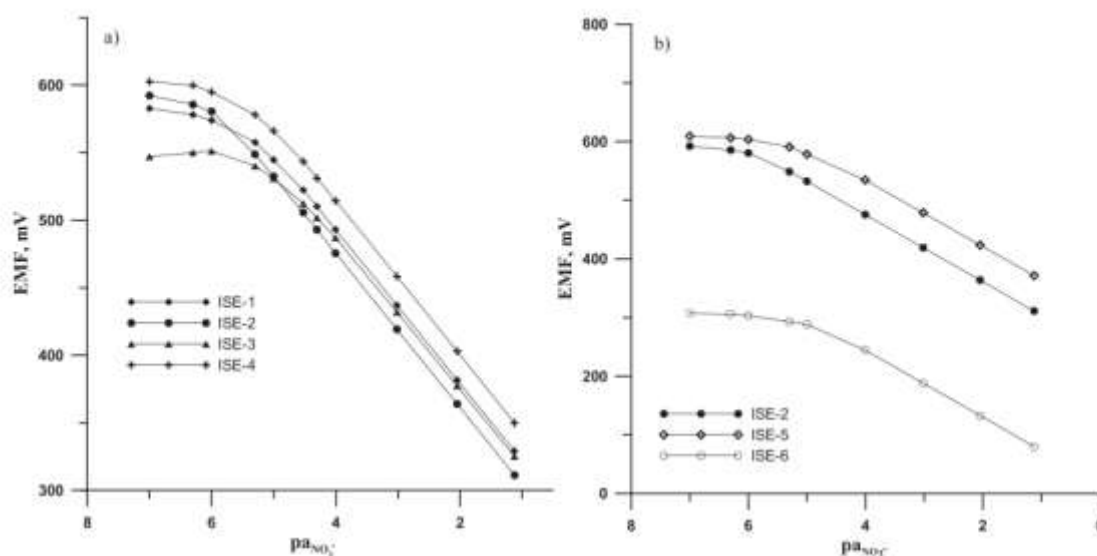
Fig. 1. Calibration curve of nitrate electrodes (a) based on different MWCNTs-IL nanocomposite (ISEs 1–4) and (b) based on MWCNTs intermediate layer (ISE-5) as well as coated disc unmodified electrode (ISE-6).

description of the study of its properties were included in the previous publication [38].

Trihexyltetradecylphosphonium chloride (THTDPCl) was purchased from Aldrich (Canada), polyvinyl chloride (PVC) from Aldrich (Milwaukee, WI, USA), while 2-nitrophenyl octyl ether (NPOE) - Fluka (Switzerland).

Four different types of carbon nanotubes were used for the research, differing mainly in size (length and diameter of the nanotube), which were as follows: I-MWCNTs length: 5–9 μm, outer diameter 6–9 nm [39]; II- MWCNTs length: 3–6 μm, outer diameter 10 nm ± 1 nm, inner diameter 4.5 nm ± 0.5 nm[40]; III-MWCNTs length: 5–9 μm, diameter 110–170 nm [41]; IV- fullerene MWCNTs length: 0.1–10 μm, outer diameter 3–20 nm [42]. I-, II- and III-MWCNTs were obtained from Sigma-Aldrich whereas IV- fullerene MWCNTs were obtained from Alfa-Aesar. The MWCNs I-III were synthesized by the method CVD (CVD - chemical vapor deposition method), while for MWCN IV-fullerene the synthesis method was not given.

Other reagents were purchased from Fluka. Freshly deionized water and pure pro-analysis salts of the highest purity available were used to prepare all aqueous solutions.

2.2. Preparation of nanocomposite and ISE membrane composition

The multiwalled carbon nanotubes-ionic liquid nanocomposite was prepared by mixing 10 mg MWCNTs with 10 mg THTDPCl dissolved in 2 mL tetrahydrofuran (THF) and sonication for 60 min. The mixture was then allowed to evaporate the solvent for 24 h then dried in an oven at 30 °C for 2 h.

In the first part of the study, 4 types of electrodes with the same qualitative composition of ion-selective membranes were constructed, differing in the type of carbon nanotubes used for nanocomposite preparation. For all electrodes, the composition of the mixtures was as follows: 1% active complex ionophore, 2% MWCNTs-THTDPCl nanocomposite, 33% PVC, 64% NPOE, while the length and diameter of the MWCNTs used were different: ISE-1: I-MWCNTs (length: 5–9 μm, outer diameter 6–9 nm); ISE-2: II-MWCNTs (length: 3–6 μm, outer diameter 10 nm ± 1 nm, inner diameter 4.5 ± 0.5 nm); ISE-3: III-MWCNTs (length: 5–9 μm, diameter 110–170 nm); ISE-4: IV-fullerene MWCNTs (length: 0.1–10 μm, outer diameter 3–20 nm).

In order to compare, two additional electrodes were made, notably the ISE-5 with the membrane without MWCNTs but the II- MWCNTS were applied as a separate layer deposited onto the inner electrode surface before membrane deposition and the ISE-6 - a simple coated disc electrode which did not contain MWCNTs both in the membrane and as a separate layer. The qualitative and quantitative composition of the membrane mixtures for ISE 5 and 6 includes: 1% active complex, 1% THTDPCl, 33% PVC, and 65% NPOE.

2.3. Preparation of the electrode

In order to prepare ion-selective electrodes, it was necessary to prepare properly the glassy carbon electrodes (GCEs). Glassy carbon discs with a diameter of 3 mm were mounted in polyetheretherketone (PEEK) housings and then used as internal electrodes in the construction of ion-selective electrodes with solid contact. The electrode surface was polished on wetted Al_2O_3 with 0.3 μm grain diameter. They were then rinsed with redistilled water, placed in an ultrasonic bath to better get rid of alumina residues, and again thoroughly rinsed with redistilled water. The next step was to immerse the electrodes in THF to get rid of the water and allow the organic solvent to evaporate under the fume cupboard in a vertical position with the electrode surface up in a suitable stand. The next step was to weigh 0.3 g of each membrane mix with the appropriate pre-determined compositions in sealable vials, add 3 mL THF to each and mix them thoroughly. The homogenization of the mixtures lasted for 1 h in an ultrasonic bath. For all electrodes, a volume of 50 μL of each mixture was dripped three times onto the previously prepared GCE surfaces, keeping half an hour between each layer. Only in the case of ISE-5, before applying the membrane mixture, a layer of the MWCNTs was deposited using 50 μL of mixture containing II-MWCNTs dispersed in THF (0.001 g mL^{-1}). The next day, the finished electrodes were soaked in a solution of 1×10^{-3} mol L^{-1} NaNO$_3$, for 48 h before first measurement. Between measurements, the electrodes were stored in the same freshly prepared solution.

2.4. The Measurement of the electromotive force

Potentiometric measurements of electromotive force (EMF) were performed in an electrochemical cell consisting of two electrodes:

working electrode – an ion selective electrode sensitive to nitrate ions (NO₃-SCISEs) and a reference electrode-a silver-chloride electrode (Metrohm 6.0750.100). All measurements were made at room temperature in mixed solutions using a 16-channel data acquisition system (Lawson Labs. Inc. USA) coupled with a computer. Additionally, an Orion 81-72 glass electrode and a multifunction computer meter CX-741 (Zabrze Mikulczyce Poland) were used for pH measurements.

2.5. Chronopotentiometry and electrochemical impedance spectroscopy measurements

Current-reversal chronopotentiometry and electrochemical impedance spectroscopy (EIS) measurements were performed in 10^{-2} mol L^{-1} NaNO₃ solution using an AUTOLAB electrochemical analyzer (Eco Chemie, Netherlands) controlled by NOVA software. For this purpose, a conventional three-electrode system was used, in which the working electrode was the tested ion-selective electrode, the auxiliary electrode was a platinum wire and the reference electrode was an Ag/AgCl silver chloride electrode (3 mol L^{-1} KCl). The impedance spectra were recorded in the frequency range 0.1–100 kHz and with the open circuit potential and an amplitude 10 mV. In the chronopotentiometry measurements a working current was applied alternately to the working electrode with a positive and negative current value (equal + 100 nA and − 100 nA respectively) each time for 60 s with simultaneous recording of the electrode potential.

3. Results and discussion

This work describes the preparation and properties of a new solid contact nitrate ion-selective electrode based on MWCNTs-ionic liquid nanocomposite. The influence of the type of MWCNTs used as nanocomposite on the parameters of nitrate ion selective electrodes was studied. In order to best compare the resulting electrodes, many of their analytical parameters were tested. The measurements made included those necessary to determine the slope and linearity range of the characteristic curve of each electrode. Appropriate detection limits as well as repeatability, and stability of the electrode potential were determined. Measurements and interpretations of the results obtained were also made in the field of electrochemical impedance spectroscopy and chronopotentiometry methods.

3.1. Potentiometric response

The measurements of the electromotive force (EMF) of the electrochemical cell constructed of the tested electrode and the reference electrode were made in NaNO₃ solutions in the concentration range of 10^{-7}–10^{-1} mol L^{-1}. The electrode calibration curves obtained are presented in Fig. 1a and b where it can be seen that all electrodes were sensitive to nitrate ions but some differences in relation to the linear ranges and slopes of the calibration curves are noticeable. From the analysis of Fig. 1a and b it can be concluded that introduction of MWCNTs-IL nanocomposite to the membrane effectively improves the electrode response. All electrodes based on MWCNTs-IL nanocomposite exhibited a wider measuring range and a higher slope compared to the ISE-6 without MWCNTs in the membrane, which showed a linear response in the range of 1×10^{-5}–1×10^{-1} mol L^{-1} with a slope of 52.1 mV/decade. It was the result of the membrane modification by the addition of nanocomposite. However the kind of MWCNTs applied for nanocomposite preparation affects the electrode response. The best response was exhibited by ISE-2. The calibration curve determined for this electrode was linear in the widest activity range 1×10^{-6}–1×10^{-1} mol L^{-1} whereas ISE-1 and ISE-4 exhibited linear response in the range 5×10^{-6}–1×10^{-1} mol L^{-1}. A shorter measuring range was exhibited by ISE-3 whose response was linear in the range of nitrate(V) concentrations within 1×10^{-5}–1×10^{-1} mol L^{-1}. The detection limits obtained were, for ISE-1, 2.3×10^{-6}, ISE-2, 5.0×10^{-7}, ISE-3, 5.1×10^{-6} and ISE-
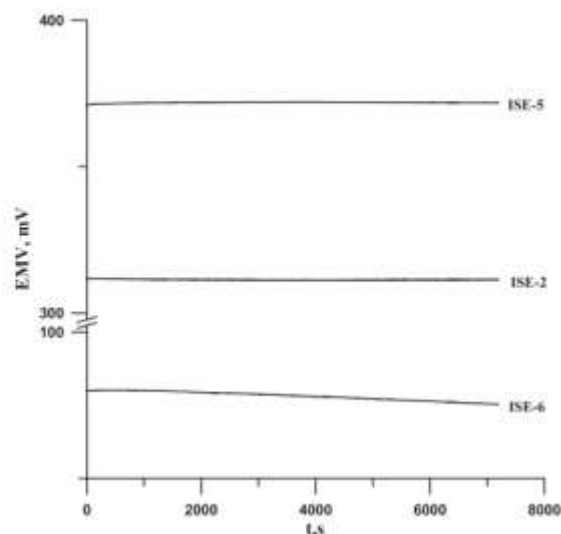

Fig. 2. Potential stability of ISE-2 based on II-MWCNTs-II nanocomposite as membrane component, ISE-5 based on II-MWCNTS as intermediate layer and unmodified ISE-6.

4, 2.5×10^{-6} mol L1, respectively. For the slope of the electrode curve, ISE-2 have the highest slope of 57.1 mV/decade. Other electrodes have lower slopes of: ISE-1 55.0, ISE-3 52.3, ISE-4 54.8 mV/decade, respectively. Since the tested electrodes differed only in the type of MWCNTs forming the nanocomposite material, the observed differences in the electrode response resulted from the differences in the structure of the nanotubes. The nanotubes used were of a similar length, but differed in diameter, and thus in porosity and specific surface area. They were also differ in terms of homogeneity. Comparing the performance of the electrodes and the structure of MWCNTs, it is easy to notice that the beneficial effect of membrane modification with the nanocomposite is the lowest in the case of the material with the lowest porosity (ISE-3) and it increases significantly for the more porous materials (ISE-1, ISE-2 and ISE-4). The best modification effect was obtained for the ISE-2 based on the II-MWCNTS-IL nanocomposite. Although the diameter of II-MWCNTs does not differ significantly from that of I-MWCNTs and IV-fullerene, they were characterized by a much greater homogenity of the structure [39,40,42] what resulted in a more homogeneous membrane and improved electrode performance.

Taking into account the course of electrode calibration curves, II-MWCNTs-IL nanocomposite is the most suitable for the preparation of nitrate electrode membranes. In order to compare the II-MWCNTs were used for preparation of ISE-5 as a separate layer deposited between the ion-sensitive membrane and the inner glassy carbon electrode. The calibration curve of ISE-5 is shown in Fig. 1b where it can be seen that using II-MWCNTs as an interlayer also improved the electrode response, but to a lesser extent than incorporating them into the membrane as a nanocomposite with an ionic liquid.

3.2. Potential stability and reversibility

It is well known that in the case of solid contact ion-selective electrodes noticeable problems with potential stability and reversibility occur. A measurement was made to determine the short-term stability of the electrode potential when soaking the electrodes for about 2 h in a 10^{-1} mol L^{-1} NaNO₃ solution and potential drift determined from $\Delta E/\Delta t$ was 0.083 µV/s for ISE-1, 0,042 µV/s for ISE-2, 0.551 µV/s for ISE-3, 0.166 µV/s for ISE-4, 0.106 µV/s for ISE-5 and 0.625 µV/s for ISE-6. The electrodes prepared with MWCNTs-IL nanocomposite except ISE-3
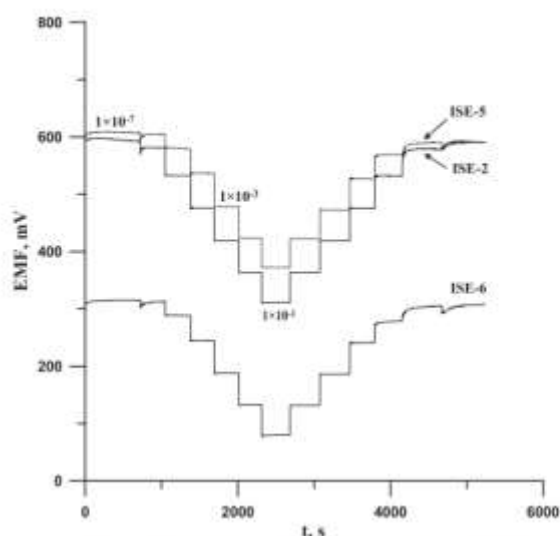
Fig. 3. Dynamic response of ISE-2 based on II-MWCNTs-II nanocomposite as membrane component, ISE-5 based on II-MWCNTS as intermediate layer and unmodified ISE-6.

exhibited better potential stability when compared with ISE-6 without MWCNTs. The best potential stability was obtained for ISE-2 with a potential drift more than ten times less than the potential drift of the unmodified ISE-6 and more than two times less than the potential drift of the ISE-5 with intermediate layer of II-MWCNTs. The worst stability was exhibited ISE-3 based on nanocomposite having III-MWCNTs with the largest diameter. It showed similar potential stability to unmodified ISE-6. Time dependent potential traces during this experiment for ISE-2, ISE-5 and ISE-6 are shown in Fig. 2.

To determine the reversibility of the electrode potential, measurements were carried out in solutions with different $NaNO_3$ concentrations. Calibration was carried out in the concentration range 1×10^{-7}–1×10^{-1} mol L^{-1} $NaNO_3$, first increasing and then decreasing concentrations, as shown in Fig. 3. In addition, potential measurements were carried out in $NaNO_3$ solutions with the following concentrations: 1×10^{-5}, 1×10^{-4} and 1×10^{-3} mol L^{-1}, of which standard deviations for 5 replicates were also counted and presented in Table 1. As it was expected electrodes prepared using MWCNTs exhibited more reversible potential than the simple coated disc electrode. Comparing the dynamic response of ISE-2 and ISE-5 prepared with the same MWCNTs but in different way it is worth to note that ISE-2 having the II-MWCNTs-IL nanocomposite as membrane component was characterized by better potential reversibility than ISE-5 with II-MWCNTs as the intermediate layer.

3.3. Dependence of EMF on pH

Measurements were made to determine the working pH range (the range, in which the potential of the electrodes does not depend on the pH of the sample solution) using a solution of 10^{-3} mol L^{-1} $NaNO_3$ and

H_2SO_4 and NaOH solutions as additives. The dependence of the potential of the tested electrodes was measured in the pH range 2.5–11.5 and it is shown in Fig. 4. The optimum pH range in which the electrodes can work effectively does not depend essentially on kind of MWCNT used for nanocomposite preparation. The determined pH range was 4.2–10.8 for ISE-2 and ISE-4 as well as 4.6–10.8 for ISE-1 and ISE-3.

3.4. Selectivity

As their name indicates, selectivity is certainly one of the most important parameters of ion-selective electrodes. The selectivity of the tested electrodes was estimated based on the obtained values of selectivity coefficients in relation to interfering ions. The selectivity coefficients of the tested electrodes were determined using the separable solution method [43] (by extrapolating the response functions to $a_i = a_j = 1$ mol L^{-1}). The selectivity coefficients obtained did not differ

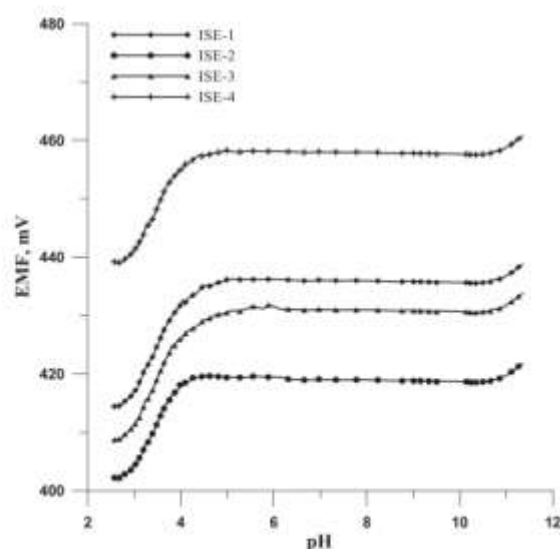**Fig. 4.** Effect of pH on the electrode potential.

Table 2

Comparison of the selectivity coefficients of ISE-2 and ISE-5 differing in the way of using II-MWCNTs.

Interfering ion	logK	
	ISE-2	ISE-5
$H_2PO_4^-$	-6,02	-6,00
SO_4^{2-}	-5,56	-5,51
CO_3^-	-5,20	-5,03
CH_3COO^-	-4,55	-4,45
F^-	-4,62	-4,63
Cl^-	-2,87	-2,80
NO_2^-	-2,29	-2,15
Br^-	-1,23	-1,11

Table 1

Mean potential values determined in the measurement of the potential reversibility (n = 5).

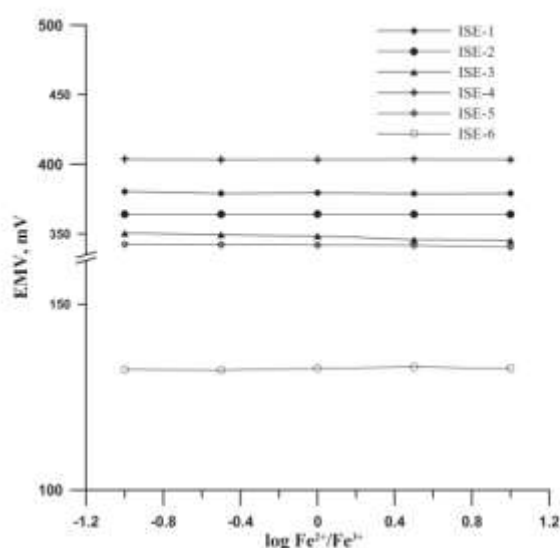| Nitrate concentration, (mol L^{-1})	Mean potential value (mV) ± SD (n = 5)					
	ISE-1	ISE-2	ISE-3	ISE-4	ISE-5	ISE-6
1×10^{-5}	544.7 ± 1.6	532.4 ± 07	532.9 ± 2.3	566.09 ± 2.1	578.5 ± 1.7	288.3 ± 4,9
1×10^{-4}	491.2 ± 1.1	475.5 ± 0.5	483.3 ± 2.2	514.34 ± 2.0	534.4 ± 1.3	241.5 ± 2.8
1×10^{-3}	436.8 ± 0.9	419.3 ± 0.4	431.84 ± 1.6	458.36 ± 1.5	478.6 ± 0.9	188.3 ± 2.1

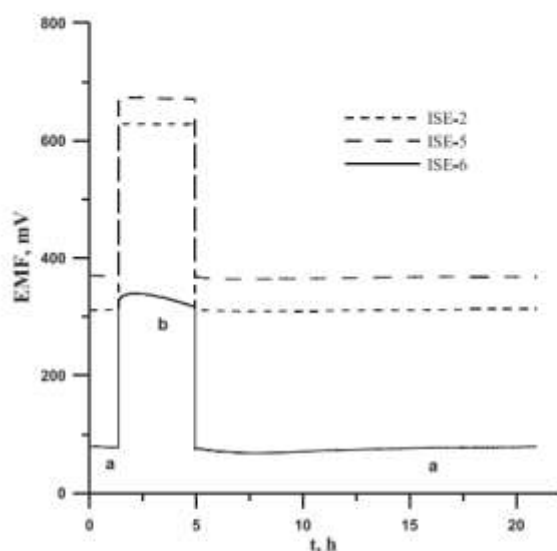**Fig. 5.** Dependence of the electrode potential on the sample redox potential.

Fig. 6. Water layer test performed for the ISE-2, ISE-5 and ISE-6 in 0.1 mol L^{-1} NaNO$_3$ (a) and 0.1 mol L^{-1} Na$_2$SO$_4$ (b).

significantly from each other. All tested electrodes were characterized by very good selectivity, among others in relation to H$_2$PO$_4^-$, SO$_4^{2-}$, CO$_3^-$, CH$_3$COO$^-$, F$^-$ and Cl$^-$ ions. It is a consequence of the same active membrane components and give us information that addition of MWCNTs-IL nanocomposite to the membrane does not impact their selectivity. Comparison of the selectivity coefficients for the electrodes, differing in the location of MWCNTs, as a membrane component (ISE-2) and as a separate layer (ISE-5) is presented in Table 2.

3.5. Redox potential sensitivity

The redox sensitivity measurements were carried out for the studied SC-ISEs. The tested solutions contained 1×10^{-3} mol L^{-1} redox couple
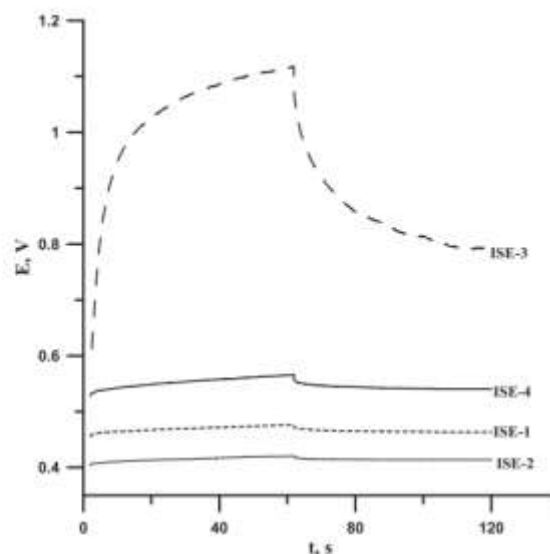
Fig. 7. Chronopotentiograms for the electrodes based on different MWCNTs-IL nanocomposite recorded in 0.01 mol L^{-1} NaNO$_3$.

Fe(CN)$_6^{3-}$ and Fe(CN)$_6^{4-}$ and 1×10^{-2} mol L^{-1} NaNO$_3$ background). For individual solutions, log [Fe^{3+}]/[Fe^{2+}] was − 1.0, − 0.5, 0.0, 0.5 and 1.0, respectively. None of the electrodes showed sensitivity to changes in redox potential of the solutions, as shown in Fig. 5. The slight changes in the potential of the ISE-3 are due to the low potential stability rather than the redox sensitivity.

3.6. Water layer test

It is known that in the case of all solid state electrodes, a thin water layer can form between the polymeric membrane and the inner electrode, which is one of the causes of the electrode potential instability [44–46]. To check the presence of water layer in the studied nanocomposite based electrodes the experimental protocol proposed by Pretsch and coworkers was adopted [44]. Studied electrodes were initially immersed in 0.1 mol L^{-1} nitrate ion solution for about 24 h then the solution was changed to 0.1 mol L^{-1} sulfate (interfering) ion solution for about 3.5 h and then the electrodes were placed back in the nitrate ions solution for about 16 h. Simultaneously, changes in the electrode potential over time were recorded. The results during this test for ISE-2, ISE-5 and ISE-6 are shown in Fig. 6. As it can be seen in this figure, both ISE-2 based on II-MWCNTs-IL nanocomposite and ISE-5 based on II-MWCNTs as intermediate layer exhibited stable potential and no potential drift was observed after replacing nitrate ions by discriminated sulfate ions. This confirms that no water layer was formed in these electrodes. Similar results were obtained for other nanocomposite based electrodes. It was due to the presence of hydrophobic properties both of nanocomposite and MWCNTs. In the case of the unmodified ISE-6 a relatively small potential drift was observed upon the change of the main ions with the interfering ions. The observed potential drift was even smaller after replacing the interfering (discriminated) ions with the main ions. The formation of a water layer between the ion-selective membrane and the inner electrode is not evident in this case. The registered electrode potential drift may be caused by a blocked membrane/inner electrode interface.

3.7. Chronopotentiometry

Current-reversal chronopotentiometry was used to evaluate and

Table 3

Electrical parameters of electrodes based on MWCNTs-IL nanocomposite determined by chronopotentiometry.

Electrode	R_{tot} (kΩ)	$\Delta E/\Delta t$ (mV/s)	C (μF)
ISE-1	20.8	0.203	687.4
ISE-2	10.7	0.106	1237
ISE-3	227	5.36	21.18
ISE-4	47.3	0.402	370.9

compare the total resistance, the potential stability and the capacitance of the studied electrodes containing different types of nanocomposite in the membrane. A current was applied to the working electrode with a positive and negative current value (equal to + 100 nA and − 100 nA respectively) each time for 60 s with simultaneous recording of the electrode potential. The obtained chronopotentiograms for the studied electrodes are shown in Fig. 7. The potential jump observed in the E-t curve after current polarity change was used to determine the total resistance of the electrode using the expression ($R_{tot} = E/2I$, where I was 100 nA). The potential drift was determined from $\Delta E/\Delta t$. For ISE-1, ISE-2 and ISE-4 dependences E(t) were linear and $\Delta E/\Delta t$ was the slope of E (t) curve. In the case of ISE-3, curve E(t) was not linear and potential drift for this electrode was estimated using potential change ΔE which occurred during negative current was applied. Determined potential drift was used to evaluate the electrode capacitance using equation $C_{if} = 1/(\Delta E/\Delta t)$ [47]. The values of the electric parameters estimated on the basis of chronopotentiometry measurements are collected in Table 3. As it can be seen the ISEs based on nanocomposite with different types of MWCNTs differ in the electric properties. The best parameters exhibited ISE-2 having the lowest total resistance of 10.7 kΩ and the highest capacitance of 1237 μF. The other electrodes had higher resistance and lower capacitance. The least favorable parameters were shown by ISE-3, which had the highest total resistance of 227 kΩ and the lowest capacitance of 21.18 μF.

The differences in the electrical parameters of the electrodes reflect the differences in their potentiometric response. as mentioned before, it is related to the different structure of the nanotubes forming the nanocomposite. Among the tested systems, the greatest differences were noticed for ISE-3 based on nanocomposite containing nanotubes with the largest diameter and the least homogeneous structure. The chronopotentiometric curve obtained for this electrode had a nonlinear course due to non ideal capacitance behavior which was the result of low homogenity of the membrane [47] as a result of the addition of nanocomposite with large differences in sizes of MWCNTs. Potential of ion-selective electrode under galvanostatic polarization conditions can be expressed by following equation $E = E_{eq} + IR + (I/C) t$ (where E_{eq} is equilibrium potential under zero current condition; I is applied constant current, C is capacitance and t-is time) [48]. ISE-3 showed the highest potential and the greatest potential drift. It was caused by high electrode resistance and low capacitance, which is related to the structure of nanotubes and their low porosity.

3.8. Electrochemical impedance spectroscopy

Similar differences in the electric properties were observed in the results obtained by EIS technique. As it can be seen in Fig. 8 the impedance spectra obtained for the studied electrodes have the same shape but a different size. They were composed of two parts, a high-frequency partial semicircle connected with bulk membrane resistance

Table 4

Electrical parameters of studied electrodes calculated determined using equivalent circuits showed in Fig. 8 (R_u-uncompensated series resistance, R_b bulk resistance, C_b geometric capacitance, R_{ct} charge transfer resistance, CPE constant phase element (Y^0 initial value for the admittance for the CPE element, N-parameter showing to what extent the CPE is the ideal capacitance, if N = 1 then CPE is ideal capacitance).

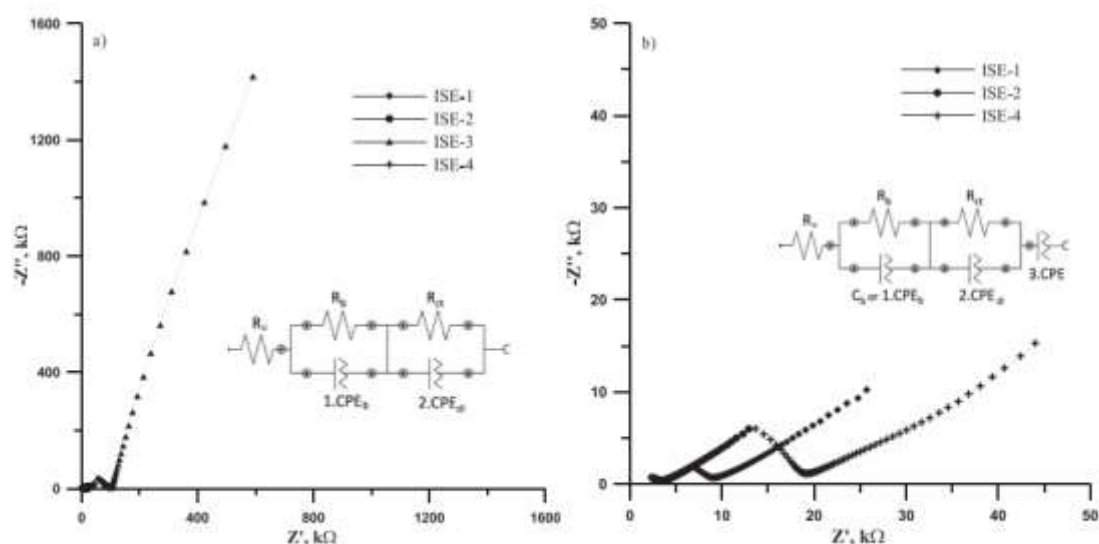| Electrode	R_u (kΩ)	R_b (kΩ)	C_b (pF)	CPE_b Y^0 (N) (pF)	R_{ct} (kΩ)	CPE_{dl} Y^0 (N) (μF)	CPE_3 Y^0 (N) (μF)
ISE-1	- 6.12	2.91	325	–	13.3	14 (0.20)	61 (0.35)
ISE-2	0.218	2.6	–	51,500 (0.89)	6.08	169 (0.22)	136 (0.42)
ISE-3	- 18.4	107	–	15 (0.85)	2980	0.05 (82)	–
ISE-4	1.19	16.5	–	242 (0.88)	29.7	77 (0.13)	50 (0.37)

Fig. 8. Impedance spectra of ISE-1, ISE-2, ISE-3 and ISE-4 determined in 0.01 mol L^{-1} NaNO$_3$ (a) and their magnification in the range 0–50 kΩ (b). The spectra were recorded at the open circuit potential in the frequency range 0.1 Hz–100 kHz. In insert equivalent electrical circuit for ISE-3 (a) and ISEs 1, 2 and 4 (b) are shown. The error of the fits (χ^2) was 1.8 × 10^{-3} (ISE-1); 6 × 10^{-4} (ISE-2); 0.012 (ISE-3) and 2.9 × 10^{-3} (ISE-4).

Table 5

Comparison of the properties of recently reported nitrate all solid state electrodes and proposed ISE-3.

Active substance	Solid contact	Slope, mV/dec	Linear range, mol L^{-1}	Detection limit, mol L^{-1}	Interfering ions with logK ≥ -2	Refs.
Nitrate ionophore V	TTF-TCNQ	-58.5	1.0×10^{-5}-1.0×10^{-1}	3.2×10^{-6}	NO$_2^-$	[52]
Ppy(NO$_3^-$)	graphite powder	-57.1	1.5×10^{-4}-1.0×10^{-1}	5.4×10^{-5}	ClO$_4^-$, Br$^-$, I$^-$, SCN$^-$, CN$^-$	[53]
Ppy(NO$_3^-$)	Au NPs	-50.4	5.3×10^{-5}-1.0×10^{-1}	5.3×10^{-5}	Cl$^-$, Br$^-$	[54]
TDMAN	laser induced graphene	-54.8	5.0×10^{-5}-1.0×10^{-1}	2.1×10^{-5}	not tested	[55]
TDMAN	MWCNTs	-57.7	3.2×10^{-6}-1.0×10^{-1}	2.5×10^{-6}	NO$_2^-$, ClO$_4^-$, Cl$^-$, SCN$^-$	[31]
TDMAN	CRGNO	-57.9	5.0×10^{-5}-1.0×10^{-1}	3.0×10^{-5}	Cl$^-$	[28]
TDMAN	POT-MoS$_2$	-64.0	7.1×10^{-4}-1.0×10^{-1}	9.2×10^{-5}	not tested	[56]
TDMA-NO$_3$	PtNPs-CB	-58.6	1.0×10^{-6}-1.0×10^{-1}	5.0×10^{-7}	NO$_2^-$, ClO$_4^-$, salicylate	[57]
THTDPCl	Ag/AgCl/Cl$^-$	-60.1	1.0×10^{-5}-1.0×10^{-1}	2.8×10^{-6}	NO$_2^-$, Br$^-$, SCN$^-$, ClO$_4^-$	[58]
Co(Bphen)$_2$(NO$_3$)$_2$	Ag/AgCl/Cl$^-$	-56.3	1.0×10^{-5}-1.0×10^{-1}	4.0×10^{-6}	ClO$_4^-$, Br$^-$, SCN$^-$	[38]
Co(Bphen)$_2$(NO$_3$)$_2$	MWCNTs-IL nanocomposite	-57.1	1.0×10^{-8}-1.0×10^{-1}	5.0×10^{-7}	Br$^-$	This work

Nit+/NO$_3^-$ – nitron(1,4-diphenyl-endoanilino-dihydrotriazole).
Ppy(NO$_3^-$) – polypyrrole doped with nitrate.
TDMAN – tridodecylmethylaminium nitrate.
TDMA-NO$_3$ – tridodecylmethyl-ammonium nitrate.
THTDPCl – trihexyl- tetradecylphosphonium chloride.
Co(Bphen)$_2$(NO$_3$)$_2$ – cobalt(II) complex with 4,7-diphenyl-1,10-phenanthroline.
TTF-TCNQ – tetrathiafulvalene-tetracyanoquinodimethane.
MWCNTs – multiwalled carbon nanotubes.
Au NPs – gold nanoparticles.
CRGNO – chemically reduced graphene oxide.
POT-MoS$_2$ – nanocomposite of poly(3-octyl-thiophene) and molybdenum disulfide.
PtNPs-CB – carbon black supporting platinum nanoparticles.
Ag/AgCl/Cl- – silver silver chloride electrode/chloride.

(R$_b$) in parallel with its geometric capacitance [49] and low frequency branch associated with interfacial processes at the interface: internal electrode/membrane and membrane/solution and diffusion processes in the membrane [50]. The impedance spectra were fitted to the equivalent circuits shown in Fig. 8 and determined data are presented in Table 4. Depending on the type of MWCNTs constituting the nanocomposite, the studied ISEs had different bulk membrane resistance R$_b$ which increased as follows 2.58, 2.91, 16.5, 107 kΩ for ISE-2, ISE-1, ISE-4 and ISE-3, respectively. The differences in the membrane resistance were due to the differences in the MWCNT porous structure. The membrane resistance R$_b$ was an order lower for electrodes based on nanocomposites with a larger porous structure. Similar results were obtained for potassium electrodes based on graphene/superhydrophobic polymer nanocomposite [51]. Even greater differences are seen for the charge transfer resistance R$_{ct}$ which was 6.08, 13.3, 29.7 and 2980 kΩ for ISE-2, ISE-1, ISE-4 and ISE-3, respectively. These results indicate that ion to electron transduction and diffusion processes in the membrane are depend essentially on the kind of nanocomposite added to the membrane. The lowest R$_{ct}$ value was obtained for the ISE- 2, which proves that ion-to-electron transduction processes proceed the most properly in this electrode. The nanocomposite based on II-MWCNTs with larger porous and the most homogeneous structure is the most suitable nanocomposite for the preparation of nitrate ion-selective nitrate electrodes among the tested systems.

4. Conclusions

A comparative study of all solid state ion-selective electrodes based on different MWCNT-ionic liquid nanocomposites has been presented. It was shown that kind of MWCNTs used for nanocomposite preparation impacts essentially the electrode performance. It seems that the structure (diameter, homogenity) of the carbon nanotubes used for the preparation of the nanocomposite is of significant importance.

The best results were obtained for the electrode prepared with nanocomposite having II-MWCNTs with a length of 3–6 µm and a diameter of 10 nm. ISE-2 exhibited the lowest detection limit and the best potential stability. This was the effect of effectively lowering the membrane resistance and increasing the electrode capacitance. The use of a nanocomposite with MWCNTs with a much larger diameter (more

than 10 times) for the preparation of electrodes did not bring the expected improvement of the electrode parameters.

The use of MWCNTs-IL nanocomposite as a membrane component simplifies the preparation of the electrode and at the same time improves its parameters to a greater extent than the use of MWCNTs as an intermediate layer.

Table 5 shows comparison of the MWCNTs-IL nanocomposite based with other all solid state nitrate ion-selective electrodes recently reported in the literature. The comparison showed that proposed ISE-2 is superior to other electrodes in terms of linear range and detection limit. Only electrode reported in [57] exhibited slightly better slope of linear range of calibration curve and the same detection limit. Nevertheless, proposed sensor shoved improved selectivity in relation to nitrite ions.

CRediT authorship contribution statement

Karolina Pietrzak: Methodology, Investigation, Data curation, Validation, Writing – original draft. **Cecylia Wardak**: Conceptualization, Methodology, Supervision, Writing – review & editing.

Declaration of Competing Interest

The authors declare that they have no known competing financial interests or personal relationships that could have appeared to influence the work reported in this paper.

References

[1] F. Li, J. Ye, M. Zhou, S. Gan, Q. Zhang, D. Han, L. Niu, All-solid-state potassium-selective electrode using graphene as the solid contact, Analyst 137 (2012) 618-623, https://doi.org/10.1039/c1an15705a.
[2] M. Fouskaki, N. Chaniotakis, Fullerene-based electrochemical buffer layer for ion-selective electrodes, Analyst 133 (2008) 1072-1075, https://doi.org/10.1039/b719759d.
[3] J. Ping, Y. Wang, J. Wu, Y. Ying, Development of an all-solid-state potassium ion-selective electrode using graphene as the solid-contact transducer, Electrochem. Commun. 13 (2011) 1529-1532, https://doi.org/10.1016/j.elecom.2011.10.018.
[4] J. Ping, Y. Wang, Y. Ying, J. Wu, Application of electrochemically reduced graphene oxide on screen-printed ion-selective electrode, Anal. Chem. 84 (2012) 3473-3479, https://doi.org/10.1021/ar203480r.
[5] C.Z. Lai, M.M. Joyer, M.A. Fierke, N.D. Petkovich, A. Stein, P. Bühlmann, Subnanomolar detection limit application of ion-selective electrodes with three-

dimensionally ordered macroporous (3DOM) carbon solid contacts, J. Solid State Electrochem. 13 (2009) 123–128, https://doi.org/10.1007/s10008-008-0579-2.

[6] Y. Fan, C. Xu, R. Wang, G. Hu, J. Miao, K. Hai, C. Lin, Determination of copper(II) ion in food using an ionic liquids-carbon nanotubes-based ion-selective electrode, J. Food Compos. Anal. 62 (2017) 63–68, https://doi.org/10.1016/j.jfca.2017.05.003.

[7] M. Ghaedi, M. Montazerozohori, R. Sahraei, Comparison of the influence of nanomaterials on response properties of copper selective electrodes, J. Ind. Eng. Chem. 19 (2013) 1356–1364, https://doi.org/10.1016/j.jiec.2012.12.040.

[8] C. Wardak, Solid contact cadmium ion-selective electrode based on ionic liquid and carbon nanotubes, Sens. Actuators B Chem. 209 (2015) 131–137, https://doi.org/10.1016/j.snb.2014.11.107.

[9] J. Guo, Y. Chai, R. Yuan, Z. Song, Z. Zou, Lead (II) carbon paste electrode based on derivatized multi-walled carbon nanotubes: application to lead content determination in environmental samples, Sens. Actuators B Chem. 155 (2011) 639–645, https://doi.org/10.1016/j.snb.2011.01.023.

[10] Y. Liu, Y. Liu, Y. Gao, P. Wang, A general approach to one-step fabrication of single-piece nanocomposite membrane based Pb2+-selective electrodes, Sens. Actuators B Chem. 281 (2019) 705–712, https://doi.org/10.1016/j.snb.2018.09.113.

[11] E.J. Parra, G.A. Crespo, J. Riu, A. Ruiz, F.X. Rius, Ion-selective electrodes using multi-walled carbon nanotubes as ion-to-electron transducers for the detection of perchlorate, Analyst 134 (2009) 1905–1910, https://doi.org/10.1039/b909224g.

[12] S.S.M. Hassan, A.G. Eldin, A.E.G.E. Amr, M.A. Al-Omar, A.H. Kamel, N.M. Khalifa, Improved solid-contact nitrate ion selective electrodes based on multi-walled carbon nanotubes (MWCNTs) as an ion-to-electron transducer, Sensors 19 (2019) 3891, https://doi.org/10.3390/s19183891.

[13] V. Schroeder, S. Savagatrup, M. He, S. Lin, T.M. Swager, Carbon Nanotube Chemical Sensors, 2019. (https://doi.org/10.1021/acs.chemrev.8b00340).

[14] N. Baig, M. Sajid, T.A. Saleh, Recent trends in nanomaterial-modified electrodes for electroanalytical applications, TrAC – Trends Anal. Chem. 111 (2019) 47–61, https://doi.org/10.1016/j.trac.2018.11.044.

[15] I. Dumitrescu, P.R. Unwin, J.V. MacPherson, Electrochemistry at carbon nanotubes: perspective and issues, Chem. Commun. 7345 (2009) 6886–6901, https://doi.org/10.1039/b909734a.

[16] C.B. Jacobs, M.J. Peairs, B.J. Venton, Review: carbon nanotube based electrochemical sensors for biomolecules, Anal. Chim. Acta 662 (2010) 105–127, https://doi.org/10.1016/j.aca.2010.01.009.

[17] C. Herrero-Latorre, J. Álvarez-Méndez, J. Barciela-García, S. García-Martín, R. M. Peña-Crecente, Characterization of carbon nanotubes and analytical methods for their determination in environmental and biological samples: a review, Anal. Chim. Acta 853 (2015) 77–94, https://doi.org/10.1016/j.aca.2014.10.008.

[18] M. Ouyang, J.L. Huang, C.M. Lieber, Fundamental electronic properties and applications of single-walled carbon nanotubes, Acc. Chem. Res. 35 (2002) 1018–1025, https://doi.org/10.1021/ar0101685.

[19] V. Sgobba, D.M. Guldi, Carbon nanotubes – electronic/electrochemical properties and application for nanoelectronics and photonics, Chem. Soc. Rev. 38 (2009) 165–184, https://doi.org/10.1039/b802652c.

[20] E.M. Jackson, P.E. Laibinis, W.E. Collins, A. Ueda, C.D. Wingard, B. Penn, Development and thermal properties of carbon nanotube-polymer composites, Compos. Part B Eng. 89 (2016) 362–373, https://doi.org/10.1016/j.compositesb.2015.12.018.

[21] Z. Spitalsky, D. Tasis, K. Papagelis, C. Galiotis, Carbon nanotube-polymer composites: chemistry, processing, mechanical and electrical properties, Prog. Polym. Sci. 35 (2010) 357–401, https://doi.org/10.1016/j.progpolymsci.2009.09.003.

[22] D. Kaluza, E. Jaworska, M. Mazur, K. Maksymiuk, A. Michalska, Multiwalled carbon nanotubes-poly(3-octylthiophene-2,5-diyl) nanocomposite transducer for ion-selective electrodes: Raman spectroscopy insight into the transducer/membrane interface, Anal. Chem. 91 (2019) 9010–9017, https://doi.org/10.1021/acs.analchem.9b01286.

[23] A. Hirsch, Functionalization of single-walled carbon nanotubes, Angew. Chem. - Int. Ed. 41 (2002) 1853–1859, https://doi.org/10.1002/1521-3773(20020603)41:11<1853::AID-ANIE1853>3.0.CO;2-N.

[24] S. Papp, J. Kozma, T. Lindfors, R.E. Gyurcsányi, Lipophilic multi-walled carbon nanotube-based solid contact potassium ion-selective electrodes with reproducible standard potentials. A comparative study, Electroanalysis 32 (2020) 867–873, https://doi.org/10.1002/elan.202000045.

[25] A.T. Lawal, Synthesis and utilization of carbon nanotubes for fabrication of electrochemical biosensors, Mater. Res. Bull. 73 (2016) 308–350, https://doi.org/10.1016/j.materresbull.2015.08.037.

[26] K. Balasubramanian, M. Burghard, Chemically functionalized carbon nanotubes, Small 1 (2005) 180–192, https://doi.org/10.1002/smll.200400118.

[27] J.H. Lehman, M. Terrones, E. Mansfield, K.E. Hurst, V. Meunier, Evaluating the characteristics of multiwall carbon nanotubes, Carbon 49 (2011) 2581–2602, https://doi.org/10.1016/j.carbon.2011.03.028.

[28] W. Tang, J. Ping, K. Fan, Y. Wang, X. Luo, Y. Ying, J. Wu, Q. Zhou, All-solid-state nitrate-selective electrode and its application in drinking water, Electrochim. Acta 81 (2012) 186–190, https://doi.org/10.1016/j.electacta.2012.07.073.

[29] S. Gupta, C.N. Murthy, C.R. Prabha, Recent advances in carbon nanotube based electrochemical biosensors, Int. J. Biol. Macromol. 108 (2018) 687–703, https://doi.org/10.1016/j.ijbiomac.2017.12.038.

[30] C. Yang, M.E. Denno, P. Pyakurel, B.J. Venton, Recent trends in carbon nanomaterial-based electrochemical sensors for biomolecules: a review, Anal. Chim. Acta 887 (2015) 17–37, https://doi.org/10.1016/j.aca.2015.05.049.

[31] D. Yuan, A.H.C. Anthis, M.G. Afshar, N. Pankratova, M. Cuartero, G.A. Crespo, E. Bakker, All-solid-state potentiometric sensors with a multiwalled carbon nanotube inner transducing layer for anion detection in environmental samples, Anal. Chem. 87 (2015) 8640–8645, https://doi.org/10.1021/acs.analchem.5b01941.

[32] R. Liang, T. Yin, W. Qin, A simple approach for fabricating solid-contact ion-selective electrodes using nanomaterials as transducers, Anal. Chim. Acta 853 (2015) 291–296, https://doi.org/10.1016/j.aca.2014.10.003.

[33] J.S. Wilkes, A short history of ionic liquids – from molten salts to neoteric solvents, Green Chem. 4 (2002) 73–80, https://doi.org/10.1039/b110838g.

[34] D.S. Silvester, Recent advances in the use of ionic liquids for electrochemical sensing, Analyst 136 (2011) 4871–4882, https://doi.org/10.1039/c1an15699c.

[35] M. Koel, Ionic liquids in chemical analysis, Ion. Liq. Chem. Anal. 35 (2005) 177–192, https://doi.org/10.1201/9781420046472.

[36] M.J. Earle, K.R. Seddon, Ionic liquids. Green solvents for the future, Pure Appl. Chem. 72 (2000) 1391–1398, https://doi.org/10.1351/pac200072071391.

[37] J.L. Anderson, J. Ding, T. Welton, D.W. Armstrong, Characterizing ionic liquids on the basis of multiple solvation interactions, J. Am. Chem. Soc. 124 (2002) 14247–14254, https://doi.org/10.1021/ja028156h.

[38] K. Pietrzak, C. Wardak, R. Łyszczek, Solid contact nitrate ion-selective electrode based on cobalt(II) Complex with 4,7-diphenyl-1,10-phenanthroline, Electroanalysis 31 (2019) 1–9, https://doi.org/10.1002/elan.201900462.

[39] ⟨https://www.sigmaaldrich.com/catalog/product/aldrich/724769⟩ (Accessed 22 July 2021).

[40] ⟨https://www.sigmaaldrich.com/catalog/product/aldrich/773840⟩ (Accessed 22 July 2021).

[41] ⟨https://www.sigmaaldrich.com/catalog/product/aldrich/659258⟩ (Accessed 22 July 2021).

[42] ⟨https://www.alfa.com/en/catalog/044945⟩ (Accessed 22 July 2021).

[43] E. Bakker, E. Pretsch, P. Bühlmann, Selectivity of potentiometric ion sensors, Anal. Chem. 72 (2000) 1127–1133, https://doi.org/10.1021/ac9911402.

[44] M. Fibbioli, W.E. Morf, M. Badertscher, N.F. De Rooij, E. Pretsch, Potential drifts of solid-contacted ion-selective electrodes due to zero-current ion fluxes through the sensor membrane, 2007, pp. 1286–1292.

[45] T. Lindfors, F. Sundfors, L. Höfler, R.E. Gyurcsányi, FTIR-ATR study of water uptake and diffusion through ion-selective membranes based on plasticized poly (vinyl chloride), Electroanalysis 21 (2009) 1914–1922, https://doi.org/10.1002/elan.200904009.

[46] T. Lindfors, F. Sundfors, L. Hofler, R.E. Gyurcsanyi, The water uptake of plasticized poly(vinyl chloride) solid-contact ion-selective electrodes, Electroanalysis 23 (2011) 2156–2163, https://doi.org/10.1002/elan.201100219.

[47] J. Bobacka, Potential stability of all-solid-state ion-selective electrodes using conducting polymers as ion-to-electron transducers, 71, 1999, pp. 4932–4937.

[48] J. Bobacka, A. Lewenstam, A. Ivaska, Equilibrium potential of potentiometric ion sensors under steady-state current by using current-reversal chronopotentiometry, J. Electroanal. Chem. 509 (2001) 27–30, https://doi.org/10.1016/S0022-0728(00)00515-5.

[49] K. Tóth, E. Gráf, G. Horvai, E. Pungor, R.P. Buck, Plasticized poly(vinyl chloride) properties and characteristics of valinomycin electrodes. 1. High-frequency resistances and dielectric properties, Anal. Chem. 58 (1986) 2736–2740, https://doi.org/10.1021/ac00126a034.

[50] J. Bobacka, A. Ivaska, A. Lewenstam, Plasticizer-free all-solid-state potassium-selective electrode based on poly(3-octylthiophene) and valinomycin, Anal. Chim. Acta 385 (1999) 195–202, https://doi.org/10.1016/S0003-2670(98)00667-9.

[51] B. Paczosa-Bator, Ion-selective electrodes with superhydrophobic polymer/carbon nanocomposites as solid contact, Carbon 95 (2015) 879–887, https://doi.org/10.1016/j.carbon.2015.09.006.

[52] M. Pięk, R. Piech, B. Paczosa-Bator, TTF-TCNQ solid contact layer in all-solid-state ion-selective electrodes for potassium or nitrate determination, J. Electrochem. Soc. 165 (2018) B60–B65, https://doi.org/10.1149/2.0161803jes.

[53] G.A. Álvarez-Romero, M.E. Palomar-Pardavé, M.T. Ramírez-Silva, Development of a novel nitrate-selective composite sensor based on doped polypyrrole, Anal. Bioanal. Chem. 387 (2007) 1533–1541, https://doi.org/10.1007/s00216-006-1021-1.

[54] L. Zhang, Z. Wei, P. Liu, An all-solid-state NO3- ion-selective electrode with gold nanoparticles solid contact layer and molecularly imprinted polymer membrane, PLoS One 15 (2020) 1–14, https://doi.org/10.1371/journal.pone.0240173.

[55] N.T. Garland, E.S. McLamore, N.D. Cavallaro, D. Mendivelso-Perez, E.A. Smith, D. Jing, J.C. Claussen, Flexible laser-induced graphene for nitrogen sensing in soil, ACS Appl. Mater. Interfaces 10 (2018) 39124–39133, https://doi.org/10.1021/acsami.8b10991.

[56] M.A. Ali, X. Wang, Y. Chen, Y. Jiao, N.K. Mahal, S. Moru, M.J. Castellano, J. C. Schnable, P.S. Schnable, L. Dong, Continuous monitoring of soil nitrate using a miniature sensor with poly(3-octyl-thiophene) and molybdenum disulfide nanocomposite, ACS Appl. Mater. Interfaces 11 (2019) 29195–29206, https://doi.org/10.1021/acsami.9b07120.

[57] B. Paczosa-Bator, L. Cabaj, R. Piech, K. Skupień, Potentiometric sensors with carbon black supporting platinum nanoparticles, Anal. Chem. 85 (2013) 10255–10261.

[58] C. Wardak, Solid contact nitrate ion-selective electrode based on ionic liquid with stable and reproducible potential, Electroanalysis 26 (2014) 864–872, https://doi.org/10.1002/elan.201300590.

Karolina Pietrzak received the M.Sc. degree in chemistry from Maria Curie Sklodowska University (MCSU), Lublin, Poland, in 2018, where she is currently pursuing the Ph.D. degree with the Department of Analytical Chemistry. Her main scientific interests are

str. 92

research, development, and analytical applications of ion-selective electrodes with solid contact.

Cecylia Wardak received the Ph.D. degree in analytical chemistry in 2004 and her D.Sc. degree in analytical chemistry and electrochemistry in 2015 from Maria Curie Sklodowska University (MCSU), Lublin, Poland. Since then she has been working as associate professor in the Department of Analytical Chemistry of Maria Curie-Sklodowska University. She was a Postdoctoral Researcher with Warsaw University, Poland (2003) and with AGH University of Science and Technology in Krakow, Poland (2016). She is an active COST member. She participated in technical meeting on problems related to diffuse pollution sources in Koblenz, Germany, and completed a course related to miniaturize analytical systems. Her main scientific interests are research, development, and analytical applications of electrochemical sensors and biosensors.

D3

NITRATE ION-SELECTIVE ELECTRODES – NEW CONSTRUCTIONS AND APPLICATIONS IN THE MONITORING OF NITRATE IONS IN ENVIRONMENTAL SAMPLES

NITRATE ION-SELECTIVE ELECTRODES – NEW CONSTRUCTIONS AND APPLICATIONS IN THE MONITORING OF NITRATE IONS IN ENVIRONMENTAL SAMPLES

C. Wardak, K. Pietrzak

Department of Analytical Chemistry, Institute of Chemical Sciences, Faculty of Chemistry, Maria Curie-Skłodowska University, Maria Curie-Skłodowska Sq. 3, 20-031 Lublin, Poland

Abstract

Ion-selective electrodes, due to many advantages, such as simplicity of use, low cost and high speed of measurements, as well as very good analytical parameters (low detection limits and high selectivity), have been widely used in recent years to determine various types of ions in environmental samples. Nitrates are ubiquitous in the environment, both in air, soil and water, and are essential for the proper growth of plants and animals. Research is still ongoing to unambiguously determine the influence of consumption of increased doses of nitrates on human health. Therefore, it is important to develop appropriate methods for determining their content in natural samples and in food products. The paper reviews articles on the latest knowledge on the influence of nitrates on human health as well as on the development and application of potentiometric sensors for determining the content of nitrates in environmental samples, including food products and various types of natural waters.

Keywords: nitrates, potentiometry, ion selective electrodes, solid contact

Nitrates are abundant in the natural environment, both in soil and water, as well as in all living organisms. They are also widely used by humans, inter alia, as artificial fertilizers to increase the yield of agricultural crops (Iammarino et al. 2013) and as preserving additives for meats and cold cuts, to improve the taste and color of products, inhibit the growth of bacteria and delay food spoilage as a result of rancidity (Bryan and Ivy 2015; Sindelar and Milkowski 2012).

Nitrates supplied to the body with food and drinking water are certainly very important biological compounds and have a good effect on human health. They have a protective effect on the cardiovascular system, lowering blood pressure and improving its flow in blood vessels (Sindelar and Milkowski 2012). Nitrates and nitrites are also nutrients necessary to maintain the homeostasis of nitric oxide (II) in the body, which, being a product of enzymatic synthesis, is involved in the process of wound healing and in the immune and neurological response (Bryan et Ivy 2015; Sindelar and Milkowski 2012). The fact that nitrates and nitrites are necessary in the human diet is also evidenced by, inter alia, the fact that in the early postpartum period in breast milk there is a relatively high concentration of these compounds, with the nitrite concentration outweighing the nitrate concentration, due to the absence of appropriate bacteria in the gastrointestinal tract of the newborn, which ensure the reduction of nitrates to nitrites. Later, however, this ratio is gradually reversed to the benefit of nitrates with obtaining appropriate commensal bacteria (Bryan et Ivy 2015).

In the right concentration, nitrates provide health benefits, but as with other chemicals, taking them in more than recommended amounts can have negative health effects, in this case mainly related to problems with the digestive system. Although nitrates have been used by humans for many different applications for centuries, the alarming results concerning the ill effects of increased doses of nitrates on human health resulting from numerous scientific studies conducted in the last century caused the use of nitrates to almost be banned in the 1970s, due to fears of carcinogenic nitrosamine formed during the thermal processing of meat products (Bedale et al. 2016). It was believed that their excessive consumption may also be associated with the occurrence of cancer and Parkinson's disease. At the beginning of the 20th century, research was also carried out on the so-called "blue baby syndrome", otherwise known as methaemoglobinaemia. The disease was expected to affect mainly infants and cause a significant reduction in the oxygen content in the blood of children (Alahi and Mukhopadhyay 2018; McKnight et al. 2009).

The main source of nitrates and nitrites in the human diet are vegetables and fruits, as well as, to a lesser extent, drinking water, animal products and grains. Nitrates are essential for the proper growth of plants, but the excess of nitrates absorbed by the plant, which the plant is no longer able to absorb, can accumulate in its tissues, especially in the leaves. Therefore, it is the leafy vegetables (lettuce, arugula, spinach, parsley) that contain the highest nitrate concentrations among various other vegetable species (Colla et al. 2018; McKnight and al. 2009). The content of nitrates in plant tissue may also be influenced by plant growth conditions (e.g. CO_2 content in the air, temperature and sunlight), as well as the harvest time and the conditions for their subsequent storage (Colla et al. 2018). The content of nitrates and nitrites in the body is due to both their consumption and their endogenous production due to the presence of denitrifying bacteria and oxidation of nitric oxide (II). The bioavailability of food nitrates is 100% (Bryan and Ivy 2015).

All nutrients should be supplied to the body in appropriate amounts so as not to cause negative health effects related to both their deficiency and excess. Also, nitrates and nitrites should be present in appropriate doses that enable proper growth and functioning. The increased content of nitrate ions has a negative effect on the balance in the environment and the proper functioning of living organisms. Therefore, in order to ensure the safety of humans and animals, it is necessary to monitor the state of the natural environment. For many essential vitamins as well as macro- and microelements, the optimal intake and the recommended diet for maintaining health and good condition of the body have been determined based on research. Therefore, governmental and international organizations have developed certain regulations to define and control

the maximum concentration of nitrates in food and the environment (Alahi and Mukhopadhyay 2018). Recommendations established by the World Health Organization (WHO) allow a maximum concentration of nitrate in drinking water of 50 mg L^{-1} in Europe and 44 mg L^{-1} in the United States (Bryan and Ivy 2015), while the average daily nitrate intake was estimated at 43-141 mg. For nitrates and nitrites, optimal doses are much lower than harmful and lethal doses (Sindelar and Milkowski 2012).

According to scientists, the main risk of consuming increased levels of nitrates is their derivatives, such as nitrites, oxides and N-nitroso compounds (Colla et al. 2018). The nitrosation process is thought to be very important. There is S-nitrosation and N-nitrosation, the latter of which is harmful to the body and may result in the formation of carcinogenic compounds. According to scientists, however, this process does not occur under conditions of normal metabolism (Bryan et al. 2012). Although scientists currently claim that many civilizational diseases are mainly caused by poor nutrition, physical inactivity and stimulants, and there are no clear results of studies on the carcinogenic effect of nitrates in humans, not only in laboratory animals, there is still a need for further research and control of consumed nitrates in the diet. There are many review articles that collect research on the effects of nitrates and nitrites on animal organisms depending on the doses taken (Bedale et al. 2016; Bryan et al. 2012; Bryan and Ivy 2015; McKnight et al. 2009; Sindelar and Milkowski 2012).

Deviating from the subject of human health, poor management of available natural resources by people, excessive use of nitrate fertilizers in agriculture and the production of pollutants and waste also disturb the balance of the natural environment and the nitrogen cycle in nature by significantly increasing the concentration of nitrates and nitrites. Water is particularly susceptible to pollution, the purity of which should be particularly important to us nowadays. Too high concentration of nitrates in surface water bodies causes excessive growth of algae and phytoplankton, which contribute to the death of aquatic organisms that do not have access to dissolved oxygen in the water and to overgrowth of water bodies (eutrophication phenomenon) (Alahi and Mukhopadhyay 2018).

Concerns about the impact of increased consumption of nitrates and nitrites both on human health and the state of the natural environment made it very important to monitor their content in both the environment and in food products and drinking water. Therefore, it is important to develop effective, quick and accurate methods for determining the content of these ions in natural samples.

Scientists developed and implemented many analytical methods to determine nitrates in various types of natural samples, including spectrophotometry (Yue et al. 2004), gas chromatography (Akyüz and Ata 2009; Campanella et al. 2017), liquid chromatography (Akyüz and Ata 2009; Croitoru 2012), colorimetry (Woollard and Indyk 2014), spectrophotometry (García-Robledo et al. 2014), spectrofluorimetry (Biswas et al. 2004), amperometry (Can et al. 2012), voltammetry (Guadagnini and Tonelli 2013).

Potentiometric methods are often used to determine the concentration of nitrate ions in water samples because they allow for direct, quick and cheap measurements and do not require a complicated sample preparation process. In

addition, potentiometric sensors with special parameters can be used for real-time and in situ research, which is particularly useful in monitoring the state of the natural environment. Ion-selective electrodes often show very good selectivity for selected main ions and they also reach lower and lower detection limits each year. In addition, the use of solids contact in ion-selective sensors, enabling the removal of the internal solution, allowed to increase the mechanical resistance of the electrodes, facilitate their storage and transport, and allowed for their miniaturization, which is particularly useful in the construction of multi-sensor platforms for applications in environmental measurements (Alahi and Mukhopadhyay 2018).

The first use of potentiometry for the determination of nitrate ions in water took place in the 1980s (Alahi and Mukhopadhyay 2018). Since then, there are still new research articles describing the innovative use of active substances and solid contacts, making it possible to obtain sensors with better and better analytical parameters.

In 2007, the Álvarez-Romero team constructed a potentiometric sensor using a composite material, polypyrrole doped with nitrate as recognition agent, to ensure selectivity for nitrate ions. The sensors obtained in this way were characterized by extended life time (~ 6 months) compared to unmodified electrodes and the possibility of regeneration of the sensor's active surface. Efficacy was tested in a real sample – in a drug (determination of isosorbide mononitrate, the active ingredient of Elantan) (Álvarez-Romero et al. 2007).

All-solid-state potentiometric sensors for nitrate determination using graphene as an ion-electron transducer were also constructed. The water layer test and impedance measurements were performed, confirming a significant reduction of the charge transfer resistance for the tested electrodes. In this way, sensors with a very good slope of the electrode characteristic curve (-57.9 mV / dec) and a fast response time (~ 10 s) were obtained, which were then successfully used to determine the nitrate content in drinking water samples (Tang et al. 2012).

Lipophilic multiwalled carbon nanotubes (f-MWCNT) were also used as the ion-electron transducer placed between the solid electrode material and the ion-selective membrane layer. According to the authors, the obtained sensors showed many advantages, such as insensitivity to pressure and light, the possibility of vertical or horizontal orientation, and high mechanical and chemical strength, which may be particularly useful in the construction of multi-sensor research platforms for determining the content of selected ions in the environment in situ (Yuan et al. 2015).

An interesting solution was proposed by scientists from the Garland team, who used laser induced graphene (LIG) as an innovative way to produce ion-selective electrodes. According to the authors, it is to be a one-step, easy and cheap process of producing laser recording on polyamide substrates, which can then be used for scalable roll production and disposable sensors in technologies. The publication focuses on the determination of nitrogen available to plants in soil in the form of both nitrate (NO_3^-) and ammonium (NH_4^+) (Garland et al. 2018).

also used as a component of the ion-selective membrane consisting of polyvinyl chloride (PVC) and a plasticizer (NPOE). The ionic liquid played a very important role in this case, both the ionophores and the ionic lipophilic component reducing the resistance of the ion-selective membrane, as well as the converter aimed at stabilizing the potential of the internal electrode. It is an inexpensive and easy to manufacture sensor with good potential stability and selectivity. It was used in samples of water and vegetables, in which the content of nitrate ions was successfully determined (Wardak 2014).

Table 1. presents a summary of analytical parameters for selected sensors sensitive to nitrate ions, which have been described in the literature over the last 15 years.

Table 1. Comparison of basic analytical parameters of nitrate ion-selective electrodes with solid contact.

Active substance	Contact	Slope [mV/dec]	LOD [mol L⁻¹]	Linear range [mol L⁻¹]	Response time [s]	Life time [months]	Refence
Ppy(NO$_3$) composite	graphite powder	-57.1	5.4×10^{-6}	1.5×10^{-4} – 1.0×10^{-5}	20	-6	(Alvarez-Romero et al., 2007)
MTDDA-NO$_3$	graphene	-57.9	3.0×10^{-6}	5.0×10^{-6} – 1.0×10^{-1}	~10	-	(Tang et al., 2012)
TDMAN	f-MW-CNTs	-57.7	2.5×10^{-6}	3.2×10^{-6} – 1.0×10^{-1}	-	-	(Yuan et al., 2015)
TDMAN	laser induced graphene	-54.8	2.1×10^{-6}	5.0×10^{-5} – 1.0×10^{-2}	-	-	(Garland et al., 2018)
TDMAN	POT-MoS$_2$ nanocomposite	-64.0	9.2×10^{-8}	7.1×10^{-4} – 1.0×10^{-8}	-	-	(Ali et al., 2019)
TDMAN	PNPs-CB	-58.6	5.0×10^{-7}	1.0×10^{-6} – 1.0×10^{-1}	5	~5	(Paczosa-Bator et al., 2013)
(Nit+/NO$_3$-) complex	MWCNTs	-55.1	2.8×10^{-6}	8.0×10^{-6} – 1.0×10^{-2}	<10	2	(Hassan et al., 2019)
poly(N-methylpyrrole)	-	-56.3	2.8×10^{-6}	5.0×10^{-6} – 1.0×10^{-1}	-	6	(Bomar et al., 2017)
nitrate ionophore V	TTF(NO$_3$)	-59.4	6.3×10^{-7}	1.0×10^{-6} – 1.0×10^{-1}	-	-	(Piek et al., 2015)

Again, in order to test soil samples, sensors were constructed using a novel nanocomposite of poly(3-octyl-thiophene) and molybdenum disulfide (POT-MoS$_2$) as a solid contact layer. The nanocomposite is characterized by high hydrophobicity and redox properties. Based on the research, it was found that the modification of the POT chain with MoS$_2$ increased both the conductivity and the anion exchange, and minimized the formation of a water layer at the interface between the ion-selective membrane and the substrate (in this case, the Au electrode). The purpose of the sensor is long-term use and continuous monitoring of nitrate content in the soil (Ali et al. 2019).

Sensors with very good stability, repeatability and potential reproducibility were produced by using platinum nanoparticles on a carbon black support (Pt-NPs-CB) as solid contact. The research used chronopotentiometry with current reversal and the potentiometric test of the water layer. Additionally, the use of this type of transducer made it possible to significantly reduce the resistance of the ion-selective membrane (Paczosa-Bator et al. 2013).

The use of the association complex of nitron–nitrate ions (Nit⁺/NO$_3$⁻) and multi-wall carbon nanotubes (MWCNT) as an intermediate layer between the ion-selective membrane (ISM) and the glassy carbon substrate made it possible to significantly reduce the potential drift after modification and over 10-fold increase in double layer capacitance compared to a conventional ion selective electrode. The generated sensors were successfully used to test real samples for the presence of nitrate ions – wastewater, fertilizers and gun powder samples (Hassan et al. 2019).

Another method of obtaining ion-selective electrodes sensitive to nitrate ions was electropolymerization of N-methylpyrrole with the use of potassium nitrate as an auxiliary electrolyte by the Bomar research team. It has been found that N-methylpyrrole is better than pyrrole for this purpose, and electrodes with an ionic imprinted polymer exhibit very good selectivity and stability of potential and a long lifetime (Bomar et al. 2017).

The electrodes were also constructed with a graphene–tetrathiafulvalene interlayer acting as a solid contact. The use of graphene allowed to obtain a much lower resistance of the ion-selective membrane and a potential drift compared to the unmodified electrode. In this case, the best parameters were obtained for the electrode modified with GR-TTF(NO$_3$) nanocomposite (Piek et al. 2016).

A completely new active substance used in the ion-selective electrodes was a cobalt(II) complex with 4,7-diphenyl-1,10-phenanthroline (Bphen) with the formula Co(Bphen)$_2$(NO$_3$)$_2$(H$_2$O)$_2$. The obtained sensor with simple operation and construction, without an additional intermediate layer, which was characterized by very good analytical parameters, a wide measuring range and pH range in which the sensors could work (5.4 – 10.6), fast response time and very good potential stability. The electrodes worked properly for many months. Their practical application has been checked in the determination of nitrate ions in natural samples: water (mineral, tap and river water) and in vegetables (Pietrzak et al. 2020).

In order to improve the analytical parameters of the electrodes, an addition of ionic liquid (IL) – trihexyltetradecylphosphonium chloride (THTDPCl) was

Type of ISE (solid contact/inner electrode)	Sample	Method	Ref
Ionic liquid(TDMACl)/Ag/AgCl	Mineral water, Tap water	Multiple standard addition	(Wardak et Grabarczyk, 2016)
	Vegetables (Iceberg lettuce Butterhead lettuce Fresh spinach)	Multiple standard addition	
MWCNTs/GCE	Waste waters (Aerated lagoon effluent, Raw sewage plant inflo, Nitrate fertilizer factory, outfalls)	Calibration curve	(Hassan et al., 2019)
Ionic liquid(TDMACl)/Ag/AgCl	Tap water, Mineral water, River water	Calibration curve	(Pietrzak et al., 2020)

Recently our team developed all solid state nitrate ion-selective electrodes in which ionic liquid and multiwalled carbon nanotubes were used as additional membrane components (Pietrzak and Wardak 2020). Such modification of membrane composition caused noticeable improvement in the electrode performance especially in potential stability and reversibility. The electrode with the best analytical parameters was successfully used for nitrate determination in natural waters samples (water from Bystrzyca River and Zemorzyce Lake) and vegetables. The water samples were analyzed without pretreatment, whereas vegetables were analyzed after minimum sample preparation without mineralization. They were collected from local markets during the period of March –April 2019. A 5g portion of previously homogenized vegetable samples was mixed with deionized water and the mixtures were stirred and heated (80°C) for 30 min. After cooling the solutions were transferred to a 500 mL volumetric flask and diluted to volume with deionized water.

Potentiometric measurements of electromotive force (EMF) were performed in a two-electrode system with an ion-selective electrode sensitive to nitrate ions (NO_3-SCISE) as an electrode working against a silver–chloride electrode as a reference electrode. The determination of nitrate was performed by the standard addition method. Recovery was also examined. Obtained results are presented in Table 3 where it can be seen that our electrode is suitable for nitrate monitoring in environmental samples.

Active substance	Contact	Slope [mV/dec]	LOD [mol L⁻¹]	Linear range [mol L⁻¹]	Response time [s]	Life time [months]	Reference
nitrate ionophore V	GR-TTF	-59.1	6.3×10^{-7}	$1.0 \times 10^{-6} – 1.0 \times 10^{-2}$	-	-	(Pięk et al., 2016)
Co(Bphen)₂ (NO₃)₂	Ag/AgCl/Cl	-56.3	4.0×10^{-6}	$1.0 \times 10^{-5} – 1.0 \times 10^{-1}$	-	> 3	(Pietrzak et al., 2020)
THTDPCl	Ag/AgCl/Cl	-60.1	2.8×10^{-6}	$1.0 \times 10^{-5} – 1.0 \times 10^{-1}$	5-10	> 4	(Wardak, 2014)

LOD – limit of detection;
MTDDA-NO₃ – methyltridodecylammonium nitrate,
TTF-TCNQ – tetrathiafulvalene-tetracyanoquinodimethane;
f-MWCNTs – lipophilic multiwalled carbon nanotubes;
TDMAN – tridodecylmethylaluminium nitrate;
THTDPCl – trihexyl- tetradecylphosphonium chloride;
Ppy(NO₃) composite – composite comprising graphite powder, polypyrrole doped with nitrate and epoxy resin;
CRGNO – chemically reduced graphene oxide;
PtNPs-CB – carbon black supporting platinum nanoparticles;
(Nit⁺/NO₃⁻) – nitron-nitrate ion association complex;
GR-TTF – graphene–tetrathiafulvalene nanocomposite;
TDMACl – tridodecylmethylammonium chloride;

Table 2 shows examples of the application of solid contact ISEs for the determination of nitrates in natural samples, e.g. in various water samples and vegetables using ion-selective electrodes.

Table 2. Examples of application of solid contact ISEs for the determination of nitrates in real samples.

Type of ISE (solid contact/inner electrode)	Sample	Method	Ref
Graphene/GCE	Mineral water, Tap water	Calibration curve	(Tang et al., 2012)
TTF/NO₃⁻/GCE	Ground water, Well water, Tap water, River water	Calibration curve	(Piek et al. 2015)

lower detection limits and better potential stability, at the same time with very good selectivity, which is a special feature of ion-selective electrodes. This creates more and more possibilities to monitor nitrate in the environment in different samples, also online.

References

1. Akyüz M., Ata S. (2009) Determination of low level nitrite and nitrate in biological, food and environmental samples by gas chromatography – mass spectrometry and liquid chromatography with fluorescence detection. Talanta 79: 900–904.

2. Alahi E.E, Mukhopadhyay S.C. (2018) Detection methods of nitrate in water: A review. Sensors & Actuators: A Physical 280: 210–221.

3. Ali M.A., Wang X., Chen Y., Jiao Y., Mahal N.K., Moru S., Castellano M.J., Schnable J.C., Schnable P.S., Dong L. (2019) Continuous Monitoring of Soil Nitrate Using a Miniature Sensor with Poly(3-octyl-thiophene) and Molybdenum Disulfide Nanocomposite. ACS Applied Materials and Interfaces 11(32): 29195–29206.

4. Álvarez-Romero G.A., Palomar-Pardavé M.E., Ramírez-Silva M.T. (2007) Development of a novel nitrate-selective composite sensor based on doped polypyrrole. Analytical and Bioanalytical Chemistry 387(4): 1533–1541.

5. Bedale W., Sindelar J.J., Milkowski A.L. (2016) Dietary nitrate and nitrite: Benefits, risks, and evolving perceptions. Meat Science 120: 85–92.

6. Biswas S., Chowdhury B., Ray B.C. (2004) A novel spectrofluorimetric method for the ultra trace analysis of nitrite and nitrate in aqueous medium and its application to air, water, soil and forensic samples. Talanta 64: 308–312.

7. Bomar E., Owens G., Murray G. (2017) Nitrate Ion Selective Electrode Based on Ion Imprinted Poly(N-methylpyrrole). Chemosensors 5(1): 2.

8. Bryan N.S., Alexander D.D., Coughlin J.R., Milkowski A.L., Boffetta P. (2012) Ingested nitrate and nitrite and stomach cancer risk: An updated review. Food and Chemical Toxicology 50(10): 3646–3665.

9. Bryan N. S., Ivy, J. L. (2015) Inorganic nitrite and nitrate: evidence to support consideration as dietary nutrients. Nutrition Research 35(8): 643–654.

10. Campanella B., Onor M., Pagliano E. (2017) Rapid determination of nitrate in vegetables by gas chromatography mass spectrometry. Analytica Chimica Acta 980: 33–40.

11. Can F., Ozoner S.K., Ergenekon P., Erhan E. (2012) Amperometric nitrate biosensor based on Carbon nanotube/Polypyrrole/Nitrate reductase biofilm electrode. Materials Science & Engineering C 32(1): 18–23.

12. Colla G., Kim H., Kyriacou M.C., Rouphael Y. (2018) Nitrate in fruits and vegetables. Scientia Horticulturae 237: 221–238.

13. Croitoru M.D. (2012) Nitrite and nitrate can be accurately measured in samples of vegetal and animal origin using an HPLC-UV/VIS technique. Journal of Chromatography B 911: 154–161.

14. García-Robledo E., Corzo A., Papaspyrou S. (2014) A fast and direct spectrophotometric method for the sequential determination of nitrate and nitrite at low concentrations in small volumes. Marine Chemistry 162: 30–36.

15. Garland N.T., Mclamore E.S., Cavallaro N.D., Mendivelso-Perez D., Smith E.A., Jing D., Claussen J.C. (2018) Flexible Laser-Induced Graphene for Nitrogen Sensing in Soil. ACS Applied Materials and Interfaces 10(45): 39124–39133.

Table 3. Result of nitrates determination in various samples (unspiked and spiked) using nitrate ion-selective electrode.

Sample	Nitrate found by NO₃⁻SCISE, mg L⁻¹ or mg kg⁻¹	Recovery, %
River water	14.6 ± 0.4	-
River water +50 mg L⁻¹ NO₃⁻	65.2 ± 0.6	100.9
Lake water	17.2 ± 0.7	-
Lake water +50 mg L⁻¹ NO₃⁻	66.8 ± 1.1	99.4
butterhead lettuce	916 ± 18	-
butterhead lettuce + 300 mg kg⁻¹ NO₃⁻	1226 ± 23	100.8
Radish	396 ± 16	-
Radish +300 mg kg⁻¹ NO₃⁻	732 ± 19	105
Fresh spinach	1322 ± 11	-
Fresh spinach + 300 mg kg⁻¹ NO₃⁻	1546 ± 13	95.3
Cucumber	532 ± 23	-
Cucumber + 300 mg kg⁻¹ NO₃⁻	815 ± 27	97.9
Cabbage	312 ± 23	-
Cabbage + 300 mg kg⁻¹ NO₃⁻	612 ± 22	100
Tomato	414 ± 16	-
Tomato + 300 mg kg⁻¹ NO₃⁻	688 ± 27	96.4

Conclusions

Ion-selective electrodes are a cheap and simple analytical tool for determination of many ions in environmental samples, including nitrates. In recent years scientists constructed many types of ion-selective electrodes with lower and

POLYCARBONATES – SYNTHESIS, PROPERTIES AND ENVIRONMENTAL IMPACT

K. Wnuczek, B. Podkościelna

Maria Curie-Skłodowska University, Institute of Chemical Science, Faculty of Chemistry, Department of Polymer Chemistry, Gliniana 33, 20-614, Lublin, Poland

Abstract

In this work a synthesis of commercially available polycarbonates as well as selected applications of these unique polymers are discussed. A traditional method of synthesis using phosgene and Bisphenol A, as well as methods based on the transesterification of methyl carbonate and diphenyl carbonate are presented. The advantages and disadvantages of the above procedures are shown. The possibilities of replacing the phosgene technology, used by most polycarbonate manufacturers, with more environmentally friendly methods were assessed. In addition, the work includes general characteristics of polycarbonates and their wide application.

Keywords: polycarbonate, Bisphenol A, phosgene

Introduction

Polycarbonates are materials we encounter every day. It is a class of thermoplastic polymers that are formally esters of carbonic acid. They have a lot of advantages such as hardness, ductility, rigidity, transparency, toughness and excellent mechanical properties. These materials are amorphous and polar polymers (Hammami et al. 2012, Shu et al. 2019). Polycarbonate, as a commercial thermoplastic engineering plastic, has been widely applied in electronics, medical equipment, food packaging, automotive industries, aerospace because of its unique thermal, mechanical, electrical and optical properties (Hauenstein et al. 2016, Zhencai et al. 2020). Due to this set of favorable properties, polycarbonates have many applications. The most advantageous properties, compared to other thermoplastics, are as follows: high impact strength, good dielectric properties, good dimensional stability, wide operating temperature range, creep strength, low water absorption, and self-extinguishing tendency. In addition, most polycarbonates, are non-toxic, very hard, abrasion and chemical resistant materials (Schnell 1964, Tabell et al. 1959, Hubacher 1957).

A number of properties of this polymer depends on the chemical structure of a polycarbonate particle. Polycarbonate macromolecules are characterized by high stiffness, limited rotation of aromatic rings and relatively long segments without polar groups (Serini 2000, Distaso et al. 2006, Darensbourg et al. 2011). The general characteristics of polycarbonates have been well described in literature. The thermal properties of unmodified polycarbonate, which can operate

16. Guadagnini L., Tonelli D. (2013) Carbon electrodes unmodified and decorated with silver nanoparticles for the determination of nitrite, nitrate and iodate. Sensors and Actuators: B. Chemical 188: 806–814.

17. Hassan S.S.M., Eldin A.G., Amr A.E.-G. E., Al-Omar M.A., Kamel A.H., Khalifa N.M. (2019) Improved Solid-Contact Nitrate Ion Selective Electrodes Based on Multi-Walled Carbon Nanotubes (MWCNTs) as an Ion-to-Electron Transducer. Sensors 19(18): 3891.

18. Iammarino M., Taranto A.D., Cristino M. (2013) Endogenous levels of nitrites and nitrates in wide consumption foodstuffs: Results of five years of official controls and monitoring. Food Chemistry 140(4): 763–771.

19. McKnight G.M., Duncan C.W., Leifert C., Golden M.H. (2009) Dietary nitrate in man: friend or foe? British Journal of Nutrition 81: 349–358.

20. Paczosa-Bator B., Cabaj L., Piech R., Skupień K. (2013) Potentiometric sensors with carbon black supporting platinum nanoparticles. Analytical Chemistry 85(21): 10255–10261.

21. Piech R., Paczosa-Bator B. (2015) Improved nitrate sensing using solid contact ion-selective electrodes based on TTF and its radical salts. Journal of The Electrochemical Society 162:B257-B263.

22. Piech M., Piech R., Paczosa-Bator B. (2016) All-solid-state nitrate selective electrode with graphene/tetrathiafulvalene nanocomposite as high redox and double layer capacitance solid contact. Electrochimica Acta 210: 407–414.

23. Pietrzak K., Wardak C., Łyszczek R. (2020) Solid Contact Nitrate Ion-selective Electrode Based on Cobalt(II) Complex with 4,7-Diphenyl-1,10-phenanthroline. Electroanalysis 32(4): 724–731.

24. Pietrzak K., Wardak C. (2020) Influence of membrane modification with various types of carbon nanotubes on the parameters of electrodes dedicated to the determination of nitrate ions. [in:] Danielewska A., Maciąg M.(eds.) Life Sciences Research – New Trends, Ed. House TYGIEL, Lublin pp. 239-247.

25. Sindelar J.J., Milkowski A.L. (2012) Human safety controversies surrounding nitrate and nitrite in the diet. Nitric Oxide 26(4): 259-266.

26. Tang W., Ping J., Fan K., Wang Y., Luo X., Ying Y., Wu J., Zhou Q. (2012) All-solid-state nitrate-selective electrode and its application in drinking water. Electrochimica Acta 81: 186–190.

27. Wardak C. (2014) Solid contact nitrate ion-selective electrode based on ionic liquid with stable and reproducible potential. Electroanalysis 26(4): 864–872.

28. Wardak C., Grabarczyk M. (2016) Analytical application of solid contact ion-selective electrodes for determination of copper and nitrate in various food products and drinking water. Journal of Environmental Science and Health – Part B 51(8): 519-524.

29. Woollard D. C., Indyk H. E. (2014) Colorimetric determination of nitrate and nitrite in milk and milk powders – Use of vanadium(III) reduction. International Dairy Journal 35(1): 88-94.

30. Yuan D., Anthis A.H.C., Ghahraman Afshar M., Pankratova N., Cuartero M., Crespo G.A., Bakker E. (2015) All-Solid-State Potentiometric Sensors with a Multiwalled Carbon Nanotube Inner Transducing Layer for Anion Detection in Environmental Samples. Analytical Chemistry 87(17): 8640-8645.

31. Yue X., Zhang Z., Yan H. (2004) Flow injection catalytic spectrophotometric simultaneous determination of nitrite and nitrate. Talanta 62: 97–101.

D4

APPLICATION OF POLYANILINE NANOFIBERS FOR THE CONSTRUCTION OF NITRATE ALL-SOLID-STATE ION-SELECTIVE ELECTRODES

ORIGINAL ARTICLE

Application of polyaniline nanofibers for the construction of nitrate all-solid-state ion-selective electrodes

Karolina Pietrzak[1] · Cecylia Wardak[1] · Szymon Malinowski[2]

Abstract

The application of polyaniline nanofibers doped with chloride and nitrate ions (PANINFs-Cl and PANINFs-NO_3) in potentiometry was described. Both kinds of nanofibers were used as an ion-to-electron transducer in ion-selective electrodes with solid contact (SCISEs). Extensive research on the properties of the nanofibers themselves (SEM, UV–Vis spectroscopy, FTIR) and the constructed electrodes (potentiometric methods, electrochemical impedance spectroscopy) has been carried out. Basic analytical parameters of electrodes containing various nanofibers contents in the ion-selective membrane and with nanofibers as an intermediate layer were determined. It was found that application of PANI nanofibers resulted in improvement of electrode performance (among others, better stability and reversibility of the electrode potential). The obtained sensors were characterized by a high slope of the calibration curve, a wide measuring range and a fast response time. Moreover, they were insensitive to change of redox potential, as well as light and the presence of oxygen in the solution, what is important from a practical point of view. They were also successfully used for nitrate determination in real environmental samples.

Keywords Ion-selective electrodes · Solid contact · Potentiometry · Nitrate · PANI nanofibers

Introduction

Thanks to their numerous technical advantages (easy operation of the equipment, speed of analysis, cheap apparatus, no need for special preparation of liquid samples) and analytical ones (very good selectivity, low detection limits) potentiometric methods are still very popular, especially in environmental chemistry (De Marco et al. 2007; Crespo 2017). The most popular sensors used in potentiometric methods are ion-selective electrodes (ISEs). The principle of measurement using them is to measure the electrochemical force of the cell (EMF), which is made of an ion-selective electrode (whose potential depends on the activity of ions in the solution) and a reference electrode (whose potential is constant) (Hu et al. 2016).

The first designs of ion-selective electrodes consisted of an inner electrode, an ion-selective membrane and also an internal solution placed between them, which was in direct contact with the membrane and provided the proper charge transfer mechanism between the membrane and the discharge electrode. They showed very good analytical parameters, but due to the presence of the solution inside the electrode the sensors had a relatively large size and their storage and transport were difficult. Air bubbles could have occurred inside such an electrode and moreover, it was necessary to replenish the solution which, when leaking into the sample solution, could cause an artificial increase in the detection limit by triggering an increase in the concentration of the analyte (main ion) in the nearest sample-electrode layer. The solution in this case was to eliminate of internal solution (coated-wire electrodes); however, this was associated with deterioration in the stability and reversibility of the electrode potential as a result of the direct connection of two materials with different conductivity, notably the substrate electrode (electronic conductivity) and the ion-selective membrane (ionic conductivity), thus blocking the flow of charge at the interface (Bobacka 2006). To obtain a satisfactory potential

✉ Cecylia Wardak
cecylia.wardak@mail.umcs.pl

[1] Department of Analytical Chemistry, Faculty of Chemistry, Institute of Chemical Sciences, Maria Curie-Sklodowska University, Maria Curie-Sklodowska Sq. 3, 20-031 Lublin, Poland

[2] Faculty of Civil Engineering and Architecture, Lublin University of Technology, Nadbystrzycka 40, 20-618 Lublin, Poland

stability, at the same time with no internal solution, additional material with mixed conductivity (ion–electron transducer) placed as an intermediate layer between them, was used to construct the electrodes (Michalska 2012). In this way, ion-selective electrodes with solid contact (SCISEs) were created (Bieg et al. 2017). The use of this additive contributed to ensuring the appropriate stability and reversibility of the sensors' potential, facilitated their operation under changing pressure and temperature conditions, and enabled their miniaturization and shape change (Bobacka et al. 2008; Lindner and Gyurcsányi 2009).

The first conductive polymers to be used for this purpose were as follows: poly(pyrrole) (PPy) (Michalska et al. 1994; Sutter et al. 2004), poly(3-octylthiophene) (POT) (Konopka et al. 2004; Chumbimuni-Torres et al. 2006; Rubinova et al. 2007), poly(3,4-ethylenedioxythiophene) (PEDOT) (Bobacka et al. 2001; Vázquez et al. 2002; Ocypa et al. 2006) or polianiline (PANI) (An et al. 2000; Han et al. 2004; Lindfors et al. 2007). The characteristics of the SCISEs in which they are used as ion–electron transducers have improved significantly over the years and they are still widely used for this purpose (Bobacka 2006). Conductive polymers belong to a group of materials with unique electrical, electrochemical and optical properties (Abdolahi et al. 2012). Due to its synthesis simplicity, high environmental stability (Jiang et al. 2018), good redox properties, attractive price and unique chemical structure polyaniline (PANI) is particularly important in designing sensors and biosensors (Ahmed et al. 2021). The PANI can be synthesized by oxidative chemical or electrochemical polymerization (Zhang and Wang 2006) and can exist in three forms with different oxidation states and protonation level: leucoemeraldine, pernigraniline and emeraldine base (Najim and Salim 2017). These forms have different conductivities and only emeraldine base PANI in half oxidation state is conductive (Dan et al. 2009). As is reported in the work by Jiang et al. (2018) nanostructured conductive polymers in the form of nanofibers (Zhang et al. 2021), nanowires (Zhang et al. 2020; Zeng et al. 2021) or nanotubes (Das et al. 2021) are particularly important in the field of chemical sensors. In comparison to globular PANI nanostructured forms exhibit greater sensitivity and faster time due to their higher surface area (Huang and Kaner 2004). The PANI nanostructures with controllable length and diameter can be synthesized using hard-template synthesis method that utilizes pores and/or channels of porous materials, i.e., membranes, zeolites or anodic aluminum oxide. However, removal of the template is relatively difficult, which makes this method unpopular (Zhang and Wang 2006). The soft-template synthesis methods, also known as template-free method or self-assembly method to obtain PANI nanostructures uses various structure-directing molecules i.e., surfactants (Zhang and Manohar 2004), deoxyribonucleic acid (DNA) or polyelectrolytes.

Procedures that do not use any matrix, either hard or soft, are a completely separate group of methods for synthesis of nanostructured polymers. This group of methods includes interfacial, radiolytic, rapid mixing, sonochemical and electrochemical polymerization (Zhang and Wang 2006).

This study described the properties of synthesized polyaniline (PANI) nanofibers doped with chloride (PANINFs-Cl) and nitrate (PANINFs-NO_3) ions and their use as solid contact in ion-selective electrodes sensitive to nitrate ions. The synthesized nanofibers were characterized using SEM, UV–Vis and FTIR spectrophotometry. They were then used in two ways: as an intermediate layer between the inner glassy carbon electrode and the ion-selective membrane, and as the ion-selective membrane component. The basic analytical parameters of the constructed sensors were examined in order to investigate the influence of PANI nanofibers on their performance. On the basis of potentiometric measurements, information was obtained about the slope of the electrode characteristic curve, their linearity range and the limit of detection, as well as the stability and reversibility of the potential. In addition, research was conducted to investigate the influence of variable conditions on the proper operation of the sensors (the effect of changes in solution pH and redox potential, the presence of light and oxygen) were carried out. Electrochemical impedance spectroscopy (EIS) was used to determine and compare the electrical parameters of the electrodes, whose values could have changed after the modification of the sensors.

Materials and methods

Apparatus

To carry out research enabling the characterization of the obtained structures (PANINFs-Cl and PANINFs-NO_3), their solutions with a concentration of 1 mg mL^{-1} in THF were prepared. The images of PANINFs structure were recorded using a high-resolution scanning electron microscope Quanta 3D FEG (FEI Hillsboro, USA). Ultraviolet–visible spectra (UV–Vis) were recorded on Helios Gamma (Thermo Scientific) ultraviolet–visible spectrometer in wavelength ranged from 200 to 900 nm. FT–IR/DRS spectra were collected using a Nicolet 380 spectrophotometer purchased from Thermo Scientific. The spectra of PANI nanostructures obtained in presence of Cl^- and NO_3^- ions were recorded in range of 4000–400 cm^{-1} with resolution of 4 cm^{-1} at room temperature. To guarantee good signal/noise ratio, the spectra were consisted of 2048 scans.

Potentiometric measurements were performed for a cell which consisted of the tested ion-selective electrodes and the Ag/AgCl reference electrode (Metrohm 6.0750.100). The electrodes were immersed in solutions of the main ion

salt (KNO_3) mixed with a magnetic stirrer. A potentiometer (Lawson Labs, Inc.) coupled to a computer was used to obtain and collect data. Additionally, an ORION 81-72 glass electrode and an Elmetron CX-741 potentiometer were used to determine the pH of the solutions. All measurements were made at room temperature.

Measurements obtained by the electrochemical impedance spectroscopy (EIS) were performed in a 1×10^{-2} mol L^{-1} KNO_3 solution. The system included three kinds of electrodes: our tested ISE as working electrode, Ag/AgCl reference electrode (Metrohm 6.0733.100) and the auxiliary electrode—a GC rod 2 mm/65 mm (Metrohm). As the measuring device the AUTOLAB electrochemical analyzer (Eco Chemie, Netherlands) controlled by NOVA software. The impedance spectra were recorded in the frequency range 0.1–100 kHz at the open circuit potential with an amplitude 10 mV.

Reagents

Substances necessary for the synthesis of aniline nanofibers: aniline monomer, ammonium peroxydisulfate (APS), hydrochloric acid, nitric acid, tetrahydrofuran (THF) were purchased from Chempur.

Ion-selective membrane components for electrodes construction: o-nitrophenyl octyl ether (NPOE), low molecular weight poly(vinylchloride) (PVC), tridodecyl dimethyl ammonium nitrate ($TDMANO_3$) were purchased from Aldrich. Salts for the preparation of solutions with different redox potential were obtained from Alfa Aesar ($Na_4Fe(CN)_6 \times 10\ H_2O$) and from POCh—Polish Chemical Reagents ($K_3Fe(CN)_6$). The remaining substances, including potassium salts for testing the selectivity of sensors, sulfuric acid and sodium base for changes of pH of the solutions, were obtained from Fluka. Compounds of the highest purity and freshly redistilled water were used to prepare all solutions.

PANI nanofibers synthesis

PANI nanofibers were synthesized by interfacial polymerization according to procedure described in paper (Huang and Kaner 2004) and shown in Fig. 1. A 50 mmol amount of aniline monomer was dissolved in mixture of EtOH and distilled water to obtain solution with concentration of 5×10^{-2} mol L^{-1}. Then, in two separate vials, 0.08 mmol of APS was dissolved in 1 mol L^{-1} HCl and HNO_3 solution, respectively. To carry out the polymerization reaction, the aniline monomer and oxidant solutions were carefully transferred to a beaker to form static interface of two phases: organic phase and water phase. After 12 h the resulting precipitate was filtered and cleaned using deionized water several times. Directly before using, the synthesized PANI nanofibers were dried at 60 °C for 24 h.

Preparation of the ion-selective membrane

To prepare every membrane mixture, all their components were weighed out on an analytical balance in accordance with the previously calculated mass values, and then the dry ingredients were combined with an organic solvent (THF) and homogenized for half an hour in an ultrasonic water bath until a homogeneous mixtures were obtained. 1 ml of solvent was added per 0.1 g of ingredients. In the case of both types of nanofibers, 4 types of membrane mixtures were prepared: basic mixture (62% NPOE, 32% PVC, 6% $TDMANO_3$); I mixture (61.5% NPOE, 32% PVC, 6% $TDMANO_3$, 0.5% nanofibers); II mixture (61% NPOE, 32% PVC, 6% $TDMANO_3$, 1% nanofibers); III mixture (60% NPOE, 32% PVC, 6% $TDMANO_3$, 2% nanofibers).

Preparation of all-solid-state ion-selective electrodes

Glassy carbon electrodes (GCE) (0.3 cm diameter) were polished thoroughly with 5000 grit sandpaper and then polished with wetted alumina powder (0.3 μm grain diameter). The electrodes were rinsed thoroughly with distilled water, immersed in water in an ultrasonic bath, and rinsed again with distilled water to remove dust residues. To get rid of organic residues, the electrodes were immersed in THF and allowed to dry in a stand. For both types of nanofibers, 5 types of electrodes were made: unmodified electrodes containing only the basic mixture without nanofibers—GCE/ISM, electrodes with 0.5; 1.0 and 2% nanofibers in the ion-selective membrane (GCE/(ISM + 0.5%PANINFs-Cl); GCE/(ISM + 1.0%PANINFs-Cl) and GCE/(ISM + 2.0%PANINFs-Cl) for PANI-Cl nanofibers and GCE/(ISM + 0.5%PANINFs-NO_3); GCE/(ISM + 1.0%PANINFs-NO_3) and GCE/(ISM + 2.0%PANINFs-NO_3) for PANI-NO_3 nanofibers, respectively) and electrodes with an intermediate layer of nanofibers (15 μl of 0.01 g/ml nanofibers in THF)—GCE/PANINFs-Cl/ISM and GCE/PANINFs-NO_3/ISM. On the dry surfaces of the electrodes, 3 times 50 μl of membrane mixtures were spotted with an interval of 30 min. The electrodes were then allowed to dry overnight and the next day immersed in a conditioning solution of KNO_3 salt at a concentration of 1×10^{-3} mol L^{-1}. Between measurements all electrodes were stored in separate containers, immersed in the conditioning solution, closed in a dark place.
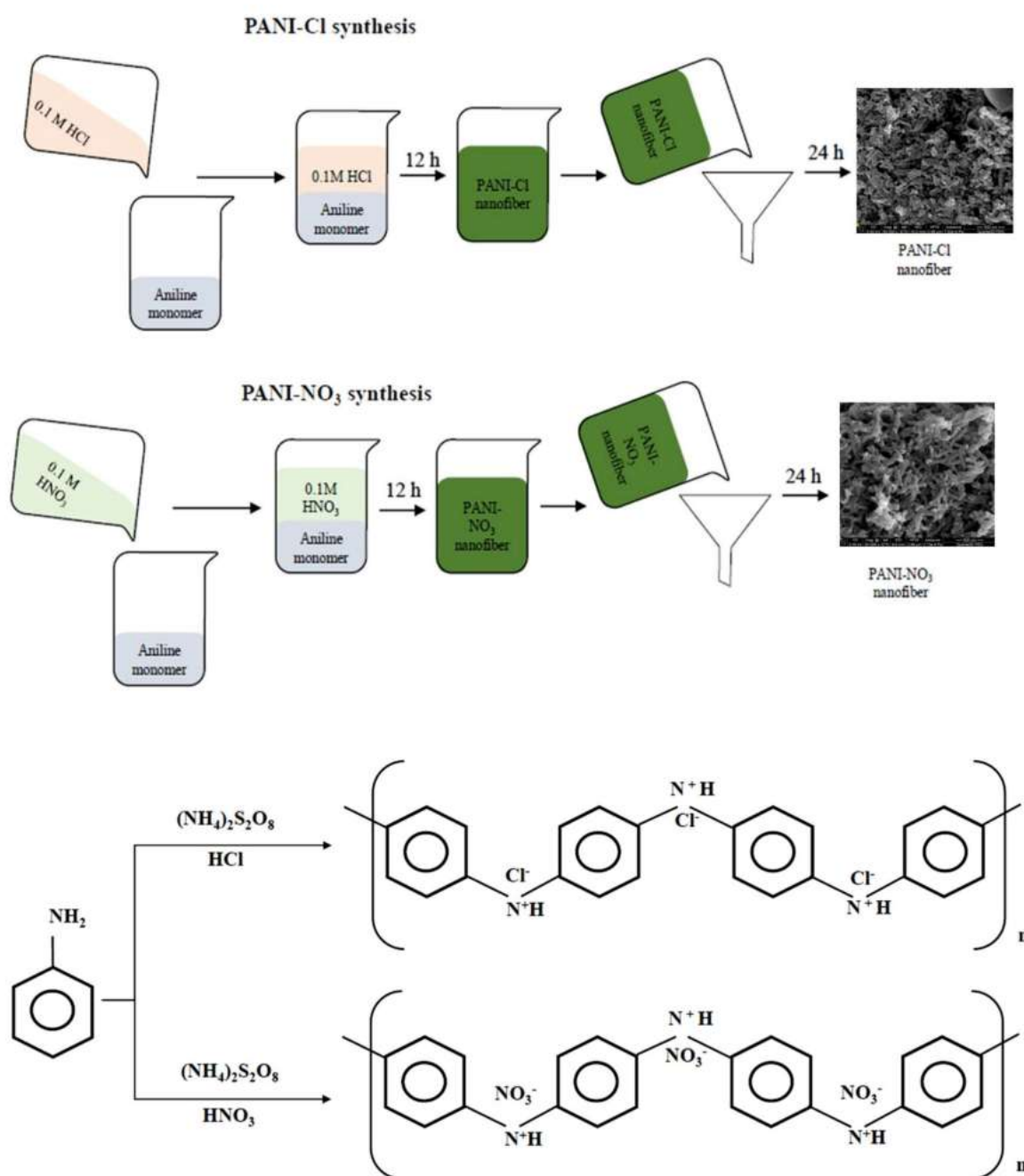
PANI-Cl synthesis

PANI-NO₃ synthesis

Fig. 1 Procedure for the synthesis of polyaniline nanofibers (PANINFs-Cl and PANINFs-NO₃) and equation of the occurring chemical reaction

Results and discussion

Modified polyaniline nanofibers were used for the construction of the electrodes as a solid contact placed both as an intermediate layer between the glassy carbon electrode (GCE) material and the ion-selective membrane material, and as a component of the membrane with different contents. A series of potentiometric measurements were performed to determine the parameters of the electrodes. The slopes of the calibration curves, their linearity ranges and the limits of

str. 105

detection were determined for all types of sensors. In addition, the reversibility and stability of the electrode potential were also investigated. The pH range in which the sensors can work properly and their selectivity for interfering ions were determined. The sensitivity tests of sensors to changing measurement conditions (redox potential change, presence of oxygen and light) were performed. For a more complete analysis, using the electrochemical impedance spectroscopy (EIS) technique, the electrical parameters of the obtained electrodes were also determined and compared.

PANI nanofibers characterization

The scanning electron micrographs shown in Fig. 2 clearly confirm the preparation of PANI in the form of nanofibers embedded in compact polymeric structures. Structural analysis indicates that the applied ion directly affects the microstructure of the obtained nanofibers, as also observed in the paper (Bednarczyk et al. 2021). The oxidative polymerization reaction carried out in the presence of NO_3^- ions allows the synthesis of longer and better formed nanofibers. However, the presence of both studied ions results in relatively cohesive structures of polymeric PANI nanofibers. Compact PANI structures may be formed due to the synthesis method, the reaction system oxidizability and the monomer concentration in the reaction system. Applied to PANI nanofibers synthesis interfacial polymerization belongs to static methods where the system is not continuously stirred during the chemical reaction. Secondly, obtaining of compact PANI nanofibers structure may also result from the high oxidizability of the reaction system (Zeng et al. 2015). APS is a relatively strong oxidant, so during the initial stage of the aniline polymerization reaction, a large number of oligomers are probably formed, and their further combination led to the compact nanofiber structure. In addition, the compact nanofiber structure may be due to the high monomer
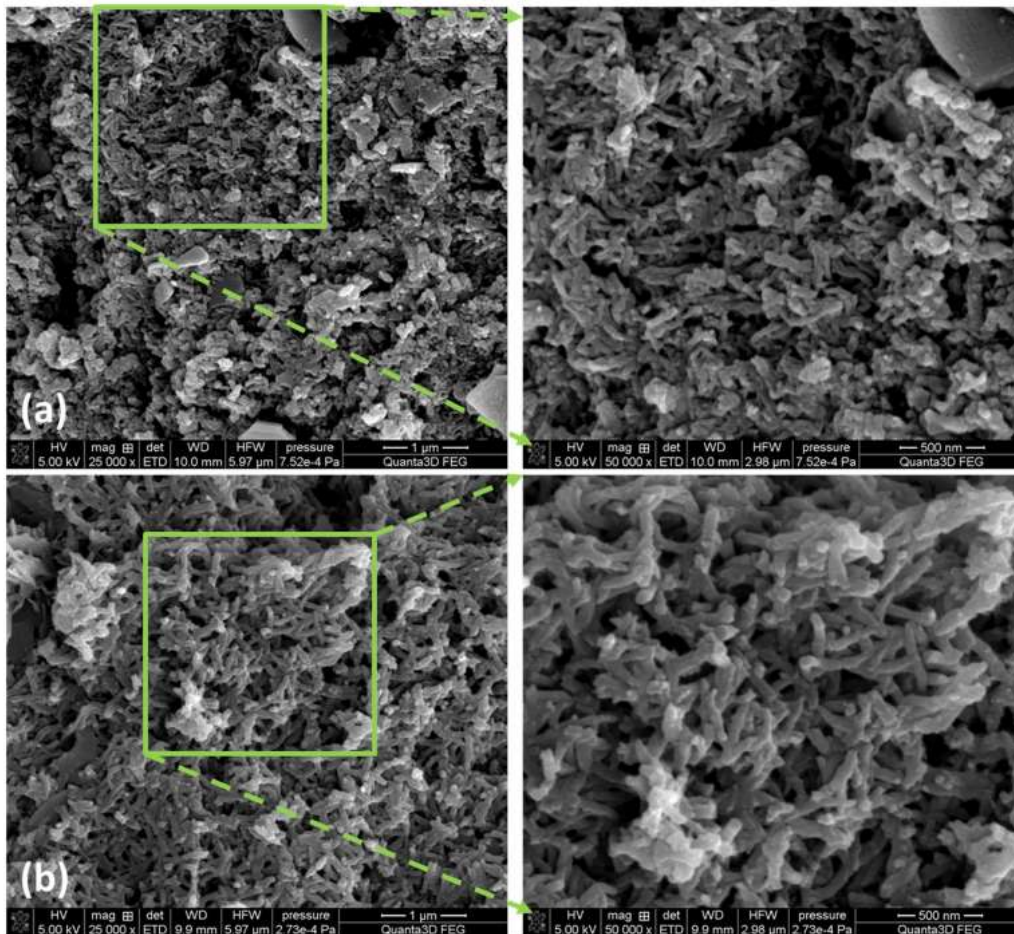
Fig. 2 SEM images of PANINFs-Cl (**a**) and PANINFs-NO$_3$ (**b**)

concentration, which causes subsequent nanofibers to be deposited on previously synthesized polymers.

Figure 3 shows the UV–Vis spectrum of PANI nanofibers synthesized in the presence of Cl^- and NO_3^- ions. These spectra show three main absorption bands with different intensities depending on the ion employed. This means that the type of used ion does not significantly influence the optical structure of the obtained PANI nanofibers. Both PANI nanofibers contain a cation radical in their structure, as indicated by the presence of absorption bands at 238 nm (PANINFs-Cl) and 232 nm (PANINFs-NO_3) corresponded to π–π^* transition in benzenoid structure (Zeng et al. 2015; El-ghaffar et al. 2016). The absorption bands appearing at wavelengths above 300 nm correspond to polar on band $\rightarrow \pi^*$ transition indicating that both PANINFs-Cl and PANINFs-NO_3 are partially doped (Zhang et al. 2009). These characteristic peaks clearly confirm synthesis of conductive emeraldine salt form.

Figure 4 shows the FTIR spectra of PANI nanofibers synthesized in the presence of Cl^- and NO_3^- ions. Analysis indicates that the type of ion used does not affect the molecular
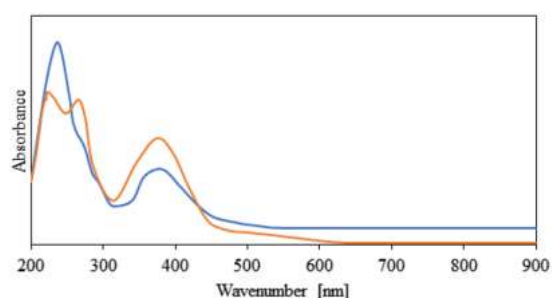
Fig. 3 UV–Vis spectrum of PANI nanofibers synthesized in the presence of Cl^- (blue line) and NO_3^- (orange line) ions
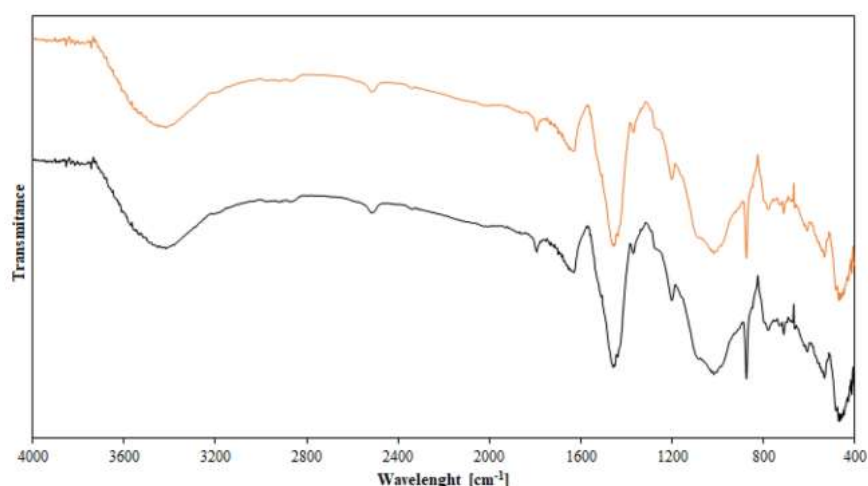
structure of the synthesized fibers either. The FTIR spectra obtained indicate the presence of bands characteristic for PANI. The broad band appearing at a wavelength of about 3500 cm^{-1} is attributed to –NH_2 stretching. At wavelengths of about 3200 cm^{-1} and 2850 cm^{-1} two small peaks attributed, respectively to –N–H^+ and C–H bonds vibrations are observed. The existence of a protonated amine group is also confirmed by peaks at about 1630 cm^{-1} and 1090 cm^{-1} assigned to –N–H and C–$NH^+\bullet$–C vibrations, respectively. The vibration of the C–$NH + \bullet$–C group and –N–H^+ bond clearly confirm that the synthesis of PANI in both the presence of Cl^- and NO_3^- ions leads to the formation of a nanostructured polymer in salt form. The benzenoid structure of obtained PANI nanostructures is confirmed by peaks at 1450 cm^{-1}, 1200 cm^{-1} and 880 cm^{-1} corresponding, respectively to C–C bond stretching vibration, C–C–H group vibration and out-of-plane bending vibration of C–H bond (Zhang et al. 2009; Zeng et al. 2015; Ahmed et al. 2021).

Potentiometric response

The dependence of the potential of the tested electrodes on nitrate ions concentration was measured in KNO_3 solutions in the concentration range of 1×10^{-7}–1×10^{-1} mol L^{-1} in relation to the silver chloride electrode as the reference electrode. The obtained calibration curves for all electrodes are shown in the Fig. 5. The slopes of the calibration curves obtained by these measurements, their linearity ranges and detection limits are summarized in Table 1.

As it can be seen in Fig. 5 and Table 1 use of PANINFs to the nitrate ion-selective electrodes preparation had the beneficial effect on their potentiometric response. In each case, the modified electrode showed a wider measuring range, a lower limit of detection and a greater slope of the calibration curve than the electrode without nanofibers. Considering
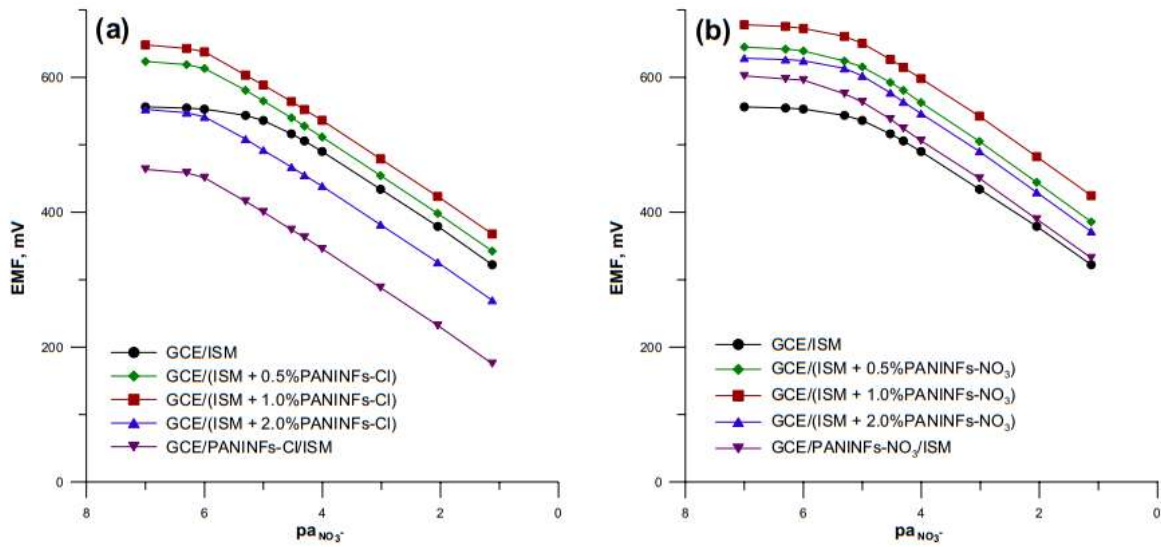
Fig. 4 FTIR spectra of PANI nanofibers synthesized in the presence of Cl^- (black line) and NO_3^- (orange line) ions

Fig. 5 Calibration curves of the electrodes with: **a** PANINFs-Cl, **b** PANINFs-NO$_3$ determined in the KNO$_3$ solution in the concentration range of 1×10^{-7}–1×10^{-1} mol L^{-1}

Table 1 Selected analytical parameters obtained for the tested electrodes

Electrode	Slope [mV/decade]	Limit of detection [mol L^{-1}]	Linear range [mol L^{-1}]	Short term potential drift [mV/h]	Reversibility (in 1×10^{-4} mol L^{-1} solution)		pH range
					Mean [mV]	SD [mV]	
GCE/ISM	55.75	3.98×10^{-6}	1×10^{-5}–1×10^{-1}	4.74	486.13	2.43	4.0–11.0
GCE/(ISM + 0.5%PANINFs-Cl)	56.07	3.47×10^{-7}	1×10^{-6}–1×10^{-1}	1.08	512.35	0.45	4.0–12.5
GCE/(ISM + 1.0%PANINFs-Cl)	56.67	3.39×10^{-7}	1×10^{-6}–1×10^{-1}	1.02	537.52	0.52	4.0–12.5
GCE/(ISM + 2.0%PANINFs-Cl)	56.17	3.55×10^{-7}	1×10^{-6}–1×10^{-1}	1.26	439.92	0.51	4.0–12.5
GCE/PANINFs-Cl/ISM	56.78	3.16×10^{-7}	1×10^{-6}–1×10^{-1}	0.53	346.35	0.33	4.0–12.5
GCE/(ISM + 0.5%PANINFs-NO$_3$)	57.20	1.58×10^{-6}	5×10^{-6}–1×10^{-1}	1.04	562.91	0.48	4.0–11.5
GCE/(ISM + 1.0%PANINFs-NO$_3$)	57.22	1.41×10^{-6}	5×10^{-6}–1×10^{-1}	1.12	596.85	0.29	4.0–11.5
GCE/(ISM + 2.0%PANINFs-NO$_3$)	57.50	1.51×10^{-6}	5×10^{-6}–1×10^{-1}	1.13	545.70	0.36	4.0–11.5
GCE/PANINFs-NO$_3$/ISM	57.80	1.12×10^{-6}	5×10^{-6}–1×10^{-1}	0.84	504.43	0.14	4.0–11.5

Short term potential drift value—given in absolute values

both types of nanofibers used, it can be seen that PANI-Cl nanofibers have a greater influence on the improvement of electrode's analytical parameters. The electrodes containing them both in the membrane and as an intermediate layer show wider linearity range of 1×10^{-6}–1×10^{-1} mol L^{-1} and also achieved lower limits of detection than other electrodes. The lowest limit of detection of 3.16×10^{-7} mol L^{-1} was obtained for the GCE/PANINFs-Cl/ISM). In the case of electrodes containing PANINFs-NO$_3$ in the membrane also, an improvement in the electrode response was observed compared to the unmodified electrode, but to a lesser degree. For these electrodes the detection limit decreased by about

0.5 orders of magnitude. However, for the electrode based on PANINFs-NO$_3$ as an intermediate layer, similar results were obtained as for electrodes based on PANINFs-Cl.

Potential reversibility

The reversibility of the electrode potential was tested in the KNO$_3$ solution with concentrations of 1×10^{-4} and 1×10^{-3} mol L^{-1}. The obtained results are shown in Fig. 6. The electrodes modified with both PANI-Cl and PANI-NO$_3$ nanofibers show a noticeably more stable potential compared to the unmodified electrode. The average potentials
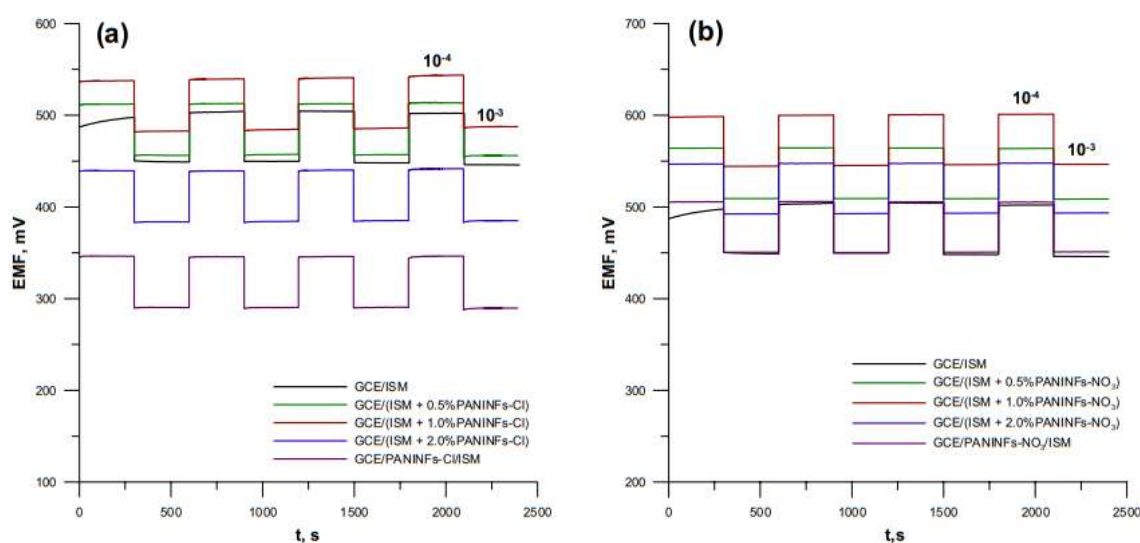
Fig. 6 Reversibility of the electrodes response: **a** PANINFs-Cl, **b** PANINFs-NO$_3$

and standard deviations obtained for 4 measurements in a solution of the main ion with a concentration of 1×10^{-4} mol L^{-1} are summarized in the Table 1. The electrodes were stable and gave a fast response after changing the solution concentration. Except for the unmodified electrode (GCE/ISM), for which the calculated SD for a results obtained in a solution with a concentration of 1×10^{-4} mol L^{-1} was 2.43 mV, for all other modified electrodes SD was more than two times smaller <1 mV.

Short-term stability of the potential

The short-term stability of the electrode potential was measured in a KNO$_3$ solution with a concentration of 1×10^{-1} mol L^{-1}. Figure 7 shows the potential change that occurred in the solution during 3 h (time selected as optimal, during which it is possible to successfully perform calibration and series of measurements with reserve). The addition of nanofibers both to the membrane and as an intermediate layer had a good effect on improving the stability of the sensors, the stability of which was significantly improved compared to the unmodified electrode (4.74 mV/h) (Table 1). Among the modified electrodes, the electrodes with the intermediate layer of PANI-Cl and PANI-NO$_3$ nanofibers were characterized by a lower potential drift of 0.53 and 0.84 mV/h, respectively.

pH range

Measurements of the electrode potential were also performed in solutions of various pH, with the main NO$_3^-$ ion

concentration equal to 1×10^{-3} mol L^{-1}. The pH range at which the potential was constant was very broad for all electrodes, while for the PANINFs-Cl based electrodes the pH range was somewhat wider in the alkaline range. Measurements with these electrodes can be successfully performed even in the range of pH 4.0–12.5 (Table 1). It is a very wide pH range, which does not significantly limit the possibility of determining nitrate ions in liquid samples.

Selectivity

The selectivity of ion-selective electrodes is a very important analytical parameter, necessary for their proper operation and obtaining correct analysis results. The good selectivity of the sensors allows to determine the concentration of the analyte (main ion) in the presence of other ions present in the solution. The components of the ion-selective membrane are responsible for selectivity, the most important of which is the ionophore, but also other ionic additions. The selectivity of the obtained sensors was tested using the separate solutions method (SSM) (Bakker et al. 2000). The addition of PANINFs did not significantly change the selectivity of the sensors. However, in all cases the selectivity also did not deteriorate. A greater difference in improved selectivity coefficients was noted for electrodes with nanofibers in the membrane than for electrodes with an intermediate layer. The results obtained for electrodes based on PANINFs-Cl nanofibers are shown in the Fig. 8. The selectivity coefficients for PANINFs-NO$_3$ electrodes were determined with the same method.
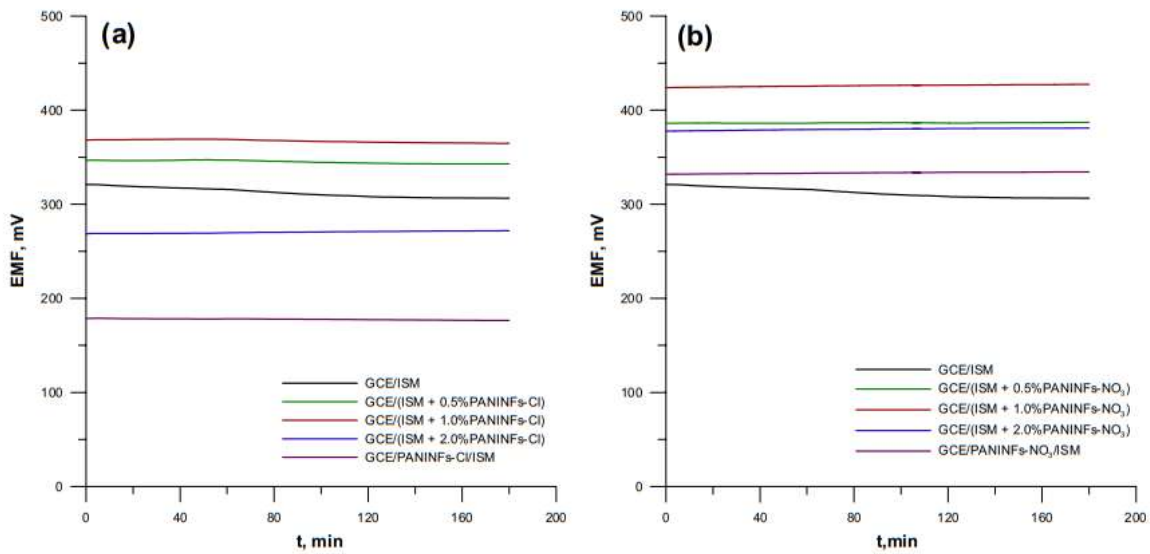
Fig. 7 Time dependence of the potential in a KNO_3 solution with a concentration of 1×10^{-1} mol L^{-1} for the **a** PANINFs-Cl, **b** PANINFs-NO_3 electrodes
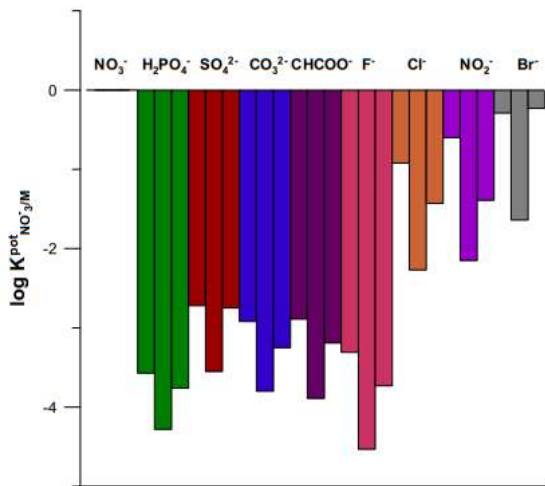

Fig. 8 Comparison of selectivity coefficients values for the studied sensors: GCE/ISM (1st column); GCE/(ISM + 1.0%PANINFs-Cl) (2nd column) and GCE/PANINFs-Cl/ISM (3rd column)

The obtained values were comparable to those obtained for the electrodes with PANINFs-Cl.

Effects of light and O_2

The resistance of the electrodes to changes in measurement conditions is very important to ensure the correctness of the obtained results. Electrodes containing conductive polymers as solid contact, unfortunately, are often sensitive to light, the presence of gases (CO_2, O_2) and pH changes, therefore it is very important to check whether the sensors are able to work properly regardless of external conditions (Vázquez et al. 2002). The research on the influence of light and the presence of oxygen in solutions on the electrode potential was performed. The potential measurements were made in the KNO_3 solution with a concentration of 1×10^{-1} mol L^{-1}. The dependence of the electrode potential with the light on and off is shown in Fig. 9, while in a deoxygenated and containing oxygen solution, in Fig. 10. The solution was deoxygenated by bubbling nitrogen through it for half an hour. All sensors worked properly, regardless of exposure to light and different oxygen content in the solution. The value of the potential does not change significantly, so it can be concluded that they are not sensitive to changes of these parameters.

Redox sensitivity

Redox sensitivity measurements were performed in solutions containing a pair of redox ions Fe^{2+} and Fe^{3+} ($Na_4Fe(CN)_6$ and $K_3Fe(CN)_6$) in the constant ionic background of 1×10^{-3} mol L^{-1} KNO_3. The log Fe^{2+}/Fe^{3+} ratio was -1; -0.7; 0; 0.7 and 1. Figure 11 shows the dependence of the measured potential on the value of the redox potential of the solution. For all electrodes, the change of redox potential does not impact on the electrode potential, which was almost constant ($sd_{max} \pm 1.37$ mV) in all solutions. Therefore, it can

⦿ Springer
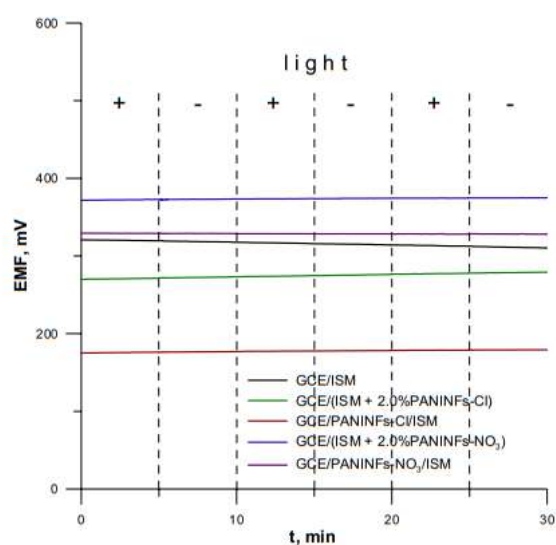
Fig. 9 Light sensitivity tests for chosen electrodes
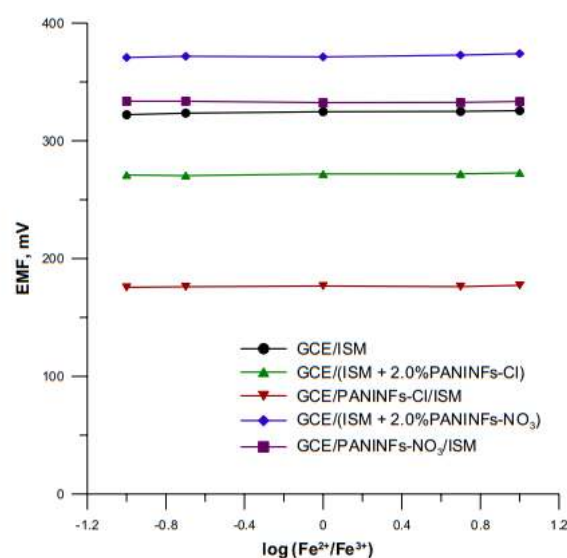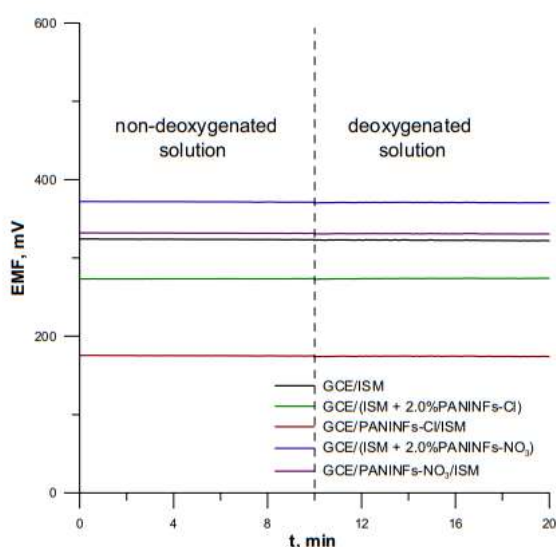
Fig. 10 Measurement of chosen electrodes potential in non-deoxygenated and deoxygenated solutions

be concluded that the tested electrodes are not sensitive to changes in the redox potential of the sample.

Life time

To establish the minimum time during which the electrodes are able to work properly, calibration curves were made in freshly prepared nitrate ions solutions regularly twice a week

Fig. 11 Redox sensitivity tests for chosen electrodes

for 3 months. After this time, linear ranges of calibration curves unchanged and the slopes decreased slightly, while for all electrodes it was over 97% of the initial value. Therefore, it was found that the electrodes were still working properly, and their lifetime is at least 3 months.

Electrochemical impedance spectroscopy

To study the effect of electrode modification by use of PANINFs the electrochemical impedance spectroscopy measurements were conducted. This technique allows the determination of the membrane resistance and the tracking of the processes at the interface: the ion-selective membrane/the inner electrode. The obtained impedance spectra for PANINFs-Cl based electrodes and unmodified electrode are shown in Fig. 12. As seen in Fig. 12, all obtained impedance spectra showed the same shape, but in different size. They had high-frequency semicircle connected to the bulk resistance (R_b) of the ion-selective membrane and its geometric capacitance (C_g) (Horvai et al. 1986) and low frequency branch, which arose from the double layer capacitance and charge transfer resistance at the interface between polymeric membrane and the inner GCE electrode. The bulk membrane resistance (R_b) determined from high frequency semicircle diameter was relatively low, even for unmodified electrode GCE/ISM due to presence in the membrane phase of ion-exchanger TDMANO$_3$ in relatively high concentration. After membrane modification with the PANINFs addition, the resistance of the membranes decreased gradually as the content of nanofibers increased. A similar decrease in the membrane resistance was observed in the case of
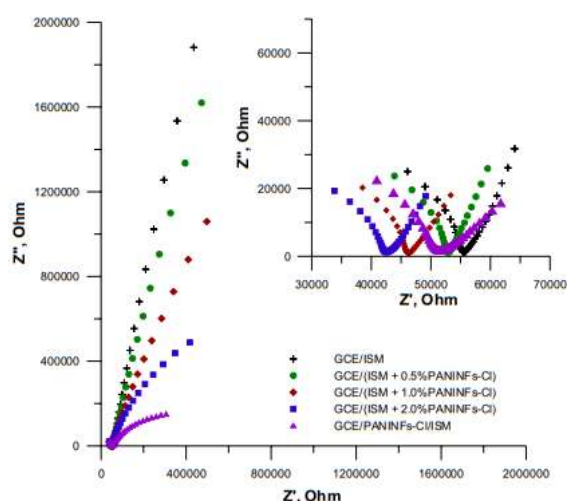
Fig. 12 Impedance spectra for GCE/ISM electrode and PANINFs-Cl based electrodes

Table 2 Electric parameters of studied electrodes determined by EIS measurements

Electrode	Membrane resistance [$k\Omega$]	Low frequency capacitance [μF]
GCE/ISM	87	0.85
GCE/(ISM + 0.5%PANINFs-Cl)	79	1.1
GCE/(ISM + 1.0%PANINFs-Cl)	67	1.4
GCE/(ISM + 2.0%PANINFs-Cl)	64	3.0
GCE/PANINFs-Cl/ISM	76	11
GCE/(ISM + 0.5%PANINFs-NO$_3$)	80	1.0
GCE/(ISM + 1.0%PANINFs-NO$_3$)	68	1.3
GCE/(ISM + 2.0%PANINFs-NO$_3$)	62	1.4
GCE/PANINFs-NO$_3$/ISM	68	10

electrodes in which the PANINFs were used as intermediate layer (Table 2).

Larger differences in the impedance spectra were observed in the low frequency range. As the content of nanofibers in the membrane increases, the low-frequency branch of the spectrum will decrease significantly, which is related to the increase in the double layer capacitance. The low frequency capacitance C_{lf} determined from the low frequency limit on the basis on following dependence $C_{lf} = 1/(2\pi f Z")$, where $f = 0.1$ Hz was 0.85 μF for unmodified GCE/ISM electrode. The C_{lf} value increased to the values of 1.1; 1.4 and 3.0 μF for electrodes GCE/(ISM + 0.5%PANINFs-Cl), GCE/(ISM + 1%PANINFs-Cl) and GCE/(ISM + 2%PANINFs-Cl), respectively. Of course, it was achieved due to the presence of nanofibers in the membrane. The greatest increase in capacitance to the value 11 μF was observed for the electrode GCE/PANINFs-Cl/ISM, in which nanofibers were used as an intermediate layer. Analogous results were obtained for electrodes modified with PANINFs-NO$_3$. The obtained results clearly show that the use of PANI nanofibers in the construction of electrodes improves their electrical parameters, especially increasing the electrical capacity, thanks to which the transfer of the charge between the membrane and the internal electrode is facilitated and the electrodes show a stable and reproducible potential (Table 2).

Analytical application

Practical usefulness of PANINFs based electrodes was tested by determination of nitrates content in drinking water, river water and ground water samples. An important advantage of the potentiometric methods is the lack of necessity or only minimal sample preparation before the measurements. Therefore, water samples were analyzed as soon as collected using the calibration curve method. The only modification was the addition of 0.5 ml of 1 mol L^{-1} Na$_2$SO$_4$ solution to 50 ml of the sample in order to ensure constant activity of the ions in the solution (Na$_2$SO$_4$ as an ionic strength buffer). The obtained results are summarized in Table 3, where it can be seen that there is a good agreement between the nitrate ions content determined with the proposed electrodes and the spectrophotometric method. This confirms that the obtained electrodes are a cheap and simple analytical device for nitrates monitoring in various water samples.

Conclusions

The successful usage of PANINFs for the construction of ion-selective electrodes is presented. It was found that the use of PANI nanofibers had a positive effect on the operation of potentiometric sensors. In particular, the stability and reversibility of the electrode potential has improved significantly. The electrodes modified with PANI-Cl nanofibers were characterized by a wider range of linearity of the calibration curves (1×10^{-6}–1×10^{-1} mol L^{-1}) and lower limits of detection. Both kinds of sensors with PANINFs-Cl and PANINFs-NO$_3$ as an intermediate layer were able to work in a wide range of pH (4.0–12.5) of solutions and under variable lighting conditions and the presence of gases (O$_2$) in the solution. The electrodes were used successfully for a period of 2 months and continued to function properly after that time. Obtained all-solid-state electrodes based on PANI nanofibers are suitable for nitrate monitoring in real water samples. Differences in the parameters of electrodes based on different PANI nanofibers result from differences in the microstructure of these nanofibers. The successful usage

Table 3 Results of nitrate ions determination in real water samples by proposed electrodes and by spectrophotometry

Sample	Nitrate ions content found [mg L^{-1}]^a			
	GCE/ (ISM + 2.0%PAN-INFs-Cl)	GCE/PANINFs-Cl/ISM	GCE/PAN-INFs-NO$_3$/ISM	Spectrophotometry
Drinking water	5.35 ± 0.02	5.33 ± 0.01	5.31 ± 0.02	5.52 ± 0.04
River water	16.23 ± 0.03	16.20 ± 0.02	16.11 ± 0.02	16.22 ± 0.05
Ground water	23.22 ± 0.03	23.22 ± 0.03	23.20 ± 0.03	23.03 ± 0.07

^{a}Results are based on five measurements

PANINFs doped with chloride or nitrate ions the construction of nitrate ion-selective electrodes is presented.

Declarations

Conflict of interest On behalf of all authors, the corresponding author states that there is no conflict of interest.

References

Abdolahi A, Hamzah E, Ibrahim Z, Hashim S (2012) Synthesis of uniform polyaniline nanofibers through interfacial polymerization. Materials 5:1487–1494. https://doi.org/10.3390/ma5081487

Ahmed HM, Ghali M, Zahra W, Ayad MM (2021) Preparation of carbon quantum dots/polyaniline nanocomposite: towards highly sensitive detection of picric acid. Spectrochim Acta Part A Mol Biomol Spectrosc 260:119967. https://doi.org/10.1016/j.saa.2021.119967

An WH, Ark MP, Hung KC et al (2000) Enhanced electrochemical performance of poly (aniline) solid-contact pH electrodes based on alkyldibenzylamine. Anal Sci 16:1145–1149

Bakker E, Pretsch E, Bühlmann P (2000) Selectivity of potentiometric ion sensors. Anal Chem 72:1127–1133. https://doi.org/10.1021/ac991146n

Bednarczyk K, Matysiak W, Tański T et al (2021) Effect of polyaniline content and protonating dopants on electroconductive composites. Sci Rep 11:1–11. https://doi.org/10.1038/s41598-021-86950-4

Bieg C, Fuchsberger K, Stelzle M (2017) Introduction to polymer-based solid-contact ion-selective electrodes—basic concepts, practical considerations, and current research topics. Anal Bioanal Chem 409:45–61

Bobacka J (2006) Conducting polymer-based solid-state ion-selective electrodes. Electroanalysis. https://doi.org/10.1002/elan.200503384

Bobacka J, Lewenstam A, Ivaska A (2001) Equilibrium potential of potentiometric ion sensors under steady-state current by using current-reversal chronopotentiometry. J Electroanal Chem 509:27–30. https://doi.org/10.1016/S0022-0728(00)00515-5

Bobacka J, Ivaska A, Lewenstam A (2008) Potentiometric ion sensors. Chem Rev 108:329–351

Chumbimuni-Torres KY, Rubinova N, Radu A et al (2006) Solid contact potentiometric sensors for trace level measurements. Anal Chem 78:1318–1322. https://doi.org/10.1021/ac050749y

Crespo GA (2017) Recent advances in ion-selective membrane electrodes for in situ environmental water analysis. Electrochim Acta 245:1023–1034

Dan LI, Huang J, Kaner RB (2009) Polyaniline nanofibers: a unique polymer nanostructure for versatile applications. Acc Chem Res 42:135–145. https://doi.org/10.1021/ar800080n

Das P, Mondal S, Malik S (2021) Fully organic polyaniline nanotubes as electrode material for durable supercapacitor. J Energy Storage. https://doi.org/10.1016/j.est.2021.102662

De Marco R, Clarke G, Pejcic B (2007) Ion-selective electrode potentiometry in environmental analysis. Electroanalysis 19:1987–2001. https://doi.org/10.1002/elan.200703916

El-ghaffar MAA, Shaffei KA, Zikry AAF et al (2016) Novel conductive nano-composite ink based on poly aniline, silver nanoparticles and nitrocellulose. Egypt J Chem 4:429–443

Han WS, Chung KC, Kim MH et al (2004) A hydrogen ion-selective poly(aniline) solid contact electrode based on dibenzylpyrenemethylamine ionophore for highly acidic solutions. Anal Sci 20:1419–1422. https://doi.org/10.2116/analsci.20.1419

Horvai G, GráF E, TóTh K et al (1986) Plasticized poly(vinyl chloride) properties and characteristics of valinomycin electrodes. 1. High-frequency resistances and dielectric properties. Anal Chem 58:2735–2740. https://doi.org/10.1021/ac00126a034

Hu J, Stein A, Bühlmann P (2016) Rational design of all-solid-state ion-selective electrodes and reference electrodes. TrAC Trends Anal Chem 76:102–114

Huang J, Kaner RB (2004) A general chemical route to polyaniline nanofibers. J Am Chem Soc 126:851–855. https://doi.org/10.1021/ja0371754

Jiang Y, Liu Z, Zeng G et al (2018) Polyaniline-based adsorbents for removal of hexavalent chromium from aqueous solution: a mini review. Environ Sci Pollut Res 25:6158–6174. https://doi.org/10.1007/s11356-017-1188-3

Konopka A, Sokalski T, Michalska A et al (2004) Factors affecting the potentiometric response of all-solid-state solvent polymeric membrane calcium-selective electrode for low-level measurements. Anal Chem 76:6410–6418. https://doi.org/10.1021/ac0492158

Lindfors T, Aarnio H, Ivaska A (2007) Potassium-selective electrodes with stable and geometrically well-defined internal solid contact based on nanoparticles of polyaniline and plasticized poly(vinyl chloride). Anal Chem 79:8571–8577. https://doi.org/10.1021/ac071344b

Lindner E, Gyurcsányi RE (2009) Quality control criteria for solid-contact, solvent polymeric membrane ion-selective electrodes. J Solid State Electrochem. https://doi.org/10.1007/s10008-008-0608-1

Michalska A (2012) All-solid-state ion selective and all-solid-state reference electrodes. Electroanalysis 24:1253–1265. https://doi.org/10.1002/elan.201200059

Michalska A, Hulanicki A, Lewenstam A (1994) All solid-state hydrogen ion-selective electrode based on a conducting poly(pyrrole) solid contact. Analyst 119:2417–2420. https://doi.org/10.1039/AN9941902417

Najim TS, Salim AJ (2017) Polyaniline nanofibers and nanocomposites: preparation, characterization, and application for Cr(VI) and phosphate ions removal from aqueous solution. Arab J Chem 10:S3459–S3467. https://doi.org/10.1016/j.arabjc.2014.02.008

Ocypa M, Michalska A, Maksymiuk K (2006) Accumulation of Cu(II) cations in poly(3,4-ethylenedioxythiophene) films doped by hexacyanoferrate anions and its application in Cu2+- selective electrodes with PVC based membranes. Electrochim Acta 51:2298–2305. https://doi.org/10.1016/j.electacta.2005.03.080

Rubinova N, Chumbimuni-Torres K, Bakker E (2007) Solid-contact potentiometric polymer membrane microelectrodes for the detection of silver ions at the femtomole level. Sensors Actuators B Chem 121:135–141. https://doi.org/10.1016/j.snb.2006.09.007

Sutter J, Lindner E, Gyurcsányi RE, Pretsch E (2004) A polypyrrole-based solid-contact Pb2+-selective PVC-membrane electrode with a nanomolar detection limit. Anal Bioanal Chem 380:7–14. https://doi.org/10.1007/s00216-004-2737-4

Vázquez M, Bobacka J, Ivaska A, Lewenstam A (2002) Influence of oxygen and carbon dioxide on the electrochemical stability of poly(3,4-ethylenedioxythiophene) used as ion-to-electron transducer in all-solid-state ion-selective electrodes. Sensors Actuators B Chem 82:7–13. https://doi.org/10.1016/S0925-4005(01)00983-2

Zeng F, Qin Z, Liang B et al (2015) Polyaniline nanostructures tuning with oxidants in interfacial polymerization system. Prog Nat Sci Mater Int 25:512–519. https://doi.org/10.1016/j.pnsc.2015.10.002

Zeng X, Liu Y, Jiang X et al (2021) Improving the stability of Pb2+ ion-selective electrodes by using 3D polyaniline nanowire arrays as the inner solid-contact transducer. Electrochim Acta 384:138414. https://doi.org/10.1016/j.electacta.2021.138414

Zhang X, Manohar SK (2004) Polyaniline nanofibers: chemical synthesis using surfactants. Chem Commun. https://doi.org/10.1039/b409309g

Zhang D, Wang Y (2006) Synthesis and applications of one-dimensional nano-structured polyaniline: an overview. Mater Sci Eng B Solid-State Mater Adv Technol 134:9–19. https://doi.org/10.1016/j.mseb.2006.07.037

Zhang C, Li G, Peng H (2009) Large-scale synthesis of self-doped polyaniline nanofibers. Mater Lett 63:592–594. https://doi.org/10.1016/j.matlet.2008.11.041

Zhang T, Yue H, Gao X et al (2020) A novel electrode material of polyaniline nanowire array/three-dimensional hollow graphene balls-graphene oxide for symmetric supercapacitor. Ionics 26:2063–2070. https://doi.org/10.1007/s11581-019-03360-3

Zhang Y, Tao Y, Wang K et al (2021) Two kinds of polyaniline fiber photo sensor with interdigital electrode and flexible hydrogel. J Appl Polym Sci 138:1–12. https://doi.org/10.1002/app.50628

D5

CHLORIDE ION-SELECTIVE ELECTRODE WITH SOLID-CONTACT BASED ON POLYANILINE NANOFIBERS AND MULTIWALLED CARBON NANOTUBES NANOCOMPOSITE

Chloride Ion-Selective Electrode with Solid-Contact Based on Polyaniline Nanofibers and Multiwalled Carbon Nanotubes Nanocomposite

Karolina Pietrzak [1,*], Klaudia Morawska [1], Szymon Malinowski [2] and Cecylia Wardak [1]

[1] Department of Analytical Chemistry, Institute of Chemical Sciences, Faculty of Chemistry, Maria Curie-Sklodowska University, Maria Curie-Sklodowska Sq. 3, 20-031 Lublin, Poland

[2] Faculty of Civil Engineering and Architecture, Lublin University of Technology, Nadbystrzycka 40, 20-618 Lublin, Poland

* Correspondence: karolina.pietrzak@poczta.umcs.lublin.pl

Abstract: Use of the nanocomposite of chloride-doped polyaniline nanofibers and multiwalled carbon nanotubes (PANINFs-Cl:MWCNTs) for construction of ion-selective electrodes with solid-contact sensitive to chloride ions has been described. Many types of electrodes were tested, differing in the quantitative and qualitative composition of the layer placed between the electrode material and the ion-selective membrane. Initial tests were carried out, including tests of electrical properties of intermediate solid-contact layers. The obtained ion-selective electrodes had a theoretical slope of the electrode characteristic curve (-61.3 mV dec^{-1}), a wide range of linearity (5×10^{-6}–1×10^{-1} mol L^{-1}) and good potential stability resistant to changing measurement conditions (redox potential, light, oxygen). The chloride contents in the tap, mineral and river water samples were successfully determined using the electrodes.

Keywords: ion-selective electrodes; solid-contact; nanofibers; nanocomposite; potentiometry; chlorides

1. Introduction

Chlorides are widely distributed in the natural environment as salts. They are used in the chemical industry, fertilizer production and food production. It is very important to know the concentration of chloride ions and to monitor them in various types of natural samples and other materials. They are very important, especially in determining the quality of water and its degree of salinity, control of industrial processes or in medicines [1]. It is important to determine their content in food, especially in processed products that are additionally salted in order to preserve them and prevent deterioration. Chlorides, which are naturally present in food products at low levels, can increase significantly during their processing, cooking and seasoning. The chloride concentration in drinking water is, on average, below 50 mg L^{-1}. The balance of electrolytes in the body is maintained by regulating total intake and excretion through the kidneys and the gastrointestinal tract. Considering the average chloride excretion from the body, an intake of 3.1 g/day for adults was considered recommended. No toxicity of chlorides was found in adults where metabolism of sodium chloride was working properly without any disturbances [2]. A number of methods have been developed that can be used to determine chloride content in various products and materials, including chronopotentiometry in long-term monitoring of chloride content in cement-based materials [3–5], chromatography methods in meat samples [6] or electrochemical methods—in sea water [7], desalted water [8], blood [9], milk [10] and food [11,12].

Among electrochemical techniques, potentiometry distinguishes itself due to its low cost, simplicity and high speed of measurements. This method enables determination of ions in colored and muddy samples, which usually do not require any pretreatment [13,14].

str. 116

The most popular group of potentiometric sensors are ion-selective electrodes (ISEs), which work by converting the activity of the ion into an electric potential that can be measured [15]. ISEs can be used to determine the content of selected ions in various types of liquid samples (water, drinks and even blood). However, to be considered fully functional and working properly, ISEs should meet a number of conditions. In their case, the key parameter is high selectivity, which makes it possible to determine the main ion concentration in real samples containing other ions [16]. In addition, the stability and reversibility of the potential are crucial so that the sensors can be used to perform measurements repeatedly over a longer period of time and the results obtained can be considered reliable. What is more, the electrical parameters of the electrodes are also important, which can be estimated on the basis of measurements using impedance spectroscopy and chronopotentiometry [17,18]. It is particularly important to develop electrodes with smaller sizes, different shapes and better mechanical resistance so that they can be used for automatic and direct determination of the content of selected ions in an in situ environment even without the need to collect samples and analyze them in the lab [1,19,20]. Such advantages are characteristic of ion-selective electrodes with solid-contact (SCISEs) in which the internal solution has been eliminated. However, to ensure the stability of the potential, solid-contact was used as a transducer, enabling the charge transfer between the solid electrode material and the ion-selective conductive membrane [21]. SCISEs, unlike conventional electrodes with an internal solution, are insensitive to liquid evaporation and changes in sample temperature and pressure and are easier to store and transport [17].

Thus far, research on obtaining various types of ion-selective electrodes sensitive to chloride ions has been described in the scientific literature several times. Depending on the materials and chemicals used, the sensors had different analytical parameters. In the work described by Legin et al., after optimizing the composition of the ion-selective membrane containing tridodecylmethylammonium chloride (TDMACl) as the active substance, a chloride electrode was obtained, characterized by a calibration slope of -48.4 mV dec^{-1} [22]. In order to analyze chlorides in pharmaceutical solutions, indium(III) octaethyl-porphyrin was used as an ionophore and electrodes with a super-Nernstian slope were obtained [23]. Electrodes with a slope of -55.0 mV dec^{-1} and linearity of the concentration range of 1×10^{-3}–1×10^{-1} mol L^{-1} were obtained in studies by Kim et al. The effect of a number of interfering ions that may be present in the sample solution was investigated, including CN$^-$, Br$^-$, ClO$_4{}^-$, SCN$^-$, acetate, hydrogen carbonate, lactate, citrate and salicylate ions [24]. Graphitic carbon nitride/silver chloride composite was also used for construction of chloride carbon paste electrodes to generate sensors with a linearity range of 1×10^{-6}–1×10^{-1} mol L^{-1} and a slope of -55.4 mV dec^{-1}. In their case, the interfering ions were CN$^-$, I$^-$, Br$^-$. They were then used to test samples of river water, sea water and drinking water with satisfactory results [25]. A wide range of linearity of the calibration curve of 5×10^{-8}–1×10^{-1} mol L^{-1} and a low detection limit were achieved for electrodes in which the anionic receptor 2-(1-H-imidazo [4,5-f][1,10]phenanthroline-2-yl)-6-methoxyphenol (HIPM) was used as the main membrane component. These electrodes were also successfully used to determine chloride ions in water, although the pH range declared by the authors in which the electrodes can be used was only 6.5–8.0 [26]. Sensors that can work in a wide range of pH changes were obtained for the purpose of research on corrosive processes. For the glass capillary microelectrodes constructed for this purpose, a slope of -58.7 mV dec^{-1} was achieved in the range 1×10^{-4}–1×10^{-1} mol L^{-1} [27]. Research on a potentiometric chip-based flow system for simultaneous determination of chlorides, fluorides, pH and redox potential in water samples [28] and an MIP-202-catalyst-integrated chloride sensor for detection of a sulfur mustard stimulant [29] has also been described. However, a review of the literature in the field of chloride electrodes shows that there is still a need for research on development of electrodes showing good analytical parameters.

Regarding SCISEs, the properties of the solid-contact material have a significant impact on the parameters of the electrodes. Substances that can be successfully used as solid-contacts in ISEs should meet a number of requirements. They should have electric and ionic

conductivity, reversibility and be sufficiently chemically stable not to undergo undesirable reactions during this process. In addition, they should be sufficiently hydrophobic to prevent formation of a water layer between the solid electrode material and the ion-selective membrane and have high bulk capacitance to ensure stable potential [30]. Conductive polymers were the first to be used as SC, such as poly(pyrrole) [31], poly(3-octylthiophene) [32] or polyaniline [33]. In recent years, nanomaterials, especially carbon-based nanomaterials, have gained great popularity in potentiometry. Properties such as high charge transfer, remarkable electrical capacities and good hydrophobicity make them ideal for use as transducer elements in potentiometric sensors [34]. Thus far, many types of nanomaterials (e.g., nanotubes, nanofibers, nanorods, nanowires, nanoparticles, nanocomposites and others) were used for this purpose [30]. From nanoparticles, scientists have described research on use of mainly metal nanoparticles: gold [35], silver [36], platinum [37] or metal oxide nanoparticles [38]. Recently, we reported successful use of polyaniline nanofibers doped with chloride and nitrate ions as solid-contact in nitrate ion-selective electrodes [39]. Polyaniline nanofibers (PANINFs) combine the unique properties of nanomaterials with the mixed ionic and electronic conductivity of conductive polymers. PANINFs and multi-walled carbon nanotubes (MWCNTs) form a nanocomposite with better electrical properties than its individual components (lower resistance and higher capacitance). It seems that such a nanocomposite is a good candidate as solid-contact for preparation of potentiometric sensors. In combination with a polymer membrane containing a highly selective ionophore, it provides hope for obtaining electrodes with good analytical and operational parameters. This work reports the study of electric properties of PANINFs and MWCNTs nanocomposite and its first usage as solid-contact in electrodes sensitive to chloride ions.

2. Materials and Methods

2.1. Apparatus

For potentiometric research, a cell consisting of the tested ion-selective electrodes (suitably modified glassy carbon electrodes (GCEs)) and a silver/silver chloride reference electrode with a double junction system (6.0750.100, Metrohm, Herisau, Switzerland) was used. The electromotive force (EMF) measurements were made at room temperature in mixed solutions using a magnetic stirrer. A 16-channel data acquisition system (Lawson Labs. Inc., Malvern, PA, USA) connected to a computer with appropriate software was used for data collection.

Electrochemical impedance spectroscopy and chronopotentiometry measurements were carried out for a 3-electrode system in which the tested electrode (GCE covered by the studied nanomaterial or ion-selective electrode) was the working electrode, Ag/AgCl (6.0733.100, Metrohm, Herisau, Switzerland)—reference electrode and GC rod 2 mm/65 mm (Metrohm, Herisau, Switzerland)—auxiliary electrode. All measurements were conducted in a NaCl solution with a concentration of 10^{-1} mol L^{-1}. The impedance spectra were recorded in the frequency range 0.1–100 kHz and 0.01–100 kHz (for the intermediate layers and ion-selective electrodes, respectively) at the open circuit potential with an amplitude of 10 mV. In chronopotentiometry measurements, a constant current of +1 μA and +100 nA (for the intermediate layers and ion-selective electrodes, respectively) was applied on the working electrode for 60 s, followed by a current of −1 μA and −100 nA for next 60 s, with simultaneous recording of the electrode potential. The AUTOLAB electrochemical analyzer (Eco Chemie, Utrecht, The Netherlands) and NOVA 2.1 software were used to perform the above measurements, collect them and adjust the electric circuit to the obtained impedance spectra.

The images of PANI/MWCNTs nanocomposite structure were recorded using a high-resolution scanning electron microscope Quanta 3D FEG (FEI Hillsboro, Hillsboro, OR, USA).

2.2. Reagents

Chemical substances used for synthesis of aniline nanofibers, aniline monomer, hydrochloric acid (HCl), ammonium persulfate (APS) and tetrahydrofuran (THF), were purchased from Chempur (Piekary Slaskie, Poland). Polyaniline nanofibers doped with Cl^- ion-synthesized following the procedure described in the publication [39]. Substances necessary for preparation of the membrane mixture were purchased from Sigma-Aldrich (Saint Louis, MO, USA) (chloride ionophore III-selectophore, tridodecylmethylammonium chloride (TDMACl) and high-molecular-weight poly(vinyl chloride) (PVC)) and Fluka (Buchs, Switzerland) (bis(2-ethylhexyl) sebacate (DOS)). Sulfuric acid and sodium hydroxide used to measure the dependence of the electrode potential on changes in pH were obtained from Chempur, while the salts of iron(II) ($Na_4Fe(CN)_6 \times 10H_2O$) and iron(III) ($K_3Fe(CN)_6$) were used to prepare the solutions differing in redox potential, respectively, from Alfa Aesar (Haverhill, MA, USA) and PPH (Polish Chemical Reagents, Gliwice, Poland). Other substances, such as inorganic salts, used to prepare the solution of the main ion (NaCl) and sodium salts of selected interfering anions (NaH_2PO_4, CH_3COONa, Na_2CO_3, $NaNO_3$, $NaNO_2$, Na_2SO_4, NaF, NaBr) were purchased from Fluka. Salts of the highest purity available (pure pro analysis) and freshly deionized water were used to prepare all solutions.

2.3. Preparation of Intermediate Solid-Contact Layers

Both the nanofibers (PANINFs-Cl) and the nanotubes (MWCNTs) as well as different nanocomposites made of them were used as intermediate layers of solid-contact in the ion-selective electrodes. Nanocomposites with a weight ratio of PANINFs-Cl:MWCNTs equal to 1:2, 1:1 and 2:1 were obtained by mixing the weighed components in THF, thoroughly homogenizing the mixture in an ultrasonic bath for one hour. Each time, the mass of components equal to 0.01 g was weighed on an analytical balance, to which 1 mL of THF was then added to obtain the initial concentration of components equal to 10 mg mL^{-1}. Then, in order to perform preliminary tests involving the examination of electrical parameters of materials and their nanocomposites, 10 µL volumes of their homogenized suspensions were spotted onto properly cleaned and dried glassy carbon electrode surfaces (GCE) and were allowed to evaporate the solvent.

2.4. Preparation of the Ion-Selective Membrane

The ion-selective membrane mixture was prepared by weighing its components on an analytical balance and thoroughly mixing it with THF using an ultrasonic bath. Ingredients with a total weight of 0.3 g were prepared and then added with 3 mL of THF. The qualitative and quantitative composition of the membrane was as follows: 2.0% chloride ionophore III, 1.2% TDMACl, 33% PVC and 63.8% DOS (as recommended by the producer [40]). After all the membrane components were homogenized completely in the organic solvent, the membrane was ready to be applied to the properly prepared electrode surface.

2.5. Preparation of Solid-Contact Ion-Selective Electrodes

For the construction of ion-selective electrodes, glassy carbon electrodes (GCEs) with a diameter of 0.3 cm were used. The surface of the electrodes was properly prepared before the application of successive layers. They were cleaned with sandpaper, grain sizes 2500 and 5000, then polished with alumina powder (0.3 µm size), wetted with distilled water and rinsed thoroughly. An ultrasonic bath was used to get rid of the residual alumina. Finally, the electrodes were rinsed again abundantly with distilled water, then with an organic solvent, THF, which was also used to prepare the membrane mixture. The electrodes were allowed to dry. Then, 10 µL of nanomaterials dispersed in THF were dropped on each electrode to thoroughly coat the solid-contact interlayer (except for the electrodes intended to act as basic electrodes containing the ion-selective membrane itself placed directly on the electrode material). Next day, the ion-selective membrane was dropped on

every electrode—3 layers of 30 μL, each time allowing the solvent to evaporate for 30 min. The electrodes with the spotted ion-selective membrane were allowed to dry overnight. Then, all electrodes were stored immersed in a conditioning solution—10^{-3} mol L^{-1} NaCl in a dark and dry place.

3. Results and Discussion

3.1. Characterization of Solid-Contact Materials

3.1.1. SEM Images

In order to compare the structure of the used types of solid-contact, they were studied by scanning electron microscopy technique. The scanning electron micrographs shown in Figure 1 clearly confirm the difference in the structure of the MWCNTs (A), PANINFs-Cl (B) and the nanocomposite (C) obtained from both of these components. In image 1C, polyaniline nanofibers entwined by carbon nanotubes can be observed.
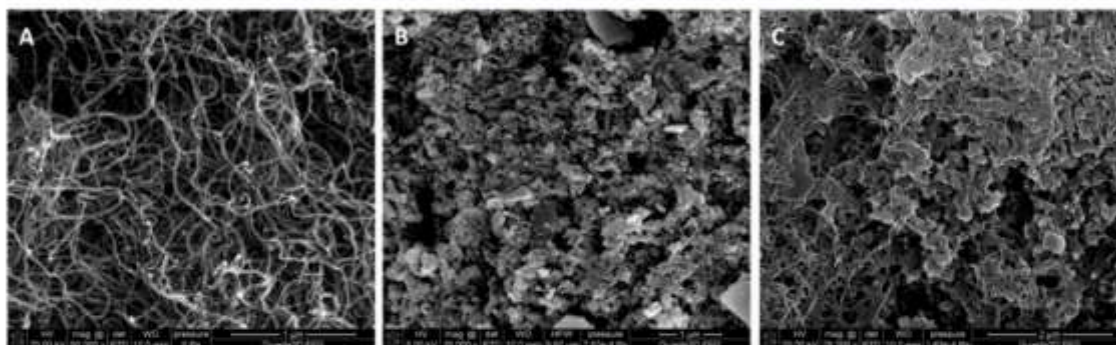

Figure 1. SEM images obtained for the layers of (**A**) MWCNTs, (**B**) PANINFs-Cl, (**C**) (2:1)PANINFs-Cl:MWCNTs nanocomposite.

3.1.2. Chronopotentiometric Tests of the Intermediate Layer

The next step of the study was to examine the electric properties of the studied nano-materials using chronopotentiometry (CP) and electrochemical impedance spectroscopy (EIS). First, the electric parameters of the obtained layers were determined by the chronopotentiometry method in a NaCl solution of 10^{-1} mol L^{-1}. The electric capacity of the tested materials was so large that it was necessary to use a current of 1 μA for measurements involving only the intermediate layers (without the spotted membranes). The results obtained for the GCE modified by PANINFs, MWCNTs and their nanocomposites are presented in Figure 2. Based on the course of the chronopotentiometric curves and formulas: $R = E/i$; drift $= \Delta E/\Delta t = i/C$ (where E–potential change, i–applied current, t–time change), the electric capacitance (C) and resistance of the electrode (R) were determined (Table 1) [18]. As all the electrodes differed only in the type of nanomaterial covering the GCE, the observed differences resulted from their different properties.

In the case of the nanocomposite, a synergistic effect was observed. It was found that all the electrodes obtained from the nanocomposites showed higher electric capacitance and lower resistance than the electrodes obtained only from PANINFs-Cl or MWCNTs. The nanocomposite obtained from PANINFs-Cl and MWCNTs with a 2:1 weight ratio showed the most favorable electric properties.
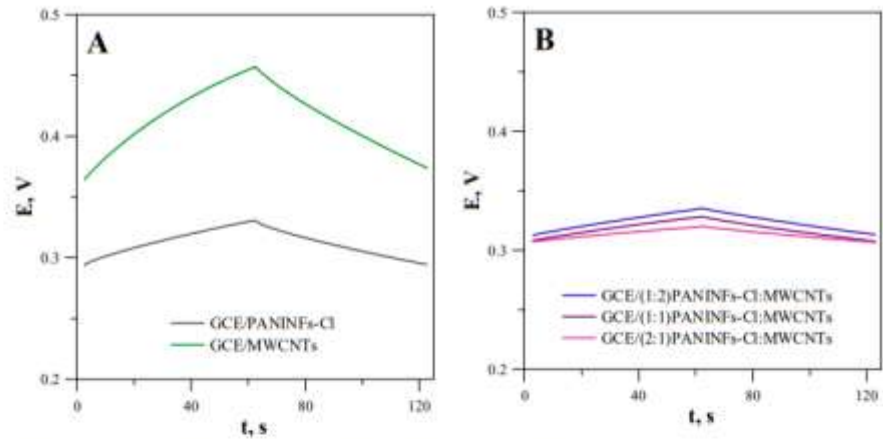
Figure 2. Chronopotentiometric curves obtained for the layers of (**A**) PANINFs-Cl and MWCNTs; (**B**) nanocomposites PANINFs-Cl:MWCNTs.

Table 1. Estimated values of electric capacitance (C) and resistance (R) for the tested solid-contact layers determined by chronopotentiometry.

Layer Material	C, mF	R, kΩ
PANINFs-Cl	1.82	0.64
MWCNTs	0.68	0.61
(1:2)PANINFs-Cl:MWCNTs	2.70	0.37
(1:1)PANINFs-Cl:MWCNTs	3.01	0.31
(2:1)PANINFs-Cl:MWCNTs	7.16	0.21

3.1.3. Initial Electrochemical Impedance Spectroscopy Tests of the Intermediate Layer

The intermediate solid-contact layers were also tested by EIS. The impedance spectra were recorded in the frequency range 0.1–100 kHz at the open circuit potential, with an amplitude of 10 mV. The obtained impedance spectra and the electrical circuit that was matched for the electrodes are shown in Figure 3. The electrical circuit consists of the uncompensated series resistance (R), mainly electrolyte resistance, the Warburg impedance (W) connected to the ion transport in the solid-contact layer and double layer capacitance (C_{dl}) [41]. The determined data are presented in Table 2, where it is evident that the studied nanomaterials show different capacities. In each case, the nanocomposite had a greater double layer capacitance C_{dl} than its constituent components, i.e., PANINFs-Cl and MWCNTs. The nanocomposite (2:1)PANINFs-Cl:MWCNTs was characterized by the largest value of $C_{dl} = 7.01$ mF, which was over ten times greater than the C_{dl} value obtained for MWCNTs (0.59 mF) and more than three times greater than the C_{dl} value obtained for PANINFs-Cl (2.10 mF).

Table 2. Electrical parameters for the tested electrodes determined by EIS.

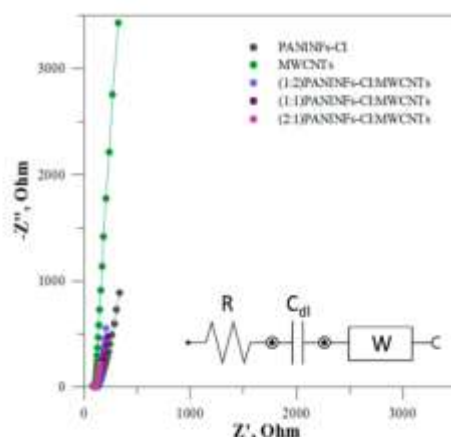| Layer Material	R [Ω]	C_{dl} (mF)	W (mOhm $\times$ s$^{(1/2)}$)	x^2
PANINFs-Cl	123.0	2.10	4.78	0.089
MWCNTs	95.0	0.59	5.76	0.092
(1:2)PANINFs-Cl:MWCNTs	108.0	3.12	7.95	0.096
(1:1)PANINFs-Cl:MWCNTs	103.0	3.40	8.59	0.054
(2:1)PANINFs-Cl:MWCNTs	101.0	7.01	13.6	0.058

Figure 3. Impedance spectra for all solid-contact layers measured in 10^{-1} mol L^{-1} NaCl with an equivalent electrical circuit (solid lines represent data fits; the error of the fits χ^2 is given in Table 2).

3.2. Characterization of Ion-Selective Electrodes

3.2.1. Electrical Parameters of Ion-Selective Electrodes

In order to check the extent to which the properties of the intermediate layer of nanomaterials affect the electrical parameters of ion-selective electrodes, complete sensors with an intermediate layer and an ion-selective membrane were also tested using the CP and EIS methods. For prepared electrodes that, in addition to the intermediate layer, also had a membrane layer, a current of 100 nA was selected for chronopotentiometric measurements. Figure 4 shows the chronopotentiometric curves obtained for the electrodes with intermediate layers and for the unmodified electrode (GCE/ISM). As was expected, the electrodes with the intermediate layer exhibited better electric parameters (higher capacitance and lower total resistance) than the simple coated disc electrode. Due to this, the modified electrodes showed reduced potential drifts upon galvanostatic polarization compared with the unmodified electrode (Table 3). This effect was the largest for the electrode based on the nanocomposite (2:1)PANINFs-Cl:MWCNTs/ISM. The potential stabilizing effect is connected with the presence of the nanomaterial layer that was placed between the ion-sensitive membrane and the inner electrode and depends on its capacitance.

The beneficial effect of the presence of the interfacial layer on the electrodes' electric parameters was confirmed by EIS study. Electrochemical impedance spectroscopy is a very useful technique to study electrochemical processes. In relation to ion-selective electrodes, it allows for the determination of, inter alia, charge transfer resistance, which provides us information about the efficiency of the intermediate layer. Impedance spectra were recorded at an open circuit potential with an amplitude of 10 mV, while the frequency range was 0.01–100 kHz. The obtained impedance spectra for the best electrode GCE/(2:1)PANINFs-Cl:MWCNTs/ISM and the unmodified electrode GCE/ISM are shown in Figure 5. The fitted equivalent circuit is presented in the insert. In the case of the electrode without the intermediate layer, a large semicircle in the high frequency region and a huge partial semicircle in the low frequency region are observed. Both parts of the impedance spectra are dramatically diminished in the case of the nanocomposite ((2:1)PANINFs-Cl:MWCNTs)-modified electrode. The high-frequency semicircle can be attributed to the bulk resistance (R_b) and geometric capacitance (C_g) of the ISM, while the low-frequency part of the semicircle can be connected to the charge transfer resistance (R_{ct}) in parallel with double layer capacitance (C_{dl}) at the interface between the polymeric membrane and the inner GC electrode. The obtained impedance spectra were fitted to the equivalent circuit shown in the insert of Figure 5 and the particular electric parameters of the electrodes were determined. The bulk membrane resistance R_b decreased from 3.4 MΩ for the unmodified GCE/ISM to 0.91 MΩ for the GCE/(2:1)PANINFs-Cl:MWCNTs/ISM,

respectively. The same effect but to a much greater extent was observed for the charge transfer resistance R_{ct}, which decreased from 29.7 MΩ for the unmodified CGE/ISM to 0.14 MΩ for the nanocomposite-based electrode, respectively. Concurrently, the low frequency layer capacitance (C_{dl}) increased drastically. It was 7.3 pF for the unmodified GCE/ISM, much smaller than the value obtained for the nanocomposite-based electrode, whose C_{dl} was 1.4 μF. These results confirm that the studied nanocomposite (2:1)PANINFs-Cl:MWCNTs significantly facilitates the diffusion processes and charge transport at the membrane/GCE interface and is a promising material for intermediate layers in solid-contact ISEs.
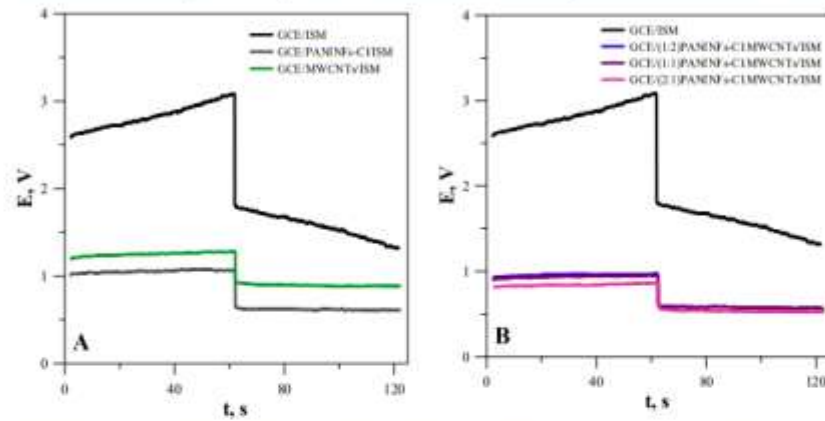

Figure 4. Chronopotentiometric curves obtained for the electrodes: (**A**) unmodified GCE/ISM and with intermediate layers of nanofibers GCE/PANINFs-Cl/ISM or nanotubes GCE/MWCNTs/ISM; (**B**) unmodified GCE/ISM and with intermediate layers of nanocomposites.

Table 3. Estimated values of electric capacitance (C) and resistance (R) for the tested electrodes determined by chronopotentiometry.

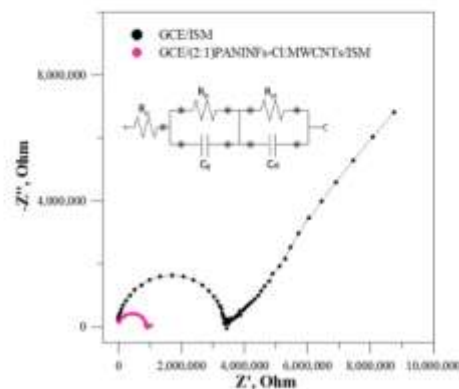| Electrode	C, mF	$\Delta E/\Delta t$, mV s^{-1}	R, MΩ
GCE/ISM	0.013	7.7	8.01
GCE/PANINFs-Cl/ISM	0.12	0.81	4.11
GCE/MWCNTs/ISM	0.10	0.96	3.49
GCE/(1:2)PANINFs-Cl:MWCNTs/ISM	0.28	0.36	3.66
GCE/(1:1)PANINFs-Cl:MWCNTs/ISM	0.26	0.34	3.48
GCE/(2:1)PANINFs-Cl:MWCNTs/ISM	0.32	0.31	2.97

Figure 5. Impedance spectra for GCE/ISM and GCE/(2:1)PANINFs-Cl:MWCNTs/ISM measured in 10^{-1} mol L^{-1} NaCl and equivalent circuit (solid lines represent data fits, the error of the fits χ^2 was 0.056 for GCE/ISM and 0.012 for GCE/(2:1)PANINFs-Cl:MWCNTs/ISM).

3.2.2. Potentiometric Response

The potentiometric response of the sensors was tested in NaCl solutions in the concentration range of 10^{-7}–10^{-1} mol L^{-1} (every half unit). The electromotive force (EMF) of the cell was measured in mixed solutions. Measurements to obtain calibration curves of the tested electrodes were performed twice a week for a period of 2 months. The slope of the calibration curve as well as the range of its linearity and the limit of detection were checked. The E^0 value was also determined each time by extrapolating the linear segment of the response function to paCl$^-$ = 0. The exemplary calibration curves obtained one week after preparation of individual sensors (the graph of the potential versus the negative logarithm of the activity of chloride ions in the solution) are shown in Figure 6. As can be seen, all the obtained electrodes were sensitive to chloride ions and showed a characteristic slope close to the theoretical value. The electrode response differed in the measuring range and limit of detection. The unmodified electrode had the shortest linear range of the calibration curve (5×10^{-5}–1×10^{-1} mol L^{-1}) and the highest limit of detection, which was 6.3×10^{-6} mol L^{-1}. The modified electrodes, regardless of the type of the intermediate layer, showed a similar potentiometric response. Compared to the unmodified electrode, their measurement range was wider by one unit pa, and the detection limit was much lower (Table 4).
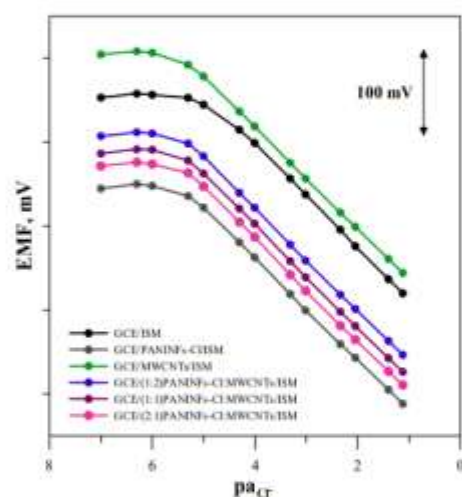

Figure 6. Potentiometric calibration plots recorded for the tested electrodes in NaCl solutions (concentration range 10^{-7}–10^{-1} mol L^{-1}).

Table 4. Selected analytical parameters obtained for the tested electrodes.

Electrode	Slope, mV dec^{-1}		Linear Range, mol L^{-1}		Limit of Detection, mol L^{-1}		Long-Term Stability $E^0 \pm$ SD, mV
	1. Week	2. Month	1. Week	2. Month	1. Week	2. Month	
GCE/ISM	−59.7	−59.6	5×10^{-5}–1×10^{-1}	1×10^{-4}–1×10^{-1}	6.3×10^{-6}	1.9×10^{-5}	205.0 ± 56
GCE/PANINFs-Cl/ISM	−59.6	−60.2	5×10^{-6}–1×10^{-1}	1×10^{-5}–1×10^{-1}	2.6×10^{-6}	6.5×10^{-6}	69.0 ± 8.5
GCE/MWCNTs/ISM	−60.3	−60.2	5×10^{-6}–1×10^{-1}	5×10^{-6}–1×10^{-1}	2.8×10^{-6}	4.8×10^{-6}	225.2 ± 6.3
GCE/(1:2)PANINFs-Cl:MWCNTs/ISM	−61.1	−60.1	5×10^{-6}–1×10^{-1}	5×10^{-6}–1×10^{-1}	2.7×10^{-6}	4.8×10^{-6}	126.4 ± 6.1
GCE/(1:1)PANINFs-Cl:MWCNTs/ISM	−61.2	−60.5	5×10^{-6}–1×10^{-1}	5×10^{-6}–1×10^{-1}	2.7×10^{-6}	3.8×10^{-6}	105.7 ± 3.5
GCE/(2:1)PANINFs-Cl:MWCNTs/ISM	−61.3	−61.1	5×10^{-6}–1×10^{-1}	5×10^{-6}–1×10^{-1}	2.3×10^{-6}	3.6×10^{-6}	89.5 ± 1.8

The electrode performance changed over time but to a different extent. Over the two-month period, all the electrodes kept a very good slope of the calibration curve. In the case of the unmodified electrode, the measurement range shortened and the detection limit increased by half an order. On the other hand, the electrodes with an intermediate layer (except GCE/PANINFs-Cl/ISM) showed an unchanged measuring range and a slightly worse detection limit.

The greatest differences were observed in the value of E^0. This parameter is a measure of the long-term stability of the potential, and changes in the value of E^0 are a source of measurement errors. An electrode characterized by a stable E^0 value does not require control calibrations and allows correct results of determinations to be obtained. The average values of E^0 determined from successive measurements and the standard deviation from the mean value are provided in Table 4, where the modified electrodes showed much better stability of the E^0 potential compared to the unmodified electrode. The improvement in long-term stability (E^0 potential change) is related to the electric capacitance of the intermediate layer and is the greatest for the electrode GCE/(2:1)PANINFs-Cl:MWCNTs/ISM with a nanocomposite layer characterized by the best electrical parameters.

3.2.3. Short-Term Stability and Reversibility of the Electrode Potential

The short-term stability of the electrode potential was measured in a 1×10^{-3} mol L^{-1} NaCl solution for 3 h. From the recorded potential change in time (Figure 7), the potential drift under zero current conditions was determined as ($\Delta E / \Delta t$) and the calculated values are provided in the last column of Table 5. As was expected, all the modified electrodes show very good potential stability. They exhibited potential drift much smaller than the electrode without an intermediate layer. It is within this time (Figure 7).

The reversibility of the potential of the tested electrodes was also measured. For this purpose, the solutions of the main ion salt (NaCl) with a concentration of 1×10^{-4} and 1×10^{-3} mol L^{-1} were changed every 10 min and the obtained potential values were read. The operation was repeated five times for each of the solutions, then the mean potentials and standard deviation were calculated; the results obtained are summarized in Table 5. A quantitative measure of the reversibility of the electrode potential is the value of the standard deviation from the mean value of the potential measured in successive tests in a solution with a given concentration. From the analysis of the data in Table 5, it can be concluded that, in each case, the introduction of the intermediate layer causes a significant improvement in the reversibility of the potential, the effect being the greatest for (2:1)PANINFs-Cl:MWCNTs-nanocomposite-modified electrodes.
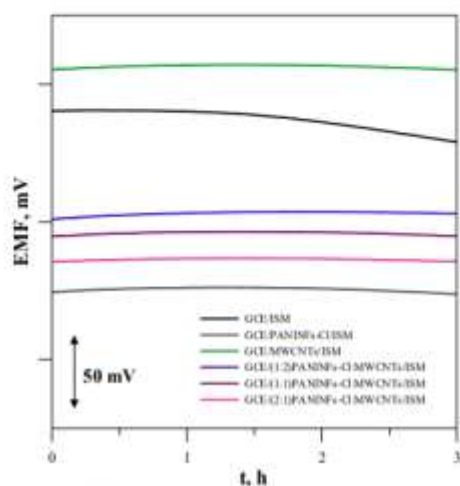

Figure 7. The short-term potential stability measured in 10^{-3} mol L^{-1} NaCl.

Table 5. Reversibility and short-term stability of the electrode potential determined in NaCl solutions with a concentration of 10^{-4} and 10^{-3} mol L^{-1}. Mean values and standard deviation obtained for 5 results.

Electrode	10^{-4} mol L^{-1}		10^{-3} mol L^{-1}		Potential Drift, mV h^{-1}
	Mean, mV	SD, mV	Mean, mV	SD, mV	
GCE/ISM	438.83	13.24	402.58	7.85	7.60
GCE/PANINFs-Cl/ISM	310.78	4.21	250.12	2.78	0.56
GCE/MWCNTs/ISM	470.10	3.82	405.58	2.26	0.08
GCE/(1:2)PANINFs-Cl:MWCNTs/ISM	370.48	3.17	310.81	2.39	0.35
GCE/(1:1)PANINFs-Cl:MWCNTs/ISM	350.39	2.19	290.98	1.87	0.09
GCE/(2:1)PANINFs-Cl:MWCNTs/ISM	335.26	1.42	270.80	0.71	0.03

3.2.4. Selectivity

The selectivity of the tested electrodes was estimated by determining the selectivity coefficients by the method of separate solutions. The variant of this method proposed by Bakker [42] was applied, in which the values of the selectivity coefficients are calculated from the equation $\log K^{pot}_{Cl/X} = -(E_X - E_{Cl})/S$, where E_X is electrode potential in the interfering ion solution with activity $a_X = 1$; E_{Cl} is electrode potential in the chloride solution with activity $a_{Cl} = 1$ and S is the slope of the electrode response in chloride solution.

Selectivity coefficients for various anions were estimated, including $H_2PO_4^-$, CH_3COO^-, HCO_3^-, NO_3^-, NO_2^-, SO_4^{2-}, F^- and Br^- ions. The tested electrodes did not differ significantly in terms of selectivity. The obtained selectivity coefficients had similar values for all the modified and unmodified electrodes. This proves that the type of solid-contact material does not affect the selectivity of the electrode, which is determined by the composition of the polymeric membrane (mainly ionophore). In this case, all the electrodes had the same membrane, and, therefore, they showed similar values of the selectivity coefficients. The determined values of $\log K^{pot}_{Cl/X}$ for the GCE/(2:1)PANINFs-Cl:MWCNTs/ISM decreased in the order -1.6, -4.6, -4.8, -5.0, -5.1, -5.6, -6.4 and -6.6 for Br^-, NO_3^-, HCO_3^-, NO_2^-, SO_4^{2-}, $H_2PO_4^-$, CH_3COO^- and F^-, respectively. Such values indicate very good selectivity of the electrodes, which makes them suitable for determination of chloride ions in various samples.

3.2.5. pH Range

The measurements were performed to determine the pH range in which the tested electrodes can be successfully used to determine the concentration of chloride ions. The electrode potential was measured in solutions of the main ion with a concentration of 10^{-3} mol L^{-1} with different pH values. Sulfuric acid and sodium base were used to obtain the appropriate pH of the solutions. All the electrodes showed a stable potential over a similar pH range of around 4–9. Since the same membrane mixture was used to construct the electrodes, it was found that the use of different materials as an intermediate layer of solid-contact is irrelevant to the pH range in which the sensors can be used. Figure 8 shows the dependence of the electrode potential on pH for the unmodified GCE/ISM and nanocomposite-based electrode GCE/(2:1)PANINFs-Cl:MWCNTs/ISM.

3.2.6. Redox Sensitivity

Potentiometric measurements were performed in solutions with different redox potential in order to check the redox sensitivity of the tested electrodes (Figure 9). Solutions with a concentration of 10^{-2} mol L^{-1} NaCl were used, which contained $Fe(CN)_6^{3-}$ and $Fe(CN)_6^{4-}$ redox coupled with $\log([Fe^{2+}]/[Fe^{3+}])$ equal to -1, -0.7, 0, 0.7 and 1. The potential of the electrodes measured in solutions with different redox potential does not change significantly. It can, therefore, be considered that they work properly regardless of the redox potential of the sample.
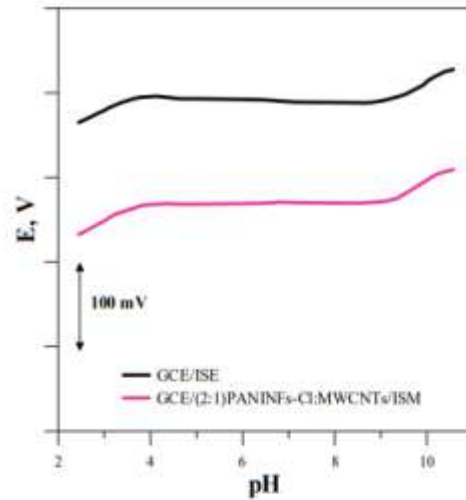
str. 126

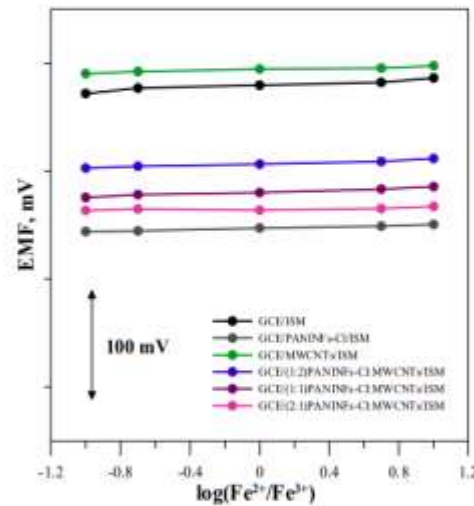**Figure 8.** Dependence of electrode potential on pH.

Figure 9. Redox sensitivity for tested electrodes.

3.2.7. Sensitivity to Light and Oxygen

It is known that SCISEs based on conducting polymers can be sensitive to light and the presence of gases, such as oxygen or carbon dioxide [43,44]. Therefore, the influence of the presence of light and gases on the stability of the electrode potential was investigated. The potential was measured in a solution of the main ion with a concentration of 10^{-1} mol L^{-1}. To examine the effect of the presence of gases on changes in the electrode potential, measurements were performed in solutions saturated with gases, alternately with solutions deoxygenated by passing nitrogen through the solution for one hour. The obtained dependence of the potential on time under changing lighting conditions is presented in Figure 10A, while variable conditions regarding the presence of oxygen in the sample solution are in Figure 10B. As can be seen in these figures, all the tested electrodes were resistant to changes in light and the presence of gases (O_2, CO_2).
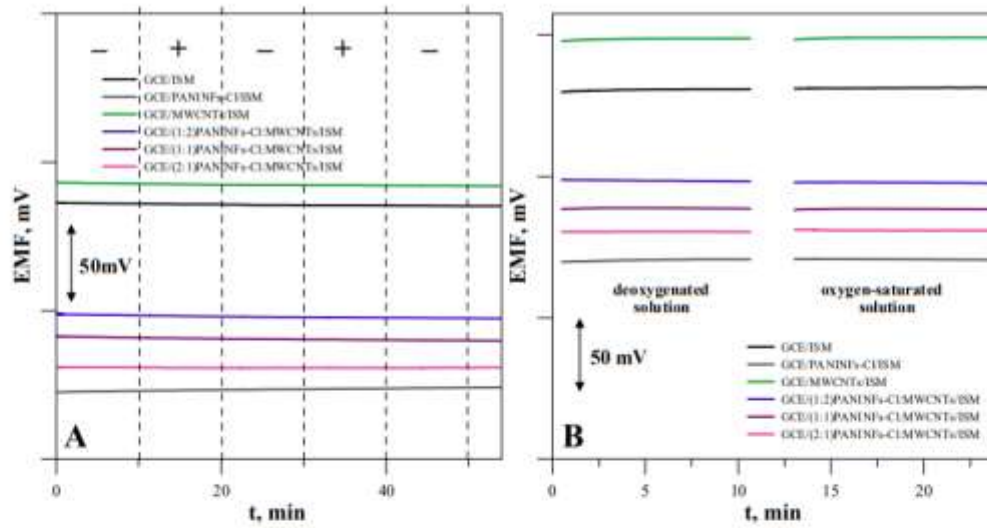
Figure 10. The effect of (**A**) light, (**B**) O$_2$ on the electrode potential.

3.3. Determination of Chlorides in Real Samples Using the Proposed Electrode

In order to check the effectiveness of using the electrodes in the study of real samples, determination of chloride concentrations in the samples of drinking water (tap water and mineral water) and river water was performed using the GCE/(2:1)PANINFs-Cl:MWCNTs/ISM. The method of classical quantitative analysis was used as a comparative method: determination of chlorides by Mohr's method. Classical quantitative analysis methods in comparison to instrumental methods have the following characteristics: if it is necessary to observe the visual endpoint of titration, i.e., the change in color of the solution from one drop of the titrant, this method depends to a large extent on the person performing the analysis. In addition, it is necessary to have the right type of glass and access to appropriate reagents and indicators, the addition of which enables detection of the endpoint of titration (here, potassium chromate) and solutions of substances acting as a titrant, the titer of which has been correctly and accurately determined. In addition, such analysis takes much more time, and, if the concentration range of the substance in the sample is not known, it may be necessary to dilute the sample and/or the titrant appropriately to fit the titrant volume not exceeding the burette volume, and for greater accuracy of the read volume—preferably within the range 20–80% of its volume. In the case of instrumental methods, and more precisely in potentiometry using ISEs, the measurements are much faster, less complicated and rely to a much lesser extent on the senses of the person. In addition, depending on the type of electrodes, the range of linearity of their calibration curves covers several levels of concentration, so it is possible to determine samples that differ significantly in the content of the tested ions.

In the case of potentiometric measurements, the only step in the preparation of the sample was the addition of sodium acetate as an ionic strength buffer, each time obtaining its concentration of 10^{-2} mol L^{-1}. In the same environment, a calibration curve for the tested electrodes was previously prepared. Chloride concentration in water samples was estimated by the standard addition method for each sample and electrode in three replicates. In the case of classical quantitative analysis, the titration was performed using of silver nitrate titrant in the presence of a color indicator of potassium chromate. It is worth noting that, in the case of the potentiometric method, the required sample volume is much smaller than in the case of classical analysis. The obtained mean results, including standard deviations, are summarized in Table 6.

Table 6. Determination of chlorides in water samples by direct potentiometry and comparison with the classic Mohr's method.

Sample	Chloride Content Found by Proposed ISE, mmol L^{-1}	Chloride Content Found by Classic Mohr's Method, mmol L^{-1}
Tap water	0.737 ± 0.016	0.745
Mineral water	0.311 ± 0.018	0.302
River water	1.07 ± 0.026	1.01

4. Conclusions

The modified electrodes were characterized by a wider measuring range and a lower detection limit compared to the unmodified electrode without a solid-contact layer. The obtained sensors had a high slope of the calibration curve, a wide measuring range, a very good potential stability, and a fast response time. This effect was the largest in the case of the PANINFs-MWCNTs nanocomposite-based electrode (in particular, for a 2:1 ratio of PANINFs-Cl:MWCNTs). Moreover, they were insensitive to change in redox potential, as well as light and oxygen, which is important from the practical point of view. The obtained electrodes were successfully used to test water samples (tap water, mineral water and river water). Due to their wide measuring range and very good selectivity, they can be used, for example, to control the efficiency of water desalination.

Chloride ion-selective electrodes are available commercially, including from the companies ELMETRON, HACH, MERA, VERNIER and THERMOFISHER (Table 7). The obtained electrodes with a composite interlayer of (2:1)PANINFs-Cl:MWCNTs are characterized by a wider range of linearity compared to the vast majority of them and have better selectivity and a fast sensor response. Most manufacturers declare a very wide pH range (2–11) in which the electrodes can be used; for testing natural water samples, usually a pH range of 4–9 should be sufficient. In addition, it is possible to add a buffer to the sample, ensuring an appropriate pH of the solution. Whenever the selectivity of chloride electrodes over other ions is tested, a list of interfering ions is available, confirming that there is no ideally selective chloride electrode available. The price of the sensors is also an important aspect as crystalline chloride electrodes are usually quite expensive.

Table 7. Comparison of the parameters for the tested chloride electrodes and commercially available electrodes.

Name of Electrode	Producer	Ion-Sensitive Membrane Type	Slope, mV dec^{-1}	Linear Range, mol L^{-1}	Detection Limit, mol L^{-1}	Interfering Ions with logK $\geq$ -2	Response Time, s	pH Range	Ref.
Chloride ISE GCE/(2:1)PANINFs-Cl:MWCNTs/ISM	-	PVC	-61.3	5×10^{-6}–1×10^{-1}	2.56×10^{-6}	Br-	<10	4–9	This work
Chloride electrode ECl-01	ELMETRON	Polycrystalline	-56 ± 3	5×10^{-5}–1	-	Br$^-$, S$_2$O$_3^{2-}$, I$^-$, S^{2-}	30–60	2–11	[45]
Intellical ISECL181 chloride ISE (Cl$^-$)	HACH	Solid-state crystal membrane	-	3×10^{-6}–1	-	-	-	-	[46]
ISE Hanna HI 4107	MERA	Semiconductor, combined	-	1×10^{-5}–1	-	-	-	2–11	[47]
Chloride ISE	VERNIER	-	-56 ± 3	3×10^{-5}–1	-	CN$^-$, Br$^-$, I$^-$, OH$^-$, S^{2-}, NH$_3$	-	2–12	[48]
Orion™ Chloride Electrode 9417SC	THERMOFISHER	-	-	1×10^{-5}–1	-	-	-	-	[49]

References

1. Ke, X. Micro-Fabricated Electrochemical Chloride Ion Sensors: From the Present to the Future. *Talanta* **2020**, *211*, 120734. [CrossRef] [PubMed]
2. Turck, D.; Castenmiller, J.; de Henauw, S.; Hirsch-Ernst, K.I.; Kearney, J.; Knutsen, H.K.; Maciuk, A.; Mangelsdorf, I.; McArdle, H.J.; Pelaez, C.; et al. Dietary Reference Values for Chloride. *EFSA J.* **2019**, *17*, e05779. [CrossRef] [PubMed]
3. de Graaf, D.B.; Abbas, Y.; Bomer, J.G.; Olthuis, W.; van den Berg, A. Sensor-Actuator System for Dynamic Chloride Ion Determination. *Anal. Chim. Acta* **2015**, *888*, 44–51. [CrossRef] [PubMed]
4. Angst, U.; Elsener, B.; Larsen, C.K.; Vennesland, Ø. Potentiometric Determination of the Chloride Ion Activity in Cement Based Materials. *J. Appl. Electrochem.* **2010**, *40*, 561–573. [CrossRef]
5. Junsomboon, J.; Jakmunee, J. Determination of Chloride in Admixtures and Aggregates for Cement by a Simple Flow Injection Potentiometric System. *Talanta* **2008**, *76*, 365–368. [CrossRef]
6. Lopez-Moreno, C.; Perez, I.V.; Urbano, A.M. Development and Validation of an Ionic Chromatography Method for the Determination of Nitrate, Nitrite and Chloride in Meat. *Food Chem.* **2016**, *194*, 687–694. [CrossRef]
7. Cuartero, M.; Crespo, G.; Cherubini, T.; Pankratova, N.; Confalonieri, F.; Massa, F.; Tercier-Waeber, M.L.; Abdou, M.; Schäfer, J.; Bakker, E. In Situ Detection of Macronutrients and Chloride in Seawater by Submersible Electrochemical Sensors. *Anal. Chem.* **2018**, *90*, 4702–4710. [CrossRef]
8. Díaz, P.; González, Z.; Granda, M.; Menéndez, R.; Santamaría, R.; Blanco, C. Evaluating Capacitive Deionization for Water Desalination by Direct Determination of Chloride Ions. *Desalination* **2014**, *344*, 396–401. [CrossRef]
9. Oka, S.; Sibazaki, Y.; Tahara, S. Direct Potentiometric Determination of Chloride Ion in Whole Blood. *Anal. Chem.* **1981**, *53*, 588–593. [CrossRef]
10. De Clercq, H.L.; Mertens, J.; Massart, D.L. Analysis of Chloride in Milk with a Specific Ion Electrode. *J. Agric. Food Chem.* **1974**, *22*, 153–154. [CrossRef]
11. Chapman, B.R.; Goldsmith, I.R. Determination of Chloride, Sodium and Potassium in Salted Foodstuffs Using Ion-Selective Electrodes and the Dry Sample Addition Method. *Analyst* **1982**, *107*, 1014–1018. [CrossRef] [PubMed]
12. Capuano, E.; van der Veer, G.; Verheijen, P.J.J.; Heenan, S.P.; van de Laak, L.F.J.; Koopmans, H.B.M.; van Ruth, S.M. Comparison of a Sodium-Based and a Chloride-Based Approach for the Determination of Sodium Chloride Content of Processed Foods in the Netherlands. *J. Food Compos. Anal.* **2013**, *31*, 129–136. [CrossRef]
13. Düzgün, A.; Zelada-Guillén, G.A.; Crespo, G.A.; Macho, S.; Riu, J.; Rius, F.X. Nanostructured Materials in Potentiometry. *Anal. Bioanal. Chem.* **2010**, *399*, 171–181. [CrossRef] [PubMed]
14. Lindner, E.; Gyurcsányi, R.E. Quality Control Criteria for Solid-Contact, Solvent Polymeric Membrane Ion-Selective Electrodes. *J. Solid State Electrochem.* **2009**, *13*, 51–68. [CrossRef]
15. Bieg, C.; Fuchsberger, K.; Stelzle, M. Introduction to Polymer-Based Solid-Contact Ion-Selective Electrodes—Basic Concepts, Practical Considerations, and Current Research Topics. *Anal. Bioanal. Chem.* **2017**, *409*, 45–61. [CrossRef]
16. Bobacka, J.; Ivaska, A.; Lewenstam, A. Potentiometric Ion Sensors. *Chem. Rev.* **2008**, *108*, 329–351. [CrossRef]
17. Hu, J.; Stein, A.; Bühlmann, P. Rational Design of All-Solid-State Ion-Selective Electrodes and Reference Electrodes. *Trends Anal. Chem.* **2016**, *76*, 102–114. [CrossRef]
18. Bobacka, J. Potential Stability of All-Solid-State Ion-Selective Electrodes Using Conducting Polymers as Ion-to-Electron Transducers. *Anal. Chem.* **1999**, *71*, 4932–4937. [CrossRef]
19. Crespo, G.A. Recent Advances in Ion-Selective Membrane Electrodes for in Situ Environmental Water Analysis. *Electrochim. Acta* **2017**, *245*, 1023–1034. [CrossRef]
20. Cuartero, M.; Crespo, G.A. All-Solid-State Potentiometric Sensors: A New Wave for in Situ Aquatic Research. *Curr. Opin. Electrochem.* **2018**, *10*, 98–106. [CrossRef]
21. Michalska, A. All-Solid-State Ion Selective and All-Solid-State Reference Electrodes. *Electroanalysis* **2012**, *24*, 1253–1265. [CrossRef]
22. Legin, A.; Makarychev-Mikhailov, S.; Kirsanov, D.; Mortensen, J.; Vlasov, Y. Solvent Polymeric Membranes Based on Tridodecylmethylammonium Chloride Studied by Potentiometry and Electrochemical Impedance Spectroscopy. *Anal. Chim. Acta* **2004**, *514*, 107–113. [CrossRef]

str. 131

23. Pimenta, A.M.; Araújo, A.N.; Montenegro, M.C.B.S.M.; Pasquini, C.; Rohwedder, J.J.R.; Raimundo, I.M. Chloride-Selective Membrane Electrodes and Optodes Based on an Indium(III) Porphyrin for the Determination of Chloride in a Sequential Injection Analysis System. *J. Pharm. Biomed. Anal.* **2004**, *36*, 49–55. [CrossRef] [PubMed]

24. Kim, W.; Sung, D.D.; Cha, G.S.; Park, S.B. Chloride-Selective Membranes Prepared with Different Matrices Including Polymers Obtained by the Sol-Gel Method. *Analyst* **1998**, *123*, 379–382. [CrossRef]

25. Alizadeh, T.; Rafiei, F.; Akhoundian, M. A Novel Chloride Selective Potentiometric Sensor Based on Graphitic Carbon Nitride/Silver Chloride (g-C$_3$N$_4$/AgCl) Composite as the Sensing Element. *Talanta* **2022**, *237*, 122895. [CrossRef]

26. Gupta, V.K.; Goyal, R.N.; Sharma, R.A. Chloride Selective Potentiometric Sensor Based on a Newly Synthesized Hydrogen Bonding Anion Receptor. *Electrochim. Acta* **2009**, *54*, 4216–4222. [CrossRef]

27. Nazarov, V.A.; Taryba, M.G.; Zdrachek, E.A.; Andronchyk, K.A.; Egorov, V.V.; Lamaka, S.V. Sodium- and Chloride-Selective Microelectrodes Optimized for Corrosion Studies. *J. Electroanal. Chem.* **2013**, *706*, 13–24. [CrossRef]

28. Chango, G.; Palacio, E.; Cerdà, V. Potentiometric Chip-Based Multipumping Flow System for the Simultaneous Determination of Fluoride, Chloride, PH, and Redox Potential in Water Samples. *Talanta* **2018**, *186*, 554–560. [CrossRef]

29. Sandhu, S.S.; Chang, A.Y.; Fernando, P.U.A.I.; Morales, J.F.; Tostado, N.; Jernberg, J.; Moores, L.C.; Wang, J. MIP-202 Catalyst-Integrated Solid-Contact Potentiometric Chloride Sensor for Versatile Multiphasic Detection of a Sulfur Mustard Simulant. *Sens. Actuators B Chem.* **2023**, *375*, 132818. [CrossRef]

30. Yin, T.; Qin, W. Applications of Nanomaterials in Potentiometric Sensors. *Trends Anal. Chem.* **2013**, *51*, 79–86. [CrossRef]

31. Michalska, A.; Hulanicki, A.; Lewenstam, A. All Solid-State Hydrogen Ion-Selective Electrode Based on a Conducting Poly(Pyrrole) Solid Contact. *Analyst* **1994**, *119*, 2417–2420. [CrossRef]

32. Konopka, A.; Sokalski, T.; Michalska, A.; Lewenstam, A.; Maj-Zurawska, M. Factors Affecting the Potentiometric Response of All-Solid-State Solvent Polymeric Membrane Calcium-Selective Electrode for Low-Level Measurements. *Anal. Chem.* **2004**, *76*, 6410–6418. [CrossRef] [PubMed]

33. Han, W.-S.; Park, M.-Y.; Chung, K.-C.; Cho, D.-H.; Hong, T.-K. Enhanced Electrochemical Performance of Poly(Aniline) Solid-Contact PH Electrodes Based on Alkyldibenzylamine. *Anal. Sci.* **2000**, *16*, 1145–1149. [CrossRef]

34. Liang, R.; Yin, T.; Qin, W. A Simple Approach for Fabricating Solid-Contact Ion-Selective Electrodes Using Nanomaterials as Transducers. *Anal. Chim. Acta* **2015**, *853*, 291–296. [CrossRef] [PubMed]

35. Zhang, L.; Wei, Z.; Liu, P. An All-Solid-State NO3- Ion-Selective Electrode with Gold Nanoparticles Solid Contact Layer and Molecularly Imprinted Polymer Membrane. *PLoS ONE* **2020**, *15*, e0240173. [CrossRef] [PubMed]

36. Yin, T.; Han, T.; Li, C.; Qin, W.; Bobacka, J. Real-Time Monitoring of the Dissolution of Silver Nanoparticles by Using a Solid-Contact Ag+-Selective Electrode. *Anal. Chim. Acta* **2020**, *1101*, 50–57. [CrossRef] [PubMed]

37. Paczosa-Bator, B.; Cabaj, L.; Piech, R.; Skupień, K. Platinum Nanoparticles Intermediate Layer in Solid-State Selective Electrodes. *Analyst* **2012**, *137*, 5272–5277. [CrossRef]

38. Pietrzak, K.; Krstulović, N.; Blažeka, D.; Car, J.; Malinowski, S.; Wardak, C. Metal Oxide Nanoparticles as Solid Contact in Ion-Selective Electrodes Sensitive to Potassium Ions. *Talanta* **2022**, *243*, 123335. [CrossRef]

39. Pietrzak, K.; Wardak, C.; Malinowski, S. Application of Polyaniline Nanofibers for the Construction of Nitrate All-solid-state Ion-selective Electrodes. *Appl. Nanosci.* **2021**, *11*, 2823–2835. [CrossRef]

40. Available online: https://www.sigmaaldrich.cn/deepweb/assets/sigmaaldrich/product/documents/523/464/24894.pdf (accessed on 20 October 2022).

41. Sundfors, F.; Bobacka, J. EIS Study of the Redox Reaction of Fe(CN)63-/4- at Poly(3,4-Ethylenedioxythiophene) Electrodes: Influence of Dc Potential and COx: CRed Ratio. *J. Electroanal. Chem.* **2004**, *572*, 309–316. [CrossRef]

42. Bakker, E.; Pretsch, E.; Bühlmann, P. Selectivity of Potentiometric Ion Sensors. *Anal. Chem.* **2000**, *72*, 1127–1133. [CrossRef] [PubMed]

43. Vázquez, M.; Bobacka, J.; Ivaska, A.; Lewenstam, A. Influence of Oxygen and Carbon Dioxide on the Electrochemical Stability of Poly(3,4-Ethylenedioxythiophene) Used as Ion-to-Electron Transducer in All-Solid-State Ion-Selective Electrodes. *Sens. Actuators B Chem.* **2002**, *82*, 7–13. [CrossRef]

44. Lindfors, T. Light Sensitivity and Potential Stability of Electrically Conducting Polymers Commonly Used in Solid Contact Ion-Selective Electrodes. *J. Solid State Electrochem.* **2009**, *13*, 77–89. [CrossRef]

45. ELMETRON. Available online: https://elmetron.com.pl/index_eng.html (accessed on 20 October 2022).

46. HACH. Available online: https://www.hach.com/intellical-isecl181-chloride-cl-ion-selective-electrode-ise-1-m-cable/product?id=7640513801 (accessed on 20 October 2022).

47. Hannainst. Available online: https://www.hannainst.com/hi4107-chloride-combination-ion-selective-electrode.html (accessed on 20 October 2022).

48. Vernier. Available online: https://www.vernier.com/product/chloride-ion-selective-electrode/ (accessed on 20 October 2022).

49. Thermofisher. Available online: https://www.thermofisher.com/order/catalog/product/9417SC (accessed on 20 October 2022).

D6

COPPER ION-SELECTIVE ELECTRODES BASED ON NEWLY SYNTHESIZED SALEN-TYPE SCHIFF BASES AND THEIR COMPLEXES

ORIGINAL PAPER

Copper ion-selective electrodes based on newly synthesized salen-type Schiff bases and their complexes

Karolina Pietrzak[1] · Cecylia Wardak[1] · Beata Cristóvão[2]

Abstract

The paper describes research on ion-selective electrodes sensitive to copper(II) ions, in which Schiff bases and their Cu(II) complexes were used as active components of ion-selective membranes. The Schiff bases differ in the type and amount of substituents in the benzene ring and/or in the aliphatic chain. A multi-stage process of optimization of the ion-selective membrane composition was carried out. Apart from the selection of the best ionophore, the influence of the type of plasticizer and lipophilic salt as well as the active substance content was also investigated. The best results were obtained for N,N'-bis(5-bromo-2-hydroxy-3-methoxybenzylidene)2-hydroxypropylene-1,3-diamine and its dinuclear copper(II) complex. The ion-selective membrane composition was optimized, resulting in obtaining electrodes with a very good slope of 29.68 mV/decade in a wide measuring range $1 \times 10^{-6} - 1 \times 10^{-1}$ mol L^{-1} and good potential stability and selectivity. The electrodes could successfully work in the pH range of 2.4–5.5 for a minimum period of 2 months.

Keywords Ion-selective electrodes · Schiff base complexes · Potentiometry · Copper ionophore

Introduction

Copper is an element quite widespread in nature, occurring both in metallic form and in various ores and minerals [1]. It is also found both in the form of complexes and solid particles in various types of waters, in groundwater, surface water, seawater, and drinking water [2]. Food such as offal, seafood, mushrooms, grains, and nuts is a source of copper in human diet. On the other hand, a large percentage of copper is supplied to the body from drinking water (about 25%). Copper is a micronutrient necessary for the proper functioning of living organisms, but in inappropriate amounts, it is toxic and dangerous to health [3]. There is approximately 100 mg of copper in the human body

[4], while the recommended daily intake of this element is about 2 mg, and 10–15 mg is considered toxic [1]. In the case of copper, both its excess and deficiency can cause many adverse health effects [1]. This element takes part in many physiological processes, is involved in the synthesis of neuropeptides, has an immunological function, and is a cofactor of many redox enzymes [4]. Insufficient copper in a human's diet can have negative consequences throughout his life. Copper deficiency may cause, among others, the occurrence of disorders in the functioning of the circulatory system and the central nervous system, while its excess may cause many side effects such as dizziness, nausea, muscle, and abdominal pain, as well as disturbances in the functioning of the internal organs and the digestive system [1, 4, 5].

Nowadays, it is very important to control the condition of the natural environment. Due to the use of copper in many industries because of its unique properties, such as high electrical conductivity, flexibility, chemical stability, and the possibility of creating alloys with many metals and therefore the increased release of this element into the environment, it is very important to monitor its content in various environmental samples, including soil, sewage, and water samples [6, 7] but also in food samples [8, 9].

Ion-selective electrodes are still widely used for the determination of metal and non-metal ions in such samples. The most

✉ Cecylia Wardak
cecylia.wardak@mail.umcs.pl

1 Department of Analytical Chemistry, Institute of Chemical Sciences, Faculty of Chemistry, Maria Curie-Sklodowska University, Maria Curie-Sklodowska Sq. 3, 20-031 Lublin, Poland

2 Department of General Chemistry, Coordination and Crystallography, Institute of Chemical Sciences, Faculty of Chemistry, Maria Curie-Sklodowska University, Maria Curie-Sklodowska Sq. 2, 20-031 Lublin, Poland

Springer

important element of the ion-selective electrodes is the ion-selective membrane, the composition of which is optimized in order to obtain the best analytical parameters of the sensors. Thanks to them, it is possible to transform the chemical potential of the determined ion into an electric potential, which ensures the proper operation of the chemical sensor [10]. There is still a search for effective and efficient substances that can be used as an ionophore (active substance), imparting selective properties to the ion-selective membrane in these sensors. However, this is not an easy task, as the design and synthesis of compounds are often a long and complicated process.

So far, many different substances have been used as active substances (ionophores) in the ion-selective membranes of potentiometric sensors sensitive to copper(II) ions, including Schiff complexes. Several commercial selectophores are available (such as, for example, copper(II) ionophore I, copper(II) ionophore IV). In the literature there are many studies of electrodes constructed using synthesized active substances in the literature. Most of them are organic and inorganic substances with a complex structure. N-hydroxy-succinimide and succinimide [3], o-xylylenebis(N,N-diisobutyldithiocarbamate) [8], 4-amino-6-methyl-1,2,4-triazin-5-one-3-thione [11], bis(2-hydroxynaphthaldehydene)-1,6-hexanediamine [12], N,N,N',N'-tetracyclohexyl-2,2'-thiodiacetamide (copper(II) ionophore IV) [13], ethambutol-copper(II) complex [14], 5,7,12,14-tetramethyldibenzo[b,i]-1,4,8,11-tetraazacyclotetradecane [15], 2-(indol-3-yl)vinyl)-1,3,4-thiadiazole-2-thiol [16], or Schiff base complex derived from 2,3-diaminopyridine and o-vanilin [17] have been used thus far as electroactive materials in different copper(II)-selective membrane sensors.

Schiff bases are the condensation products of carbonyl compounds with primary amines [18]. The first described condensation of an aldehyde with an amine described Schiff took place in 1864 [19], and since then, compounds from this group have been widely synthesized and studied by many scientists. Schiff base ligands are easily synthesized and widely used in coordination chemistry to synthesize their complexes with most of transition metals [20]. Many of these compounds exhibit excellent catalytic activity in a variety of reactions under conditions of increased humidity and higher temperatures (> 100 °C) [18]. Thanks to their stability and high sensitivity and selectivity to specific metal cations, these compounds are widely used in many fields of analytical, coordination, and materials chemistry as well as in organic synthesis. They are also used in magnetic materials, adsorption, and fluorescence [21]. Schiff's bases are a very large and important group of compounds, which due to their unique properties and high versatility are widely described in the literature, both in the form of review articles [18, 19, 22, 23], and research papers containing descriptions of the synthesis of these compounds and their properties. They have typical chemical applications, but it is also very popular to obtain compounds of this type, including

both Schiff bases and their complexes, and study not only their catalytic properties, but also biological ones, including antifungal, antibacterial, and anti-inflammatory properties, which enables their use in clinical and pharmacological areas [24–32]. Schiff base complexes with copper are commonly synthesized and studied [20, 33–38]. Compounds of this type were also used in the present study.

In the work, newly synthesized compounds belonging to the group of Schiff base complexes were used for the construction of ion-selective electrodes sensitive to copper(II) ions. Electrodes were constructed which differed in the type and amount of active substances, the type of plasticizer, and the type of lipophilic salt in the membrane. The basic analytical parameters of the obtained sensors were compared, such as characteristic curve slope, linearity range, and detection limit of the electrodes, as well as pH ranges. Selectivity coefficients for selected cations were determined, and measurements of the reversibility and stability of the sensor potential were also made. The aim of the research was to optimize the composition of the ion-selective membrane for the electrode sensitive to copper(II) ions.

Materials and methods

Apparatus

Potentiometric measurements were performed for a cell composed of an Ag/AgCl (Metrohm 6.0750.100) reference electrode containing a 1 mol L^{-1} concentration of lithium acetate in an external electrolytic key and the tested ion-selective electrodes with a different composition of ion-selective membranes. All measurements were performed at room temperature using a magnetic stirrer. This was connected to a potentiometer (Lawson Labs, Inc.) coupled with a computer that collected and analyzed the data. Additionally, an ORION 81-72 glass electrode and an Elmetron CX-741 potentiometer were used to measure the dependence of the electrode potential on pH.

Reagents

Schiff base ligands and their complexes with copper(II), synthesized according to the described procedures [20], were used as active components of the ion-selective membranes: N,N'-bis(5-bromo-2-hydroxy-3-methoxybenzylidene)2-hydroxypropylene-1,3-diamine (H_3L^1), mononuclear copper(II) complex of N,N'-bis(5-bromo-2-hydroxy-3-methoxybenzylidene)2-hydroxypropylene-1,3-diamine ([Cu(HL^1)]·H_2O) (HL^{1}Cu), dinuclear copper(II) complex of N,N'-bis(5-bromo-2-hydroxy-3-methoxybenzylidene)2-hydroxypropylene-1,3-diamine([Cu$_2$(L^1)(OAc)(MeOH)]·2H_2O·MeOH)

Table 1 The formulas, masses, and schemes of compounds used as components of ion-selective membranes

Abbreviation	Formula	Molecular weight [u]	Scheme of compound
H_3L^1	$C_{19}H_{20}Br_2N_2O_5$	516.18	
HL^1Cu	$C_{19}H_{18}Br_2CuN_2O_5$	577.71	
L^1Cu_2	$C_{22}H_{26}Br_2Cu_2N_2O_8$	733.35	
H_5L^2	$C_{17}H_{18}N_2O_5$	330.34	
H_2L^3	$C_{19}H_{20}Br_2N_2O_4$	500.18	
H_4L^4	$C_{19}H_{22}N_2O_4$	342.39	
H_4L^5	$C_{17}H_{18}N_2O_4$	314.34	

Table 1 (continued)

H_3L^1, N,N'-bis(5-bromo-2-hydroxy-3-methoxybenzylidene) 2-hydroxypropylene-1,3-diamine

HL^1Cu, mononuclear complex of N,N'-bis(5-bromo-2-hydroxy-3-methoxybenzylidene) 2-hydroxypropylene-1,3-diamine with copper(II)

L^1Cu_2, dinuclear complex of N,N'-bis(5-bromo-2-hydroxy-3-methoxybenzylidene) 2-hydroxypropylene-1,3-diamine with copper(II)

H_5L^2, N,N'-bis(2,3-dihydroxybenzylidene) 2-hydroxypropylene-1,3-diamine

H_2L^3, N,N'-bis(5-bromo-2-hydroxy-3-methoxybenzylidene) propylene-1,3-diamine

H_4L^4, N,N'-bis(2,3-dihydroxybenzylidene) -2,2-dimethyl propylene-1,3-diamine

H_4L^5, N,N'-bis(2,3-dihydroxybenzylidene) propylene-1,3-diamine

(L^1Cu_2) [20, 21], N,N'-bis(2,3-dihydroxybenzylidene)2-hydroxypropylene-1,3-diamine (H_5L^2), N,N'-bis(5-bromo-2-hydroxy-3-methoxybenzylidene)propylene-1,3-diamine (H_2L^3), N,N'-bis(2,3-dihydroxybenzylidene)-2,2-dimethyl propylene-1,3-diamine (H_4L^4) [39], and N,N'-bis(2,3-dihydroxybenzylidene)propylene-1,3-diamine (H_4L^5) [40]. To prepare the membrane, mixtures were also used poly(vinyl chloride) cz. d. a. (Sigma-Aldrich); plasticizers, tris(2-ethylhexyl)phosphate (TEHP, Fluka), tributyl phosphate (TBP, Merck), o-nitrophenyloctylether (NPOE, Fluka), bis(butylpentyl)adipate (BBPA, Fluka), and bis(2-ethylhexyl)sebacate (DOS, Fluka), and lipophilic salts, potassium tetrakis(4-chlorophenyl)borate (KTpClPB, Fluka), potassium tetra[3,5-bis(trifluoromethyl)phenyl] borate (KTFPB, Sigma-Aldrich), and sodium tetraphenylborate (NaTPB, Merck). Cation salts for which the electrode selectivity were tested, and the main ion salt $(Cu(NO_3)_2)$ necessary for the preparation of aqueous stock solutions and $NaOH_{(aq)}$ and $HNO_{3(aq)}$ used to test the electrode pH range were obtained from Fluka. Redistilled water was used to prepare all solutions.

Preparation of the ion-selective electrodes and membrane composition

Pure silver wires (previously cleaned with fine sandpaper and degreased with acetone and dried) were electrochemically anodized with constant 5 V current in 4 mol L^{-1} HCl for 2 min to form an Ag/AgCl electrodes. The inner electrodes prepared in this way were placed in a copper plate, immersed in a 1×10^{-3} mol L^{-1} KCl solution saturated with AgCl and left overnight in a dark place. The weighed and thoroughly mixed membrane mixtures were homogenized in an ultrasonic bath for 1 h and then purged of air bubbles using a vacuum pump and transferred to previously cleaned cylindrical Teflon containers in which silver chloride electrodes were placed. Enough membrane mixture was used in each container to completely cover the Ag/AgCl electrode. The filled Teflon containers were then placed in a laboratory drier and heated to 90 °C for about 5 min, until the mixtures gelled completely. Then they were left to cool down at room temperature and screwed to the electrode bodies. Before the first measurement, the electrodes were conditioned in 1 ×

Table 2 Qualitative and quantitative compositions of membrane mixtures

No electrode	Ionophore	[%]	Lipophilic salt	[%]	Plasticizer	[%]	PVC [%]
0	-	-	KTpClPB	0.50	NPOE	66.50	33.00
1	H_3L^1	1	KTpClPB	0.48	NPOE	65.52	33.00
2	HL^1Cu	1	KTpClPB	0.43	NPOE	65.57	33.00
3	L^1Cu_2	1	KTpClPB	0.34	NPOE	65.66	33.00
4	H_5L^2	1	KTpClPB	0.75	NPOE	65.25	33.00
5	H_2L^3	1	KTpClPB	0.50	NPOE	65.50	33.00
6	H_4L^4	1	KTpClPB	0.72	NPOE	65.28	33.00
7	H_4L^5	1	KTpClPB	0.79	NPOE	65.21	33.00
8	L^1Cu_2	1	KTpClPB	0.34	TBP	65.66	33.00
9	L^1Cu_2	1	KTpClPB	0.34	BBPA/NPOE	32.66/33.00	33.00
10	L^1Cu_2	1	KTpClPB	0.34	DOS/NPOE	32.66/33.00	33.00
11	L^1Cu_2	1	KTpClPB	0.34	TEHP/NPOE	32.66/33.00	33.00
12	L^1Cu_2	2	KTpClPB	0.34	NPOE	64.66	33.00
13	L^1Cu_2	2	KTpClPB	0.34	TEHP/NPOE	32.33/32.33	33.00
14	L^1Cu_2	4	KTpClPB	0.34	NPOE	62.66	33.00
15	L^1Cu_2	4	KTpClPB	0.34	TEHP/NPOE	31.33/31.33	33.00
16	L^1Cu_2	1	KTFPB	0.62	NPOE	65.38	33.00
17	L^1Cu_2	1	NaTPB	0.24	NPOE	65.76	33.00

10^{-3} mol L^{-1} Cu(NO$_3$)$_2$ solution for 24 h while before each subsequent measurement for 1 h.

In the preliminary tests, the membrane mixtures (except for the base mixture) contained 1% by weight of each active substance. Table 1 shows the summary and structural formulas as well as the molar masses of all compounds used for this purpose. The weight of each of them was calculated based on the determined molar mass of each compound. Then, on this basis, the weight of KTpClPB (molar mass 496 g mol^{-1}) was calculated, which was added by a half less moles compared to the active substance. In each case, the PVC content was 33.0%, while the remaining part was NPOE (in total 100%). Having examined the basic analytical parameters of the prepared electrodes containing various ionophores (such as limit of detection, selectivity, linearity, and pH range), one active substance was selected. In the next stage of the research, which included optimization of the composition of the ion-selective membranes containing the active substance, the compound L^{1}Cu$_2$, both the percentage of this compound and the types and contents of plasticizers were changed. In the last step, the electrodes containing different types of lipophilic salts were also compared. Table 2 shows the compositions of the membrane mixtures at each stage of the optimization of the ion-selective membrane composition.

Results and discussion

The study investigated the ionophoric properties of newly synthesized Schiff base ligands and their complexes with copper(II). The tested ligands have in the molecule two nitrogen atoms with free electron pairs and phenolic groups capable of dissociation. Due to this, they can interact with copper(II) ions to form mononuclear or binuclear complexes.

In the structure of the mononuclear complex (HL^{1}Cu), which crystalizes in one molecule of water, the Cu(II) ion coordinates two phenolate oxygen atoms and two imine nitrogen atoms of the doubly deprotonated Schiff base. The alcohol group of the aliphatic chain of the Schiff base remains protonated and acts as a hydrogen bond donor to a water molecule. In the structure of the binuclear complex (L^{1}Cu$_2$), which crystallizes with one methanol molecule and two water molecules, the Cu(II) ions also coordinate two phenolate oxygen and two imine nitrogen atoms of the Schiff base. Additionally, the copper(II) ions are doubly bridged by the oxygen atoms of the alkoxide group of the fully deprotonated Schiff base and the carboxylate group of the acetate ion, respectively.

The studied compounds were used as an active component of the ion-selective membrane of electrodes sensitive to copper(II) ions. The whole research on ion-selective electrodes was divided into several parts. At the beginning, the effectiveness of the use of individual ligands and their selected complexes with copper as an active substance of the polymeric membrane sensitive to copper(II) ions was tested. Electrodes without the active substance were also prepared to make the effect of other substances more noticeable. For all types of electrodes, calibration curves were made to determine the slope, linearity range, and detection limits. Selectivity coefficients and the pH ranges in which the electrodes can work properly were also determined. Taking into

Table 3 Basic parameters of electrodes with different active substances

No electrode	Slope [mV/dec]	Linear range [mol L^{-1}]	Limit of detection [mol L^{-1}]	pH range	Response time [s]
0	20.31	5×10^{-5}–1×10^{-1}	1.5×10^{-5}	-	< 15
1	28.64	1×10^{-6}–1×10^{-1}	6.3×10^{-7}	2.4–5.5	< 10
2	30.10	1×10^{-6}–1×10^{-1}	5.9×10^{-7}	2.4–5.5	< 10
3	29.68	1×10^{-6}–1×10^{-1}	6.2×10^{-7}	2.4–5.5	< 10
4	26.56	5×10^{-5}–1×10^{-1}	8.7×10^{-6}	5.2–6.0	< 10
5	55.20	5×10^{-6}–1×10^{-3}	5.5×10^{-6}	3.8–5.5	< 15
6	36.00	1×10^{-6}–1×10^{-2}	5.2×10^{-7}	2.8–5.5	< 15
7	41.00	1×10^{-6}–1×10^{-2}	4.8×10^{-7}	2.1–5.5	< 15

Table 4 Summary of selectivity coefficient values ($\log K^{pot}_{Cu/M}$) for the studied sensors determined by SSM method

No electrode	Na$^+$	K$^+$	Ca^{2+}	Mg^{2+}	Co^{2+}	Ni^{2+}	Zn^{2+}	Cd^{2+}	Pb^{2+}
1	−3.58	−1.67	−1.25	−2.22	−2.55	−1.99	−2.43	−1.26	−0.57
2	−2.74	−2.26	−1.93	−4.64	−4.12	−2.39	−3.21	−1.59	−0.87
3	−3.06	−2.33	−2.07	−5.02	−4.42	−2.58	−3.14	−1.82	−1.77
4	−0.77	1.51	−0.4	−1.78	−1.81	−0.16	−1.79	−1.2	−0.15
5	−1.31	−0.45	1.0	−0.74	−0.91	−0.67	−1.23	0.9	−0.46
6	−2.4	1.92	−1.4	0.77	−0.53	1.57	−1.57	0.77	−0.57
7	−4.39	−1.32	−1.39	−0.95	−1.66	−2.22	−3.00	−3.18	−2.17

Table 5 Comparison of selectivity coefficients ($\log K^{pot}_{Cu/M}$) for the tested electrode 3 and other electrodes available in the literature

Active substance	Interfering ion									References
	Na^+	K^+	Ca^{2+}	Mg^{2+}	Co^{2+}	Ni^{2+}	Zn^{2+}	Cd^{2+}	Pb^{2+}	
NHS	-	-	−2.41	-	−3.55	−1.49	−2.06	-	−0.59	[3]
SUCC			−1.78		−0.89	−0.91	−0.59		−0.07	
o-XBDiBDTC	−4.71	−2.42	−3.50	-	−3.80	−2.30	−5.23	−2.98	−2.50	[8]
AMTOT	−2.10	−2.19	−2.12	−2.17	−2.39	−2.66	−2.64	−2.30	−2.85	[11]
BHNHDA	-	-	-	−3.41	−2.98	−3.13	−3.15	−2.36	3.07	[12]
copper(II) ionophore IV	−4.95	−5.21	−4.93	−6.22	−3.16	−3.02	−3.39	−3.84	-	[13]
ethambutol-copper(II) complex	−1.32	−0.70	−1.50	−2.89	−1.06	−1.23	−1.66	−1.46	−1.09	[14]
$Me_4Bzo_2[14]aneN_4$	−0.15	−1.30	−2.85	−2.68	−2.33	−1.05	−2.25	−2.77	−2.41	[15]
S_2	−3.19	−3.11	−3.46	−3.77	−3.54	−4.02	−2.62	−2.01	−1.82	[16]
B	−1.07	−1.22	−1.20	−1.21	−1.10	−1.12	−1.09	−1.09	-	[17]
L^1Cu_2	−3.06	−2.33	−2.07	−5.02	−4.42	−2.58	−3.14	−1.82	−1.77	This work

Abbreviations: *NHS*, N-hydroxy-succinimide; *SUCC*, succinimide; *o-XBDiBDTC*, o-xylylenebis(N,N-diisobutydithiocarbamate); *AMTOT*, 4-amino-6-methyl-1,2,4-triazin-5-one-3-thione; *BHNHDA*, bis(2-hydroxynaphthaldehydene)-1,6-hexanediamine; *copper(II) ionophore IV*, N,N,N',N', tetracyclohexyl-2,2'-thiodiacetamide; *$Me_4Bzo_2[14]aneN_4$*, 5,7,12,14-tetramethyldibenzo[b,i]-1,4,8,11-tetraazacyclotetradecane; *S_2*, 2-(indol-3-yl)vinyl)-1,3,4-thiadiazole-2-thiol; *B*, Schiff base complex derived from 2,3-diaminopyridine and o-vanilin; *NPOE*, o-nitrophenyloctylether; *DOP*, dioctyl phthalate; *DBBP*, dibutylbutylphosphonate; *TBP*, tri-n-butylphosphate

account the characteristic slope, linear range, and selectivity, the best compound was selected for detailed studies and optimization of the membrane composition. The influence of the type of plasticizer, the type of lipophilic ionic additive, and the concentration of the active substance were also investigated. Other parameters, such as reversibility, short-term and

Fig. 1 Calibration curves of electrodes differing in the type of plasticizer in the membrane determined in the concentration range of $1 \times 10^{-7} - 1 \times 10^{-1}$ mol L^{-1} $Cu(NO_3)_2$
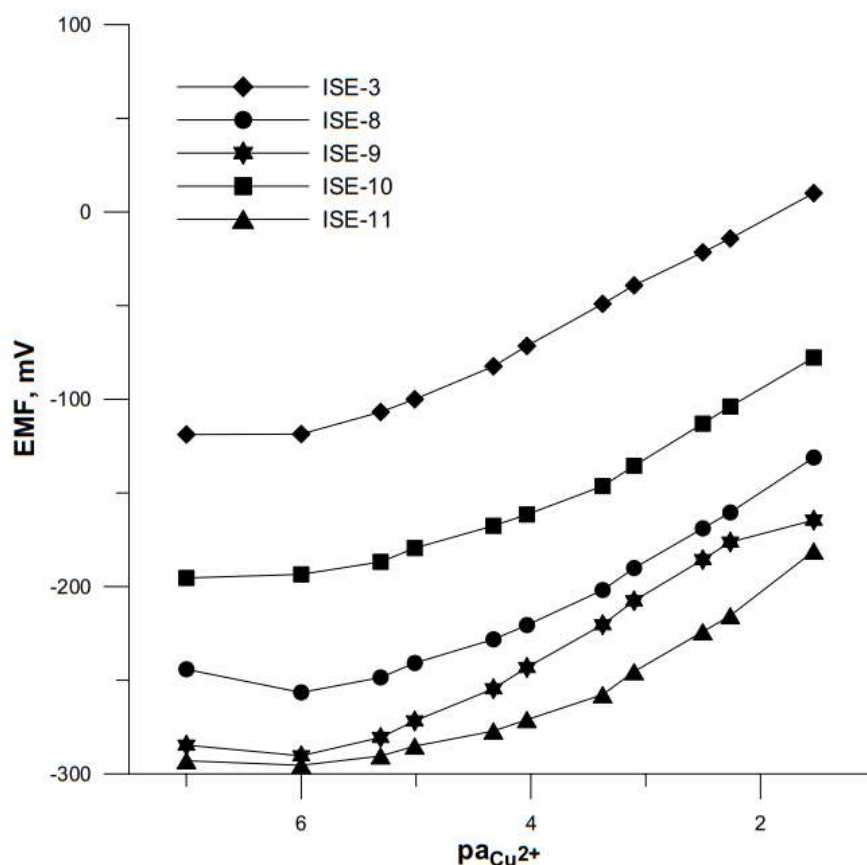
long-term stability, and electrode lifetime, were measured for the optimal ion-selective membrane composition selected on the basis of the obtained results.

Potentiometric response

The electrode potential response was measured in $Cu(NO_3)_2$ solutions in the concentration range of 1×10^{-7}–1×10^{-1} mol L^{-1}. On the basis of the obtained calibration curves, the slopes, linearity ranges, and detection limits were determined for electrodes differing in the type of active substance. The detection limit was determined as the activity level of the main ion at which the measured potential deviates $18/z$ mV from the linear response curve [41]. All the obtained values are summarized in Table 3. Depending on the type of ligand incorporated into the membrane, the electrodes differed significantly. All electrodes showed sensitivity to copper ions but with different ranges and slopes. The electrodes with ligands H_3L^1 and H_5L^2 had the slope of the calibration curve closest to the theoretical value, but electrode 1 based on H_3L^1 exhibited wider measuring range. Other electrodes based on the ligands H_2L^3, H_4L^4, and H_4L^5 had a super-Nernstian slope of the calibration curve and/or shorter linear

range of the calibration curve. For comparison, electrode 0 without the complexing ligand in the membrane showed poor response to copper ions with the slope of 20.31 mV/decade. The best results were obtained for the ligand H_3L^1, and hence, it was applied as membrane active substance also in the form of complexes with copper(II) ions. Electrodes 2 and 3 based on the mononuclear (HL^{1}Cu) and dinuclear (L^{1}Cu$_2$) complex, respectively, showed similar potentiometric response to that of electrode 1.

After selecting one active substance (L1Cu2), mixtures that differed in the type of plasticizer in the ion-selective membrane (ISEs 3, 8, 9, 10, 11) were prepared. The calibration curves of these electrodes are shown in Fig. 1. Based on this, pure NPOE was found to be the best plasticizer in this case.

Subsequently, successive mixtures differing in the content of active substance in the membrane were tested. Additional electrodes with 2 and 4% wt. of the studied L1Cu2 complex were prepared and measured.

It was concluded that the increasing active substance content in the membrane phase did not cause improvement in the electrode response. Therefore, the optimal ionophore concentration in the membrane was determined to be 1% wt.

Fig. 2 Calibration curves of electrodes differing in the type of lipophilic salt in the membrane determined in the concentration range of 1×10^{-7} – 1×10^{-1} mol L^{-1} Cu(NO$_3$)$_2$
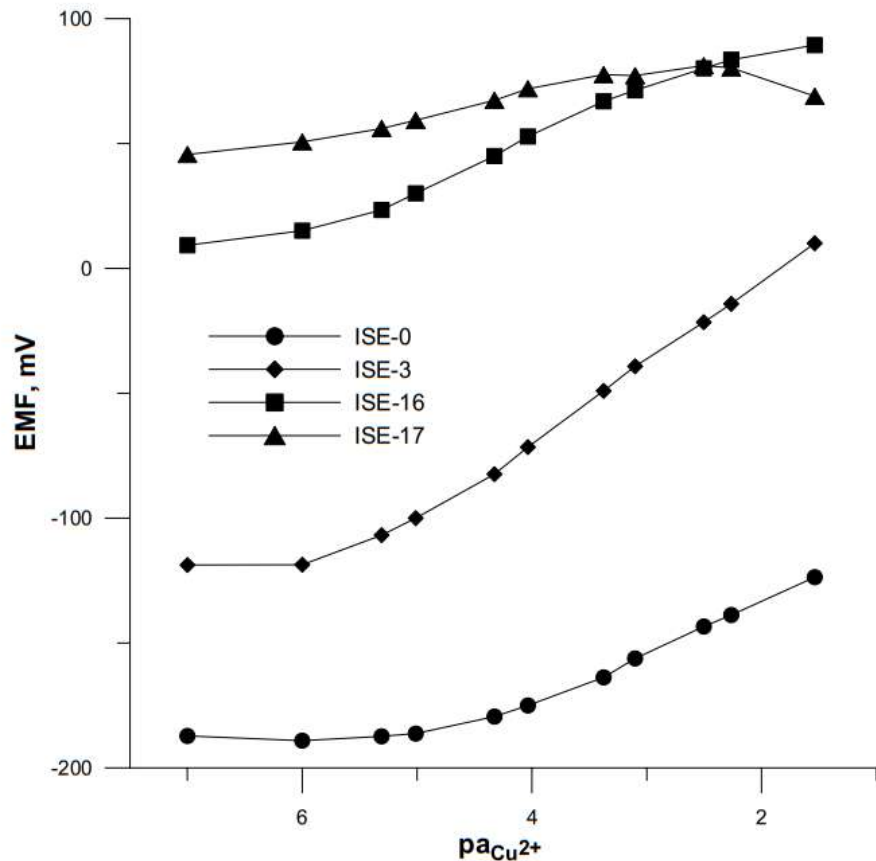
Then, the focus was on the type of lipophilic salt as a membrane additive. The previously used salt KTpClPB as well as KTFPB and NaTPB (ISE 3, 16, 17) were considered. For this group of electrodes, the calibration curves are shown in Fig. 2. In this case, it was confirmed that the KTpClPB salt used from the beginning was the best choice.

Based on extensive research on the optimal composition of ion-selective electrode membranes containing selected ligands and Schiff complexes, one optimal composition was selected for electrode 3 (Table 2). In order to test additional analytical parameters (such as reversibility, short-term and long-term stability, and electrode lifetime), several copies of these electrodes were made.

Response time

The response time of the sensors was estimated by measuring the electrode potential while adding concentrated standard solutions of the main ion to the mixed solution in which the electrodes were immersed. All standard additives were added in a way so as to obtain solution concentrations in the same concentration range in which the measurements of the electrode calibration curve were made, i.e., 10^{-7}–10^{-1} mol L^{-1}. The time during which the electrode potential reached

> 95% of the final value at a given concentration was measured, i.e., the value after the signal had stabilized over time. All electrodes were found to exhibit a fast response time (less than 15 s) (Table 3).

Dependence of the potential on pH

The dependence of the electrode potential on the pH of the solutions was measured in a 1×10^{-3} mol L^{-1} solution of the main ion in the pH range from 1.5 to 8. The appropriate pH of the solution was obtained by adding small volumes of concentrated acid ($HNO_{3(aq)}$) and base ($NaOH_{(aq)}$) to the main ion solution. The pH ranges for the electrodes with all types of ionophores did not differ significantly, and they are summarized in Table 3. The dependence of the electrode potential on the pH of the sample solution determined for electrode 3 is shown in Fig. 3. As can be seen, the electrode potential remains stable within the pH range of 2.4–5.5. Outside this range, gradual changes in potential were observed. At higher pH values, the potential decreased with increasing pH. This was associated with the formation of Cu^{2+} hydroxyl complexes in the solution. The change in electrode potential at low pH values below 2.4 was due to the interfering effect of hydrogen ions which affect the complex formation

Fig. 3 Dependence of the potential on the pH of a solution with a concentration of 10^{-3} mol L^{-1} for electrode 3
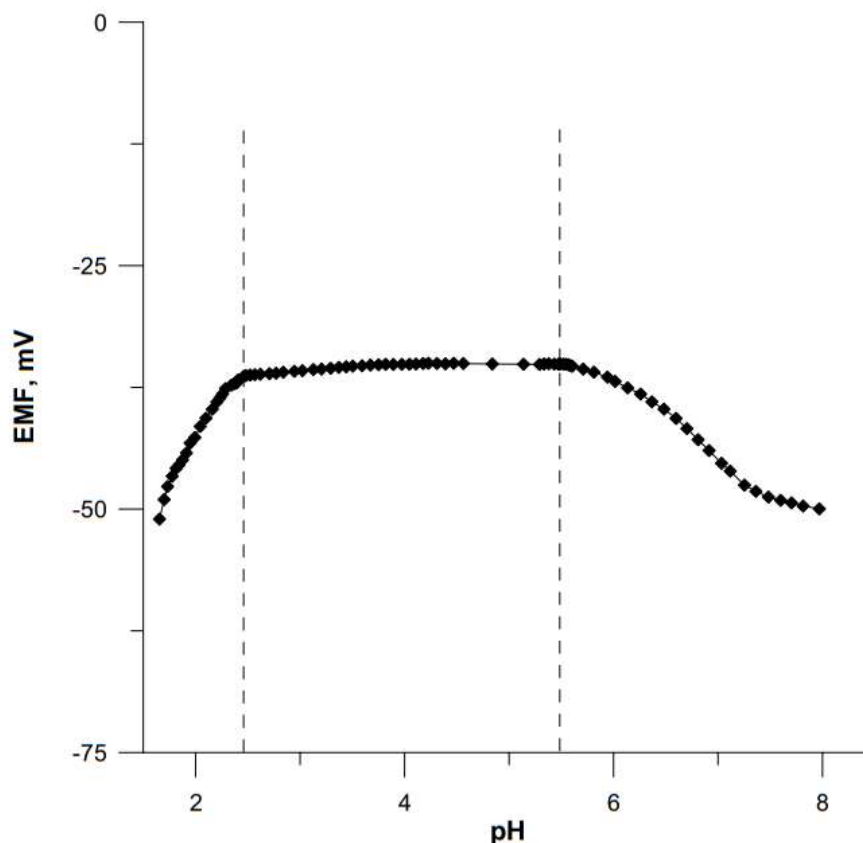
equilibrium between the ionophore and Cu^{2+} ions. For the other sensors, the dependence of the electrode potential on the pH of the solution followed a similar course.

Selectivity

The selectivity of the electrodes towards the selected cations was estimated for all the compositions of the membrane mixtures. Selectivity coefficients were determined by the separate solutions method (SSM) for the following ions: Na^+, K^+, Ca^{2+}, Mg^{2+}, Co^{2+}, Ni^{2+}, Cd^{2+}, and Pb^{2+}. The method consists in obtaining calibration curves for the main ion (i) and interfering ions (j) and then extrapolating these curves ($a_i = a_j = 0$) to obtain E^0 [42]. The obtained $logK^{pot}_{Cu/M}$ values are presented in Table 4 where it can be seen that among the electrodes based on ligands, electrodes 1 (H_3L^1) and 7 (H_4L^5) are characterized by better selectivity than the other electrodes. In turn, when comparing electrodes 1–3 based on the H_3L^1 ligand and its complexes with copper(II), a gradual improvement in electrode selectivity can be seen for the electrode containing the mono- and dinuclear complexes, respectively. It is worth noting that the electrode based on L^1Cu_2 showed good selectivity towards lead ions, which are usually a serious interferent in the case of electrodes sensitive to copper(II) ions.

The comparison of the selectivity coefficients for electrode 3 with the selectivity coefficients for other electrodes sensitive to copper(II) ions available in the literature is presented in Table 5. On the basis on analysis of this table, it can be concluded that although electrode 3 based on the L^1Cu_2 complex did not show the best selectivity among the other electrodes, its selectivity is still promising and superior than many others [3, 11, 14, 15, 17]. As regards the selectivity coefficients in relation to almost all tested ions (except for cadmium and lead), the $logK^{pot}_{Cu/M}$ values are < -2. In such case, the electrode can be used successfully for the determination of the main ion in samples where the concentration of interfering ions will not be higher than the concentration of the main ion. Otherwise, the electrode can also be used, but the results of the determination of the main ion need to be corrected based on the exact concentration of interferents present in the sample and the values of the appropriate selectivity coefficients.

Fig. 4 Potential reversibility at concentrations of 1×10^{-3} and 1×10^{-4} mol L^{-1} and the short-term stability at a concentration of 1×10^{-1} mol L^{-1} of the ISE-3 electrode
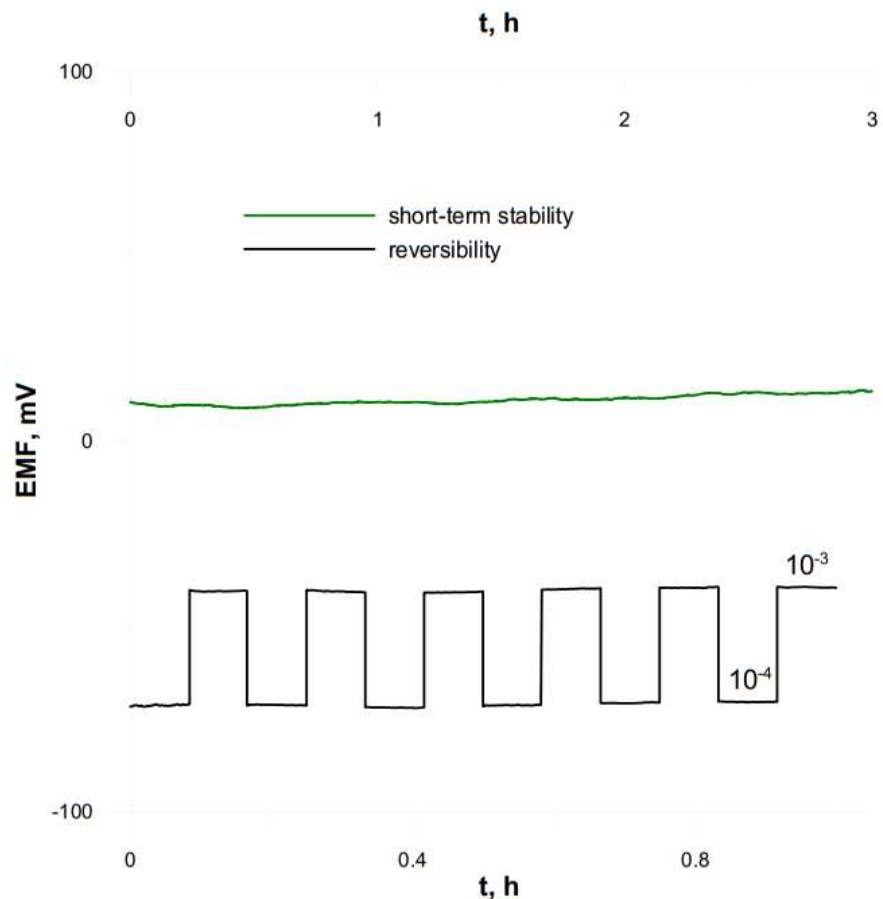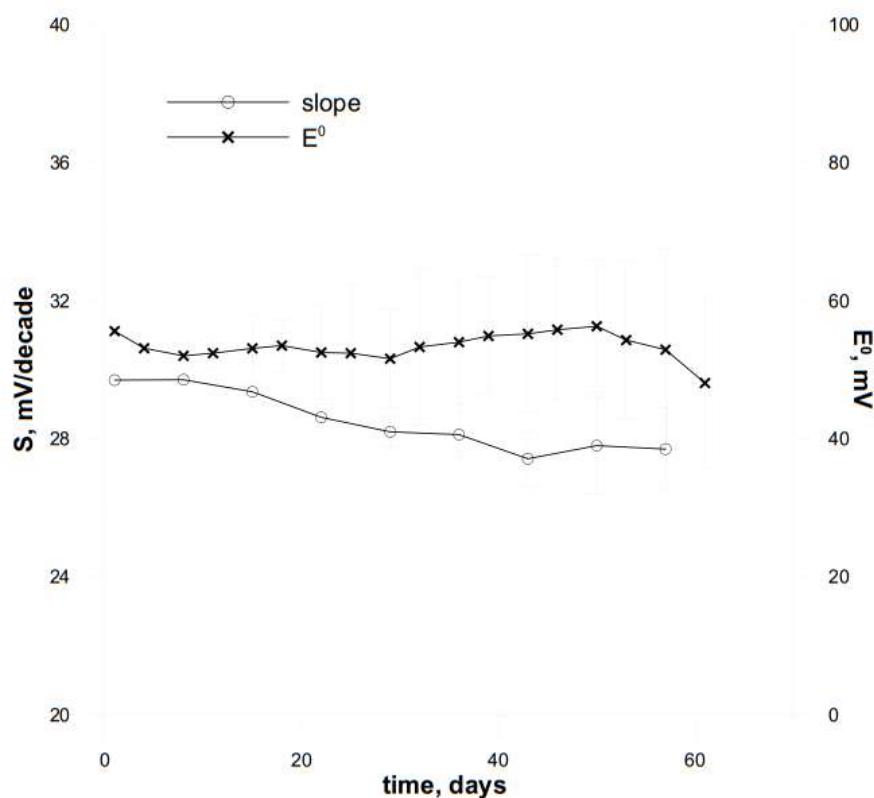
Fig. 5 Stability of the electrode based on L^1Cu_2. Change of the slope and potential E_{st}^0 in time. Standard deviations given in the plot were determined for the same electrodes no. 3

From among all the possibilities, the electrode containing the dinuclear copper(II) complex (L^1Cu_2) was selected for further research, mainly because the electrode with this compound was close to the theoretical slope of the calibration curve since its calibration curve had a wide range of linearity, and, most of all, this electrode exhibited the best selectivity.

Table 6 Comparison of the properties of various Cu^{2+}-selective electrodes

Active substance	Plasticizer	Slope [mV/Dec]	Detection limit [mol L^{-1}]	Linear range [mol L^{-1}]	Response time [s]	Life time [months]	pH range	References
NHS	NPOE	37.5	4.4×10^{-6}	1×10^{-4}–1×10^{-2}	0.25	3	2.0–6.0	[3]
SUCC	NPOE	25.4	7.3×10^{-6}	1×10^{-4}–1×10^{-2}	1	3	2.0–6.0	
o-XBDiBDTC	NPOE	31.3	4.9×10^{-7}	1×10^{-6}–1×10^{-1}	< 10	3	3.5–6.0	[8]
AMTOT	NPOE	29.3	6.2×10^{-7}	1×10^{-6}–1×10^{-1}	< 20	2	2.5–7	[11]
BHNHDA	-	29.5	3.0×10^{-5}	5×10^{-5}–1×10^{-1}	5–8	1	2.0–5.0	[12]
copper(II) ionophore IV	NPOE	28.9	3.5×10^{-7}	1×10^{-6}–1×10^{-2}	5–10	4	2.5–6.0	[13]
ethambutol-copper(II) complex	DOP	29.9	-	8×10^{-6}–1×10^{-1}	11	5	2.1–6.3	[14]
$Me_4Bzo_2[14]aneN_4$	DBBP	30.2	-	3×10^{-5}–1×10^{-1}	13	5	2.6–5.5	[15]
S_2	TBP	30.6	2.3×10^{-7}	6×10^{-7}–1×10^{-1}	13	2.5	3.0–7.5	[16]
B	DOP	29.6	3.0×10^{-7}	5×10^{-6}–1×10^{-1}	< 30	> 4	1.9–5.2	[17]
L^1Cu_2	NPOE	29.7	6.2×10^{-7}	1×10^{-6}–1×10^{-1}	< 10	> 2	2.4–5.5	This work

Abbreviations: *NHS*, N-hydroxy-succinimide; *SUCC*, succinimide; *o-XBDiBDTC*, o-xylylenebis(N,N-diisobutydithiocarbamate); *AMTOT*, 4-amino-6-methyl-1,2,4-triazin-5-one-3-thione; *BHNHDA*, bis(2-hydroxynaphthaldehyde)-1,6-hexanediamine; *copper(II) ionophore IV*, N,N,N',N'-tetracyclohexyl-2,2'-thiodiacetamide; $Me_4Bzo_2[14]aneN_4$, 5,7,12,14-tetramethyldibenzo[b,i]-1,4,8,11-tetraazacyclotetradecane; S_2, 2-(indol-3-yl)vinyl)-1,3,4-thiadiazole-2-thiol; *B*, Schiff base complex derived from 2,3-diaminopyridine and o-vanilin; *NPOE*, o-nitrophenyloctylether; *DOP*, dioctyl phthalate; *DBBP*, dibutylbutylphosphonate; *TBP*, tri-n-butylphosphate

Reversibility and short-term stability of the electrode potential

The reversibility of the electrode potential was measured in $Cu(NO_3)_2$ solutions with concentrations of 1×10^{-4} and 1×10^{-3} mol L^{-1}. The measurement of the potential was continued for about 5 min, and then the solution was changed to another solution with a different concentration. Figure 4 shows the dependence of the potential on time for electrode 3 with an optimized membrane composition where it can be seen that the electrode potential was fully reversible. The mean values of the potential obtained from six measurements for a single electrode were -71.3 ± 0.9 and -40.2 ± 0.6 for 1×10^{-4} and 1×10^{-3} mol L^{-1} of copper solutions, respectively.

In order to check the stability of the electrode potential during the measurement, the potential of the electrode immersed in a 1×10^{-1} mol L^{-1} $Cu(NO_3)_2$ solution was monitored for 3 h. Time trace potential change recorded during this test is shown in Fig. 4 where it can be seen that the electrode potential was very stable. Based on the obtained results, the potential drift was estimated at 0.017 mV/minute.

The proposed electrode 3 showed very good potential stability and reversibility. It is very important from the point of view of practical applications. It is well-known that potential drift and a change in electrode parameters over time are the main causes of errors in ion determination.

Life time and long-term potential stability and reproducibility

The stability and reproducibility of the electrode potential in the long-term were studied for a period of 2 months. Four identical sensors were measured two times per week in freshly prepared Cu^{2+} ion solutions. During this time, the linear range of the calibration curve did not change, the slope of the calibration curve of the sensors slightly decreased, and E^0 changed to a small extent with quite good reproducibility. The 2-month-old electrodes continued to work properly. Figure 5 presents the change in the slope and potential E^0 over time obtained for four identical electrodes 3.

Conclusions

Ionophoric properties of recently synthetized Schiff base ligands were studied in relation to copper(II) ions. The best parameters were exhibited by the electrode which contained the dinuclear complex of N,N'-bis(5-bromo-2-hydroxy-3-methoxybenzylidene) 2-hydroxypropylene-1,3-diamine with copper(II) ions as the ionophore in the membrane. The optimal membrane composition was 1% wt. L^1Cu_2, 0.34% wt. KTpClPB, 65.66% wt. NPOE, and 33% wt. PVC. Table 6

compares the basic analytical parameters of the proposed electrode with other previously reported Cu^{2+}-selective electrodes [3, 8, 34–40]. The presented data shows that our sensor is superior to most of the other electrodes with regard to detection limit and linear range. Only the electrode based on the commercial ionophore IV, which is currently unavailable, had comparable parameters. The electrodes have a calibration curve slope of 29.68 mV/decade and a linearity range of 10^{-6}–10^{-1} mol L^{-1}. It is worth to note that the proposed electrode was in solid contact mode and it was characterized by very good selectivity and high potential stability and reversibility. Measurements with the obtained electrode can be performed in acidic solutions in the typical pH range for electrodes sensitive to copper(II) ions (2.4–5.5).

Declarations

Conflict of interest The authors declare no competing interests.

References

1. Stern BR, Solioz M, Krewski D, et al (2007) Copper and human health: biochemistry, genetics, and strategies for modeling dose-response relationships
2. Wardak C, Grabarczyk M (2016) Analytical application of solid contact ion-selective electrodes for determination of copper and nitrate in various food products and drinking water. J Environ Sci Heal Part B 51:519–524. https://doi.org/10.1080/03601234.2016.1170545
3. Tutulea-Anastasiu MD, Wilson D, del Valle M et al (2013) A solid-contact ion selective electrode for copper(II) using a succinimide derivative as ionophore. Sensors (Switzerland) 13:4367–4377. https://doi.org/10.3390/s130404367
4. Bost M, Houdart S, Oberli M et al (2016) Dietary copper and human health: current evidence and unresolved issues. J Trace Elem Med Biol 35:107–115. https://doi.org/10.1016/j.jtemb.2016.02.006
5. Kaplan JH, Maryon EB (2016) How mammalian cells acquire copper: an essential but potentially toxic metal. Biophys J 110:7–13. https://doi.org/10.1016/j.bpj.2015.11.025
6. Rachou J, Gagnon C, Sauvé S (2007) Use of an ion-selective electrode for free copper measurements in low salinity and low ionic strength matrices. Environ Chem 4:90–97. https://doi.org/10.1071/EN06036
7. Topcu C, Lacin G, Yilmaz V et al (2018) Electrochemical determination of copper(II) in water samples using a novel ion-selective electrode based on a graphite oxide–imprinted polymer composite. Anal Lett 51:1890–1910. https://doi.org/10.1080/00032719.2017.1395035
8. Birinci A, Eren H, Coldur F et al (2016) Rapid determination of trace level copper in tea infusion samples by solid contact ion selective electrode. J Food Drug Anal 24:485–492. https://doi.org/10.1016/j.jfda.2016.02.012

9. Fan Y, Xu C, Wang R et al (2017) Determination of copper(II) ion in food using an ionic liquids-carbon nanotubes-based ion-selective electrode. J Food Compos Anal 62:63–68. https://doi.org/10.1016/j.jfca.2017.05.003

10. Ghosh T, Chung HJ, Rieger J (2017) All-solid-state sodium-selective electrode with a solid contact of chitosan/prussian blue nanocomposite. Sensors (Switzerland) 17:2536. https://doi.org/10.3390/s17112536

11. Zamani HA, Rajabzadeh G, Firouz A, Ariaii-Rad AA (2005) Synthesis of 4-amino-6-methyl-1,2,4-triazin-5-one-3-thione and its application in construction of a highly copper(II) ion-selective electrochemical sensor. J Braz Chem Soc 16:1061–1067. https://doi.org/10.1590/S0103-50532005000600025

12. Ghaedi M, Montazerozohori M, Sahraei R (2013) Comparison of the influence of nanomaterials on response properties of copper selective electrodes. J Ind Eng Chem 19:1356–1364. https://doi.org/10.1016/j.jiec.2012.12.040

13. Wardak C, Lenik J (2013) Application of ionic liquid to the construction of Cu(II) ionselective electrode with solid contact. Sensors Actuators B Chem 189:52–59. https://doi.org/10.1016/j.proeng.2012.09.107

14. Gupta VK, Prasad R, Kumar A (2003) Preparation of ethambutol-copper(II) complex and fabrication of PVC based membrane potentiometric sensor for copper. Talanta 60:149–160. https://doi.org/10.1016/S0039-9140(03)00118-8

15. Gupta VK, Prasad R, Kumar A (2003) Cu(II) selective sensor based on 5,7,12,14-tetramethyldibenzo[b,i]-1,4,8,11-tetraaza-cyclotetradecane in PVC matrix. J Appl Electrochem 33:381–386

16. Bandi KR, Singh AK, Upadhyay A (2014) Electroanalytical and naked eye determination of Cu2+ ion in various environmental samples using 5-amino-1,3,4-thiadiazole-2-thiol based Schiff bases. Mater Sci Eng C 34:149–157. https://doi.org/10.1016/j.msec.2013.09.006

17. Singh LP, Bhatnagar JM (2004) Copper(II) selective electrochemical sensor based on Schiff base complexes. Talanta 64:313–319. https://doi.org/10.1016/j.talanta.2004.02.020

18. Gupta KC, Sutar AK (2008) Catalytic activities of Schiff base transition metal complexes. Coord Chem Rev 252:1420–1450. https://doi.org/10.1016/j.ccr.2007.09.005

19. Cozzi PG (2004) Metal – salen Schiff base complexes in catalysis : practical aspects. Chem Soc Rev 33:410–421

20. Osypiuk D, Cristóvão B, Bartyzel A (2020) New coordination compounds of CuII with Schiff base ligands - crystal structure, thermal and spectral investigations. Crystals 10:1004

21. Cristóvão B, Osypiuk D, Miroslaw B, Bartyzel A (2020) Heterometallic di- and trinuclear CuIILnIII (LnIII = La, Ce, Pr, Nd) complexes with an alcohol-functionalized compartmental Schiff base ligand: syntheses, crystal structures, thermal and magnetic studies. Polyhedron 188:114703. https://doi.org/10.1016/j.poly.2020.114703

22. Vigato PA, Tamburini S (2004) The challenge of cyclic and acyclic Schiff bases and related derivatives. Coord Chem Rev 248:1717–2128. https://doi.org/10.1016/j.cct.2003.09.003

23. Al ZW, Ko YG (2016) Organometallic complexes of Schiff bases: recent progress in oxidation catalysis. J Organomet Chem 822:173–188. https://doi.org/10.1016/j.jorganchem.2016.08.023

24. Tumer M, Koksal H, Sener MK, Serin S (1999) Antimicrobial activity studies of the binuclear metal complexes derived from tridentate Schiff base ligands. Transit Met Chem 24:414–420

25. Gaber M, El-Ghamry HA, Fathalla SK, Mansour MA (2018) Synthesis, spectroscopic, thermal and molecular modeling studies of Zn2+, Cd2+ and UO22+ complexes of Schiff bases containing triazole moiety. Antimicrobial, anticancer, antioxidant and DNA binding studies. Mater Sci Eng C 83:78–89. https://doi.org/10.1016/j.msec.2017.11.004

26. Panneerselvam P, Nair RR, Vijayalakshmi G et al (2005) Synthesis of Schiff bases of 4-(4-aminophenyl)-morpholine as potential antimicrobial agents. Eur J Med Chem 40:225–229. https://doi.org/10.1016/j.ejmech.2004.09.003

27. Shakya PR, Singh AK, Rao TR (2012) Synthesis and characterization of lanthanide(III) complexes with a mesogenic Schiff-base, N,N'-di-(4-decyloxysalicylidene)-2',6'-diaminopyridine. Mater Sci Eng C 32:1906–1911. https://doi.org/10.1016/j.msec.2012.05.039

28. Bagihalli GGB, Avaji PG, Patil SA, Badami PS (2008) Synthesis, spectral characterization, in vitro antibacterial, antifungal and cytotoxic activities of Co(II), Ni(II) and Cu(II) complexes with 1, 2, 4-triazole Schiff bases. Eur J Med Chem 43:2639–2649. https://doi.org/10.1016/j.ejmech.2008.02.013

29. Creaven BS, Duff B, Egan DA et al (2010) Anticancer and antifungal activity of copper(II) complexes of quinolin-2(1H)-one-derived Schiff bases. Inorg Chim Acta 363:4048–4058. https://doi.org/10.1016/j.ica.2010.08.009

30. Raman N, Kulandaisamy A, Thangaraja C (2004) Synthesis, structural characterisation and electrochemical and antibacterial studies of Schiff base copper complexes. Transit Met Chem 29:129–135

31. Taghizadeh L, Montazerozohori M, Masoudiasl A et al (2017) New tetrahedral zinc halide Schiff base complexes: synthesis, crystal structure, theoretical, 3D Hirshfeld surface analyses, antimicrobial and thermal studies. Mater Sci Eng C 77:229–244. https://doi.org/10.1016/j.msec.2017.03.150

32. Gomathi G, Gopalakrishnan R (2016) A hydrazone Schiff base single crystal (E)-Methyl N'-(3,4,5-trimethoxybenzylidene) hydrazine carboxylate: physicochemical, in vitro investigation of antimicrobial activities and molecular docking with DNA gyrase protein. Mater Sci Eng C 64:133–138. https://doi.org/10.1016/j.msec.2016.03.084

33. Aly HM, Moustafa ME, Nassar MY, Abdelrahman EA (2015) Synthesis and characterization of novel Cu(II) complexes with 3-substituted-4-amino-5-mercapto-1,2,4-triazole Schiff bases: a new route to CuO nanoparticles. J Mol Struct 1086:223–231. https://doi.org/10.1016/j.molstruc.2015.01.017

34. Zolezzi S, Spodine E, Decinti A (2002) Electrochemical studies of copper(II) complexes with Schiff-base ligands. Polyhedron 21:55–59

35. Khorshidifard M, Amiri H, Askari B et al (2015) Cobalt(II), copper(II), zinc(II) and palladium(II) Schiff base complexes: synthesis, characterization and catalytic performance in selective oxidation of sulfides using hydrogen peroxide under solvent-free conditions. Polyhedron 95:1–13. https://doi.org/10.1016/j.poly.2015.03.041

36. El-Behery M, El-Twigry H (2007) Synthesis, magnetic, spectral, and antimicrobial studies of Cu(II), Ni(II), Co(II), Fe(III), and UO2(II) complexes of a new Schiff base hydrazone derived from 7-chloro-4-hydrazinoquinoline. Spectrochim Acta Part A 66:28–36. https://doi.org/10.1016/j.saa.2006.02.017

37. Xiao Y, Cao C (2020) Influence of substituents on the structure of Schiff bases Cu(II) complexes. J Mol Struct 1209:127916. https://doi.org/10.1016/j.molstruc.2020.127916

38. Ignatova M, Stoyanova N, Manolova N et al (2020) Electrospun materials from polylactide and Schiff base derivative of Jeffamine ED® and 8-hydroxyquinoline-2-carboxaldehyde and its complex with Cu2+: preparation, antioxidant and antitumor activities. Mater Sci Eng C 116:111185. https://doi.org/10.1016/j.msec.2020.111185

39. Cristóvão B, Osypiuk D, Miroslaw B, Bartyzel A (2018) Syntheses, crystal structures, thermal and magnetic properties of new heterotrinuclear CuII–LnIII–CuII complexes incorporating N2O4-donor Schiff base ligands. Polyhedron 144:225–233. https://doi.org/10.1016/j.poly.2018.01.023

40. Cristóvão B, Miroslaw B (2015) Tautomerism of a compartmental Schiff base ligand and characterization of a new heterometallic CuII-DyIII complex - synthesis, structure and magnetic properties. Inorg Chem Commun 52:64–68. https://doi.org/10.1016/j.inoche.2014.12.019

41. Lindner E, Umezawa Y (2008) Performance evaluation criteria for preparation and measurement of macro- and microfabricated ion-selective (IUPAC Technical Report). Pure Appl Chem 80:85–104. https://doi.org/10.1351/pac200880010085

42. Bakker E, Pretsch E, Bühlmann P (2000) Selectivity of potentiometric ion sensors. Anal Chem 72:1127–1133. https://doi.org/10.1021/ac991146n

D7

IONIC LIQUID-MULTIWALLED CARBON NANOTUBES NANOCOMPOSITE BASED ALL SOLID STATE ION-SELECTIVE ELECTRODE FOR THE DETERMINATION OF COPPER IN WATER SAMPLES

Article

Ionic Liquid-Multiwalled Carbon Nanotubes Nanocomposite Based All Solid State Ion-Selective Electrode for the Determination of Copper in Water Samples

Cecylia Wardak *, Karolina Pietrzak and Małgorzata Grabarczyk

Department of Analytical Chemistry, Institute of Chemical Sciences, Faculty of Chemistry,
Maria Curie-Sklodowska University, Maria Curie-Sklodowska Sq. 3, 20-031 Lublin, Poland;
karolina.pietrzak@poczta.umcs.lublin.pl (K.P.); malgorzata.grabarczyk@mail.umcs.pl (M.G.)
* Correspondence: cecylia.wardak@mail.umcs.pl

Abstract: A new copper sensitive all solid-state ion-selective electrode was prepared using multiwalled carbon nanotubes-ionic liquid (1-butyl-3-methylimidazolium hexafluorophosphate) nanocomposite as an additional membrane component. The effect of nanocomposite content in the membrane on the electrode parameters was investigated. The study compares, among others, detection limits, sensitivity, and the linearity ranges of calibration curves. Content 6 wt.% was considered optimal for obtaining an electrode with a Nernstian response of 29.8 mV/decade. An electrode with an optimal nanocomposite content in the membrane showed a lower limit of detection, a wider linear range and pH range, as well as better selectivity and potential stability compared to the unmodified electrode. It was successfully applied for copper determination in real water samples.

1. Introduction

Copper occurs naturally in metallic form, as well as in ores and minerals, and in the form of complexes and solid particles in various types of water: surface, drinking, ground and sea water [1,2]. Due to its many useful properties, which include: high stability, flexibility and electrical conductivity, both copper and its numerous alloys have many applications in households and industry (in electroplating and photography, microelectronics, or as catalysts) [1]. Copper is an important trace element necessary for the proper functioning of human and animal organisms, however, both the excess and deficiency of this element can cause adverse health effects [1].

Copper is, inter alia, a component of metalloenzymes in which it acts as an electron donor or acceptor in important redox reactions, including collagen cross-linking, melamine production or mitochondrial respiration. Its presence makes it possible to maintain homeostasis and the proper functioning of the body from the development and growth of the fetus. Copper plays an important role in the metabolism of iron and glucose, helps in the proper work of the brain and heart muscle. It takes part in the synthesis of neurotransmitters as well as in antioxidant and immunological processes [1,3,4]. Long-term exposure to overly high concentrations of copper can cause many health problems [5]. A high concentration of copper can lead to redox reactions of the Fenton type, and hence to oxidative damage to biological systems, and cell death [3]. Copper is indirectly associated with the occurrence of neurological disorders, including prion diseases or Alzheimer's disease [1]. People who consciously or unknowingly ingest increased doses of copper develop a number of symptoms including dizziness and nausea, headache and

str. 148

abdominal pain, diarrhea and vomiting, irritation of the eyes, nose and mouth. In such a situation, liver and kidney failure and, in severe cases, even death can occur [1,5].

The human body contains about 100 mg of copper, while the recommended daily intake of copper is about 2 mg, and a dose of 10–15 mg is considered toxic [2,3]. Copper enters the human body with food and drinking water [1]. Foods that are rich in copper include nuts, grains, legumes, potatoes and some fruits, as well as the liver of mammals, molluscs and crustaceans [1]. Depending on many factors, the copper content of drinking water may range from 0.005 to 30 mg L^{-1} [2]. The heavy metal content of the aquatic environment has increased in parallel with the rapid industrialization over the past 150 years. The average concentration of copper in uncontaminated river waters is 10 µg L^{-1} and in polluted waters it can reach 30–60 µg L^{-1}. In recreational reservoirs, concentrations of 1 mg L^{-1} and lower are used to suppress the growth of harmful algae. Taking into account both the beneficial and toxic effects of copper, its monitoring in the environment is very important. In water samples copper can be easy determined potentiometrically using a copper ion-selective electrode.

Potentiometry is one of the simpler analytical techniques using easy-to-use apparatus, and is also characterized by relatively low costs and speed of measurements [6,7]. Thanks to these advantages, potentiometry is used to determine more than 60 different analytes in many branches of science and industry (chemical and clinical analysis, environmental monitoring, process control, etc.) [7,8]. Potentiometric measurement consists of measuring the electromotive force of a cell working under near-zero current conditions consisting of a working electrode, which is an ion-selective electrode, and a reference electrode [8].

In the last decades, ion-selective electrodes with solid contact have gained great popularity, in which the liquid contact is replaced only by an additional thin layer of a substance characterized by ionic and electronic conductivity, placed between the electrode material and the membrane layer. This was made to improve the stability and reproducibility of the electrode potential, which deteriorated significantly when the ion-selective membrane was applied directly to the surface of the solid electrode, as was the case with coated wire electrodes, first proposed almost 50 years ago. By eliminating the internal solution, the electrodes were designed to be smaller in size, easier to handle and store than their predecessors, and to avoid the risk of solution evaporation or leakage [8]. Ion-selective electrodes with solid contacts are also characterized by an easier structure than their classic predecessors, with greater possibilities of shape modification and lower production costs. Moreover, these types of electrodes often allow for lower detection limits and can work in any position and under unfavorable conditions (e.g., high pressure), in which sensors of other types could be damaged [2,9].

In recent years, many electroactive substances have been used as solid contacts in ion-selective electrodes: conducting polymers (typically polypyrrole doped by chloride ions [10], ladder conjugated polymer-thieno[3,2-b]thiophene [11]), hydrogel [12], redox-active self-assembled monolayers [13], carbon nanomaterials (singlewalled carbon nanotubes (SWCNTs) and graphene [14], multiwalled carbon nanotubes (MWCNT) [15] colloid-imprinted mesoporous carbon [16], three-dimensionally ordered macroporous (3DOM) carbon [17], carbon black [18]), nanoparticles (gold [19] and platinum [20]). To achieve better properties of analytical sensors, scientists have also used combinations of several components used for this purpose (multiwalled carbon nanotubes and bimetallic nanoparticles AuCu [21]) or their modifications (gold nanoparticles functionalised with lipoic acid or lipoic amide [22] or octadecane modified MWCNT [23]).

In this work, a new all solid-state copper ion selective electrode based on multiwalled carbon nanotubes-ionic liquid nanocomposite is described. A nanocomposite was prepared using multiwalled carbon nanotubes and 1-butyl-3-methylimidazolium hexafluorophosphate (BMImPF₆). Both components play an important role in the electrode operation and contribute to the improvement of its analytical and electrical parameters. Multiwalled carbon nanotubes act as ion-to-electron transducer facilitating

the charge transfer between the membrane and the internal electrode [15,24]. As we have shown in previous works, ionic liquids can be successfully used as an ionic membrane component that reduces resistance and facilitates the transport of the main ion from the water phase to the membrane [25,26]. 1-butyl-3-methylimidazolium hexafluorophosphate (BMImPF$_6$) was successfully used as an extraction solvent for preconcentration of copper [27,28]. Therefore, we have decided to use this ionic liquid in the form of a nanocomposite with MWCNTs to prepare copper all solid-state ion-selective electrodes. The use of a nanocomposite combines the beneficial functions of both components and allows a homogeneous membrane to be obtained.

2. Materials and Methods

2.1. Reagents

N,N,N',N'-Tetracyclohexyl-2,2'-thiodiacetamide (copper(II) ionophore IV) and 2-nitrophenyl octyl ether (NPOE) were purchased from Fluka. Ionic liquid: 1-butyl-3-methylimidazolium hexafluorophosphate (BMImPF$_6$), multiwalled carbon nanotubes (MWCNTs) with 6–9 nm diameter, 5 µm length and poly(vinyl chloride) low molecular weight (PVC) were obtained from Sigma Aldrich. Copper nitrate (pure pro analysis), other nitrate salts used in the interference study and other reagents were purchased from Fluka. All aqueous solutions were prepared using freshly deionized water.

2.2. Preparation of Nanocomposite

MWCNTs- BMImPF$_6$ nanocomposite was obtained by mixing 100 mg of nanotubes with 500 mg of ionic liquid and thorough homogenization of the mixture in an ultrasonic bath for 1 h.

2.3. Preparation of the Electrode

Electrodes with different nanocomposite contents in the membrane from 0 to 8%, were made. The membranes contained, for electrode 1: 1% ionophore, 33% PVC, 66% NPOE; for electrode 2: 1% ionophore, 33% PVC, 64% NPOE, 2% nanocomposite; for electrode 3: 1% ionophore, 33% PVC, 62% NPOE, 4% nanocomposite; for electrode 4: 1% ionophore, 33% PVC, 60% NPOE, 6% nanocomposite; for electrode 5: 1% ionophore, 33% PVC, 58% NPOE, 8% nanocomposite. Membrane components were weighed in appropriate proportions into a glass vial, 1 mL THF per 0.1 g of the mixture was added and homogenized in an ultrasonic bath for 30 min, and then applied to the surface of the inner electrode. The mixture prepared in this way is visually homogeneous even after 1 month from preparation. In the case of adding nanotubes to the membrane cocktail, but without an ionic liquid, the sediment of the nanotubes is clearly visible at the bottom of the glass vial already 2 weeks after the preparation.

Glassy carbon disks with 3 mm diameters were used as the internal electrode. Before covering them with a membrane mixture, they were thoroughly polished with Al$_2$O$_3$ powder, rinsed with water in an ultrasonic bath and additionally immersed in THF and dried in the air. Next, the membrane was deposited on the electrode surface by drop casting 3 times 30 µL of membrane mixture dispersed in THF and left to dry for 24 h. Th next day, the electrode was immersed in 1×10^{-3} mol L^{-1} Cu(NO$_3$)$_2$ solution for at least 24 h. The electrode was also stored in such a solution between measurements.

For comparison purposes, a classical electrode with an internal filling solution was prepared and labeled as electrode 1*. The membrane of this electrode had the same composition as in electrode 1 without the nanocomposite (1% ionophore, 33% PVC, 66% NPOE). It was prepared exactly according to the procedure described previously [29]. A piece of the membrane in the shape of a circle with a diameter of 5 mm was mounted in a Philips IS 561 electrode body, which was then filled with an internal solution 1×10^{-3} mol L^{-1} Cu(NO$_3$)$_2$. Between measurements this electrode was stored in the same solution.

2.4. The Measurement of the Electromotive Force

The EMF measurements were performed in the system copper ion-selective electrode as the indicating electrode and a silver-chloride electrode (Metrohm 6.0750.100) as the reference electrode. All measurements were made at room temperature in mixed solutions using a 16-channel data acquisition system (Lawson Labs. Inc., Malvern, PA, USA) coupled with a computer. An Orion 81–72 glass electrode connected to a multifunction computer meter CX-741 (Zabrze-Mikulczyce, Poland) was used for pH measurements.

2.5. Electrochemical Impedance Spectroscopy Measurements

Electrochemical impedance spectroscopy (EIS) measurements were performed in 1×10^{-2} mol L^{-1} Cu(NO$_3$)$_2$ solution using an AUTOLAB electrochemical analyzer (Eco Chemie, Netherlands) controlled by NOVA software. For this purpose, a conventional three-electrode system was used, in which the working electrode was the tested ion-selective electrode, the auxiliary electrode was a platinum wire, and the reference electrode was an Ag/AgCl silver chloride electrode (3 mol L^{-1} KCl). The impedance spectra were recorded in the frequency range 0.1–100 kHz and at open circuit potential using an AC-amplitude of 10 mV.

3. Results and Discussion

Both ionic liquids and MWCNTs exhibited hydrophobic and electrically conductive properties. These features make them good candidates for the modification of polymer ion selective electrode membranes to improve their electrical and mechanical properties. As we have shown in our previous research on cadmium solid contact ISEs [30], IL and MWCNTs show synergistic properties, which means that an electrode with a membrane containing both of these components shows better performance compared to electrodes whose membranes were modified only with an ionic liquid or only with carbon nanotubes. A similar effect was reported in relation to other electrochemical sensors [31].

It is known that imidazolium based ionic liquid, due to presence of cation-π, interacts with the π electronic surface of the MWCNTs [32]. Due to this, MWCNTs are surrounded by an ionic liquid layer which provides both steric and electrostatic stabilization, and a homogenous composite material is formed. Therefore the MWCNTs-IL nanocomposite can be effectively dispersed in the membrane cocktail without the use of additional dispersing agents.

3.1. Potential Response

The effect of membrane modification by the addition of MWCNTs-IL nanocomposite was assessed first by determining the electrode response in Cu(NO$_3$)$_2$ solutions at concentrations ranging from 1×10^{-6} to 1×10^{-2} mol L^{-1}. The obtained calibration curves are shown in Figure 1 where it can be seen that electrodes with unmodified membranes showed a similar response regardless of the kind of contact. The classic electrode 1* was characterized by a slightly higher characteristic slope of 27.5 mV/decade compared to electrode 1 with the same membrane but without internal solution, the slope of which was 26.7 mV/decade. On the other hand, electrode 1 showed a slightly lower detection limit of 4.4 $\times 10^{-7}$ mol L^{-1} compared to the classic electrode 1* (5.5 $\times 10^{-7}$ mol L^{-1}). This effect is well known for electrodes without an internal solution. The improvement in the detection limit is achieved due to the elimination of transmembrane ion fluxes [33].
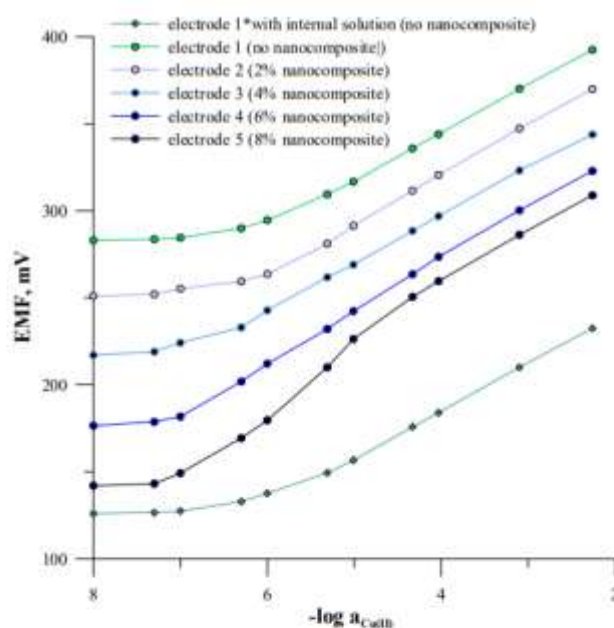
Figure 1. Calibration curves of studied electrodes.

The modified electrodes were characterized by a wider measuring range and lower detection limit compared to unmodified electrode 1 and classical electrode 1* with internal solution. A gradual improvement in the electrode response can be seen as the nanocomposite content in the membrane increases. The electrode exhibiting the best response was electrode 4 which contained 6% nanocomposite in the membrane. The calibration curve of this electrode had a linear course over the widest concentration range of 1×10^{-7}–1×10^{-2} mol L^{-1} with a slope of 29.8 mV/decade. This electrode was characterized by the lowest limit of detection 3.3×10^{-8} mol L^{-1}. Electrodes with lower composite content exhibited higher detection limits of 3.7×10^{-7} mol L^{-1} (electrode 2) and 1.0×10^{-7} mol L^{-1} (electrode 3). The range of linear response of these electrodes was also shorter compared to electrode 4 and the slope was close to the Nernstian one, at 28.3 mV/decade and 28.8 mV/decade for electrodes 2 and 3, respectively. Electrode 5, with the highest nanocomposite content (8%), tended to have a super Nernstian response at lower concentrations, and the linear range of the calibration curve was shortened. As a result, the detection limit of this electrode deteriorated to 6.6×10^{-6} mol L^{-1}.

Differences in the properties of the electrodes are due to differences in the composition of the membrane. The enrichment of the membrane with nanocomposite lowers its resistance and increases its lipophilic character. As the nanocomposite content in the membrane increases, its extraction capacity increases and the transport of Cu ions from the water phase to the membrane phase is more efficient.

The improvement in the electrode response is clearly revealed in the dynamic response, an example of which for electrodes 1 and 4 is shown in Figure 2. There is an evident difference in the potential stability and range of linearity for the modified electrode.

Taking into account the analytical parameters of the electrodes, such as the linear range of calibration curve, the slope of the characteristic and the limit of detection, electrode 4 was chosen for further studies. In parallel, an unmodified electrode 1 was also tested for comparison.
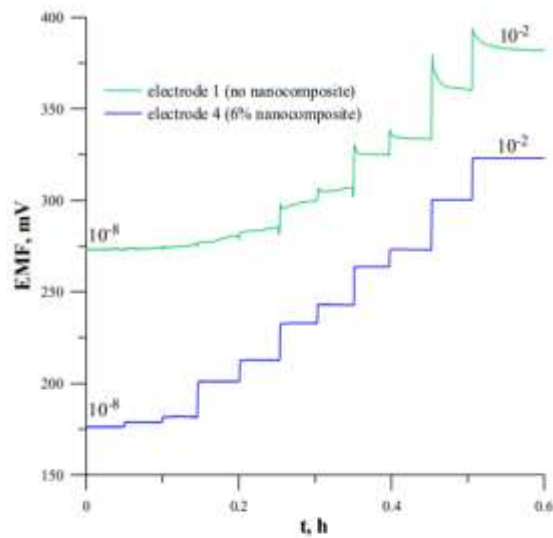
str. 152

Figure 2. Potentiometric dynamic response for tested unmodified electrode 1 and electrode 4.

3.2. Potential Stability and Reversibility

The fully conditioned electrodes were tested to evaluate parameters such as the stability and reversibility of the potential. These parameters are important in terms of the practical application of the electrodes and have a significant influence on the accuracy of determinations and analysis time. Short term potential stability was observed during 3 h measurement in the 0.01 mol L^{-1} Cu(NO$_3$)$_2$ solution. On the basis of total potential change, the potential drift of studied electrodes was calculated from dependence $\Delta E/\Delta t$. As expected, after the introduction of the MWCNTs-IL nanocomposite into the membrane phase, the stability of the electrode potential was significantly improved (Figure 3). The potential drift determined for electrode 4 (0.046 mV/min) was much smaller than the potential drift of electrode 1 (0.16 mV/min) without membrane modification.
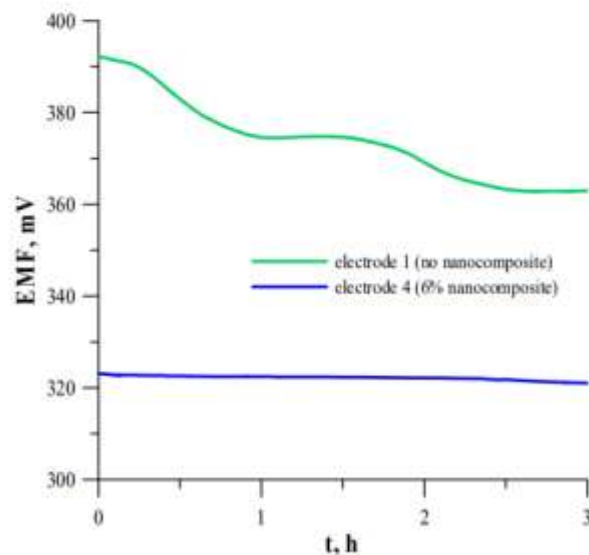

Figure 3. Comparison of potential stability of nanocomposite-based electrode 4 and unmodified electrode 1.

str. 153

The improved potential stability also results in a better potential reversibility. This parameter was studied by potential measurements repetitively in $Cu(NO_3)_2$ solutions with the concentrations: 1×10^{-5} and 1×10^{-4} mol L^{-1}. Time-dependent potential traces during this experiment for modified electrode 4 and unmodified electrode 1 are shown in Figure 4 where it can be seen that the potential of the modified electrode was fully reversible in contrast to the unmodified one.
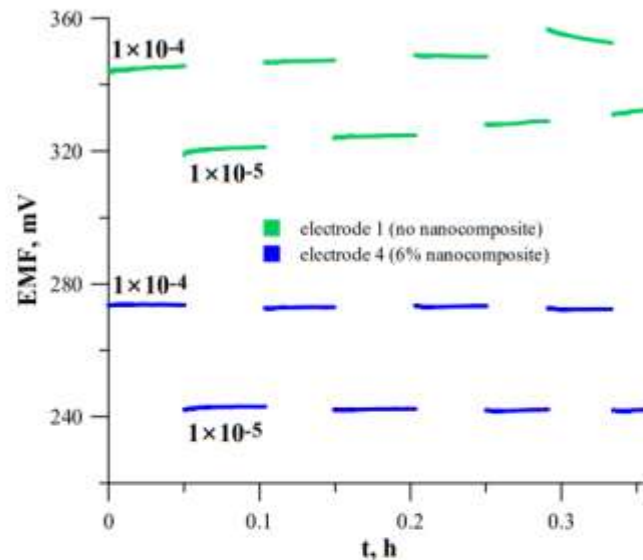

Figure 4. Potential reversibility determined in 1×10^{-4} and 1×10^{-5} mol L^{-1} $Cu(NO_3)_2$ solution.

3.3. Dependence of Electrode Potential on pH

The influence of the pH on the response of the studied electrode was investigated using 1×10^{-4} mol L^{-1} $Cu(NO_3)_2$ solution over the pH range 2.0–8.0. The pH was adjusted using HNO_3 or NaOH solutions as additives and the working pH range was determined as where the potential of the electrode was nearly constant (± 2 mV) (Figure 5). Based on this analysis, the working pH range was 5.0–6.0 and 2.5–6.0 for electrode 1 and electrode 4, respectively. In both cases, a gradual decrease in the potential at higher pH values was detected. It can be attributed to the formation of some hydroxy complexes of Cu^{2+} in solution. The pH ranges of the studied electrodes differ within acidic solutions. In this region, the change in potential is due to the interfering influence of hydrogen ions. In the case of the modified electrode, this effect is significantly reduced due to the presence of an ionic liquid in the membrane. As a result, the potential of the modified electrode does not depend on the pH in the broader range 2.5–6.0.
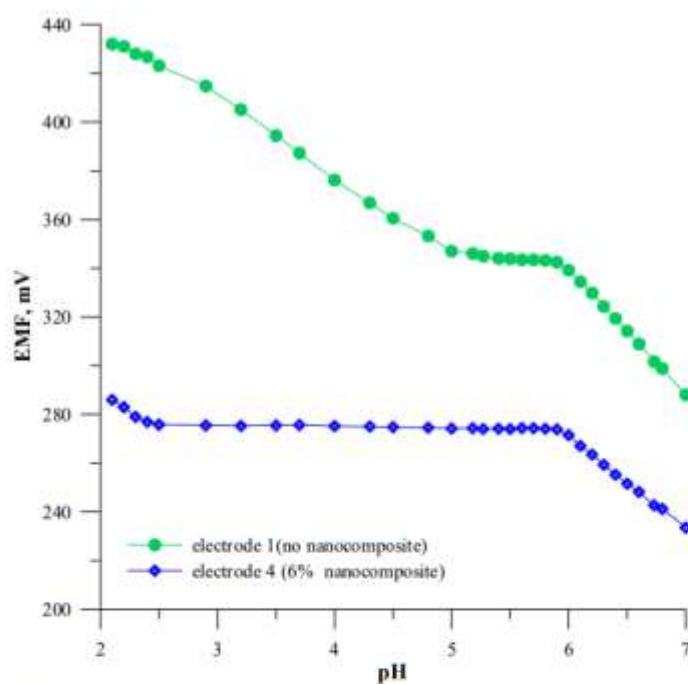
Figure 5. Dependence of electrode potential on pH.

3.4. Redox Sensitivity

Since the presence of electron conducting nanomaterial in the membrane may induce a redox response in the ion-selective electrode, the redox sensitivity test was performed. Measurements of the electrode potential in samples with different redox potential were performed in solutions containing a pair of redox ions Fe^{2+} and Fe^{3+} ($FeSO_4$ and $Fe_2(SO_4)_2$) in the constant ionic background of 10^{-3} mol L^{-1} $Cu(NO_3)_2$ ($logFe^{2+}/Fe^{3+}$ ratio: -1; -0.7; 0; 0.7 and 1) (Figure 6). The potential of the electrodes did not change much despite the change in solutions, so it was found that they are not sensitive to this type of environmental changes.
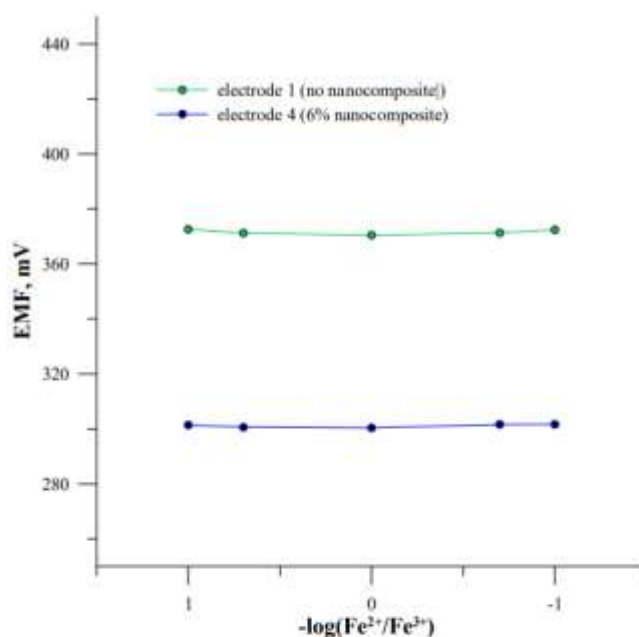
Figure 6. Redox sensitivity test for electrode 1 and modified electrode 4.

3.5. Influence of the Presence of Gases

Due to the willingness to use the described electrodes for testing environmental samples, it was considered important to check whether the presence of gases in water samples will affect the effectiveness and quality of copper ions determinations. For this purpose, the electrode potential was measured in a main ion solution of 10^{-3} mol L^{-1} previously left at room temperature in order to saturate CO_2 and O_2 from the air for half an hour. N_2 was then passed through the solution to get rid of CO_2 and O_2, and the electrode potential was measured again for half an hour. The obtained relation is shown in Figure 7. The potential value was almost constant for the modified electrode, therefore it can be concluded that the presence of gases in the sample does not affect the operation of the proposed electrode. In the case of unmodified electrode 1, potential drift was observed both in the presence and absence of CO_2 and O_2 in the solution. This was probably due to a water layer forming between the inner electrode surface and the membrane, which was confirmed by a water layer test.
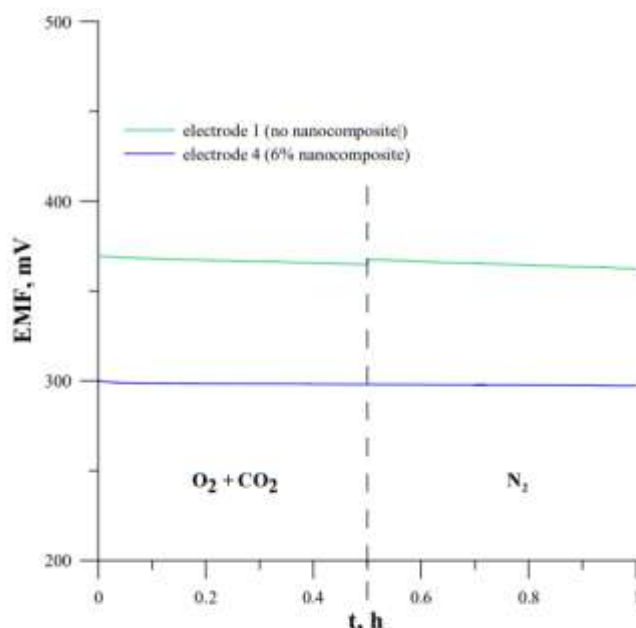
Figure 7. Influence of the presence of gases on the potential of the electrodes.

3.6. Water Layer Test

In order for ion-selective electrodes to function properly, they should meet a number of requirements. For ion-selective electrodes with solid contact, in addition to the basic parameters, such as a wide range of linearity, low detection limits and very good selectivity of sensors, resistance to changes in external conditions is also very important (e.g., the previously described sensitivity to changes in pH and redox potential of solutions and the presence of gases in samples) and to maintain the appropriate stability and reversibility of the sensors' potential. It has been confirmed that a thin water layer may form between the solid contact material and the ion selective membrane, the presence of which is undesirable, mainly due to the electrode potential changes it can cause [34]. A water layer test was performed following the procedure described by Pretch et al. [35]. The electrodes were immersed in a solution of $Cu(NO_3)_2$ with a concentration of 1×10^{-2} mol L^{-1} for 24 h. They were then transferred to a solution containing the salt of the interfering ion $(Zn(NO_3)_2)$ at the same concentration for about 3 h, and after this time were returned to the main ion solution again. Figure 8 shows the water layer test for electrode 4 with 6% nanocomposite in the membrane and for the unmodified electrode 1. In the potential time-traces recorded for the nanocomposite-based electrode, no essential potential drift was observed after replacing the main ion solution to the interfering ion solution and after the reverse change. In the case of an unmodified electrode, a significant positive potential drift was observed first, followed by a negative one. Such results give us information that the modified electrode was resistant to the formation of a water layer. It was achieved by the presence in the membrane a highly lipophilic MWCNTs-BMImPF$_6$ nanocomposite.
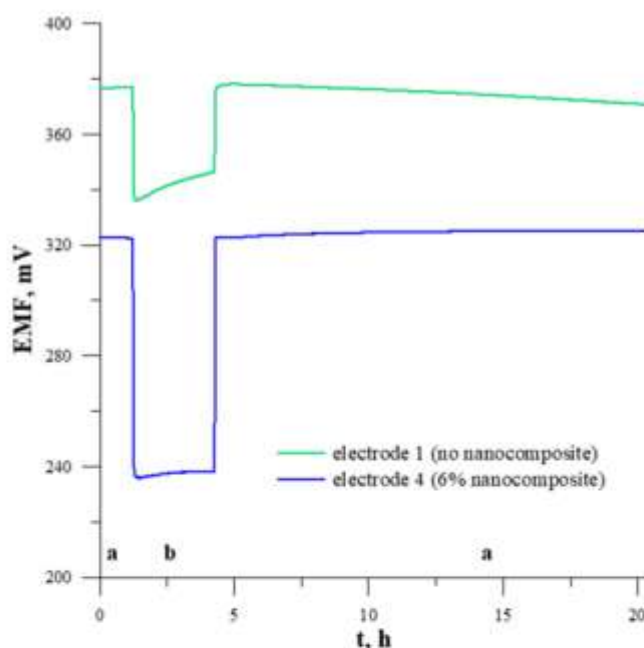
Figure 8. Water layer test of electrode 1 and 4 determined in 1×10^{-2} mol L^{-1} Cu(NO$_3$)$_2$ (a) and 1×10^{-2} mol L^{-1} Zn(NO$_3$)$_2$ (b).

3.7. Selectivity

One of the most important parameters of ion-selective electrodes is their selectivity, the numerical measure of which are the selectivity coefficients. The selectivity coefficient values were determined by the separate solution method (by extrapolating the response functions to $a_i = a_j = 1$ mol L^{-1}) [36]. A comparison of selectivity coefficients obtained for nanocomposite-based electrode 4 and unmodified electrode 1 is presented in Figure 9, where it can be seen that the addition of MWCNTs-BMImPF$_6$ nanocomposite to the membrane phase caused a noticeable improvement in the electrode selectivity. The obtained electrode was very selective to copper over all interfering ions (log $K^{pot}_{Cu/M} \leq -3$) except lead, which was the most interfering ion (log$K^{pot}_{Cu/Pb} \leq -2.1$). This was not overly surprising because lead is a well-known interferent in the case of copper selective electrodes [37,38]. The improvement of the selectivity of the nanocomposite-based electrode can be explained by the fact that the addition of the nanocomposite increases the ionic strength of the membrane and thus facilitates the selective transport of the main ion to the membrane phase.
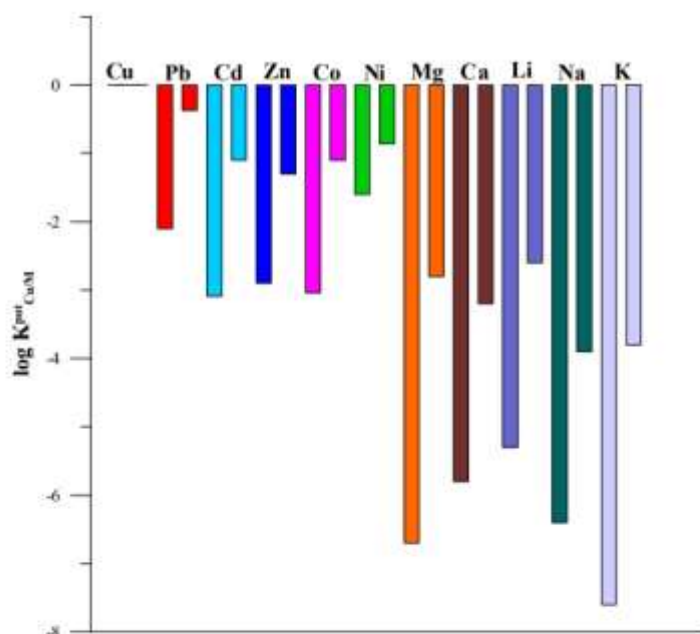
Figure 9. Comparison of selectivity coefficients of nanocomposite-based electrode 4 (1st column) and unmodified electrode 1 (2nd column).

3.8. Life Time and Long Term Potential Stability

The lifetime of the modified electrode was studied by its periodic recalibration in the Cu^{2+} copper nitrate solutions. The measurements were made 3 times a week during a period of 3 months. No significant change in the performance of the electrode was observed. Figure 10 presents the calibration curves of electrode 4 determined 1, 5 and 12 weeks after preparation. Three-month-old electrodes still worked correctly, showing a slight increase in the detection limit to the value of 5.1×10^{-8} mol L^{-1} and a small decrease in the slope of the characteristic to the value 28.6 mV/decade. It is worth noting that the modified electrode was characterized by very good long term potential stability. The mean E^0 value determined from 36 calibrations performed during the lifetime test was 393.2 ± 6.3 mV. Such a small change in the E^0 potential is a valuable feature of the electrode as it allows for its long-term use without the need for frequent recalibration.
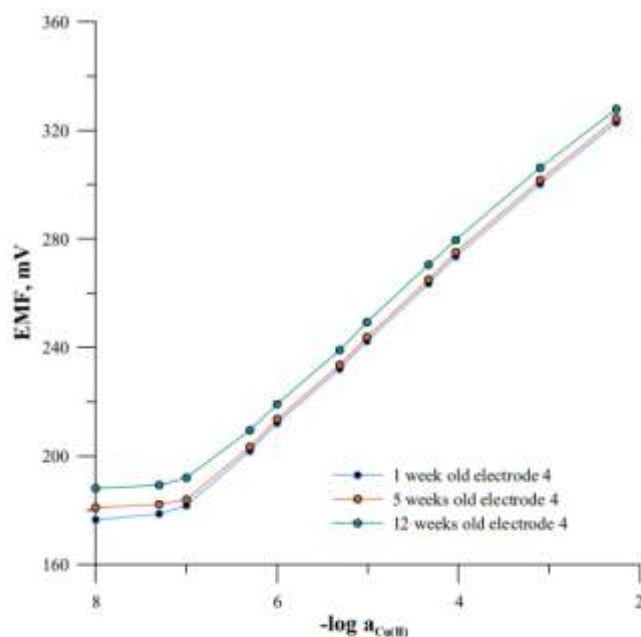
Figure 10. Change of calibration curve course in time determined for electrode 4.

3.9. Electrochemical Impedance Spectroscopy

In order to study the effect of membrane modification on the electric properties of electrodes, an impedance study was carried out for fully conditioned electrodes two weeks after preparation. The obtained impedance spectra for modified electrode 4 and unmodified electrode 1 are shown in Figure 11. As it can be seen in this figure, both obtained impedance spectra showed a high-frequency semicircle connected to the bulk resistance (R_b) of the ion-selective membrane and its geometric capacitance (C_g) [39]. However, the diameter of the semicircles, which is a measure of membrane resistance, varies dramatically. The bulk membrane resistance (R_b) determined from high frequency semicircle decreased almost ten times (from 309 to 0.36 kΩ) after modification of the membrane by MWCNTs-IL nanocomposite.
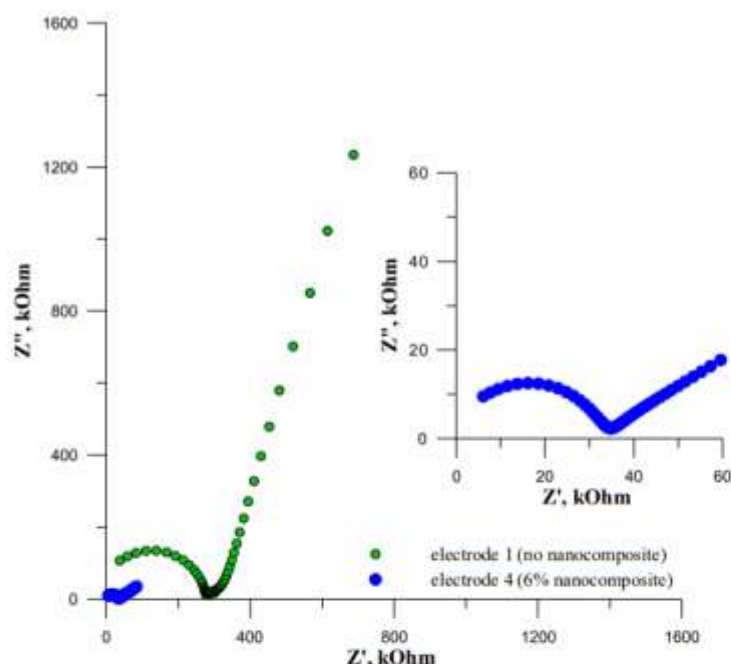
Figure 11. Impedance spectra of electrode 4 based on MWCNTs-BMImPF₆ nanocomposite and un-modified electrode 1 determined in 1×10^{-2} mol L^{-1} Cu(NO₃)₂ solution. Frequency range 0.1–100 kHz, amplitude 10 mV.

The second section of the impedance spectra determined for low frequencies is connected with the double layer capacitance in parallel with a charge-transfer resistance at the interface between the inner electrode and the ion-selective membrane [40]. The low-frequency branch in the impedance spectrum of the modified electrode was much smaller than that obtained for the unmodified one. The low-frequency capacitance was calculated from the low frequency limit using the following expression $C_{lf} = 1/(2\pi f Z'')$ [41], where f = 0.1 Hz was 45.7 μF for electrode 4 and 1.29 μF for electrode 1. These results indicate the largest capacitance and faster diffusion processes in electrode 4 containing MWCNTs-IL nanocomposite in the membrane. The reduction in the membrane resistance and the facilitated charge transfer at the interface contribute to the improvement of the analytical parameters of the electrode, especially the improvement of the stability and the reversibility of the potential.

3.10. Analytical Application

The usefulness of the proposed electrode 4 in the analysis of real samples was assessed by measuring the content of copper in certified reference material SPS-WW1 Batch 111 Waste Water. This sample was analyzed without any pretreatment directly in the form in which it had been purchased after two times dilution and addition of 0.1 mol L^{-1} NaOH to neutralize HNO₃ to reach a stable pH of 4.5. The obtained results from five measurements (*n* = 5) showed that the certified value (400 ± 2 μg L^{-1}) and the value obtained by the proposed electrode (412 ± 14 μg L^{-1}) were in good agreement. Furthermore, the electrode was used for the determination of copper in river water samples. River water was collected from local river, Czerniejówka. Water samples were acidified with HNO₃ to reach a stable pH of 4.5. Samples were spiked with Cu(II) ions to obtain final concentrations of 3×10^{-7}, 5×10^{-7} and 1×10^{-6} mol L^{-1}, in order to recover measurements. The data obtained for the samples and the corresponding spiked ones are summarized in Table 1. As it can be seen, the results of the determination of copper in all cases correspond to each other

well, which confirms the possibility of employing the proposed all solid-state electrode for the monitoring of copper in water samples.

Table 1. Results of copper determination in river water samples using proposed copper electrode 4.

Sample	Added Copper, µg L^{-1}	Found Copper by ISE, µg L^{-1} [a]	Recovery,%
	unspiked	13.6 ± 0.6	-
River water	19.2	33.1 ± 1.1	101.5
	32	44.8 ± 2.7	97.7
	64	78.1 ± 3.1	100.7

[a] standard deviations are based on six measurements.

4. Conclusions

As a result of the research, a new all solid-state copper ion-selective electrode was obtained, simple both in design and operation. The electrode obtained as a result of the membrane modification by MWCNTs-IL nanocomposite shows better selectivity than the electrode with an unmodified membrane, with a detection limit an order of magnitude lower, and a wider measuring range. Moreover, its potential is not dependent on pH over a much wider pH range. The addition of a nanocomposite to the ion-sensitive membrane also caused a noticeable reduction in the membrane resistance and an increase in capacity, which results in better potential stability.

References

1. Stern, B.R.; Solioz, M.; Krewski, D.; Aggett, P.; Aw, T.-C.; Baker, S.; Crump, K.; Dourson, M.; Haber, L.; Hertzberg, R.; et al. Copper and human health: Biochemistry, genetics, and strategies for modeling dose-response relationships. *J. Toxicol. Environ. Health Part B* **2007**, *10*, 157–222, doi:10.1080/10937400600755911.
2. Wardak, C.; Grabarczyk, M. Analytical application of solid contact ion-selective electrodes for determination of copper and nitrate in various food products and drinking water. *J. Environ. Sci. Health Part B* **2016**, *51*, 519–524, doi:10.1080/03601234.2016.1170545.
3. Bost, M.; Houdart, S.; Oberli, M.; Kalonji, E.; Huneau, J.-F.; Margaritis, I. Dietary copper and human health: Current evidence and unresolved issues. *J. Trace Elements Med. Biol.* **2016**, *35*, 107–115, doi:10.1016/j.jtemb.2016.02.006.
4. Kaplan, J.H.; Maryon, E.B. How mammalian cells acquire copper: An essential but potentially toxic metal. *Biophys. J.* **2016**, *110*, 7–13, doi:10.1016/j.bpj.2015.11.025.
5. Gupta, V.K.; Ganjali, M.R.; Norouzi, P.; Khani, H.; Nayak, A.; Agarwal, S. Electrochemical analysis of some toxic metals by ion-selective electrodes. *Crit. Rev. Anal. Chem.* **2011**, *41*, 282–313, doi:10.1080/10408347.2011.589773.
6. Huang, M.-R.; Gu, G.-L.; Ding, Y.-B.; Fu, X.-T.; Li, R.-G. Advanced solid-contact ion selective electrode based on electrically conducting polymers. *Chin. J. Anal. Chem.* **2012**, *40*, 1454–1460, doi:10.1016/s1872-2040(11)60572-0.
7. Bieg, C.; Fuchsberger, K.; Stelzle, M. Introduction to polymer-based solid-contact ion-selective electrodes—basic concepts, practical considerations, and current research topics. *Anal. Bioanal. Chem.* **2017**, *409*, 45–61, doi:10.1007/s00216-016-9945-6.
8. Hu, J.; Stein, A.; Bühlmann, P. Rational design of all-solid-state ion-selective electrodes and reference electrodes. *TrAC Trends Anal. Chem.* **2016**, *76*, 102–114, doi:10.1016/j.trac.2015.11.004.
9. Tutulea-Anastasiu, M.D.; Wilson, D.; Del Valle, M.; Schreiner, C.M.; Crețescu, I. A solid-contact ion selective electrode for copper(ii) using a succinimide derivative as ionophore. *Sensors* **2013**, *13*, 4367–4377, doi:10.3390/s130404367.
10. Kisiel, A.; Michalska, A.; Maksymiuk, K. Rectifying effect for ion-selective electrodes with conducting polymer solid contact. *Synth. Met.* **2018**, *246*, 246–253, doi:10.1016/j.synthmet.2018.10.019.

11. Yu, S.-Y.; Li, Y.-C.; Xiong, T.; Yuan, Q.; Liu, Y.-M.; Yuan, Z.-Y.; Xiao, Y. A ladder conjugated polymer transducer for solid-contact Cu^{2+}-selective electrodes. *Chin. Chem. Lett.* **2013**, *25*, 364–366, doi:10.1016/j.cclet.2013.11.015.

12. Gyurcsányi, R.E. Microfabricated ISEs: Critical comparison of inherently conducting polymer and hydrogel based inner contacts. *Talanta* **2004**, *63*, 89–99, doi:10.1016/j.talanta.2003.12.002.

13. Fibbioli, M.; Enger, O.; Diederich, F.; Pretsch, E.; Bandyopadhyay, K.; Liu, S.-G.; Echegoyen, L.; Bühlmann, P. Redox-active self-assembled monolayers as novel solid contacts for ion-selective electrodes. *Chem. Commun.* **2000**, 339–340, doi:10.1039/a909532b.

14. Liang, R.; Yin, T.; Qin, W. A simple approach for fabricating solid-contact ion-selective electrodes using nanomaterials as transducers. *Anal. Chim. Acta* **2015**, *853*, 291–296, doi:10.1016/j.aca.2014.10.033.

15. Parra, E.J.; Crespo, G.A.; Riu, J.; Ruiz, A.; Rius, F.X. Ion-selective electrodes using multi-walled carbon nanotubes as ion-to-electron transducers for the detection of perchlorate. *Analyst* **2009**, *134*, 1905–1910, doi:10.1039/b908224g.

16. Hu, J.; Zou, X.U.; Stein, A.; Bühlmann, P. Ion-selective electrodes with colloid-imprinted mesoporous carbon as solid contact. *Anal. Chem.* **2014**, *86*, 7111–7118, doi:10.1021/ac501633r.

17. Lai, C.-Z.; Joyer, M.M.; Fierke, M.A.; Petkovich, N.D.; Stein, A.; Bühlmann, P. Subnanomolar detection limit application of ion-selective electrodes with three-dimensionally ordered macroporous (3DOM) carbon solid contacts. *J. Solid State Electrochem.* **2009**, *13*, 123–128, doi:10.1007/s10008-008-0579-2.

18. Paczosa-Bator, B. All-solid-state selective electrodes using carbon black. *Talanta* **2012**, *93*, 424–427, doi:10.1016/j.talanta.2012.02.013.

19. Jaworska, E.; Wójcik, M.; Kisiel, A.; Mieczkowski, J.; Michalska, A. Gold nanoparticles solid contact for ion-selective electrodes of highly stable potential readings. *Talanta* **2011**, *85*, 1986–1989, doi:10.1016/j.talanta.2011.07.049.

20. Paczosa-Bator, B.; Piech, R.; Cabaj, L.; Skupień, K. Platinum nanoparticles intermediate layer in solid-state selective elec-trodes. *Analyst* **2012**, *137*, 5272–5277.

21. Liu, Y.; Liu, Y.; Yan, R.; Gao, Y.; Wang, P. Electrochimica acta bimetallic AuCu nanoparticles coupled with multi-walled carbon nanotubes as ion-to-electron transducers in solid-contact potentiometric sensors. *Electrochim. Acta* **2020**, *331*, 135370.

22. Matzeu, G.; Zuliani, C.; Diamond, D. Electrochimica acta solid-contact ion-selective electrodes (ISEs) based on ligand function-alised gold nanoparticles. *Electrochim. Acta* **2015**, *159*, 158–165.

23. Papp, S.; Kozma, J.; Lindfors, T.; Gyurcsányi, R.E. Lipophilic multi-walled carbon nanotube-based solid contact potassium ion-selective electrodes with reproducible standard potentials. A comparative study. *Electroanalysis* **2020**, *32*, 867–873, doi:10.1002/elan.202000045.

24. Jaworska, E.; Maksymiuk, K.; Michalska, A. Optimizing carbon nanotubes dispersing agents from the point of view of ion-selective membrane based sensors performance — introducing carboxymethylcellulose as dispersing agent for carbon nanotubes based solid contacts. *Electroanalysis* **2015**, *28*, 947–953, doi:10.1002/elan.201500609.

25. Wardak, C. Ionic liquids as new lipophilic additives to the membrane of lead ion-selective electrodes with solid contact. *Int. J. Environ. Anal. Chem.* **2009**, *89*, 735–748, doi:10.1080/03067310902887642.

26. Wardak, C.; Lenik, J. Application of ionic liquid to the construction of Cu (II) ion-selective electrode with solid contact. *Sens. Actuators B Chem.* **2013**, *189*, 52–59.

27. Huang, H.-L. Extraction of copper species from the nanoporous sorbent with an ionic liquid. *J. Mol. Liq.* **2017**, *230*, 24–27, doi:10.1016/j.molliq.2016.12.112.

28. Arain, S.A.; Kazi, T.G.; Afridi, H.I.; Arain, M.S.; Panhwar, A.H.; Khan, N.; Baig, J.A.; Shah, F. A new dispersive liquid-liquid microextraction using ionic liquid based microemulsion coupled with cloud point extraction for determination of copper in serum and water samples. *Ecotoxicol. Environ. Saf.* **2016**, *126*, 186–192, doi:10.1016/j.ecoenv.2015.12.035.

29. Wardak, C. A Comparative study of cadmium ion-selective electrodes with solid and liquid inner contact. *Electroanalysis* **2012**, *24*, 85–90, doi:10.1002/elan.201100362.

30. Wardak, C. Solid contact cadmium ion-selective electrode based on ionic liquid and carbon nanotubes. *Sens. Actuators B Chem.* **2015**, *209*, 131–137, doi:10.1016/j.snb.2014.11.107.

31. Zhao, Y.; Gao, Y.; Zhan, D.; Liu, H.; Zhao, Q.; Kou, Y.; Shao, Y.; Li, M.; Zhuang, Q.; Zhu, Z. Selective detection of dopamine in the presence of ascorbic acid and uric acid by a carbon nanotubes-ionic liquid gel modified electrode. *Talanta* **2005**, *66*, 51–57, doi:10.1016/j.talanta.2004.09.019.

32. Fukushima, T.; Aida, T. Ionic liquids for soft functional materials with carbon nanotubes. *Chem. A Eur. J.* **2007**, *13*, 5048–5058, doi:10.1002/chem.200700554.

33. Sutter, J.; Lindner, E.; Gyurcsányi, R.E.; Pretsch, E. A polypyrrole-based solid-contact Pb^{2+}-selective PVC-membrane electrode with a nanomolar detection limit. *Anal. Bioanal. Chem.* **2004**, *380*, 7–14, doi:10.1007/s00216-004-2737-4.

34. Lindner, E.; Gyurcsányi, R.E. Quality control criteria for solid-contact, solvent polymeric membrane ion-selective electrodes. *J. Solid State Electrochem.* **2009**, *13*, 51–68, doi:10.1007/s10008-008-0608-1.

35. Fibbioli, M.; Morf, W.E.; Badertscher, M.; De Rooij, N.F.; Pretsch, E. Potential drifts of solid-contacted ion-selective electrodes due to zero-current ion fluxes through the sensor membrane. *Electroanalysis* **2000**, *12*, 1286–1292, doi:10.1002/1521-4109(200011)12:163.0.CO;2-Q.

36. Bakker, E.; Pretsch, E.; Bühlmann, P. Selectivity of potentiometric ion sensors. *Anal. Chem.* **2000**, *72*, 1127–1133, doi:10.1021/ac991146n.

37. Szigeti, Z.; Bitter, I.; Tóth, K.; Latkoczy, C.; Fliegel, D.J.; Günther, D.; Pretsch, E. A novel polymeric membrane electrode for the potentiometric analysis of Cu^{2+} in drinking water. *Anal. Chim. Acta* **2005**, *532*, 129–136, doi:10.1016/j.aca.2004.10.061.

38. Ghaedi, M.; Montazerozohori, M.; Sahraei, R. Comparison of the influence of nanomaterials on response properties of copper selective electrodes. *J. Ind. Eng. Chem.* **2013**, *19*, 1356–1364, doi:10.1016/j.jiec.2012.12.040.
39. Horvai, G.; Graf, E.; Toth, K.; Pungor, E.; Buck, R.P. Plasticized poly(vinyl chloride) properties and characteristics of valinomycin electrodes. 1. High-frequency resistances and dielectric properties. *Anal. Chem.* **1986**, *58*, 2735–2740, doi:10.1021/ac00126a034.
40. Bobacka, J.; Lewenstam, A.; Ivaska, A. Electrochemical impedance spectroscopy of oxidized poly(3,4-ethylenedioxythiophene) film electrodes in aqueous solutions. *J. Electroanal. Chem.* **2000**, *489*, 17–27, doi:10.1016/s0022-0728(00)00206-0.
41. Mousavi, Z.; Teter, A.; Lewenstam, A.; Maj-Zurawska, M.; Ivaska, A.; Bobacka, J. Comparison of multi-walled carbon nanotubes and poly(3-octylthiophene) as ion-to-electron transducers in all-solid-state potassium ion-selective electrodes. *Electroanalysis* **2011**, *23*, 1352–1358, doi:10.1002/elan.201000747.

D8

METAL OXIDE NANOPARTICLES AS SOLID CONTACT IN ION-SELECTIVE ELECTRODES SENSITIVE TO POTASSIUM IONS

Metal oxide nanoparticles as solid contact in ion-selective electrodes sensitive to potassium ions

Karolina Pietrzak[a], Nikša Krstulović[b], Damjan Blažeka[b], Julio Car[b], Szymon Malinowski[c], Cecylia Wardak[a,*]

[a] Department of Analytical Chemistry, Institute of Chemical Sciences, Faculty of Chemistry, Maria Curie-Skłodowska University, Maria Curie-Skłodowska Sq. 3, 20-031, Lublin, Poland
[b] Institute of Physics, Bijenička cesta 46, 10 000, Zagreb, Croatia
[c] Faculty of Civil Engineering and Architecture, Lublin University of Technology, Nadbystrzycka 40, 20-618, Lublin, Poland

ARTICLE INFO

ABSTRACT

In recent years, various types of nanomaterials and nanoparticles have been very popular, also in analytical chemistry for sensors preparation. Ion-selective electrodes with solid contact were constructed, in which a layer of nanoparticles of selected metal oxides (zinc, copper and iron oxides) obtained by pulsed laser liquid ablation (PLAL) was placed between the glassy carbon solid electrode material and the ion-selective membrane. The basic analytical parameters of the obtained sensors were determined using potentiometric methods. Additionally, the electrochemical impedance spectroscopy method (EIS) was also used to investigate the electrical properties of the sensors. The obtained results were compared for all types of electrodes, both modified and unmodified, in order to investigate the effect of the type of nanoparticles and the thickness of their layer used as solid contact. It was found that the addition of metal oxide nanoparticles improved the analytical parameters of the sensors, mainly the potential stability and electrical parameters. The best results were obtained for an electrode with an intermediate layer of zinc oxide nanoparticles. In this case, a slope of -56.07 mV/dec, a linearity range of $1 \times 10^{-5} - 1 \times 10^{-1}$ mol L^{-1} and a limit of detection of 3.66×10^{-6} mol L^{-1} were obtained. Particularly noteworthy is the significant improvement in the stability of the potential of this electrode and the long life of more than 5 months.

1. Introduction

Potentiometric sensors have been very popular among scientists all over the world for many years. ISEs are applicable in many areas of human life. They are used in process control, clinical diagnostics [1,2] and environmental monitoring [3,4]. They owe their popularity to numerous advantages resulting from their use, which include, among others, simple operation, quick analysis time, relatively low operating costs, low detection limits and very good selectivity [5–7]. Conventional ion-selective electrodes (ISEs) between the lead-out electrode and the membrane material contain a liquid contact, the presence of which causes many difficulties in their handling or storage [8]. The elimination of the internal solution led to the formation of coated-wire electrodes (CWEs) in 1971 [9], which, however, had poor potential stability and short lifetime, mainly due to the lack of a well-defined redox pair [10], residual current flow through the membrane and the formation of a water layer on membrane-metal interface [11–14]. As a solution, therefore, a solid contact with both ionic and electronic conductivity was used. In this way, ion-selective electrodes with solid contact (SCISEs) were created [5]. The use of solid contact made it possible to modify the shape and significantly reduce the size of the sensors, which, apart from taking up much less space, can be used in multi-sensor measuring platforms [15–17] for determination of ions in natural samples. Moreover, the SCISEs created in this way are characterized by high mechanical strength, easy storage and transport, and can operate under high pressure conditions and in any position [18].

Many materials have already been used successfully as solid contact. Conducting polymers were used as the first for this purpose [19–22]. They are characterized by double conductivity, both ionic and electronic, and therefore can be successfully used as ion-electrode transducers in ion-selective electrodes. Such sensors had significantly improved membrane conductivity, but were often sensitive to light, O₂,
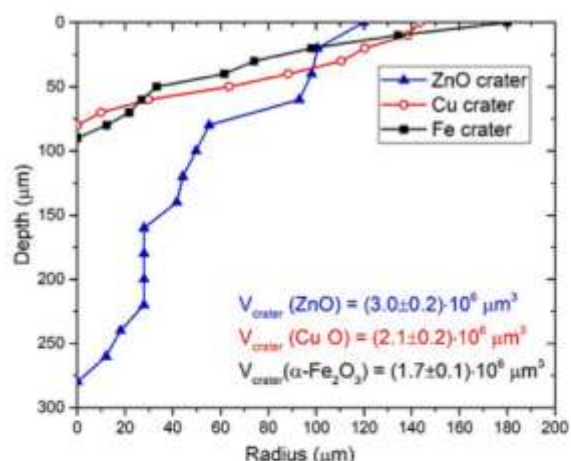
Fig. 1. Semi-profiles of ablated craters.

CO_2 and pH changes [23]. Then, scientists focused mainly on various types of nanomaterials, in particular carbon nanomaterials, including SWCNTs [5,24–26], MWCNTs [27–30], graphene [31–33], fullerenes [34], carbon nanofibers [35] and nanohorns [36], which are mainly used for their unique chemical, physical and electrical properties. High charge transfer, extraordinary electrical capacitance and good hydrophobicity make them perfect as transducer elements in potentiometric sensors [5]. Currently, research on various nanoparticles, mainly metal

and metal oxide nanoparticles, and their possible applications is emerging. One of such applications is using them to improve the analytical parameters of potentiometric sensors. So far, mainly metal nanoparticles have been used for this purpose: silver [37], gold [38–41], platinum [42–44], as well as bimetallic AuCu nanoparticles [45].

Nowadays, many methods of obtaining nanoparticles have been developed. They can be easily divided into physical (physical vaporphase deposition, mechanical milling, sputtering, laser ablation), chemical (chemical vaporphase deposition, chemical reduction, electrosynthesis) and biological (biological synthesis using bacteria, fungi, algae) methods. However, depending on the type of starting material, all of them can be assigned to two groups of methods: the bottom-up approach (building nanostructures from simple substances of small sizes) and top-down approach (obtaining nanoparticles from macroscopic material as a result of decomposition mainly by means of mechanical methods) [46].

One of the main methods of obtaining nanoparticles is laser ablation in liquid (LAL), which belongs to the group of physical methods with a top-down approach. This method allows for easy and quick preparation of high purity nanoparticles [47]. Laser ablation in liquids has been used to synthesize nanomaterials for over two decades, but the nature of this method is still not fully understood. Therefore, there are many publications aimed at in-depth knowledge and understanding of the mechanisms occurring during the processes taking place during laser operation and optimization of the process conditions in order to reduce the costs and control the size of the obtained nanoparticles [48]. They also describe the main principles, possibilities and benefits of the laser ablation method [47,49–52] and its use for the synthesis of various types of nanoparticles, including Au [53,54], Ag [55–57], Cu [58,59], Pt [60] and others [61,62]. Despite the significant cost of the equipment (laser
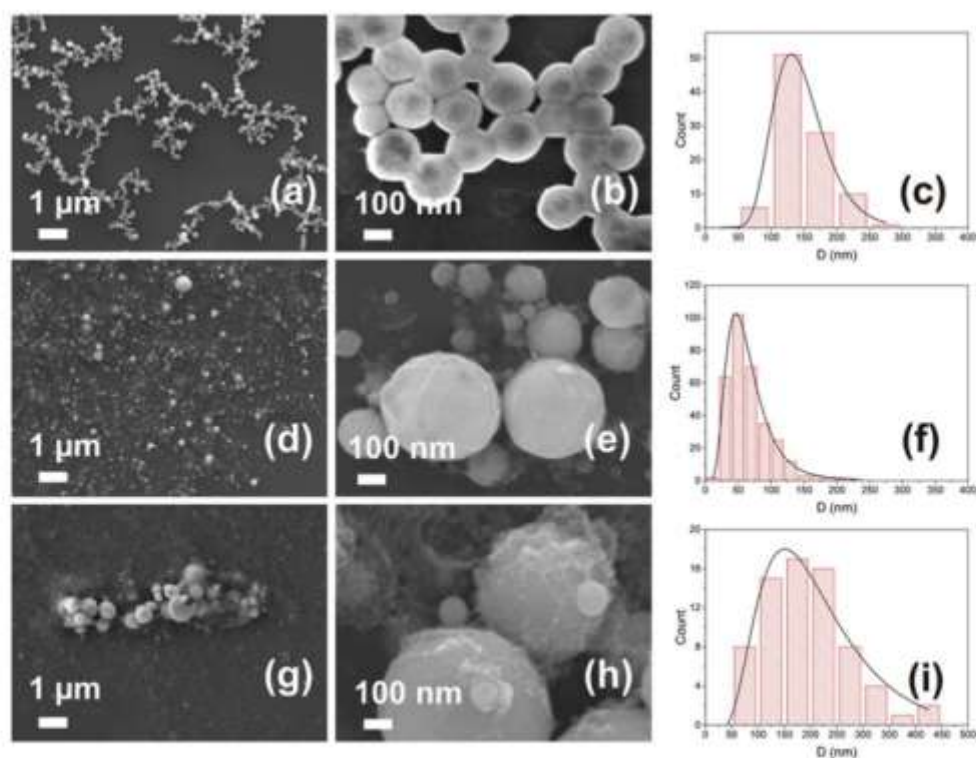

Fig. 2. SEM images of nanoparticles with corresponding size-distributions for ZnO (first row), CuO (second row) and α-Fe₂O₃ (third row). Black lines represent log-normal fit to size-distributions.
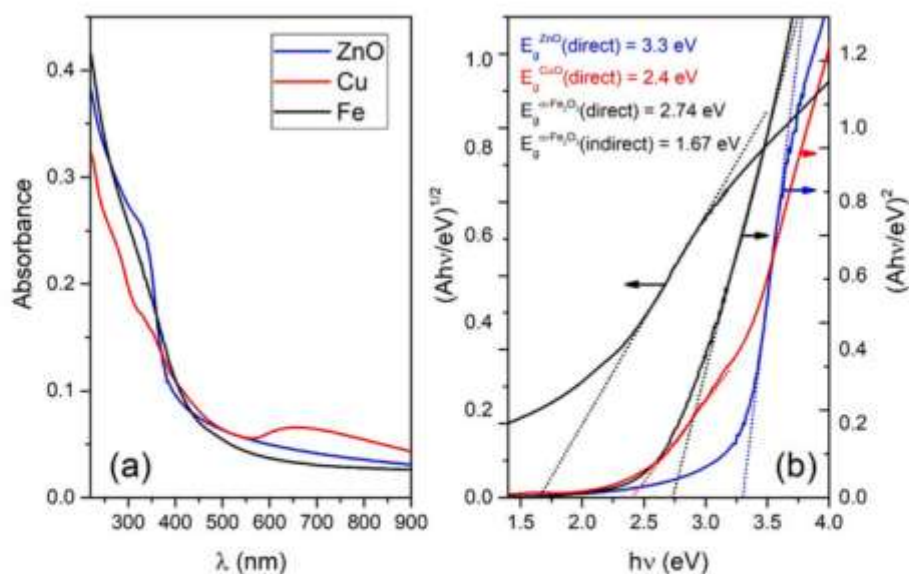
str. 167

Fig. 3. (a) UV-VIS photoabsorption spectra of ZnO, CuO and α-Fe$_2$O$_3$ colloidal solutions, (b) band gap energies of nanoparticles obtained using Tauc plot.
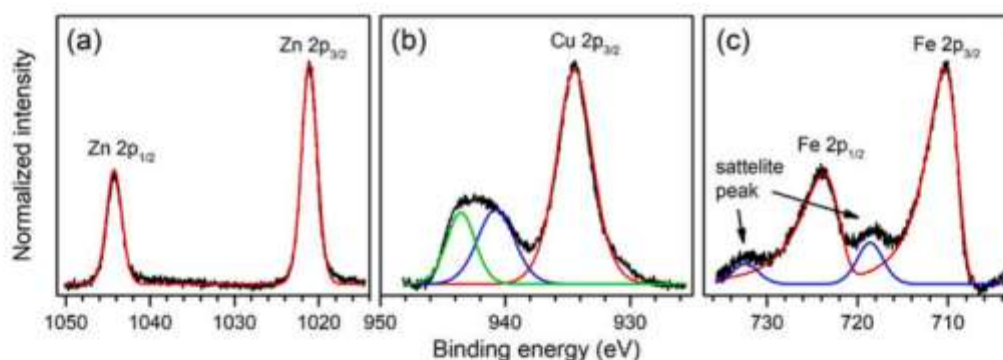

Fig. 4. High resolution XPS spectra of (a) Zn 2p, (b) Cu 2p and (c) Fe 2p.

the most expensive), laser ablation has many advantages. This method can be used to obtain nanoparticles, among others noble metals in water or organic solvents without the need to use additional substances, unlike standard methods involving the chemical reduction of metal salts in the presence of stabilizing molecules. The costs of purchasing metal salts and other chemical additives that would be necessary to produce nanoparticles by traditional chemical methods are eliminated. In addition, the amount of waste produced is significantly reduced, and although the process itself takes some time, depending on the parameters set, the manual operation of the system is also minimal [50]. The main advantage of laser ablation in liquids over the standard techniques is that it provides nanoparticles of high purity as no chemicals are required and no byproducts of the reactions and residues on the nanoparticle surface are present. Summarizing, the laser production of nanoparticles, although it is more expensive than the chemical one, is, however, chemical-freehigh yield, simpler and more ecological [48].

The main objective of the research was to investigate the effect of type and thicknesses of the layer of metal oxide nanoparticles (used as solid contact) placed as an intermediate layer between the electrode material and the ion-selective membrane on the analytical parameters of

the potassium ion-selective electrodes. For this purpose, nanoparticles of zinc oxide, copper oxide and iron oxide obtained by laser ablation were used. A number of studies were carried out in the field of potentiometric methods as well as impedance spectroscopy. Sensors were obtained that are capable of working for a long time, while maintaining a very good slope of the calibration curves, still having good potential stability and a fast response time.

2. Materials and methods

2.1. Reagents

Ion-selective membrane components, such as potassium ionophore – valinomycin and low molecular weight poly(vinylchloride) (PVC) were purchased from Aldrich; whereas potassium tetrakis(p-chlorophenyl) borate (KTPClPB), bis(2-ethylhexyl) sebacate (DOS) were purchased from Fluka. Other substances such as nitrate salts necessary for electrode selectivity studies were purchased from Fluka. All aqueous solutions in the appropriate concentrations were prepared with salts of the highest purity available (pure pro analysis) using freshly deionized water.

3

str. 168

Table 1
Analytical parameters of studied electrode and their stability in time.

Electrode	Parameter	Time [weeks]					
		1	2	4	6	8	20
ISE-ZnO(a)	Slope [mV/decade]	−56.18	−55.44	−55.63	−55.47	−55.02	−55.25
	Limit of detection [mol L^{-1}]	5.31×10^{-6}	6.80×10^{-6}	7.43×10^{-6}	7.77×10^{-6}	8.15×10^{-6}	9.48×10^{-6}
	Linearity range [mol L^{-1}]	$1 \times 10^{-5} - 1 \times 10^{-1}$	$1 \times 10^{-5} - 1 \times 10^{-1}$	$1 \times 10^{-5} - 1 \times 10^{-1}$	$1 \times 10^{-5} - 1 \times 10^{-1}$	$1 \times 10^{-5} - 1 \times 10^{-1}$	$1 \times 10^{-5} - 1 \times 10^{-1}$
	Potential E^0[mV]	552.45	554.74	560.72	564.35	566.50	579.35
ISE-ZnO(b)	Slope [mV/decade]	−56.07	−55.69	−55.38	−55.60	−55.47	−55.62
	Limit of detection [mol L^{-1}]	3.66×10^{-6}	3.86×10^{-6}	4.41×10^{-6}	4.67×10^{-6}	4.95×10^{-6}	5.47×10^{-6}
	Linearity range [mol L^{-1}]	$1 \times 10^{-5} - 1 \times 10^{-1}$	$1 \times 10^{-5} - 1 \times 10^{-1}$	$1 \times 10^{-5} - 1 \times 10^{-1}$	$1 \times 10^{-5} - 1 \times 10^{-1}$	$1 \times 10^{-5} - 1 \times 10^{-1}$	$1 \times 10^{-5} - 1 \times 10^{-1}$
	Potential E^0[mV]	350.18	355.66	361.22	366.44	370.38	383.71
ISE-CuO(a)		1	2	3	4	6	8
	Slope [mV/decade]	−56.68	−56.39	−56.20	−51.72	−52.40	−46.07
	Limit of detection [mol L^{-1}]	8.21×10^{-6}	9.44×10^{-6}	6.59×10^{-6}	4.23×10^{-6}	3.43×10^{-6}	3.67×10^{-6}
	Linearity range [mol L^{-1}]	$1 \times 10^{-5} - 1 \times 10^{-1}$	$1 \times 10^{-5} - 1 \times 10^{-1}$	$1 \times 10^{-5} - 1 \times 10^{-1}$	$1 \times 10^{-5} - 5 \times 10^{-2}$	$1 \times 10^{-5} - 5 \times 10^{-2}$	$1 \times 10^{-5} - 1 \times 10^{-3}$
	Potential E^0[mV]	496.51	509.61	522.69	498.74	500.34	464.27
ISE-CuO(b)	Slope [mV/decade]	−57.52	−56.68	−56.65	−56.51	−55.77	−53.74
	Limit of detection [mol L^{-1}]	3.12×10^{-6}	5.29×10^{-6}	5.56×10^{-6}	5.59×10^{-6}	6.47×10^{-6}	7.69×10^{-6}
	Linearity range [mol L^{-1}]	$1 \times 10^{-5} - 1 \times 10^{-1}$	$1 \times 10^{-5} - 1 \times 10^{-1}$	$1 \times 10^{-5} - 1 \times 10^{-1}$	$1 \times 10^{-5} - 1 \times 10^{-1}$	$1 \times 10^{-5} - 1 \times 10^{-1}$	$1 \times 10^{-5} - 1 \times 10^{-1}$
	Potential E^0[mV]	412.44	409.01	397.57	408.63	440.70	442.90
ISE-Fe$_2$O$_3$(a)		1	2	3	4	6	8
	Slope [mV/decade]	−55.11	−54.82	−52.50	−46.40	−46.89	−46.62
	Limit of detection [mol L^{-1}]	6.60×10^{-6}	4.21×10^{-6}	1.62×10^{-6}	1.76×10^{-6}	3.54×10^{-6}	4.33×10^{-6}
	Linearity range [mol L^{-1}]	$1 \times 10^{-5} - 1 \times 10^{-1}$	$1 \times 10^{-6} - 1 \times 10^{-1}$	$1 \times 10^{-5} - 1 \times 10^{-1}$	$1 \times 10^{-5} - 1 \times 10^{-3}$	$1 \times 10^{-5} - 5 \times 10^{-3}$	$1 \times 10^{-5} - 5 \times 10^{-3}$
	Potential E^0[mV]	367.63	399.29	397.96	441.47	489.75	422.85
ISE-Fe$_2$O$_3$(b)	Slope [mV/decade]	−56.81	−56.65	−56.14	−55.27	55.77	−55.11
	Limit of detection [mol L^{-1}]	4.54×10^{-6}	3.37×10^{-6}	6.05×10^{-6}	6.58×10^{-6}	4.26×10^{-6}	6.05×10^{-6}
	Linearity range [mol L^{-1}]	$1 \times 10^{-5} - 1 \times 10^{-1}$	$1 \times 10^{-5} - 1 \times 10^{-1}$	$1 \times 10^{-5} - 1 \times 10^{-1}$	$1 \times 10^{-5} - 1 \times 10^{-1}$	$1 \times 10^{-5} - 1 \times 10^{-1}$	$1 \times 10^{-5} - 1 \times 10^{-1}$
	Potential E^0[mV]	463.49	457.73	468.68	455.54	544.81	531.11
ISE(c)		1	2	3	4	6	8
	Slope [mV/decade]	−55.03	−55.45	−55.30	−55.27	−55.25	−54.79
	Limit of detection [mol L^{-1}]	5.86×10^{-6}	6.79×10^{-6}	7.36×10^{-6}	7.81×10^{-6}	1.14×10^{-5}	1.93×10^{-5}
	Linearity range [mol L^{-1}]	$1 \times 10^{-5} - 1 \times 10^{-1}$	$1 \times 10^{-5} - 1 \times 10^{-1}$	$1 \times 10^{-5} - 1 \times 10^{-1}$	$1 \times 10^{-5} - 1 \times 10^{-1}$	$5 \times 10^{-5} - 1 \times 10^{-1}$	$1 \times 10^{-4} - 1 \times 10^{-1}$
	Potential E^0[mV]	370.18	387.21	401.23	408.31	422.77	446.34

(a) thicker layer of the solid contact – 500 μl and (b) thinner layer of the solid contact – 100 μl of the colloidal solution of nanoparticles; (c) clear electrode – without intermediate layer.

2.2. Apparatus

Measurements of the electromotive force (EMF) of a cell consisting of a working electrode (tested ion-selective electrode with a solid contact sensitive to potassium ions) and a silver/silver chloride reference electrode with double junction system (Metrohm 6.0750.100)were performed at room temperature in mixed solutions with a magnetic stirrer using a potentiometric system consisting of a 16-channel data acquisition system (Lawson Labs. Inc., USA) connected to a computer with appropriate software.

Electrochemical impedance spectroscopy (EIS) measurements were performed in a 1×10^{-2} mol L^{-1} KNO$_3$ solution in a system consisting of three electrodes: tested ISE as working electrode, silver/silver chloride reference electrode with c(KCl) = 3 mol L^{-1} as reference electrolyte (Metrohm 6.0733.100) and the auxiliary electrode - a GC rod 2 mm/65 mm (Metrohm). An AUTOLAB electrochemical analyzer (Eco Chemie, Netherlands) controlled by NOVA software was used as the measuring device. The impedance spectra were recorded in the frequency range 0.1–100 kHz at the open circuit potential with an amplitude ±10 mV.

2.3. Synthesis and characterization of nanoparticles

Zinc oxide, copper oxide and iron oxide nanoparticles colloidal solutions were synthesized via a process of pulsed laser ablation of pure metallic targets (purity >99.99%, GoodFellow) immersed in a glass beaker containing 25 mL of deionized water. The experimental set-up is the same as we used in an article [61], with Nd:YAG laser (Quantel, Brilliant) with following parameters: number of pulses 5000, wavelength 1064 nm, repetition rate 5 Hz, output pulse energy 300 mJ (120 mJ delivered to the target) and pulse duration 4 ns. Mass concentration of ablated metallic material in as-synthesized colloids (in a form of nanoparticles and irregular material) was calculated from ablated crater-volume and known metallic density. The crater volume was determined using an optical microscope (Leica DM2700 M, Leica Microsystems). Characterization of nanoparticles deposited on silicon wafers was performed using a JEOL JSM-7800F field emission SEM instrument (Jeol Ltd., Tokyo, Japan) by detecting the secondary electrons with an electron beam accelerating voltage of 10 kV and 12 kV and a working distance (WD) of 10 mm and 3 mm, respectively. Prior to the nanoparticles deposition the substrates were ultrasonically cleaned for
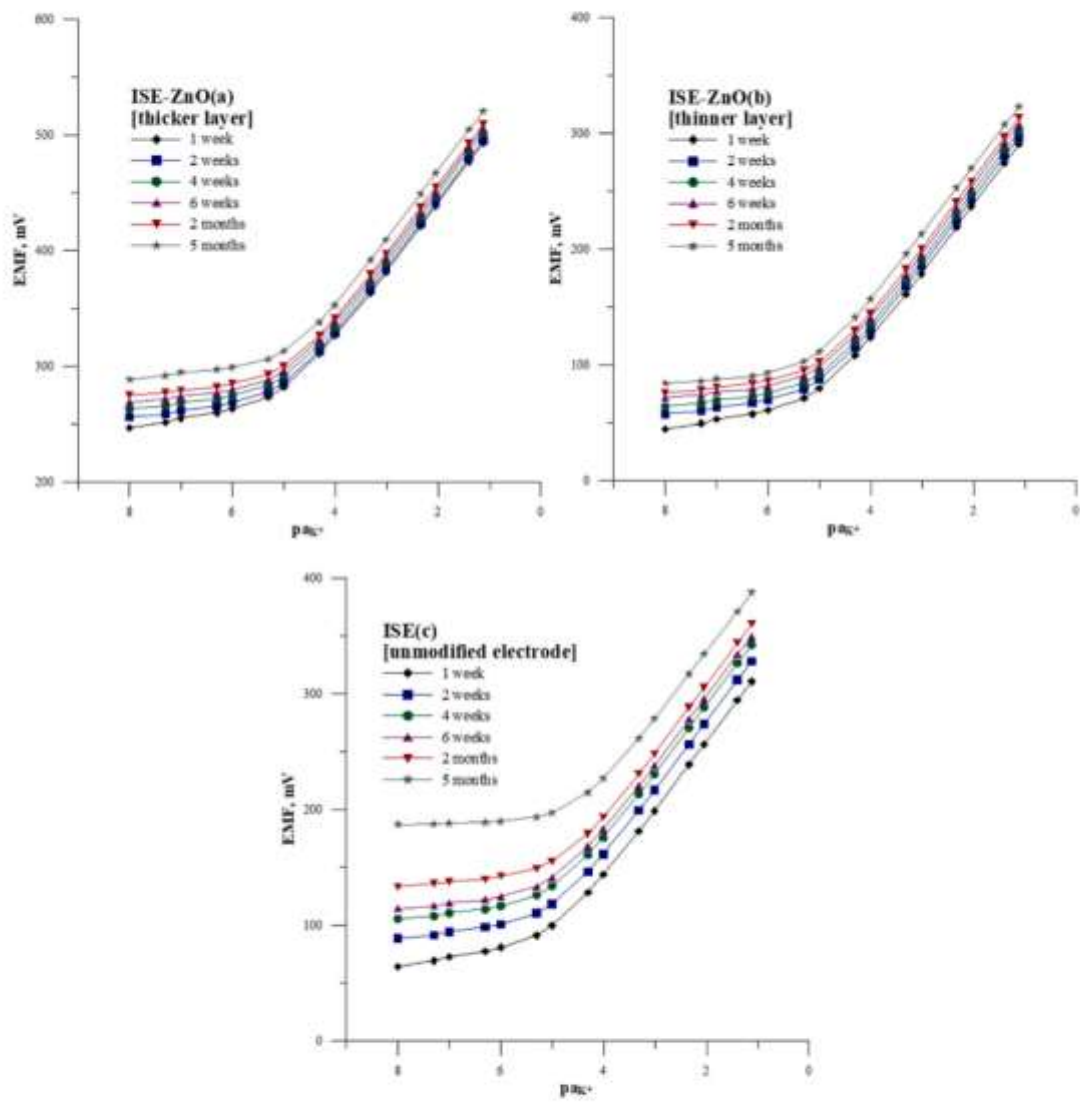
str. 169

Fig. 5. Calibration curves of electrodes: with thicker NPs layer - ISE-ZnO(a), thinner NPs layer - ISE-ZnO(b) and without intermediate layer - ISE(c), determined in time.
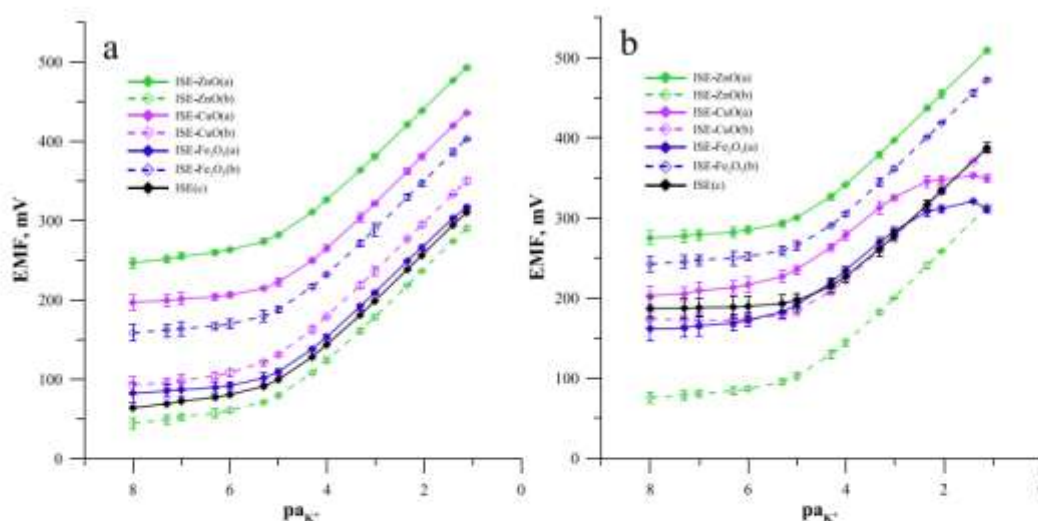
Fig. 6. Calibration curves of electrodes obtained in the KNO₃ solution in the concentration range of $1 \times 10^{-8} - 1 \times 10^{-1}$ mol L^{-1} during: a) the first week, b) after two months of testing. Standard deviations given on the plots are determined for three electrodes.

Table 2
Potential stability and response time obtained for the tested electrodes.

Parameter	ISE-ZnO (a)	ISE-ZnO (b)	ISE-CuO (a)	ISE-CuO (b)	ISE-Fe₂O₃(a)	ISE-Fe₂O₃(b)	ISE (c)
Short term potential drift [mV/h]	0.32	0.16	1.38	0.54	14.36	1.40	5.17
Long term potential drift [mV/day]	0.18	0.22	0.45	0.39	0.70	0.86	1.1
Response time [s]	4–6	4–6	4–6	4–6	6–8	6–8	6–8

10 min in acetone, distilled water and isopropanol and finally dried with N₂ gas. As-synthesized colloidal solutions were characterized by UV-VIS measurements (Lambda 25, PerkinElmer). The chemical composition and bonding were characterized by XPS in a SPECS XPS spectrometer equipped with a Phoibos MCD 100 electron analyzer and a monochromatized source of Al Kα X-rays of 1486.74 eV. The typical pressure in the UHV chamber during analysis was in the 10^{-7} Pa range. For the electron pass energy of the hemispherical electron energy analyzer of 10 eV used in the present study, the overall energy resolution was around 0.8 eV. All spectra were calibrated by the position of C 1s peak, placed at the binding energy of 284.5 eV. The XPS spectra were deconvoluted into several sets of mixed Gaussian-Lorentzian functions with Shirley background subtraction.

2.4. Preparation of the ion-selective membrane

The ion-selective membrane was prepared by weighing the appropriate masses of the membrane components on an analytical balance (totally 0.3 g) and adding 3 mL of THF to them. Qualitative and quantitative composition of the membrane: 3% valinomycin, 1% KTPClPB, 32% PVC, 64% DOS. The membrane components and the organic solvent were thoroughly mixed and placed in an ultrasonic bath until the mixture was completely homogenized.

2.5. Preparation of solid contact ion-selective electrodes

Glassy carbon electrodes (GCE) with a diameter of 0.3 cm were used for the research. The surface of the electrodes was prepared by using fine grit sandpaper (2500 and 5000), then polished with alumina powder sized 0.3 μm, rinsed with distilled water and cleaned using an ultrasonic bath. The electrodes were then rinsed again to better remove residual abrasives, rinsed with tetrahydrofuran (THF) and allowed to dry. The solid contact layer was created by repeatedly dropping small volumes of a colloidal aqueous solution of selected nanoparticles (in total volumes of 500 μl (a) and 100 μl (b)) onto the surfaces of previously prepared GCEs that were allowed to dry. Ion-selective membrane layers were then dropped (three times 30 μl) and the THF was allowed to evaporate. For comparison, unmodified electrodes were also prepared in which an ion-selective membrane was spotted directly on the GCE surface. The electrodes were left to dry for 24 h and then immersed in 1×10^{-3} mol L^{-1} of potassium ion conditioning solution (potassium nitrate salt - KNO₃). Three of the same type of electrodes were made and tested in parallel.

3. Results and discussion

3.1. Characteristics of nanoparticles

The mass concentration of as-synthesized ablated colloidal solutions was determined from ablated craters shown in Fig. 1 and according to a procedure previously described [63]. Craters were evaluated as described in the article [64].

The masses of ablated material, calculated from craters and known density, are 16.8 μg, 12.6 μg and 8.9 μg for ZnO, CuO and α-Fe₂O₃ colloidal solutions, respectively. It yields corresponding mass concentrations of produced colloids 0.67 mg/L, 0.50 mg/L and 0.36 mg/L for ZnO, CuO and α-Fe₂O₃ colloidal solutions, respectively.

A SEM imaging was used to inspect nanoparticles size, shape and morphology. From SEM images a size-distribution of nanoparticles were obtained using program ImageJ. SEM images together with corresponding size-distributions are shown in Fig. 2.

From Fig. 2 it can be seen that all nanoparticles are of spherical shape while in CuO and especially in α-Fe₂O₃ irregularly crystallized material is also present. ZnO colloid contains mostly pure nanoparticles with no irregular material. Size distributions of nanoparticles are relatively
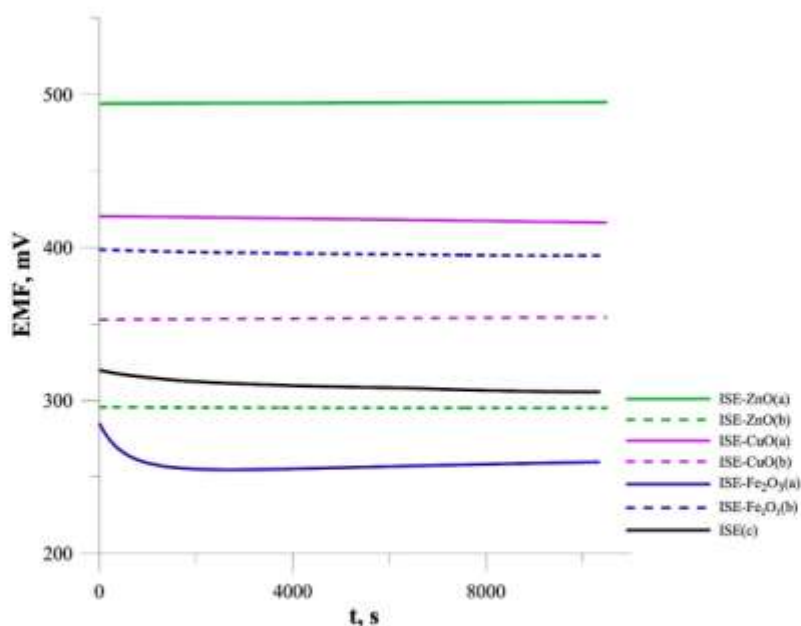
str. 171

Fig. 7. Short-term potential stability of the tested electrodes, measured in a 1×10^{-1} mol L^{-1} KNO$_3$ solution.

broad and follow log-normal distribution which is typical for laser synthesis of nanoparticles in liquids as discussed in the article [63]. Average size of ZnO nanoparticles is 140 nm, CuO is 50 nm and α-Fe$_2$O$_3$ is 150 nm.

In Fig. 3 (a) UV-VIS photoabsorption spectra of ZnO, CuO and α-Fe$_2$O$_3$ colloidal solutions are shown. Optical band gap energy is determined from UV-VIS spectra using following formula:

$$Ah\nu \sim \left(h\nu - E_g\right)^n \tag{1}$$

where: A is the absorbance, $h\nu$ is the photon energy, E_g is the band gap energy and n is exponent which depends on the type of transition. Namely, its value is ½ for indirect and 2 for direct transitions. E_g is determined by extrapolating the linear part of $(Ah\nu)^{1/n}$vs. $h\nu$ to zero (A = 0) as is shown in Fig. 3(b). It can be seen that ZnO(E_g = 3.3 eV) and CuO(E_g = 2.4 eV) possess direct band gap as expected and with the values reported in the literature [65,66]. Note that CuO band gap is about 1 eV larger that bulk material but this feature can be attributed to the reduced grain size in the case of nanoparticles prepared by pulsed laser ablation [67]. Such band gap energies indicate that laser ablated Zn and Cu oxidized in water possessing wurtzite and cuprous crystal structures of ZnO and CuO, respectively [63,68]. Laser ablation of Fe in water results in formation of Fe-oxides. They can, most probably, crystallize in two polymorphic structures α-Fe$_2$O$_3$ and γ-Fe$_2$O$_3$. As α-Fe$_2$O$_3$ possess both direct and indirect band gap and determined E_g's are 2.74 eV and 1.67 eV, respectively, it indicates that nanoparticles are of α-Fe$_2$O$_3$ structure [69].

The surface property of nanoparticles was studied by XPS analysis. In Fig. 4 (a) a high-resolution XPS core level spectrum of Zn 2p is shown. The spectrum is fitted with two components at 724.1 eV and 710.0 eV

(fit is shown with red line). Peaks correspond to Zn^{2+} states in ZnO lattice. In Fig. 4 (b) a high-resolution XPS core level spectrum of Cu 2p is shown. The spectrum consists of the main peak 2p$_{3/2}$ at binding energy 934.5 eV (red line fit) and satellite band consisting of two peaks at 944.0 eV and 941.0 eV (green and blue fit, respectively) which are typical features of cuprous oxide, CuO [70,71]. In Fig. 4 (c) a high-resolution XPS core level spectrum of Fe 2p obtained from α-Fe$_2$O$_3$ nanoparticles is shown. The spectrum is fitted with two main peaks at 724.1 eV and 710.3 eV (red line fit) while both peaks are accompanied with broad satellite structures positioned on their high binding energy side (blue line fit) at 733.0 eV and 718.5 eV, respectively. The main peaks energies are consistent with values obtained for the ferric oxides reported in literature [72].

3.2. Potentiometric measurements

3.2.1. Potentiometric response

This work describes potassium ion-selective electrodes with solid contact, in which nanoparticles of selected metal oxides (zinc, copper and iron oxide) were used as solid contact. Sensors with two thicknesses of solid contact layers (thicker - 500 µl (a) and thinner - 100 µl (b) of nanoparticles suspension) were tested. In order to obtain a better comparison, an electrode without an intermediate layer (c) was additionally prepared. The obtained electrodes have been widely studied.

Measurements were made to prepare electrode calibration curves, which also allowed to determine their linearity ranges, detection limits (LOD) and sensor response times. In addition, the stability of the short- and long-term potential of the tested electrodes and the reversibility of the potential at various concentration levels were also examined. The
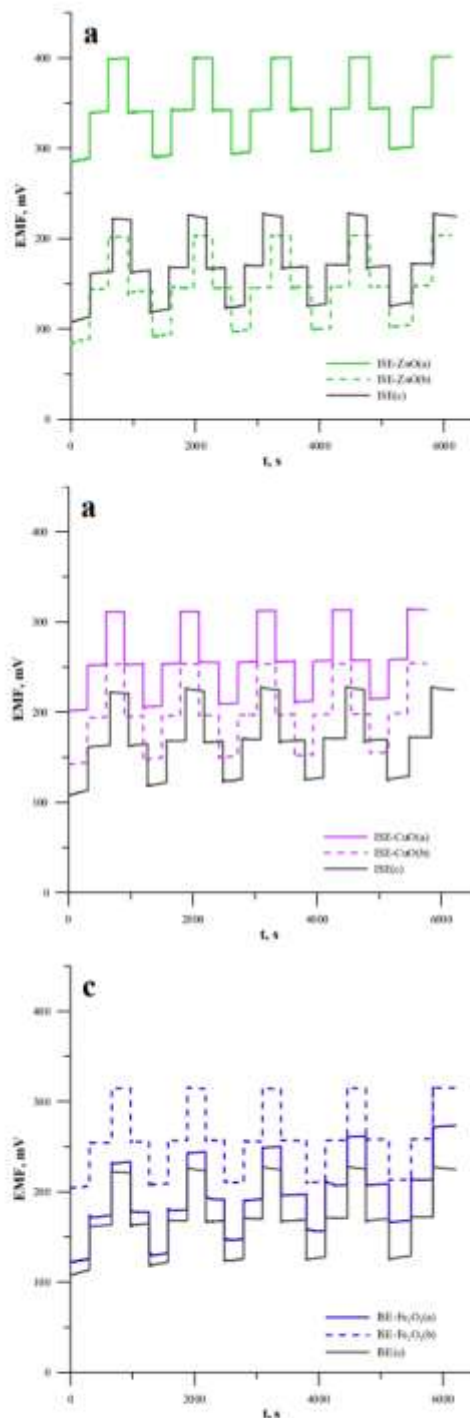
str. 172

Fig. 8. Reversibility of the potential response measured in KNO$_3$ solutions with concentrations: 1×10^{-5}, 1×10^{-4} and 1×10^{-3} mol L^{-1} for the tested electrodes: unmodified electrode and electrodes containing thicker and thinner interlayer of a) ZnO, b) CuO and c) Fe$_2$O$_3$ nanoparticles as a solid contact.

electrochemical impedance spectroscopy technique was used to test and compare the electrical properties of the sensors.

The potentiometric response of the electrodes was tested in KNO$_3$ solutions in the concentration range of $1 \times 10^{-8} - 1 \times 10^{-1}$ mol L^{-1} by measuring the electromotive force (EMF) of the cell composed of the tested electrode and the Ag/AgCl reference electrode. The measurements were made twice a week. On the basis of the obtained calibration curves, analytical parameters of the electrodes such as detection limit, characteristic slope, linear range and potential E^0 were determined. The E^0 potential values were determined from the calibration curves by extrapolation of the linear section of the response function to the pa$_{K+}$ = 0. Change of analytical parameters in time of different electrodes are presented in Table 1. Time course of the calibration curves for ZnONPs-based electrodes and unmodified electrodes is shown on Fig. 5.

In the initial period of time, the slopes of the electrode characteristics curves and the determined detection limits were comparable for all sensors. However, over time, the differences between the sensors varied more. As time passed, the slope of the electrode characteristics decreased and the detection limit increased. However, this process was much faster for electrodes without nanoparticles. Moreover, calibration curves lost their linear course at higher concentrations and the linear range shortened for electrodes with a thicker layer of nanoparticles when copper oxide and iron oxide nanoparticles were used. All electrodes with thinner layer of nanoparticles exhibited better stability in time compared to electrode without nanoparticles modification. In the case of zinc oxide nanoparticles, both types of electrodes worked properly for several months. Even five-month-old electrodes showed the same linear range and 98.3 and 95.0% of initial slope for thicker and thinner layer of nanoparticles, respectively (Fig. 5).

The improvement of electrode stability in result of introduction of metal oxide nanoparticles intermediate layer is not surprising. Transition metals nanoparticles including ZnONps, CuONPs and Fe$_2$O$_3$NPs belong to nanostructures which show excellent physical and electrochemical performance as compared to their bulk counterparts. They are characterized by high surface-to-volume ratio and exhibit semiconducting properties. Due to presence of NPs layer the electroactive surface area is enlarged and electron transfer between ion sensitive membrane and inner electrode is enhanced.

Electrodes with a thinner layer of nanoparticles showed a much longer lifetime compared to electrodes with a thicker layer of nanoparticles when copper oxide and iron oxide nanoparticles were used. In the case of zinc oxide nanoparticles, both types of electrodes worked properly for several months.

The graphs (Fig. 6) show the calibration curves for all types of electrodes obtained at the beginning of the tests and after 2 months. There is a noticeable advantage in the durability of electrodes with a thinner intermediate layer in the case of copper and iron oxide nanoparticles.

The more favorable properties of the electrodes based on ZnONPs are probably the result of greater homogenity of ZnONPs. As can be seen on SEM images (Fig. 2) ZnONPs, contrary to Fe$_2$O$_3$NPs and CuONPs, did not contain irregularly crystallized material. Homogenous structure of ZnONPs allows to obtain an evenly distributed layer of nanoparticles on the surface of the inner electrode and is not conducive to the formation of the water layer on membrane-inner electrode interface. In the case of CuONPs and Fe$_2$O$_3$NPs presence of irregularly crystallized forms can cause poorer adhesion of the membrane to the inner layer of nanoparticles and the surface of the inner electrode. This effect was more evident in the case of electrodes with thicker layer of NPs.

3.2.2. Long term potential stability

The research on the long-term stability of the electrode potential consisted in systematic (twice a week) calibration of the electrodes in freshly prepared KNO$_3$ solutions and estimating the E^0 value each time from the linear segment of the calibration curve. The stability was calculated from the difference between the E^0 values obtained for the

Table 3

Results of potential reversibility measurements, mean potential values and standard deviation.

C_{K^+} [mol L^{-1}]	Parameter	ISE-ZnO(a)	ISE-ZnO(b)	ISE-CuO(a)	ISE-CuO(b)	ISE-Fe$_2$O$_3$(a)	ISE-Fe$_2$O$_3$(b)	ISE(c)
1×10^{-5}	MeanV mV]	295.25	97.61	209.57	150.71	146.09	209.93	123.44
	SD [mV]	5.08	5.79	4.97	4.32	17.63	2.98	6.36
1×10^{-4}	MeanV mV]	342.02	144.94	254.25	196.17	182.87	255.62	166.71
	SD [mV]	1.17	1.51	1.23	0.91	8.36	1.06	2.68
1×10^{-3}	MeanV mV]	400.51	203.25	312.25	253.55	252.32	314.43	223.66
	SD [mV]	0.66	0.53	1.04	0.26	15.56	0.39	1.76

MeanV – mean value of SEM, SD – standard deviation.

Table 4

Comparison of logarithms of selectivity coefficients obtained by the method of separated solutions (SSM) for tested electrodes and selected electrodes available in the literature.

Ion	$log K_{K^+, M}^{pot}$							
	ISE-ZnO(b)	ISE-CuO(b)	ISE-Fe$_2$O$_3$(b)	ISE	[74]	[75]	[76]	[77]
Na$^+$	-4.8 ± 0.1	-4.9 ± 0.2	-4.8 ± 0.2	-4.8 ± 0.1	-4.5 ± 0.2	-4.6 ± 0.1	-4.3 ± 0.2	-3.5 ± 0.1
Ca^{2+}	-4.7 ± 0.1	-4.6 ± 0.2	-4.4 ± 0.3	-4.8 ± 0.2	-3.1 ± 0.2	-5.0 ± 0.2	-4.2 ± 0.2	-3.6 ± 0.4
Mg^{2+}	-5.4 ± 0.2	-5.3 ± 0.3	-5.3 ± 0.3	-4.8 ± 0.3	-4.5 ± 0.3	-5.5 ± 0.1	-4.5 ± 0.3	-3.7 ± 0.4
Co^{2+}	-3.7 ± 0.1	-4.0 ± 0.3	-3.7 ± 0.1	-3.8 ± 0.4	–	–	–	–
Ni^{2+}	-2.5 ± 0.3	-2.7 ± 0.3	-2.5 ± 0.4	-2.5 ± 0.3	–	–	–	–
Zn^{2+}	-5.1 ± 0.2	-5.1 ± 0.1	-5.0 ± 0.2	-5.0 ± 0.2	–	–	–	–
Cu^{2+}	-5.1 ± 0.1	-5.1 ± 0.3	-5.0 ± 0.1	-5.1 ± 0.3	–	–	–	–
Cd^{2+}	-4.9 ± 0.2	-5.0 ± 0.2	-4.9 ± 0.3	-5.0 ± 0.4	–	–	–	–
Pb^{2+}	-5.3 ± 0.3	-5.3 ± 0.4	-5.2 ± 0.4	-5.1 ± 0.4	–	–	–	–

last and first calibrations, which was then divided by the number of days in between them. As it can be seen on Fig. 5 electrodes based on ZnO nanoparticles were characterized by good long term potential stability. Calibration curves determined over five months were very repeatable for these electrodes. Similar results were obtained for ISE-CuO(b) and ISE-Fe$_2$O$_3$(b). Change of potential E^0 in time for all tested electrodes is shown in Table 1 and long term potential stability expressed as $\Delta E^0/\Delta t$ is given in Table 2 where it can be seen that all electrodes based on nanoparticles exhibited improved long term potential stability compared to simple coated disc electrode.

3.2.3. Short-term stability of the potential

Short-term potential stability was determined in a KNO$_3$ solution with a concentration of 1×10^{-1} mol L^{-1} for 3 h. The EMF dependence on time for modified and unmodified electrodes is shown in Fig. 7. Except for the ion-selective electrode with a thicker layer of iron oxide nanoparticles, all electrodes showed better potential stability compared to the unmodified electrode. The best potential stability exhibited electrodes based on ZnO nanoparticles. The determined potential drift ($\Delta E/\Delta t$) was over sixteen times smaller and over thirty-two times smaller for electrodes with a thicker and thinner layer of ZnO nanoparticles, respectively, compared to unmodified electrodes (Table 2). It is worth to note that in the case of all modified electrodes short-term stability was better for electrodes with thinner layer of metal oxide nanoparticles. Probably it was connected with diffusion processes within this layer which is faster in thinner layer and results in more effective charge transport between membrane and inner electrode.

3.2.4. Reversibility of the electrode potential

The reversibility of the potential was measured with KNO$_3$ solutions in 1×10^{-5}, 1×10^{-4} and 1×10^{-3} mol L^{-1} concentrations. Time-

dependent potential traces during reversibility measurements are presented in Fig. 8 whereas mean potential values obtained from measurement in particular concentrations and standard deviation are given in Table 3 where it can be seen that electrodes with metal oxides nanoparticles were characterized by better potential reversibility than unmodified electrode ISE(c). This is evidenced by the lower value of the standard deviation. Only the electrodes with a thicker layer of iron nanoparticles showed worse potential reversibility. Most likely, it was caused by the membrane detaching from the substrate. This hypothesis is also confirmed by the water layer test described below.

3.2.5. Selectivity

Selectivity coefficients for selected interfering ions were determined using the separate solution method (SSM) [73]. The logarithms of selectivity coefficients obtained for the tested electrodes were presented in Table 4. In addition, the table also includes data on other ion-selective electrodes sensitive to potassium ions, which are available in the literature. Placement of an intermediate layer of nanoparticles between the electrode material and the ion-selective membrane did not change the selectivity significantly. The selectivity for the chosen interfering ions is comparable for all tested sensors, and also for the given examples. The reason can be that the best known and most commonly used ionophore for this type of electrodes is valinomycin. The selectivity of sensors containing the same active substance as a component of the ion-selective membrane will not differ significantly. Additions of other substances or different types of materials used as solid contact may have a slight difference in selectivity.

3.2.6. Water layer test

The water layer test was performed to check whether there was a thin layer of water phase between the material of the inner electrode and the
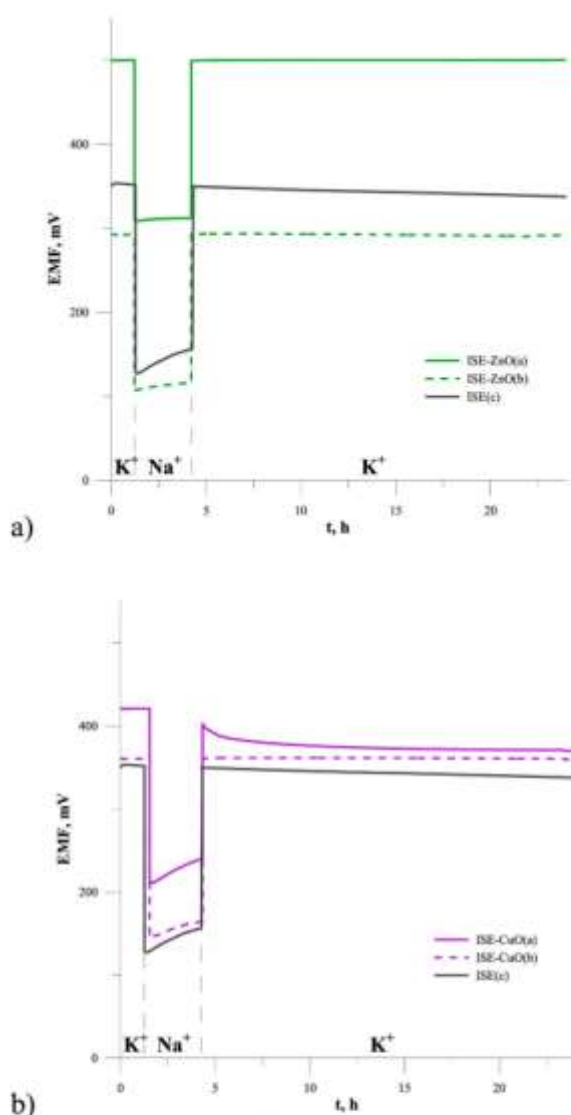
9

a)

b)

Fig. 9. Water layer test for the SCISEs with zinc oxide (a) and copper oxide (b) nanoparticles. The measurements were recorded in 1×10^{-1} mol L^{-1} KNO$_3$ and in 1×10^{-1} mol L^{-1} NaNO$_3$.

ion-selective membrane causing the deterioration of the electrode potential stability. The procedure was based on the description in the article [13]. The water layer test was carried out for each type of electrode after soaking the electrodes in 1×10^{-1} mol L^{-1} KNO$_3$ solution for 24 h. Then the signal was measured for about an hour in the main ion solution, then the solution was changed to 1×10^{-1} mol L^{-1} NaNO$_3$ (interfering ion) and the signal was measured for about 3 h. Then the electrodes were placed back in the main ion solution and the change in electrode potentials was measured again for about 20 h.

As it can be seen on Fig. 9, ISE without nanoparticles layer exhibited noticeable potential drift after replacement of primary ions by interfering ions which indicates the formation of a water layer between the membrane and inner electrode. In the case of electrodes with an additional layer of zinc oxide nanoparticles as a solid contact, a more stable potential was observed. In the case of copper oxide nanoparticles-based

electrodes lack of potential drift was observed only for electrode with thinner interlayer of CuONPs. The electrode with thicker interlayer of CuONPs exhibited similar potential readings to those observed for unmodified ISE(c). Similar results were obtained for ISEs based on iron oxide nanoparticles.

3.2.7. Effects of O_2, CO_2 and light on the electrode potential stability

In the case of potentiometric sensors, it is very important that they are able to work in changing conditions, especially due to their possible application in the study of natural samples and environmental monitoring, also directly without the need to take the samples to the laboratory. In order to test the resistance of the electrodes to changing measurement conditions, tests were carried out on the influence of the presence of gases and light on the change of the potential of the tested electrodes. For this purpose, a fresh KNO$_3$ solution with a concentration of 10^{-3} mol L^{-1} was prepared and the tested electrodes were immersed in it. In order to check the effect of the presence of gases, the electrode potential was measured alternately, each time for 10 min, in two solutions: the starting solution, which was left in the air at room temperature in order to be saturated with oxygen and carbon dioxide from the air, and the solution, which had previously been deoxidized by hour in nitrogen flow. In the case of examining the effect of the presence of light on the potential of the electrodes, they were also immersed in a KNO$_3$ solution with a concentration of 10^{-3} mol L^{-1}, and then the light was turned off and the light was turned on, also 10 min apart. Fig. 10 shows the dependence of the potential on time under varying conditions for electrodes with an intermediate layer of ZnO nanoparticles. Both in the case of this type of electrode, as well as the others, no significant influence of both the presence of gases and the change of lighting in the laboratory was noticed. The electrodes worked properly, the potential did not change much, which could result from the change of measurement conditions, and their work was not disturbed in any way.

3.3. Electrochemical impedance spectroscopy

In order to investigate the influence of the kind of metal oxide nanoparticles on electrochemical performance ISE-ZnO(a), ISE-CuO(a), ISE-Fe$_2$O$_3$(a) and unmodified ISE(c) were compared by electrochemical impedance spectroscopy. EIS spectra were recorded at open circuit potential, with an amplitude of ± 10 mV and within the frequency range from 0.1 Hz to 100 kHz. Fig. 11 shows impedance spectra obtained for the studied electrodes. As it can be seen in Fig. 11, all impedance spectra had the same shape semicircle in the high frequency region together with a part of semicircle in the low frequency region. The high-frequency semicircle can be attributed to the bulk resistance (R$_b$) and geometric capacitance (C$_g$) of the ISM, and the low-frequency part of semicircle can be connected to the charge-transfer resistance (R$_{ct}$) in parallel with a double layer capacitance (C$_{dl}$) at the interface between the polymeric membrane and inner GC electrode [78,79]. The obtained impedance spectra were fitted to the equivalent circuit presented in Fig. 12 where it can be seen that apart resistance (R) and capacitance (C), there is the constant phase element (CPE). CPE is connected with diffusion and surface imperfection and depending on the value of parameter n, it can represent ideal capacitance if n = 1, or Warburg impedance when n = 0.5. Electrical parameters of studied electrodes determined using equivalent circuit are listed in Table 5. As can be seen in result of introduction of metal oxide nanoparticles intermediate layer, the electrical parameters of studied electrodes were significantly improved. Bulk membrane resistance R$_b$ decreased from 882 kΩ for unmodified ISE(c) to 78.1, 391 and 479 kΩ for ISE-CuO(a), ISE–Fe$_2$O$_3$(a), ISE-ZnO(a), respectively. Similar change was observed for the charge transfer resistance R$_{ct}$ which decreased from 180 kΩ for unmodified ISE(c) to 9.34, 70.0 and 22.0 kΩ for ISE-CuO(a), ISE-Fe$_2$O$_3$(a), ISE-ZnO(a), respectively. At the same time, the double layer capacitance (C$_{dl}$) capacity increased significantly. It was equal 0.116 nF for unmodified ISE(c) and was much smaller than this obtained for
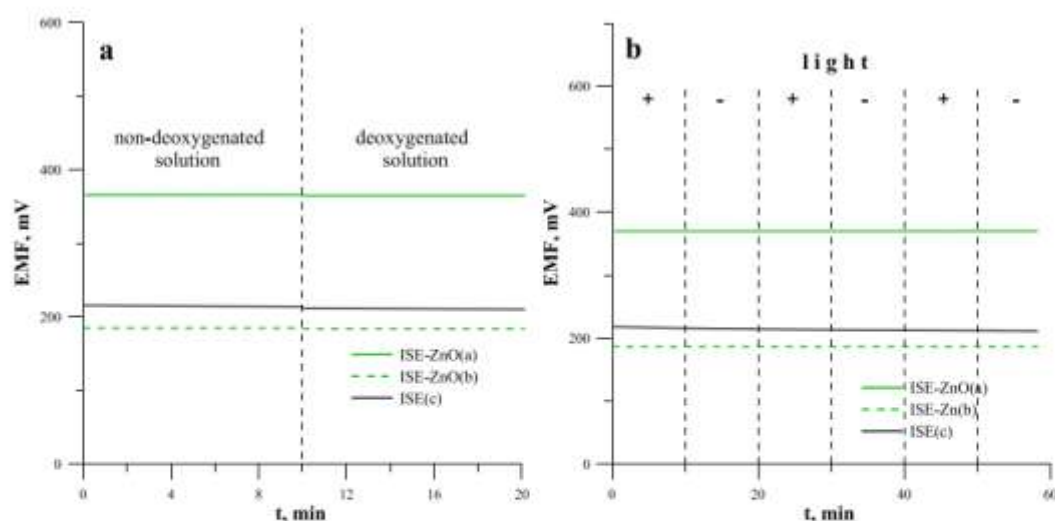
Fig. 10. The effect of the presence of gases and light on the operation of sensors: unmodified ISE(c) electrode and electrodes with ZnO nanoparticles solid contact. Measurement in 10^{-3} mol L^{-1} KNO$_3$ solution.
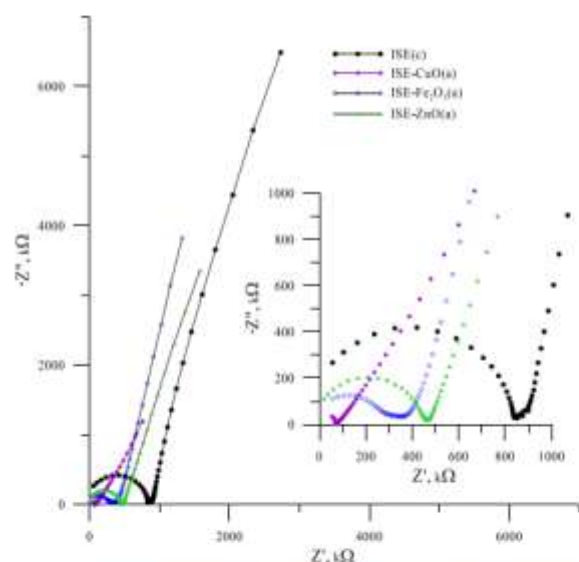

Fig. 11. Experimental data obtained from Electrochemical Impedance Spectroscopy (EIS) analysis. Spectrum of the impedance of electrodes with a thicker layer of nanoparticles and an unmodified electrode (ISE(c)) obtained in a KNO$_3$ solution with a concentration of 1×10^{-2} mol L^{-1}, recorded at the open circuit potential in the frequency range 0.1 Hz–100 kHz.

nanoparticles based electrodes whose C_{dl} was 104, 10.3 and 27.7 nF for ISE-CuO(a), ISE-Fe$_2$O$_3$(a), ISE-ZnO(a), respectively. These results indicate that the applying of metal oxide NPs as a transducing layer significantly facilitates the diffusion processes and charge transport at the interface which results in improvement the potential stability.

4. Conclusions

Potassium-sensitive ion-selective electrodes with solid contact were constructed, in which various metal oxide nanoparticles were used as
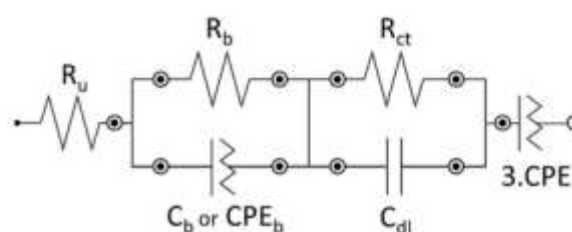

Fig. 12. The equivalent electrical circuit for electrodes. The error of the fits (χ^2) was 0.02, 0.04, 0.004 and 0.01 for ISE-CuO(a), ISE-Fe$_2$O$_3$(a), ISE-ZnO(a) and ISE(c), respectively.

solid contact. A slightly higher slopes of the calibration curves were obtained for the modified electrodes compared to the unmodified electrode. Moreover, electrodes with nanoparticles showed better stability and potential reversibility. The prepared ion-selective electrodes were characterized by a very fast response time (4–8 s). The electrodes with ZnO nanoparticles also showed a very long life, as they were still working properly after 5 months and kept a very good slope. In the case of CuO and Fe$_2$O$_3$ nanoparticles their usage as solid contact of ion-selective electrodes requires optimization of inner layer thickness.

Metal oxide nanoparticles offer a new alternative to obtain all solid state ion-selective electrodes. They are relatively cheap and readily available material. Nanoparticles obtained by laser ablation, compared to other materials used as solid contact, e.g. carbon nanomaterials, are characterized by high purity. This is due to the fact that the laser ablation process as a method of obtaining various types of metal and metal oxides nanoparticles is characterized by high speed, minimal manual operation of the equipment and cleanliness, because it is not necessary to use any organic compounds or other additives (such as metal salts) and it does not produce any products by-contaminants of the obtained end product.

Credit author statement

Karolina Pietrzak: Methodology, Investigation, Data curation, Validation, Writing – original draft. Nikša Krstulović: : Methodology, Writing – review & editing. Damjan Blažeka: Investigation, Julio Car:

str. 176

Table 5

Electrical parameters of studied electrodes determined from EIS measurements (R_u-uncompensated series resistance, R_b bulk resistance, C_b geometric capacitance, R_{ct} charge transfer resistance, CPE constant phase element (Y^0 initial value for the admittance for the CPE element, n-parameter showing to what extent the CPE is the ideal capacitance, if $n = 1$ then CPE is ideal capacitance, and when $= 0.5$ it is Warburg impedance).

Electrode	R_u [kΩ]	R_b [kΩ]	C_b [pF]	CPE$_b$ Y^0(n) [pF]	R_{ct} [kΩ]	C_{dl} (nF)	CPE$_{dl}$ Y^0(n) [nF]
ISE-CuO(a)	−6.26	78.1	12.2	–	9.34	104	994(0.629)
ISE-ZnO(a)	−28.8	479	–	40.8(0.908)	22.0	26.7	417(0.779)
ISE-Fe$_2$O$_3$(a)	−16.9	391	–	265(0.872)	70.0	10.3	381(0.829)
ISE(c)	−26.3	882	8.01	–	180	0.116	363(0.775)

Investigation. Szymon Malinowski: Validation, Formal analysis. Cecylia Wardak: Conceptualization, Methodology, Supervision, Writing – review & editing

Declaration of competing interest

The authors declare that they have no known competing financial interests or personal relationships that could have appeared to influence the work reported in this paper.

Acknowledgements

References

[1] R. Koncki, Recent developments in potentiometric biosensors for biomedical analysis, Anal. Chim. Acta 599 (2007) 7–15, https://doi.org/10.1016/j.aca.2007.08.003.

[2] L. van de Velde, E. d'Angremont, W. Olthuis, Solid contact potassium selective electrodes for biomedical applications- a review, Talanta 160 (2016), https://doi.org/10.1016/j.talanta.2016.06.050.

[3] R. De Marco, G. Clarke, B. Pejcic, Ion-selective electrode potentiometry in environmental analysis, Electroanalysis 19 (2007) 1987–2001, https://doi.org/10.1002/elan.200703916.

[4] G.A. Crespo, Recent Advances in Ion-selective membrane electrodes for in situ environmental water analysis, Electrochim. Acta 245 (2017) 1023–1034, https://doi.org/10.1016/j.electacta.2017.05.159.

[5] R. Liang, T. Yin, W. Qin, A simple approach for fabricating solid-contact ion-selective electrodes using nanomaterials as transducers, Anal. Chim. Acta 853 (2015) 291–296, https://doi.org/10.1016/j.aca.2014.10.033.

[6] E. Lindner, R.E. Gyurcsányi, Quality Control Criteria for Solid-Contact, Solvent Polymeric Membrane Ion-Selective Electrodes, 2009, pp. 51–68, https://doi.org/10.1007/s10008-008-0608-1.

[7] J. Sutter, A. Radu, S. Peper, E. Bakker, E. Pretsch, Solid-contact polymeric membrane electrodes with detection limits in the subnanomolar range, Anal. Chim. Acta 523 (2004) 53–59, https://doi.org/10.1016/j.aca.2004.07.016.

[8] T. Ghosh, H.J. Chung, J. Rieger, All-solid-state sodium-selective electrode with a solid contact of chitosan/prussian blue nanocomposite, Sensors 17 (2017) 2536, https://doi.org/10.3390/s17112536.

[9] R.W. Cattrall, H. Freiser, Coated wire ion selective electrodes, Anal. Chem. 43 (1971) 1905–1906, https://doi.org/10.1021/ac60307a032.

[10] R.P. Buck, Ion selective electrodes, Anal. Chem. 48 (1976) 23–39.

[11] T. Lindfors, F. Sundfors, L. Höfler, R.E. Gyurcsányi, FTIR-ATR study of water uptake and diffusion through ion-selective membranes based on plasticized poly (vinyl chloride), Electroanalysis 21 (2009) 1914–1922, https://doi.org/10.1002/elan.200904609.

[12] T. Lindfors, F. Sundfors, L. Höfler, R.E. Gyurcsányi, The water uptake of plasticized poly(vinyl chloride) solid-contact calcium-selective electrodes, Electroanalysis 23 (2011) 2156–2163, https://doi.org/10.1002/elan.201100219.

[13] M. Fibbioli, W.E. Morf, M. Badertscher, N.F. De Rooij, E. Pretsch, Potential drifts of solid-contacted ion-selective electrodes due to zero-current ion fluxes through the sensor membrane, Electroanalysis 12 (2000) 1286–1292, https://doi.org/10.1002/1521-4109(200011)12:16<1286::AID-ELAN1286>3.0.CO;2-Q.

[14] J. Hu, A. Stein, P. Bühlmann, Rational design of all-solid-state ion-selective electrodes and reference electrodes, Trends Anal. Chem. 76 (2016) 102–114, https://doi.org/10.1016/j.trac.2015.11.004.

[15] Z. Mousavi, K. Granholm, T. Sokalski, A. Lewenstam, All-solid-state electrochemical platform for potentiometric measurements, Sensor. Actuator. B Chem. 207 (2015) 895–899, https://doi.org/10.1016/j.snb.2014.06.067.

[16] G. Maduraiveeran, W. Jin, Nanomaterials based electrochemical sensor and biosensor platforms for environmental applications, Trends Environ. Anal. Chem. 13 (2017) 10–23, https://doi.org/10.1016/j.teac.2017.02.001.

[17] S. Anastasova-Ivanova, U. Mattinen, A. Radu, J. Bobacka, A. Lewenstam, J. Migdalski, M. Danielewski, D. Diamond, Development of miniature all-solid-state potentiometric sensing system, Sensor. Actuator. B Chem. 146 (2010) 199–205, https://doi.org/10.1016/j.snb.2010.02.044.

[18] J. Bobacka, A. Ivaska, A. Lewenstam, Potentiometric ion sensors, Chem. Rev. 108 (2008) 329–351.

[19] M. Vázquez, J. Bobacka, A. Ivaska, A. Lewenstam, Influence of oxygen and carbon dioxide on the electrochemical stability of poly(3,4-ethylenedioxythiophene) used as ion-to-electron transducer in all-solid-state ion-selective electrodes, Sensor. Actuator. B Chem. 82 (2002) 7–13, https://doi.org/10.1016/S0925-4005(01)00983-2.

[20] J. Sutter, E. Lindner, R.E. Gyurcsányi, E. Pretsch, A polypyrrole-based solid-contact Pb2+-selective PVC-membrane electrode with a nanomolar detection limit, Anal. Bioanal. Chem. 380 (2004) 7–14, https://doi.org/10.1007/s00216-004-2737-4.

[21] K.Y. Chumbimuni-Torres, N. Rubinova, A. Radu, L.T. Kubota, E. Bakker, Solid contact potentiometric sensors for trace level measurements, Anal. Chem. 78 (2006) 1318–1322, https://doi.org/10.1021/ac050749y.

[22] T. Lindfors, Light sensitivity and potential stability of electrically conducting polymers commonly used in solid contact ion-selective electrodes, J. Solid State Electrochem. 13 (2009) 77–89, https://doi.org/10.1007/s10008-008-0561-z.

[23] H. Mei-rong, G.U. Guo-li, D. Yong-bo, F.U. Xiao-tian, L. Rong-gui, Advanced solid-contact ion selective electrode based on electrically conducting polymers, Chin. J. Anal. Chem. 40 (2012) 1454–1460, https://doi.org/10.1016/S1872-2040(11)60572-0.

[24] M. Najafi, L. Maleki, A.A. Rafati, Novel surfactant selective electrochemical sensors based on single walled carbon nanotubes, J. Mol. Liq. 159 (2011) 226–229, https://doi.org/10.1016/j.molliq.2011.01.013.

[25] G.A. Crespo, S. Macho, F.X. Rius, Ion-selective electrodes using carbon nanotubes as ion-to-electron transducers, Anal. Chem. 80 (2008) 1316–1322, https://doi.org/10.1021/ac071156l.

[26] J. Ampurdanés, G.A. Crespo, A. Maroto, M.A. Sarmentero, P. Ballester, F.X. Rius, Determination of choline and derivatives with a solid-contact ion-selective electrode based on octaamide cavitand and carbon nanotubes, Biosens. Bioelectron. 25 (2009) 344–349, https://doi.org/10.1016/j.bios.2009.07.006.

[27] E.J. Parra, G.A. Crespo, J. Riu, A. Ruiz, F.X. Rius, Ion-selective electrodes using multi-walled carbon nanotubes as ion-to-electron transducers for the detection of perchlorate, Analyst 134 (2009) 1905–1910, https://doi.org/10.1039/b908224g.

[28] G.A. Crespo, D. Gugsa, S. Macho, F.X. Rius, Solid-contact pH-selective electrode using multi-walled carbon nanotubes, Anal. Bioanal. Chem. 395 (2009) 2371–2376, https://doi.org/10.1007/s00216-009-3127-8.

[29] M. Ghaedi, M. Montazerozohori, R. Sahraei, Comparison of the influence of nanomaterials on response properties of copper selective electrodes, J. Ind. Eng. Chem. 19 (2013) 1356–1364, https://doi.org/10.1016/j.jiec.2012.12.040.

[30] S.S.M. Hassan, A.G. Eldin, A.E.G.E. Amr, M.A. Al-Omar, A.H. Kamel, N.M. Khalifa, Improved solid-contact nitrate ion selective electrodes based on multi-walled carbon nanotubes (MWCNTs) as an ion-to-electron transducer, Sensors 19 (2019) 3891, https://doi.org/10.3390/s19183891.

[31] F. Li, J. Ye, M. Zhou, S. Gan, Q. Zhang, D. Han, L. Niu, All-solid-state potassium-selective electrode using graphene as the solid contact, Analyst 137 (2012) 618, https://doi.org/10.1039/c1an15705a.

[32] Z.A. Boeva, T. Lindfors, Few-layer graphene and polyaniline composite as ion-to-electron transducer in silicone rubber solid-contact ion-selective electrodes, Sensor. Actuator. B Chem. 224 (2016) 624–631.

[33] M. Pięk, R. Piech, B. Paczosa-Bator, All-solid-state nitrate selective electrode with graphene/tetrathiafulvalene nanocomposite as high redox and double layer capacitance solid contact, Electrochim. Acta 210 (2016), https://doi.org/10.1016/j.electacta.2016.05.170.

[34] M. Fouskaki, N. Chaniotakis, Fullerene-based electrochemical buffer layer for ion-selective electrodes, Analyst 133 (2008) 1072–1075, https://doi.org/10.1039/b719759d.

[35] G.D. O'Neil, R. Buiculescu, S.P. Kounaves, N.A. Chaniotakis, Carbon-nanofiber-based nanocomposite membrane as a highly stable solid-state junction for reference electrodes, Anal. Chem. 83 (2011) 5749–5753, https://doi.org/10.1021/ac201072n.

[36] C. Jiang, Y. Yao, Y. Cai, J. Ping, All-solid-state potentiometric sensor using single-walled carbon nanohorns as transducer, Sensor. Actuator. B Chem. 283 (2019) 284–289, https://doi.org/10.1016/j.snb.2018.12.040.

str. 177

[37] T. Yin, T. Han, C. Li, W. Qin, J. Bobacka, Real-time monitoring of the dissolution of silver nanoparticles by using a solid-contact Ag+-selective electrode, Anal. Chim. Acta 1101 (2020) 50–57, https://doi.org/10.1016/j.aca.2019.12.022.

[38] E. Woźnica, M.M. Wójcik, M. Wojciechowski, J. Mieczkowski, E. Bulska, K. Maksymiuk, A. Michalska, Dithizone modified gold nanoparticles films for potentiometric sensing, Anal. Chem. 84 (2012) 4437–4442, https://doi.org/10.1021/ac300155f.

[39] M. Chen, M. Zhang, X. Wang, Q. Yang, M. Wang, G. Liu, L. Yao, An all-solid-state nitrate ion-selective electrode with nanohybrids composite films for in-situ soil nutrient monitoring, Sensors (2020) 20, https://doi.org/10.3390/s20082276.

[40] E. Jaworska, M. Wójcik, A. Kisiel, J. Mieczkowski, A. Michalska, Gold nanoparticles solid contact for ion-selective electrodes of highly stable potential readings, Talanta 85 (2011) 1986–1989, https://doi.org/10.1016/j.talanta.2011.07.049.

[41] L. Zhang, Z. Wei, P. Liu, An all-solid-state NO3- ion-selective electrode with gold nanoparticles solid contact layer and molecularly imprinted polymer membrane, PLoS One 15 (2020) 1–14, https://doi.org/10.1371/journal.pone.0240171.

[42] B. Paczosa-Bator, R. Piech, L. Cabaj, K. Słupień, Platinum nanoparticles intermediate layer in solid-state selective electrodes, Analyst 137 (2012) 5272–5277.

[43] B. Paczosa-Bator, R. Piech, C. Wardak, L. Cabaj, Application of graphene supporting platinum nanoparticles layer in electrochemical sensors with potentiometric and voltammetric detection, Ionics 24 (2018) 2455–2464, https://doi.org/10.1007/s11581-017-2356-7.

[44] E. Jaworska, A. Kisiel, K. Maksymiuk, A. Michalska, Lowering the resistivity of polyacrylate ion-selective membranes by platinum nanoparticles addition, Anal. Chem. 83 (2011) 438–445, https://doi.org/10.1021/ac1019864.

[45] Y. Liu, Y. Liu, R. Yan, Y. Gao, P. Wang, Bimetallic AuCu nanoparticles coupled with multi-walled carbon nanotubes as ion-to-electron transducers in solid-contact potentiometric sensors, Electrochim. Acta 331 (2020) 135370, https://doi.org/10.1016/j.electacta.2019.135370.

[46] I. Khan, K. Saeed, I. Khan, Nanoparticles: properties, applications and toxicities, Arab. J. Chem. 12 (2019) 908–931, https://doi.org/10.1016/j.arabjc.2017.05.011.

[47] Y. Momma, G. Gal, N. Lorner, I. Bar, A simple strategy for enhanced production of nanoparticles by laser ablation in liquids, Nanotechnology 31 (2020), https://doi.org/10.1088/1361-6528/ab78ec.

[48] Y.V. Petrov, V.A. Khokhlov, V.V. Zhakhovsky, N.A. Inogamov, Laser ablation in liquid, J. Phys. Conf. Ser. 1556 (2020), https://doi.org/10.1088/1742-6596/1556/1/012002.

[49] H. Zeng, W. Cai, Y. Li, J. Hu, P. Liu, Composition/structural evolution and optical properties of ZnO/Zn nanoparticles by laser ablation in liquid media, J. Phys. Chem. B 109 (2005) 18260–18266, https://doi.org/10.1021/jp052258n.

[50] V. Amendola, M. Meneghetti, Laser ablation synthesis in solution and size manipulation of noble metal nanoparticles, Phys. Chem. Chem. Phys. 11 (2009) 3805–3821, https://doi.org/10.1039/b900654k.

[51] H. Naser, M.A. Alghoul, M.K. Hossain, N. Asim, M.F. Abdullah, M.S. Ali, F. G. Alzubi, N. Amin, The role of laser ablation technique parameters in synthesis of nanoparticles from different target types, J. Nanoparticle Res. 21 (2019), https://doi.org/10.1007/s11051-019-4690-3.

[52] L. Kroe, M. Šprung, T. Rončević, A. Maravić, V.Č. Čulić, D. Blažeka, N. Krstulović, I. Aviani, Probing the mode of antibacterial action of silver nanoparticles synthesized by laser ablation in water: what fluorescence and AFM data tell us, Nanomaterials 10 (2020) 1–20, https://doi.org/10.3390/nano10061040.

[53] F. Mafune, J. Kohno, Y. Takeda, T. Kondow, Formation of gold nanoparticles by laser ablation in aqueous solution of surfactant, J. Phys. Chem. B 105 (2001) 5114–5120, https://doi.org/10.1021/jp0037091.

[54] L. Torrisi, A. Torrisi, Laser ablation parameters influencing gold nanoparticle synthesis in water, Radiat. Eff. Defect Solid 173 (2018) 729–739, https://doi.org/10.1080/10420150.2018.1528598.

[55] G.A. Martinez-Cammon, N. Nino-Martinez, F. Martinez-Gutierrez, J.R. Martinez-Mendoza, R. Ruiz, Synthesis and antibacterial activity of silver nanoparticles with different sizes, J. Nanoparticle Res. 10 (2008) 1343–1348.

[56] C.G. Moura, R.S.F. Pereira, M. Andritschky, A.L.B. Lopes, J.P.F. de Grilo, R.M. do Nascimento, F.S. Silva, Effects of laser fluence and liquid media on preparation of small Ag nanoparticles by laser ablation in liquid, Opt Laser. Technol. 97 (2017) 20–28, https://doi.org/10.1016/j.optlastec.2017.06.007.

[57] F. Mafuné, J.Y. Kohno, Y. Takeda, T. Kondow, H. Sawabe, Formation and size control of silver nanoparticles by laser ablation in aqueous solution, J. Phys. Chem. B 104 (2000) 9111–9117, https://doi.org/10.1021/jp001336y.

[58] A.J. Mulder, R.D. Tilbury, P.J. Wright, T. Becker, M. Massi, M.A. Buntine, Laser-based formation of copper nanoparticles in aqueous solution: optical properties,

[59] particle size distributions, and formation kinetics, Aust. J. Chem. 70 (2017) 1212–1218, https://doi.org/10.1071/CH17363.

[59] S. Moniri, M. Ghoranneviss, M.R. Hantehzadeh, M.A. Asadabad, Synthesis and optical characterization of copper nanoparticles prepared by laser ablation, Bull. Mater. Sci. 40 (2017) 37–43, https://doi.org/10.1007/s12034-016-1348-y.

[60] F. Mafuné, J.Y. Kohno, Y. Takeda, T. Kondow, Formation of stable platinum nanoparticles by laser ablation in water, J. Phys. Chem. B 107 (2003) 4218–4223, https://doi.org/10.1021/jp021580k.

[61] N. Krstulović, I. Capan, Synthesis of Al-doped ZnO nanoparticles by laser ablation of ZnO:Al2O3 target in water, Mater. Res. Express 4 (2017), https://doi.org/10.1088/2053-1591/aa896d.

[62] C. Yao, W. Chen, L. Li, K. Jiang, Z. Hu, J. Lin, N. Xu, J. Sun, J. Wu, ZnO:Au nanocomposites with high photocatalytic activity prepared by liquid-phase pulsed laser ablation, Opt Laser. Technol. 133 (2021) 106533, https://doi.org/10.1016/j.optlastec.2020.106533.

[63] N. Krstulović, K. Salamon, O. Budimlija, J. Kovač, J. Dasović, P. Umek, I. Capan, Parameters optimization for synthesis of Al-doped ZnO nanoparticles by laser ablation in water, Appl. Surf. Sci. 440 (2018) 916–925, https://doi.org/10.1016/j.apsusc.2018.01.295.

[64] N. Krstulović, S. Miloševic, Drilling enhancement by nanosecond-nanosecond collinear dual-pulse laser ablation of titanium in vacuum, Appl. Surf. Sci. 256 (2010) 4142–4148, https://doi.org/10.1016/j.apsusc.2010.01.098.

[65] V. Srikant, D.R. Clarke, On the optical band gap of zinc oxide, J. Appl. Phys. 83 (1998) 5447–5451, https://doi.org/10.1063/1.367375.

[66] J.F. Pierson, A. Thobor-Keck, A. Billard, Cuprite, paramelaconite and tenorite films deposited by reactive magnetron sputtering, Appl. Surf. Sci. 210 (2003) 359–367, https://doi.org/10.1016/S0169-4332(03)00108-9.

[67] M.A. Goodal, T.F. Qahtan, M.A. Dastageer, Y.W. Maganda, D.H. Anjum, Synthesis of Cu/Cu2O nanoparticles by laser ablation in deionized water and their annealing transformation into CuO nanoparticles, J. Nanosci. Nanotechnol. 13 (2013) 5759–5766.

[68] K. Kutasi, N. Krstulović, A. Jurov, K. Salamon, D. Popović, S. Miloševic, Controlling: the composition of plasma-activated water by Cu ions, Plasma Sources Sci. Technol. 30 (2021), https://doi.org/10.1088/1361-6595/abf078.

[69] A.A. Akl, Optical properties of crystalline and non-crystalline iron oxide thin films deposited by spray pyrolysis, Appl. Surf. Sci. 233 (2004) 307–319, https://doi.org/10.1016/j.apsusc.2004.03.265.

[70] Y. Wang, S. Lany, J. Ghanbaja, Y. Fagot-Revurat, Y.P. Chen, F. Soldera, D. Horwat, F. Mücklich, J.F. Pierson, Electronic structures of Cu2O, Cu4O3, and CuO: a joint experimental and theoretical study, Phys. Rev. B 94 (2016) 1–10, https://doi.org/10.1103/PhysRevB.94.245418.

[71] W. Lv, L. Li, Q. Meng, X. Zhang, Molybdenum-doped CuO nanosheets on Ni foams with extraordinary specific capacitance for advanced hybrid supercapacitors, J. Mater. Sci. 55 (2020) 2492–2502.

[72] T. Fujii, F.M.F. de Groot, G.A. Sawatzky, F.C. Voogt, T. Hibma, K. Okada, In situ XPS analysis of various iron oxide films grown by NO2-assisted molecular-beam epitaxy, Phys. Rev. B 59 (1999) 3195–3202.

[73] E. Bakker, E. Pretsch, P. Bühlmann, Selectivity of potentiometric ion sensors, Anal. Chem. 72 (2000) 1127–1133, https://doi.org/10.1021/ac9911146n.

[74] J. Ping, Y. Wang, J. Wu, Y. Ying, Development of an all-solid-state potassium ion-selective electrode using graphene as the solid-contact transducer, Electrochem. Commun. 13 (2011) 1529–1532, https://doi.org/10.1016/j.elecom.2011.10.018.

[75] B. Paczosa-Bator, L. Cabaj, M. Pięk, R. Piech, W.W. Kubiak, Carbon-supported platinum nanoparticle solid-state ion selective electrodes for the determination of potassium, Anal. Lett. 48 (2015) 2773–2785.

[76] Q. An, L. Jiao, F. Jia, J. Ye, F. Li, S. Gan, Q. Zhang, A. Ivaska, L. Niu, Robust single-piece all-solid-state potassium-selective electrode with monolayer-protected Au clusters, J. Electroanal. Chem. 781 (2016) 272–277, https://doi.org/10.1016/j.jelechem.2016.10.053.

[77] D. Kałuża, E. Jaworska, M. Mazur, K. Maksymiuk, A. Michalska, Multiwalled carbon nanotubes-poly(3-octylthiophene-2,5-diyl) nanocomposite transducer for ion-selective electrodes: Raman spectroscopy insight into the transducer/membrane interface, Anal. Chem. 91 (2019) 9010–9017, https://doi.org/10.1021/acs.analchem.9b01286.

[78] A. Radu, S. Anastasova-Ivanova, B. Paczosa-Bator, M. Danielewski, J. Bobacka, A. Lewenstam, D. Diamond, Diagnostic of functionality of polymer membrane-based ion selective electrodes by impedance spectroscopy, Anal. Methods 2 (2010) 1490–1498, https://doi.org/10.1039/c0ay00249f.

[79] E. Barsoukov, J.R. Macdonald (Eds.), Impedance Spectroscopy Theory, Experiment, and Applications, Second, A John Wiley & Sons, Inc., Publication, Hoboken, New Jersey, 2005.

13

str. 178

D9

SOLID STATE ION-SELECTIVE ELECTRODE BASED ON SILVER NANOPARTICLES

Solid state ion-selective electrode based on silver nanoparticles

Karolina Pietrzak[a, *], Nikša Krstulović[b], Cecylia Wardak[a], Szymon Malinowski[c]

[a] *Maria Curie-Sklodowska University, Faculty of Chemistry, Institute of Chemical Sciences, Department of Analytical Chemistry, Maria Curie-Sklodowska Sq. 3, 20-031 Lublin, Poland*
    ✉ *karolina.pietrzak@poczta.umcs.lublin.pl*
[b] *Institute of Physics, Bijenička cesta 46, 10 000 Zagreb, Croatia*
[c] *Lublin University of Technology, Faculty of Civil Engineering and Architecture, Nadbystrzycka 40, 20-618 Lublin, Poland*

Keywords

ion-selective electrodes
potassium
potentiometry
silver nanoparticles

Abstract

The research on the use of silver nanoparticles as an ion to electron transducer in ion-selective electrodes with solid contact sensitive to potassium ions was described. Silver nanoparticles were obtained using the laser ablation technique. Basic analytical parameters were determined for electrodes with two thicknesses of silver nanoparticles placed between the electrode material and the membrane. The obtained modified electrodes had a very good slope of the characteristic curve (56.16 mV dec^{-1}), fast response (< 6 s), good potential stability (0.32 mV h^{-1}), and long life time (> 5 months). In the case of modified electrodes, a significant improvement in the stability of the potential and an increase in life time compared to unmodified electrodes have been noticed.

1. Introduction

All modifications in the design of ion-selective electrodes are aimed at improving their most important analytical parameters, including increasing the slope of the calibration curves, extending the linearity ranges, and lowering the detection limit, which will enable the determination of ions at lower concentration levels. Apart from the above, a very important parameter, which has been improved in recent years, characterizing the ion-selective electrodes is their selectivity, i.e., their ability to determine the selected main ion to which the ion-selective membrane is sensitive, in the presence of other interfering ions in the sample [1]. In addition, in the case of potentiometric sensors, the stability of the measured potential over time and under various, also changing environmental conditions (change of the light intensity, pH of the sample, presence of O_2 and CO_2) is very important, which favors their subsequent use in environmental analysis and measurements in the in situ environment. In addition to changing the active ingredients of ion-selective membranes, in the case of solid contact ion-selective

electrodes, intermediate layers and additional membrane components acting as solid contact are also used. Due to the elimination of the internal solution, these electrodes can be miniaturized, their shape can be modified, they are easier to transport and store, and they are much more mechanically resistant and durable [2].

Nanomaterials have found applications in many fields of science and industry. Recently, they have been successfully used to construct electrochemical sensors, including ion-selective electrodes. So far, carbon nanomaterials (carbon nano-tubes [3, 4], graphene [5], fullerenes [6], carbon black [7]) and metal nanopar-ticles (Ag [8], Au [9], Pt [10]) have already been used for this purpose.

2. Experimental

2.1 Reagents and chemicals

Ion selective membrane components were obtained from Aldrich (potassium ionophore-valinomycin, and low molecular weight poly(vinylchloride)) and Fluka (potassium tetrakis(*p*-chlorophenyl)borate and bis(2-ethylhexyl)sebacate). Salts of the highest purity available (pure pro analysis) and freshly deionized water were used for the preparation of aqueous ion solutions. These substances were mainly obtained from Fluka. Silver nanoparticles (precisely silver nanoparticles in water) were obtained using the laser ablation in liquid method at the Institute of Physics in Zagreb.

2.2 Instrumentation

All potentiometric measurements were made for a cell consisting of an Ag/AgCl reference electrode (Metrohm 6.0750.100) and the tested ion-selective electro-des (unmodified electrodes containing only the membrane and electrodes with an intermediate layer of silver nanoparticles of different thickness). The tests were carried out at room temperature in mixed solutions. A 16-channel data acquisition system (Lawson Labs, USA) connected to a computer was used to collect and process the results.

2.3 Preparation of solid contact ion-selective electrodes

The qualitative and quantitative composition of the membrane was as follows: 3% valinomycin, 1% potassium tetrakis(*p*-chlorophenyl)borate, 32% poly(vinyl-chloride), 64% bis(2-ethylhexyl)sebacate. Weighing amounts of 0.3 g of the ingredients were weighed, followed by the addition of 3 ml of tetrahydrofuran. Everything was homogenized with an ultrasonic water bath. The surface of glassy carbon electrodes with a diameter of 3 mm was polished with sandpaper and an alumina powder (size 0.3 μm). Then the electrodes were rinsed with distilled
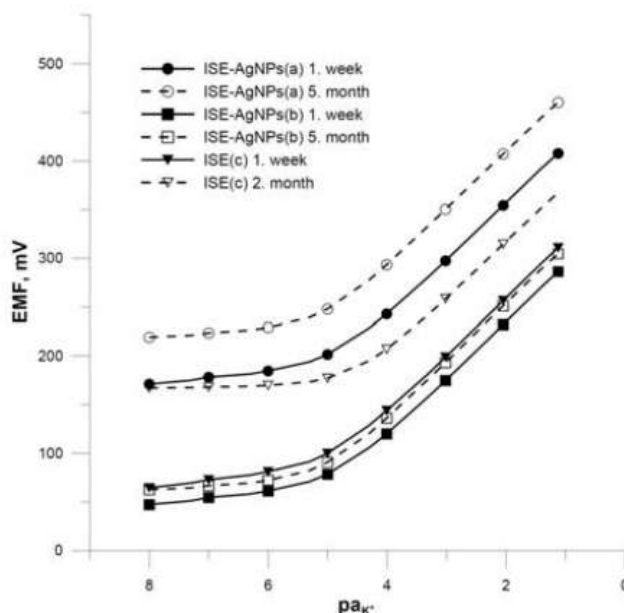
Fig. 1 Calibration curves of electrodes determined after 1 week and 5 months of electrode operation (for electrodes with silver nanoparticles).

water and additionally an ultrasonic water bath was used to get rid of the residual abrasive material. The electrodes were immersed in tetrahydrofuran to degrease the surface and allowed to dry. Small volumes of nanoparticles in water were then spotted (500 and 100 µL in total) and allowed to dry again. Finally, a membrane mix was spotted on the previously prepared electrodes (3×30 µL of the mixture with an interval of half an hour), and the next day, after complete drying, they were immersed in a conditioning solution (1×10^{-3} mol L^{-1} KNO$_3$). For comparison, apart from electrodes with intermediate layers of nanoparticles (500 µL – AgNPs (a), and 100 µL - AgNPs (b)), unmodified electrodes, containing only the ion-selective membrane (c) were also made.

3. Results and discussion

The cell electromotive force measurements were performed in KNO$_3$ solutions in the concentration range of 10^{-8}–10^{-1} mol L^{-1}. On the basis of the obtained calibration curves (Fig. 1), the values of the basic analytical parameters were determined: slopes and linear ranges of calibration curve as well as detection limits for all sensors (Table 1).

The reversibility of the potential of the tested sensors in 10^{-5}, 10^{-4}, and 10^{-3} mol L^{-1} solutions was also investigated. The numerical values including the average potentials and standard deviations for five repetitions are presented in Table 2. In each case, the values of the standard deviation were lower for the modified electrodes as compared to the unmodified ones, which proves the beneficial effect of silver nanoparticles intermediate layer on the reversibility of the electrode potential.

Table 1
Selected analytical parameters obtained for the tested electrodes (LOD – limit of detection; 5. month – for ISE-Ag(a) and ISE-Ag(b) electrodes; 2. month – for ISE(c)).

Parameter	ISE-Ag(a)	ISE-Ag(b)	ISE(c)
Slope / mV dec^{-1}			
1. week	−55.51	−56.16	−55.03
5./2. month	−55.17	−56.60	−54.79
Linear range / mol L^{-1}			
1. week	10^{-5}–10^{-1}	10^{-5}–10^{-1}	10^{-5}–10^{-1}
5./2. month	10^{-5}–10^{-1}	10^{-5}–10^{-4}	10^{-4}–10^{-1}
LOD /mol L^{-1}			
1. week	5.38×10^{-6}	5.17×10^{-6}	5.86×10^{-6}
5./2. month	7.58×10^{-6}	5.05×10^{-6}	1.93×10^{-5}
Short term potential drift / mV h^{-1}	1.85	0.32	5.17
Long term potential drift / mV day^{-1}	0.38	0.15	1.1
Response time / s	< 6	< 6	< 8

Table 2
Mean values of potentials (E) and standard deviations (SD) obtained for the tested electrodes for five measurements.

$c(K^+)$ / mol L^{-1}	Parameter	ISE-Ag(a)	ISE-Ag(b)	ISE(c)
10^{-5}	E / mV	220.25	78.12	123.44
	SD / mV	4.22	5.06	6.36
10^{-4}	E / mV	268.61	136.30	166.71
	SD / mV	0.93	1.52	2.68
10^{-3}	E / mV	324.45	182.23	223.66
	SD / mV	0.75	0.46	1.76

The selectivity of the tested electrodes was estimated thanks to the determination of the selectivity coefficients by the method of separate solutions. The selectivity coefficients obtained for selected metal cations (Na^+, Ca^{2+}, Mg^{2+}, Co^{2+}, Zn^{2+}, Cu^{2+}, Cd^{2+}, Pb^{2+}) were compared. For the ion sequences given above, the log K are respectively: for the ISE-AgNPs electrode (a) [−5.03; −4.30; −5.40; −4.08; −4.85; −4.82; −4.77; −5.06], for the ISE-Ag electrode (b) [−4.90; −4.37 −5.46; −3.86; −5.19; −5.18; −5.14; −5.46] and for the ISE electrode [−4.75; −4.76; −4.82; −3.75; −5.04; −5.11; −4.95; −5.13]. No significant influence of the modification of the electrodes on their selectivity was noticed, as the values of all obtained selectivity coefficients were comparable for all types of electrodes. Slightly better selectivity coefficients for the tested electrodes were obtained for Mg^{2+} and Co^{2+} cations.

The short and long term stability of the electrode potential was also investigated. The short-term stability of the potential was measured for 3 h in a KNO_3 solution with a concentration of 10^{-1} mol L^{-1}. Figure 2 shows a graph of electrode potential change versus time. Modified electrodes are characterized by better
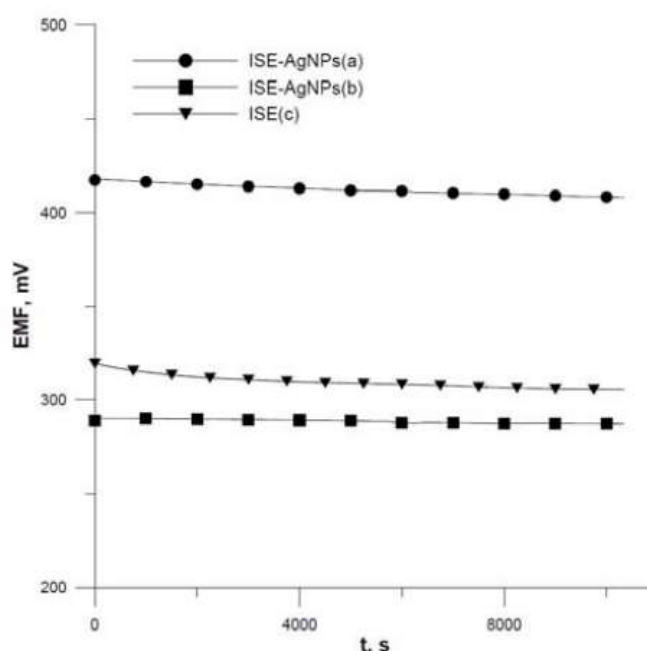
Fig. 2 Short-term stability of the electrode potential in a solution of 10^{-1} mol L^{-1} KNO$_3$.

potential stability, while the lowest potential change over time is shown by electrodes with a thinner layer of silver nanoparticles.

In order to determine the long-term stability of the electrode potential and their lifetime, electrodes were tested for 5 months. Figure 1 shows a comparison of calibration curves for each type of electrode determined for one week and five months old electrode. During this time, both the slope and the linearity range did not change much, and the modified electrodes continued to function properly. In the case of unmodified electrodes, the linearity range of the calibration curve decreased by an order of magnitude (from 10^{-5}–10^{-1} mol L^{-1} to 10^{-4}–10^{-1} mol L^{-1}). Moreover, modified electrodes showed much better long term potential stability. Change of E_{st}^{o} was much smaller for modified electrodes compared to unmodified ones. The electrodes with a thinner layer of nanoparticles showed the lowest long term potential drift over time.

4. Conclusions

Modification of the electrodes mainly influenced the improvement of the stability and reversibility of the electrode potential and their durability compared to electrodes without an intermediate layer. The electrodes with an additional layer of silver nanoparticles worked properly for over at least five months, showing an unchanged slope of the calibration curve and also maintaining the same linear range as at the beginning of measurements. In addition, they are simple and convenient to use and allow for quick measurements and results obtained.

Acknowledgments

References

[1]   Pretsch E.: The new wave of ion-selective electrodes. *TrAC, Trends Anal. Chem.* **26** (2007), 46–51.

[2]   Bobacka J., Ivaska A., Lewenstam A.: Potentiometric ion sensors. *Chem. Rev.* **108** (2008), 329–351.

[3]   Parra E.J., Crespo G.A., Riu J., Ruiz A., Rius F.X.: Ion-selective electrodes using multi-walled carbon nanotubes as ion-to-electron transducers for the detection of perchlorate. *Analyst* **134** (2009), 1905–1910.

[4]   Hassan S.S.M., Eldin A.G., Amr A.E.G.E., Al-Omar M.A., Kamel A.H., Khalifa N.M.: Improved solid-contact nitrate ion selective electrodes based on multi-walled carbon nanotubes (MWCNTs) as an Ion-to-electron transducer. *Sensors* **19** (2019), 3891.

[5]   Li F., Ye J., Zhou M., Gan S., Zhang Q., Han D., Niu L.: All-solid-state potassium-selective electrode using graphene as the solid contact. *Analyst* **137** (2012), 618–623.

[6]   Fouskaki M., Chaniotakis N.: Fullerene-based electrochemical buffer layer for ion-selective electrodes. *Analyst* **133** (2008), 1072–1075.

[7]   Paczosa-Bator B.: All-solid-state selective electrodes using carbon black. *Talanta* **93** (2012), 424–427.

[8]   Qi L., Jiang T., Liang R., Qin W.: Polymeric membrane ion-selective electrodes with anti-biofouling properties by surface modification of silver nanoparticles. *Sens. Actuators, B* **328** (2021), 129014.

[9]   Jaworska E., Wójcik M., Kisiel A., Mieczkowski J., Michalska A.: Gold nanoparticles solid contact for ion-selective electrodes of highly stable potential readings. *Talanta* **85** (2011), 1986–1989.

[10]   Paczosa-Bator B., Piech R., Wardak C., Cabaj L.: Application of graphene supporting platinum nanoparticles layer in electrochemical sensors with potentiometric and voltammetric detection. *Ionics* **24** (2018), 2455–2464.

D10

URANYL ION-SELECTIVE ELECTRODE WITH SOLID CONTACT

Uranyl ion-selective electrode with solid contact

Karolina Pietrzak*, Cecylia Wardak

Department of Analytical Chemistry, Institute of Sciences, Faculty of Chemistry, Maria Curie-Sklodowska University, Maria Curie-Sklodowska Sq. 3, 20-031 Lublin, Poland
✉ *karolina.pietrzak@poczta.umcs.lublin.pl*

Keywords

ion-selective electrode
solid contact
uranyl

Abstract

New all solid state uranyl ion-selective electrodes with low detection limits (7.1×10^{-7} mol L^{-1}), short response time, good selectivity and stable and reproducible potential were developed. Many types of electrodes with different active ingredient content in ion-selective membrane (bis(2,4,4-trimethylpentyl)phosphonium acid, Cyanex-272) were tested. As an additive, an ionic liquid 1-octyl-3-methyl-imidazole chloride was used. The optimal composition of the ion-selective membrane was chosen from all electrodes based on the determination and comparison of analytical parameters of the sensors.

1. Introduction

Uranium belongs to the group of hazardous elements. It is a highly harmful and radioactive element, toxic to humans and all living organisms [1, 2]. Inhaled with air, it has a particularly destructive effect on the kidneys, and as a result of accumulation in white blood cells, it can also cause impairment of the immune system [2]. Uranium occurs at several degrees of oxidation, however in aqueous solutions the most stable form is uranyl ion ($UO_2(II)$) [1, 2]. The presence of uranium in the environment is caused by, among others natural soil and rock erosion. Environmental pollution with this element is also constantly increasing due to human activity: coal combustion, uranium ore mining and processing, the arms industry, and the use of uranium as nuclear fuel in fission reactors [3]. It is very important to constantly monitor the concentration of uranium both in the natural environment in order to assess its state and safety (especially in the case of drinking water), as well as in all stages of processing processes associated with the nuclear industry to avoid the occurrence of nuclear pollution [1, 3].

Scientists have made many attempts to develop research methods to determine the content of uranyl compounds in liquid samples. Efforts were made to use many analytical methods for this purpose, including spectrophotometry,

plasma spectrometry, luminescence spectroscopy, voltammetry or chromatography methods [2].

Due to many advantages of potentiometric methods (among them lower costs, easier operation of devices, quick response and the ability to perform measurements in flow mode) [3], a number of potentiometric sensors have also been developed that could be successfully used in this type of research. The most popular potentiometric sensors include ion-selective electrodes (ISEs), which are characterized by low-energy consumption, small size and portability and are successfully widely used for the determination of both inorganic and organic ions in clinical analysis, process technology as well as in control the state of the natural environment [4, 5]. Removal of the internal solution containing the same analyte to which the electrode is sensitive resulted in the so-called solid contact ISEs, which are much smaller in size than their predecessors, are more convenient to use and more mechanically resistant. In this type of sensors, however, it is important to achieve satisfactory potential stability, which is necessary to obtain satisfactory results [5]. A very important part of ISEs is the ion-selective membrane, whose composition determines the analytical parameters of the sensors. Researchers are currently focusing on the production and testing of new substances that could be successfully used as membrane components and solid contacts that would allow to obtain new sensors with lower detection limits, longer lifetime and better potential stability, and to determine new, previously unattainable analytes [4].

As the active components of the membrane sensitive to uranyl ion, scientists have already used: Kryptofix 22DD (4,13-didecyl-1,7,10,16-tetraoxa-4,13-diaza-cyclooctadecane) [2], Cyanex extractants (bis(2,4,4-trimethylpentyl)phosphinic acid, bis(2,4,4-trimethylpentyl)monothiophosphinic acid, and bis(2,4,4-trimethylpentyl)dithiophosphinic) acid [3], DBBP (dibutyl butylphosphonate) and DOPP (di-*n*-octyl phenylphosphonate) [6], DMSO (dimethylsuphoxide) [7], TTPTP (5,6,7,8-tetrahydro-8-thioxopyrido[4',3',4,5]thieno[2,3-*d*]pyrimidine-4(3H)one) [8] or TEHP (tris(2-ethylhexyl)phosphate) and TPTU (*O*-(1,2-dihydro-2-oxo-1-pyridyl)-*N*,*N*,*N'*,*N'*-bis(tetra-methylene)uronium hexafluorophosphate) [9].

2. Experimental

2.1 Reagents and chemicals

This paper presents research on the design and properties of ion-selective electrodes with solid contact for the determination of uranyl ions. Bis(2,4,4-trimethylpentyl)phosphonium acid (Cyanex-272) was used as the active component of the membrane, which was described in the literature as a good uranyl extractant [10]. In order to ensure a constant potential of this electrode and reduce the electrode resistance, the ion-sensitive membrane was enriched with a few percent addition of 1-octyl-3-methylimidazole chloride ionic liquid.

Table 1

Quantitative and qualitative composition of electrode membranes: Cyanex-272 (bis(2,4,4-tri-methylpentyl)phosphoric acid), TBP (tri-*n*-butyl phosphate), and OMImCl (1-octyl-3-methyl-imidazole chloride).

Abbreviation of electrode	Membrane composition / % (*w/w*)			
	Cyanex-272	PVC	TBP	OMImCL
ISE-1	0.0	33	62.0	5
ISE-2	0.5	33	61.5	5
ISE-3	1.0	33	61.0	5
ISE-4	3.0	33	59.0	5
ISE-5	5.0	33	57.0	5
ISE-6	10.0	33	52.0	5

Several types of ion-selective electrodes were prepared using an Ag/AgCl electrode as an internal electrode, which differ in the quantitative and qualitative composition of the membranes. All compositions are listed in Table 1.

2.2 Instrumentation

Measurements were made at room temperature using a 16-channel data collection system (Lawson Labs. Inc. USA) coupled to a computer in solutions mixed with a mechanical stirrer. A silver / silver chloride electrode with double junction was used as the reference electrode.

3. Results and discussion

The effect of ion-selective membrane composition on the properties of the obtained potentiometric sensors was examined by determining their basic analytical parameters, including: slope of the electrode characteristics, detection limit, measuring range (concentration range in which the course of the electrode characteristics is rectilinear), pH range (in which it has no effect for electrode potential) and response time. The obtained values of the tested parameters are shown in Table 2.
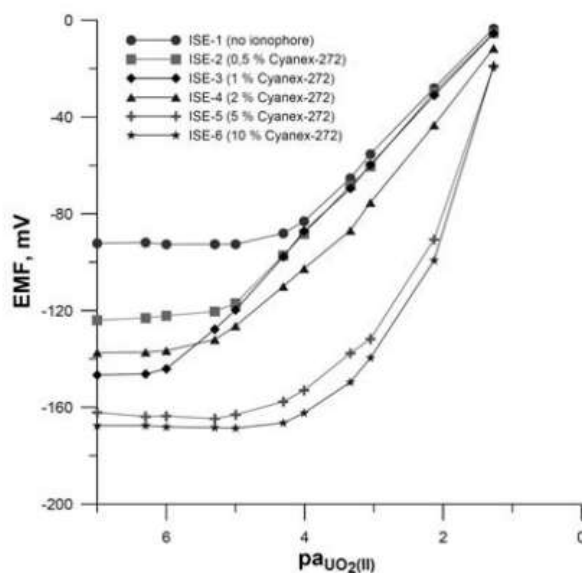
Figure 1 shows the calibration curves of the tested electrodes determined in $UO_2(NO_3)_2$ solutions in the concentration range $1 \times 10^{-7} - 1 \times 10^{-1}$ mol L^{-1}. As it can be seen in Fig. 1 and Table 2 all electrodes were sensitive to uranyl ions, but in different extend. The best response exhibited ISE-3 containing 1% (*w/w*) of ionophore. Increasing the ionophore content in the membrane shortened the linearity range of the calibration curve and its supernenstian slope.

The selectivity of the tested electrodes was estimated by determining the selectivity coefficients in relation to interfering ions. For this purpose, the separate solution method was used (extrapolating response curves to $a_i = a_j = 1$ mol L^{-1}). Comparison of ISE-1 and ISE-3 electrode selectivity is shown in Fig. 2.

Table 2
Selected parameters and their determined values of tested ion selective electrodes.

Abbreviation of electrode	Slope / mV/$pa(UO_2^{2+})$	Detection limit / mol L^{-1}	Linear range / mol L^{-1}	Response time / s	pH range
ISE-1	29.7	2.5×10^{-5}	$5\times10^{-5}-1\times10^{-1}$	5–8	2.8–4.2
ISE-2	29.2	6.5×10^{-6}	$1\times10^{-5}-1\times10^{-1}$	5–8	2.5–6.0
ISE-3	29.8	7.1×10^{-7}	$1\times10^{-5}-1\times10^{-1}$	5–8	2.4–6.0
ISE-4 (I)	35.7	3.1×10^{-6}	$5\times10^{-4}-1\times10^{-1}$	5–8	n.d.
ISE-4 (II)	24.2	3.1×10^{-6}	$5\times10^{-6}-5\times10^{-4}$	5–8	n.d.
ISE-5 (I)	63.8	n.d.	$1\times10^{-3}-1\times10^{-1}$	5–10	n.d.
ISE-5 (II)	23.4	n.d.	$5\times10^{-5}-1\times10^{-3}$	5–10	n.d.
ISE-6 (I)	73.3	n.d.	$1\times10^{-3}-1\times10^{-1}$	5–10	n.d.
ISE-6 (II)	22.2	n.d.	$5\times10^{-5}-1\times10^{-3}$	5–10	n.d.

Fig. 1 Calibration curves of the tested electrodes obtained in $UO_2(NO_3)_2$ solutions in the concentration range from 1×10^{-7} to 1×10^{-1} mol L^{-1}.
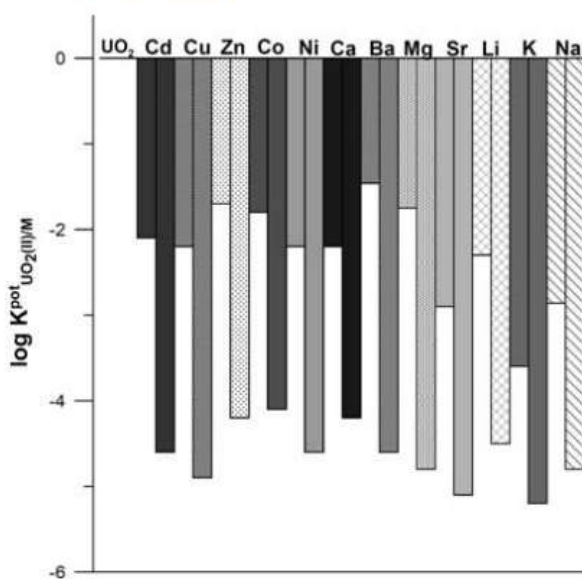
Fig. 2 Comparison of selectivity coefficients (log $K^{pot}(UO_2(II))$/M) for electrodes ISE-1 (1st column) and ISE-3 (2nd column).
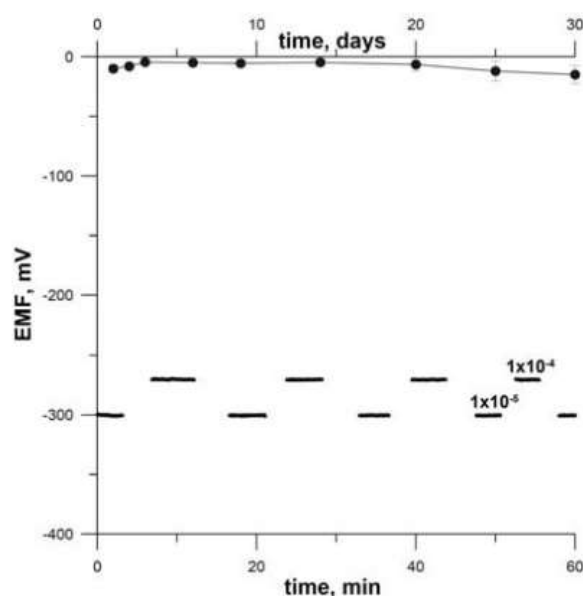
Fig. 3 Stability (●), reproducibility and reversibility (–) of the potential of ISE-3. Standard deviations given on the plot are determined for the same three ISE-3.

In order to examine the reversibility of the potential of the tested electrodes, potential measurements were made alternately in solutions 1×10^{-4} mol L^{-1} and 1×10^{-5} mol L^{-1} of $UO_2(NO_3)_2$. The recorded potential readings are shown in Fig. 3. Long-term potential stability and sensor reproducibility were evaluated by determining the average value of the electrode potential in a 0.1 mol L^{-1} $UO_2(II)$ ion solution over time for three identical ISE-3. These measurements were made to observe changes in the potential of electrodes with the same concentration over a long period of time (30 days). Figure 3 shows the long-term potential stability and reproducibility determined for three identical sensors.

4. Conclusions

As a result of the tests, ion-selective electrode for the determination of uranyl ions was obtained which is easy to design and use. The best analytical parameters exhibited ISE-3 containing 1% ionophore in the ion-selective membrane. For this type of electrodes, the detection limit of 7.1×10^{-7} mol L^{-1}, linearity of the electrode calibration curve in the range 1×10^{-6}–1×10^{-1} mol L^{-1} and response time 5–8 s were obtained. In addition, the manufactured sensors also showed stable, reproducible and reversible potential, and very good selectivity in relation to the tested interferents.

References

[1]   Ansari R., Mosayebzadeh Z.: Construction of a new solid-state U(VI) ion-selective electrode based on polypyrrole conducting polymer. *J. Radioanal. Nucl. Chem.* **299** (2014), 1597–1605.

[2]   Ghanbari M., Rounaghi G.H., Ashraf N.: An uranyl solid state PVC membrane potentiometric sensor based on 4,13-didecyl-1,7,10,16-tetraoxa-4,13-diazacyclooctadecane and its application for environmental samples. *Int. J. Environ. Anal. Chem.* **97** (2017), 189–200.

[3]   Badr I.H.A., Zidan W.I., Akl Z.F.: Cyanex based uranyl sensitive polymeric membrane electrodes. *Talanta* **118** (2014), 147–155.

[4]   Bieg C., Fuchsberger K., Stelzle M.: Introduction to polymer-based solid-contact ion-selective electrodes: basic concepts, practical considerations, and current research topics. *Anal. Bioanal. Chem.* **409** (2017), 45–61.

[5]   Bobacka J., Ivaska A., Lewenstam A.: Potentiometric ion sensors. *Chem. Rev.* **108** (2008), 329–351.

[6]   Zidan W.I., Badr I.H.A., Akl Z.F.: Development of potentiometric sensors for the selective determination of UO_2^{2+} ions. *J. Radioanal. Nucl. Chem.* **303** (2015), 469–477.

[7]   Saleh M.B., Soliman E.M., Gaber A.A.A., Ahmed S.A.: Novel PVC membrane uranyl ion-selective sensor. *Sens. Actuators B* **114** (2006), 199–205.

[8]   Saleh M.B., Hassan S.S.M., Abdel A.A., Abdel N.A.: A novel uranyl ion-selective PVC membrane sensor based on 5,6,7,8-tetrahydro-8-thioxopyrido[4',3',4,5]thieno[2,3-*d*]pyrimidine-4(3H)one. *Sens. Actuators B* **94** (2003), 140–144.

[9]   Hassan S.S.M., Ali M.M., Attawiya A.M.Y.: PVC membrane based potentiometric sensors for uranium determination. *Talanta* **54** (2001), 1153–1161.

[10]   Prabhu D.R., Ansari S.A., Raut D.R., Murali M.S., Mohapatra P.K.: Extraction behaviour of dioxouranium(VI) cation by two phosphorous-based liquid cation-exchangers in room-temperature ionic liquids. *Sep. Sci. Technol.* **52** (2017), 2328–2337.

SUPLEMENT Z OŚWIADCZENIAMI WSPÓŁAUTORÓW

mgr Karolina Pietrzak
Katedra Chemii Analitycznej
Instytut Nauk Chemicznych
Wydział Chemii UMCS
pl. Marii Curie-Skłodowskiej 3, 20-031 Lublin
karolina.pietrzak@poczta.umcs.lublin.pl

Lublin, dnia 01.12.2022

Rada Naukowa Instytutu Chemii
Uniwersytetu Marii Curie-Skłodowskiej
w Lublinie

Oświadczenie o współautorstwie

Niniejszym oświadczam, że w pracach:

D1   K. Pietrzak, C. Wardak, R. Łyszczek, Solid contact nitrate ion-selective electrode based on cobalt(II) complex with 4,7-diphenyl-1,10-phenanthroline, Electroanalysis. 32 (2020) 724–731.

D2   K. Pietrzak, C. Wardak, Comparative study of nitrate all solid state ion-selective electrode based on multiwalled carbon nanotubes-ionic liquid nanocomposite, Sensors and Actuators B: Chemical. 348 (2021) 130720.

D3 C. Wardak, K. Pietrzak, Nitrate ion-selective electrodes – new constructions and applications in the monitoring of nitrate ions in environmental samples, Post-conference monograph Modern Problems and Solutions in Environmental Protection, Białystok 2021, 11-28, ISBN. 978-83-7431-692-1.

D4   K. Pietrzak, C. Wardak, S. Malinowski, Application of polyaniline nanofibers for the construction of nitrate all-solid-state ion-selective electrodes, Applied Nanoscience. 11(12) (2021) 2823-2835.

D5   K. Pietrzak, K. Morawska, S. Malinowski, C. Wardak, Chloride ion-selective electrode with solid-contact based on polyaniline nanofibers and multiwalled carbon nanotubes nanocomposite, Membranes. 12 (2022) 1150.

str. 194

D6   K. Pietrzak, C. Wardak, B. Cristóvão, Copper ion-selective electrodes based on newly synthesized salen-type Schiff bases and their complexes, Ionics. 28 (2022) 2423-2435.

D7   C. Wardak, K. Pietrzak, M. Grabarczyk, Ionic liquid-multiwalled carbon nanotubes nanocomposite based all solid state ion-selective electrode for the determination of copper in water samples, Water. 13 (2021) 2869.

D8   K. Pietrzak, N. Krstulović, D. Blažeka, J. Car, S. Malinowski, C. Wardak, Metal oxide nanoparticles as solid contact in ion-selective electrodes sensitive to potassium ions, Talanta. 243 (2022) 123335.

D9   K. Pietrzak, N. Krstulović, C. Wardak, S. Malinowski, Solid state Ion-selective electrode based on silver nanoparticles, Proceedings of the 17th International Students Conference "Modern Analytical Chemistry", Charles University, Prague 2021, 85-90, ISBN 978-80-7444-089-2.

D10   K. Pietrzak, C. Wardak, Uranyl ion-selective electrode with solid contact, Proceedings of the 16th International Students Conference "Modern Analytical Chemistry", Charles University, Prague 2020, 45-50, ISBN 978-80-7444-079-3.

mój udział polegał na:

- opracowywaniu koncepcji prac badawczych,

- wykonywaniu elektrod do badań,

- wykonaniu całości/większości prac badawczych obejmujących pomiary potencjometryczne oraz całości prac badawczych obejmujących pomiary chronopotencjometryczne i impedancyjne,

- interpretacji otrzymanych wyników,

- napisaniu całości bądź przeważającej części manuskryptu,

- dokonaniu poprawek do manuskryptów na podstawie otrzymanych recenzji i udział w przygotowywaniu odpowiedzi na pytania recenzentów.

Karolina Pietrzak

podpis

dr hab. Cecylia Wardak, prof. UMCS
Katedra Chemii Analitycznej
Instytut Nauk Chemicznych
Wydział Chemii UMCS
pl. Marii Curie-Skłodowskiej 3, 20-031 Lublin
cecylia.wardak@mail.umcs.pl

Rada Naukowa Instytutu Chemii
Uniwersytetu Marii Curie-Skłodowskiej
w Lublinie

Oświadczenie o współautorstwie

Niniejszym oświadczam, że w pracach:

D1   K. Pietrzak, C. Wardak, R. Łyszczek, Solid contact nitrate ion-selective electrode based on cobalt(II) complex with 4,7-diphenyl-1,10-phenanthroline, Electroanalysis. 32 (2020) 724–731.

D2   K. Pietrzak, C. Wardak, Comparative study of nitrate all solid state ion-selective electrode based on multiwalled carbon nanotubes-ionic liquid nanocomposite, Sensors and Actuators B: Chemical. 348 (2021) 130720.

D3 C. Wardak, K. Pietrzak, Nitrate ion-selective electrodes – new constructions and applications in the monitoring of nitrate ions in environmental samples, Post-conference monograph Modern Problems and Solutions in Environmental Protection, Białystok 2021, 11-28, ISBN. 978-83-7431-692-1.

D4   K. Pietrzak, C. Wardak, S. Malinowski, Application of polyaniline nanofibers for the construction of nitrate all-solid-state ion-selective electrodes, Applied Nanoscience. 11(12) (2021) 2823-2835.

D5   K. Pietrzak, K. Morawska, S. Malinowski, C. Wardak, Chloride ion-selective electrode with solid-contact based on polyaniline nanofibers and multiwalled carbon nanotubes nanocomposite, Membranes. 12 (2022) 1150.

D6   K. Pietrzak, C. Wardak, B. Cristóvão, Copper ion-selective electrodes based on newly synthesized salen-type Schiff bases and their complexes, Ionics. 28 (2022) 2423-2435.

D7   C. Wardak, K. Pietrzak, M. Grabarczyk, Ionic liquid-multiwalled carbon nanotubes nanocomposite based all solid state ion-selective electrode for the determination of copper in water samples, Water. 13 (2021) 2869.

D8   K. Pietrzak, N. Krstulović, D. Blažeka, J. Car, S. Malinowski, C. Wardak, Metal oxide nanoparticles as solid contact in ion-selective electrodes sensitive to potassium ions, Talanta. 243 (2022) 123335.

D9   K. Pietrzak, N. Krstulović, C. Wardak, S. Malinowski, Solid state Ion-selective electrode based on silver nanoparticles, Proceedings of the 17th International Students Conference "Modern Analytical Chemistry", Charles University, Prague 2021, 85-90, ISBN 978-80-7444-089-2.

D10   K. Pietrzak, C. Wardak, Uranyl ion-selective electrode with solid contact, Proceedings of the 16th International Students Conference "Modern Analytical Chemistry", Charles University, Prague 2020, 45-50, ISBN 978-80-7444-079-3.

mój udział polegał na:

- opiece merytorycznej podczas planowania oraz realizacji prac badawczych,

- udziale w interpretacji oraz dyskusji wyników badań,

- nadzorze merytorycznym nad treścią manuskryptów,

- udziale w odpowiadaniu na pytania recenzentów.

Cecylia Wode

podpis

dr hab. Renata Łyszczek, prof. UMCS
Katedra Chemii Ogólnej, Koordynacyjnej i Krystalografii
Instytut Nauk Chemicznych
Wydział Chemii UMCS
pl. Marii Curie-Skłodowskiej 2, 20-031 Lublin
renata.lyszczek@mail.umcs.pl

Rada Naukowa Instytutu Chemii
Uniwersytetu Marii Curie-Skłodowskiej
w Lublinie

Oświadczenie o współautorstwie

Niniejszym oświadczam, że w pracy:

D1   K. Pietrzak, C. Wardak, R. Łyszczek, Solid contact nitrate ion-selective electrode based on cobalt(II) complex with 4,7-diphenyl-1,10-phenanthroline, Electroanalysis. 32 (2020) 724–731.

mój udział polegał na:

- syntezie substancji aktywnej – kompleks Co(II) z 4,7-difenylo-1,10-fenantroliną;

- wykonaniu badań dotyczących określenia struktury substancji aktywnej i pomoc w interpretacji ich wyników.

podpis

dr Szymon Malinowski
Wydział Budownictwa i Architektury
Politechnika Lubelska
Nadbystrzycka 40, 20-618 Lublin
s.malinowski@pollub.pl

Lublin, dnia 28.11.2022

**Rada Naukowa Instytutu Chemii
Uniwersytetu Marii Curie-Skłodowskiej
w Lublinie**

Oświadczenie o współautorstwie

Niniejszym oświadczam, że w pracach:

D4   K. Pietrzak, C. Wardak, S. Malinowski, Application of polyaniline nanofibers for the construction of nitrate all-solid-state ion-selective electrodes, Applied Nanoscience. 11(12) (2021) 2823-2835.

D5   K. Pietrzak, K. Morawska, S. Malinowski, C. Wardak, Chloride ion-selective electrode with solid-contact based on polyaniline nanofibers and multiwalled carbon nanotubes nanocomposite, Membranes. 12 (2022) 1150.

D7   K. Pietrzak, N. Krstulović, D. Blažeka, J. Car, S. Malinowski, C. Wardak, Metal oxide nanoparticles as solid contact in ion-selective electrodes sensitive to potassium ions, Talanta. 243 (2022) 123335.

D8   K. Pietrzak, N. Krstulović, C. Wardak, S. Malinowski, Solid state Ion-selective electrode based on silver nanoparticles, Proceedings of the 17th International Students Conference "Modern Analytical Chemistry", Charles University, Prague 2021, 85-90, ISBN 978-80-7444-089-2.

mój udział polegał na:

-syntezie nanowłókien polianiliny, wykonaniu badań wstępnych dotyczących identyfikacji nanowłókien,

- wykonaniu pomiarów metodą FTIR,

- pomocy w interpretacji wyników uzyskanych metodą FTIR.

....
podpis

lic Klaudia Morawska
Katedra Chemii Analitycznej
Instytut Nauk Chemicznych
Wydział Chemii UMCS
pl. Marii Curie-Skłodowskiej 3, 20-031 Lublin

Lublin, dnia 29.11.2022

Rada Naukowa Instytutu Chemii
Uniwersytetu Marii Curie-Skłodowskiej
w Lublinie

Oświadczenie o współautorstwie

Niniejszym oświadczam, że w pracach:

D5   K. Pietrzak, K. Morawska, S. Malinowski, C. Wardak, Chloride ion-selective electrode with solid-contact based on polyaniline nanofibers and multiwalled carbon nanotubes nanocomposite, Membranes. 12 (2022) 1150.

mój udział polegał na:

- wykonaniu oznaczenia jonów chlorkowych metodą Mohra.

Klaudia Morawska
....
podpis

str. 200

Lublin, dnia 12.10.2022r

dr hab. Beata Cristóvao, prof. UMCS
Katedra Chemii Ogólnej, Koordynacyjnej I Krystalografii
Instytut Nauk Chemicznych
Wydział Chemii UMCS
pl. Marii Curie-Skłodowskiej 2, 20-031 Lublin
beata.cristovao@mail.umcs.pl

**Rada Naukowa Instytutu Chemii
Uniwersytetu Marii Curie-Skłodowskiej
w Lublinie**

Oświadczenie o współautorstwie

Niniejszym oświadczam, że w pracy:

D6   K. Pietrzak, C. Wardak, B. Cristóvão, Copper ion-selective electrodes based on newly synthesized salen-type Schiff bases and their complexes, Ionics. (2022).

mój udział polegał na:

- syntezie zasad Schiffa i ich kompleksów wykorzystywanych w pracy jako substancje aktywne.

Beata Cristóvão

podpis

str. 201

Lublin, dnia 21.09.2022

prof. dr hab. Małgorzata Grabarczyk
Katedra Chemii Analitycznej
Instytut Nauk Chemicznych
Wydział Chemii UMCS
pl. Marii Curie-Skłodowskiej 3, 20-031 Lublin
małgorzata.grabarczyk@mail.umcs.pl

Rada Naukowa Instytutu Chemii
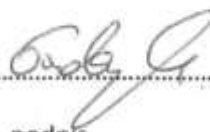Uniwersytetu Marii Curie-Skłodowskiej
w Lublinie

Oświadczenie o współautorstwie

Niniejszym oświadczam, że w pracy:

D7   C. Wardak, K. Pietrzak, M. Grabarczyk, Ionic liquid-multiwalled carbon nanotubes nanocomposite based all solid state ion-selective electrode for the determination of copper in water samples, Water. 13 (2021) 2869.

mój udział polegał na:

- pomocy w przygotowaniu elektrod.

....
podpis

Zagreb, date 1.9.2022.

doc. dr Nikša Krstulović
Institute of Physics, Bijenicka cesta 46
10 000, Zagreb, Croatia
+385 1 469 8803
niksak@ifs.hr

Scientific Council of the Institute of Chemistry

Maria Curie-Sklodowska University

in Lublin

Declaration of co-authorship

I hereby declare that in the work:

D8   K. Pietrzak, N. Krstulović, D. Blažeka, J. Car, S. Malinowski, C. Wardak, Metal oxide nanoparticles as solid contact in ion-selective electrodes sensitive to potassium ions, Talanta. 243 (2022) 123335.

D9   K. Pietrzak, N. Krstulović, C. Wardak, S. Malinowski, Solid state Ion-selective electrode based on silver nanoparticles, Proceedings of the 17th International Students Conference "Modern Analytical Chemistry", Charles University, Prague 2021, 85-90, ISBN 978-80-7444-089-2.

my participation consisted in:

- development of a part of the research concept,

- synthesis and study of nanoparticles, interpretation of part of the results,

- writing part of the manuscript.

signature

str. 203

Zagreb, date 1.9.2022.

dr Damjan Blažeka
Institute of Physics, Bijenicka cesta 46
10 000, Zagreb, Croatia
+385 1 469 8803
dblazeka@ifs.hr

Scientific Council of the Institute of Chemistry
Maria Curie-Sklodowska University
in Lublin

Declaration of co-authorship

I hereby declare that in the work:

D8   K. Pietrzak, N. Krstulović, D. Blažeka, J. Car, S. Malinowski, C. Wardak, Metal oxide nanoparticles as solid contact in ion-selective electrodes sensitive to potassium ions, Talanta. 243 (2022) 123335.

my task consisted in:

- participation in synthesis of nanoparticles and their characteristics.

Damjan Blažeka

signature

mgr Julio Car
Institute of Physics, Bijenicka cesta 46
10 000, Zagreb, Croatia
+385 1 469 8803
jcar@ifs.hr

Zagreb, date
01.09 2022.

Scientific Council of the Institute of Chemistry

Maria Curie-Sklodowska University

in Lublin

Declaration of co-authorship

I hereby declare that in the work:

D6   K. Pietrzak, N. Krstulović, D. Blažeka, J. Car, S. Malinowski, C. Wardak, Metal oxide nanoparticles as solid contact in ion-selective electrodes sensitive to potassium ions, Talanta. 243 (2022) 123335.

my task consisted in:

- participation in synthesis of nanoparticles and their characteristics.

signature

DOROBEK NAUKOWY AUTORA

Wykaz wszystkich publikacji naukowych:

1) K. Tyszczuk-Rotko, **K. Pietrzak**, A. Sasal, *Adsorptive stripping voltammetric method for the determination of caffeine at integrated three-electrode screen-printed sensor with carbon/carbon nanofibers working electrode*, Adsorption 25 (2019) 913–921, https://doi.org/10.1007/s10450-019-00116-3. (IF$_{2019}$ = 1,949; punktacja MEiN: 70)

2) [**D1**] **K. Pietrzak**, C. Wardak, R. Łyszczek, *Solid contact nitrate ion-selective electrode based on cobalt(II) complex with 4,7-diphenyl-1,10-phenanthroline*, Electroanalysis 32 (2020) 724-731, DOI: 10.1002/elan.201900462. (IF$_{2020}$ = 3,223; punktacja MEiN: 70)

3) S. Malinowski, C. Wardak, J. Jaroszyńska-Wolińska, P. A. F. Herbert, **K. Pietrzak**, M. Malinowski, *New electrochemical laccase-based biosensor for dihydroxybenzene isomers determination in real water samples*, Journal of Water Process Engineering 34 (2020) 101150, https://doi.org/10.1016/j.jwpe.2020.101150. (IF$_{2020}$ = 5,485; punktacja MEiN: 100)

4) S. Malinowski, C. Wardak, **K. Pietrzak**, *Effect of multi-walled carbon nanotubes on analytical parameters of laccase-based biosensors received by soft plasma polymerization technique*, IEEE Sensors Journal 20 (2020) 8423-8428. https://doi.org/10.1109/JSEN.2020.2982742. (IF$_{2020}$ = 3,301; punktacja MEiN: 100)

5) **K. Pietrzak**, C. Wardak, *Characteristics of carbon nanomaterials and their application in the construction of potentiometric sensors – review*, Annales Universitatis Mariae Curie-Skłodowska Lublin – Polonia, Sectio AA, Vol. LXXIV, 2 (2019), 0.17951/aa.2019.74.2.41-52. (punktacja MEiN: 20)

6) [**D2**] **K. Pietrzak**, C. Wardak, *Comparative study of nitrate all solid state ion-selective electrode based on multiwalled carbon nanotubes-ionic liquid nanocomposite*, Sensors & Actuators: B. Chemical 348 (2021) 130720. https://doi.org/10.1016/j.snb.2021.130720. (IF$_{2021}$ = 9,221; punktacja MEiN: 140)

7) [D7] C. Wardak, **K. Pietrzak**, M. Grabarczyk, *Ionic Liquid-Multiwalled Carbon Nanotubes Nanocomposite Based All Solid State Ion-Selective Electrode for the Determination of Copper in Water Samples*, Water 13 (2021) 2869. https://doi.org/10.3390/w13202869. (IF$_{2021}$ = 3,530; punktacja MEiN: 100)

8) [D6] **K. Pietrzak**, C. Wardak, B. Cristóvão, *Copper ion-selective electrodes based on newly synthesized salen- type Schiff bases and their complexes*, Ionics 0123456789 (2022). https://doi.org/10.1007/s11581-022-04482-x. (IF$_{2021}$ = 2,961; punktacja MEiN: 70)

9) [D4] **K. Pietrzak**, C. Wardak, S. Malinowski, *Application of polyaniline nanofibers for the construction of nitrate all-solid-state ion-selective electrodes*, Applied Nanoscience (2021). https://doi.org/10.1007/s13204-021-02228-1. (IF$_{2021}$ = 3,869; punktacja MEiN: 100)

10) [D8] **K. Pietrzak**, N. Krstulović, D. Blažeka, J. Car, S. Malinowski, C. Wardak, *Metal oxide nanoparticles as solid contact in ion-selective electrodes sensitive to potassium ions*, Talanta 243 (2022) 123335. https://doi.org/10.1016/j.talanta.2022.123335. (IF$_{2021}$ = 6,556; punktacja MEiN: 100)

11) [D5] **K. Pietrzak**, K. Morawska, S. Malinowski, C. Wardak, *Chloride ion-selective electrode with solid-contact based on polyaniline nanofibers and multiwalled carbon nanotubes nanocomposite*, Membranes. 12 (2022) 1150. https://doi.org/10.3390/membranes12111150. (IF$_{2021}$ = 4,562; punktacja MEiN: 100)

Łączny IF zgodnie z rokiem opublikowania*: 44,657.

Łączna liczba punktów MEiN zgodnie z rokiem opublikowania*: 970.

* dla publikacji z roku 2022 – dane z roku poprzedniego.

Wykaz monografii i recenzowanych materiałów pokonferencyjnych:

1) M. Suljkanović, M. Grabarczyk, C. Wardak, M. Adamczyk, **K. Pietrzak**, *Electrochemical sensors as simple and cheap devices for rapid determination of various species in environmental samples*, ENVIRONMENTAL ENGINEERING - INŽENJERSTVO OKOLIŠA, Special Issue, Portable, affordable and simple analytical platforms, Vol. 6, Nr 1, July 2019, 1-6. ISSN 1849-4714 (Print), ISSN 1849-5079 (Online).

2) C. Wardak, **K. Pietrzak**, *Wpływ cieczy jonowej na właściwości elektrody jonoselektywnej czułej na jony Cu(II)*, Elektroliza – sensory i metody pomiarowe, Wydawnictwo Naukowe AKAPIT, Kraków 2019, str. 247-254, ISBN 978-83-65955-36-4.

3) **K. Pietrzak**, C. Wardak, *Zastosowanie nanomateriałów węglowych do konstrukcji elektrod jonoselektywnych ze stałym kontaktem*, w: Innowacje W Praktyce konferencja - warsztaty - wystawa - spotkania panelowe, wydawnictwo: Centrum Innowacji Naukowo-Edukacyjnych, Lublin, 4-5 kwietnia 2019, str. 158-159, ISBN 978-83-943796-5-0.

4) **K. Pietrzak**, C. Wardak, *Konstrukcja i właściwości jonoselektywnej elektrody ołowiowej typu solid contact*, w: Nauka i przemysł – lubelskie spotkania studenckie, Praca zbiorowa pod redakcją dr hab. Doroty Kołodyńskiej, str. 9-12, 2019, ISBN: 978-83-227-9220-9.

5) **K. Pietrzak**, C. Wardak, *Zastosowanie nanomateriałów węglowych w konstrukcji czujników potencjometrycznych*, str. 92-100, 2019, Oficyna Edukacyjna Krzysztof Pazdro Sp. z o.o., ISBN 978-83-7594-191-3 (Rozdział w monografii „Kwadrans Dla Chemii").

6) C. Wardak, **K. Pietrzak**, *All solid state ion-selective electrode for lead monitoring in the environment* in Eds. J. Karpińska, M. Bartoszewicz, R. Sawczuk; Modern problems and solutions in environmental protection, 2019 pp.110-115, University of Bialystok Press, ISBN 978-83-7431-615-6.

7) **K. Pietrzak**, C. Wardak: *Czujniki potencjometryczne w kontroli środowiska naturalnego, Nauka i praktyka w bezpieczeństwie pracy, środowisku i zarządzaniu*, Katowice 2019, Wyższa Szkoła Zarządzania Ochroną Pracy w Katowicach (WSZOP), str. 239-255, ISBN 978-83-61378-67-9.

8) **K. Pietrzak**, C. Wardak, S. Malinowski, J. Jaroszyńska-Wolińska, *Bioczujnik elektrochemiczny do oznaczania rezorcyny w obecności katecholu i hydrochinonu*, Praca zbiorowa pod redakcją L. Dawidowicz i T. Cłapy: Nauka dla środowiska Tom IV, Wydawnictwo Naukowe GSP, str. 119-129, 2020, Zgorzelec, ISBN 978-83-952571-2-4.

9) [**D10**] **K. Pietrzak**, C. Wardak, *Uranyl ion-selective electrode with solid contact*, Proceedings of the 16th International Students Conference "Modern Analytical Chemistry", Charles University, Prague 2020, 45-50, ISBN 978-80-7444-079-3.

10) **K. Pietrzak**, C. Wardak: *Wpływ modyfikacji membrany różnymi rodzajami nanorurek węglowych na parametry elektrod dedykowanych do oznaczania jonów azotanowych (V)*, Badania z zakresu nauk przyrodniczych – nowe trendy, Lublin 2020, Wydawnictwo Naukowe TYGIEL, str. 239-247, ISBN 978-83-66489-08-0.

11) C. Wardak, S. Malinowski, **K. Pietrzak**, J. Kosik, *Bioczujniki elektrochemiczne do jednoczesnego oznaczania izomerów dihydroksybenzenu*, Praca zbiorowa pod redakcją Z. Hubickiego; Nauka i Przemysł - metody spektroskopowe w praktyce, nowe wyzwania i możliwości, 2020, 144-153, Wyd. UMCS Lublin, ISBN. 978-83-227-93695.

12) **K. Pietrzak**, C. Wardak, B. Cristóvão, *Badania kompleksów miedzi z ligandami typu zasada Schiffa jako jonoforów na jony miedzi*, Praca zbiorowa pod redakcją Z. Hubickiego; Nauka i Przemysł - metody spektroskopowe w praktyce, nowe wyzwania i możliwości, 2020, 140-143, Wyd. UMCS Lublin, ISBN. 978-83-227-93695.

13) [**D9**] **K. Pietrzak**, N. Krstulović, C. Wardak, S. Malinowski, *Solid state Ion-selective electrode based on silver nanoparticles*, Proceedings of the 17th International Students Conference "Modern Analytical Chemistry", Charles University, Prague 2021, 85-90, ISBN 978-80-7444-089-2.

14) **K. Pietrzak**, C. Wardak, S. Malinowski, N. Krstulović, *Zastosowanie elektrochemicznej spektroskopii impedancyjnej do badania mechanizmu działania nanocząstek tlenków metali w elektrodach jonoselektywnych*, Praca zbiorowa pod redakcją Z. Hubickiego; Nauka i Przemysł - metody spektroskopowe w praktyce, nowe wyzwania i możliwości, 2021, 129-132, Wyd. UMCS Lublin, ISBN. 978-83-227-9503-3

15) C. Wardak, S. Malinowski, **K. Pietrzak**, J. Kosik, R. Sobkiewicz, *Zastosowanie nanomateriałów węglowych w konstrukcji bioczujników elektrochemicznych z enzymatyczną warstwą receptorową*, Praca zbiorowa pod redakcją Z. Hubickiego; Nauka i Przemysł - metody spektroskopowe w praktyce, nowe wyzwania i możliwości, 2021, 44-48, Wyd. UMCS Lublin, ISBN. 978-83-227-9504-0.

16) [**D3**] C. Wardak, **K. Pietrzak**, *Nitrate ion-selective electrodes – new constructions and applications in the monitoring of nitrate ions in environmental samples*, Post-conference monograph Modern Problems And Solutions In Environmental Protection, Białystok 2021, 11-28, ISBN. 978-83-7431-692-1

17) **K. Pietrzak**, C. Wardak, S. Malinowski, *Wpływ rodzaju domieszkowanego jonu na właściwości włókien polianilinowych oraz parametry analityczne elektrod jonoselektywnych*, Praca zbiorowa pod redakcją prof. dr hab. Doroty Kołodyńskiej; Nauka i Przemysł – lubelskie spotkania studenckie, 2022, 103-106, Wyd. UMCS Lublin, ISBN. 978-83-227-9603-0

18) C. Wardak, **K. Pietrzak**, *Azotanowe elektrody jonoselektywne z membraną modyfikowaną nanokompozytem - wpływ struktury nanokompozytu na właściwości elektrod*, Praca zbiorowa pod redakcją Z. Hubickiego; Nauka i Przemysł – metody spektroskopowe w praktyce, nowe wyzwania i możliwości, 2022, 320-323 Wyd. UMCS Lublin, ISBN 978-83-227-9602-3.

19) C. Wardak, **K. Pietrzak**, S. Malinowski, *Optymalizacja właściwości plazmy w konstrukcji bioczujników przeznaczonych do oznaczania dopaminy*, Praca zbiorowa pod redakcją Z. Hubickiego; Nauka i Przemysł – metody spektroskopowe w praktyce, nowe wyzwania i możliwości, 2022, 316-319 Wyd. UMCS Lublin, ISBN 978-83-227-9602-3

Udział w konferencjach krajowych:

Komunikaty ustne:

1) **K. Pietrzak***, *Krótka charakterystyka elektrod jonoselektywnych*, National Scientific Conference for PhD Students – 2nd edition, Kraków, 2.03.2019

2) **K. Pietrzak***, C. Wardak, *Zastosowanie nanomateriałów węglowych do konstrukcji elektrod jonoselektywnych ze stałym kontaktem*, VI Ogólnopolska Konferencja Naukowa Innowacje w Praktyce, Lublin, 4-5.04.2019

3) **K. Pietrzak***, C. Wardak, S. Malinowski, J. Jaroszyńska-Wolińska, *Bioczujnik elektrochemiczny do oznaczania rezorcyny w obecności katecholu i hydrochinonu*, VI Ogólnopolska Konferencja Młodych Naukowców, Poznań, 24-27.04.2019

4) **K. Pietrzak***, C. Wardak, *Konstrukcja, właściwości i zastosowanie elektrody jonoselektywnej ze stałym kontaktem czułej na jony ołowiu(II)*, Ogólnopolska Konferencja Naukowa Ochrona Środowiska – Rozwiązania I Perspektywy, Lublin, 17.05.2019

5) **K. Pietrzak***, C. Wardak, *Czujniki potencjometryczne w kontroli środowiska naturalnego*, VIII Konferencja Bezpieczeństwo Pracy - Środowisko - Zarządzanie, Szczyrk, 8-9.10.2019

6) **K. Pietrzak***, C. Wardak, Wpływ rodzaju nanorurek węglowych na parametry elektrod azotanowych, V Ogólnopolska Konferencja Naukowa Nanotechnologia wobec oczekiwań XXI w., Lublin, 13.12.2019

7) **K. Pietrzak***, C. Wardak, Wpływ stężenia substancji aktywnej w membranie na parametry analityczne elektrod uranylowych, VII Ogólnopolska konferencja naukowa Innowacje w Praktyce, Lublin online, 20.10.2020

8) **K. Pietrzak***, C. Wardak, S. Malinowski, Wpływ rodzaju domieszkowanego jonu na właściwości włókien polianilinowych oraz parametry analityczne elektrod jonoselektywnych, w których zostały one wykorzystane jako stały kontakt, X Ogólnopolskie Sympozjum „Nauka i przemysł – lubelskie spotkania studenckie", Lublin online, 27.06.2022r.

9) C. Wardak*, S. Malinowski, **K. Pietrzak**, J. Kosik, R. Sobkiewicz, Wykład pt.: Zastosowanie nanomateriałów *węglowych w konstrukcji bioczujników elektrochemicznych z enzymatyczną warstwą receptorową*, Nauka i Przemysł, Metody spektroskopowe w praktyce, nowe wyzwania i możliwości, Lublin online, 29-30.06.2021r.

10) C. Wardak*, **K. Pietrzak**, J. Lenik, Wykład pt.: *Zastosowanie materiałów kompozytowych w konstrukcji elektrod jonoselektywnych typu all solid state*, Fizykochemia granic faz - metody instrumentalne, Lublin, 23-26.08.2021

11) C. Wardak*, **K. Pietrzak**, Wykład pt.: *Azotanowe elektrody jonoselektywne z membraną modyfikowaną nankompozytem- wpływ struktury nanokompozytu na właściwości elektrod*, Nauka i Przemysł, Metody spektroskopowe w praktyce, nowe wyzwania i możliwości, Lublin online, 28-29.06.2022r.

12) C. Wardak*, **K. Pietrzak**, S. Malinowski, Wykład pt.: *Zastosowanie nanomateriałów polimerowych i ich kompozytów w konstrukcji elektrod jonoselektywnych ze stałym kontaktem*, 64. Zjazd PTChem, Lublin, 11-16.09.2022r.

Postery:

1) **K. Pietrzak***, Alicja Niczyporuk, *Sekret wiecznej młodości czy przekleństwo raka? Ile jeszcze tajemnic kryją w sobie przeciwutleniacze?* Zjazd Zimowy Sekcji Studenckiej PTChem, Kraków, 5.12.2015

2) **K. Pietrzak***, *Kawa – napój, który zachwycił świat*, Zjazd Zimowy Sekcji Studenckiej PTChem, Lublin, 17.12.2016

3) **K. Pietrzak***, *Kofeina – charakterystyka substancji*, Zjazd Zimowy Sekcji Studenckiej PTChem, Bydgoszcz, 9.12.2017

4) **K. Pietrzak***, *Woltamperometryczne metody oznaczania kofeiny*, Zjazd Zimowy Sekcji Studenckiej PTChem, Skorzęcin, 25.04.2018

5) **K. Pietrzak***, C. Wardak, *Elektroda jonoselektywna do oznaczania miedzi z membraną modyfikowaną nanorurkami węglowymi i cieczą jonową*, Zjazd Zimowy Sekcji Studenckiej PTChem, Warszawa, 8.12.2018

6) **K. Pietrzak***, *Oznaczanie jonów miedzi(II) za pomocą elektrod jonoselektywnych - przegląd metod*, National Scientific Conference for PhD Students – 2nd edition, Kraków, 2.03.2019

7) **K. Pietrzak***, *Zastosowanie elektrod jonoselektywnych w badaniu wód i ścieków*, XI Interdyscyplinarna Konferencja Naukowa TYGIEL, Lublin, 23-24.03.2019

8) **K. Pietrzak***, C. Wardak, *Zastosowanie nanomateriałów węglowych do konstrukcji czujników potencjometrycznych*, Zjazd Wiosenny Sekcji Studenckiej PTChem, Ustroń, 10-14.04.2019

9) **K. Pietrzak***, C. Wardak, *Konstrukcja i właściwości jonoselektywnej elektrody ołowiowej typu solid contact*, VII Ogólnopolskie Sympozjum Nauka i przemysł - lubelskie spotkania studenckie, Lublin, 24.06.2019

10) **K. Pietrzak***, C. Wardak, *Wpływ rodzaju elektrody wewnętrznej i jej modyfikacji na właściwości elektrod jonoselektywnych ze stałym kontaktem*, XVII Konferencja – Elektroanaliza w Teorii i Praktyce, Kraków online, 19-20.11.2020

11) **K. Pietrzak***, C. Wardak, S. Malinowski, N. Krstulović, *Zastosowanie elektrochemicznej spektroskopii impedancyjnej do badania mechanizmu działania nanocząstek tlenków metali w elektrodach jonoselektywnych*, IX Ogólnopolskie Sympozjum „Nauka i przemysł – lubelskie spotkania studenckie", Lublin online, 28.06.2021

12) **K. Pietrzak***, C. Wardak, S. Malinowski, *Zastosowanie modyfikowanych nanowłókien polianiliny w konstrukcji elektrod jonoselektywnych ze stałym kontaktem czułych na jony azotanowe(V)*, VIII Ogólnopolska konferencja naukowa Innowacje w Praktyce, Lublin online, 14.10.2021

13) C. Wardak*, S. Malinowski, **K. Pietrzak**, *Bioczujnik elektrochemiczny do oznaczania dopaminy z enzymatyczną warstwą receptorową otrzymaną metodą polimeryzacji plazmowej*, Fizykochemia granic faz – metody instrumentalne, Lublin, 13-17.05.2019

14) C. Wardak*, S. Malinowski, **K. Pietrzak**, *Wpływ modyfikacji elektrody podłożowej na rozdzielenie sygnałów izomerów dihydroksybenzenu rejestrowanych dla bioczujnika na*

bazie lakazy, XVII Konferencja – Elektroanaliza w Teorii i Praktyce, Kraków online, 19-20.11.2020

15) C. Wardak*, **K. Pietrzak**, A. Czaplicka, *Miedziowe elektrody jonoselektywne za stałym kontaktem na bazie wielościennych nanorurek węglowych i nanocząstek tlenku miedzi(II)*, Fizykochemia granic faz - metody instrumentalne, Lublin, 23-26.08.2021

16) C. Wardak*, **K. Pietrzak**, S. Malinowski, *Chlorkowe elektrody jonoselektywne ze stałym kontaktem na bazie nanokompozytu wielościennych nanorurek węglowych i nanowłókien polianiliny*, XI Polska Konferencja Chemii Analitycznej, PoKoChA 2022, Łódź, 19-23.06.2022

17) C. Wardak*, **K. Pietrzak**, J. Lenik, *Zastosowanie złotych mikroelektrod zespolonych w konstrukcji azotanowych elektrod jonoselektywnych typu all solid state*, XI Polska Konferencja Chemii Analitycznej, PoKoChA 2022, Łódź, 19-23.06.2022

18) C. Wardak*, **K. Pietrzak**, S. Malinowski, *Optymalizacja właściwości plazmy w konstrukcji bioczujników przeznaczonych do oznaczania dopaminy*, Nauka i Przemysł, Metody spektroskopowe w praktyce, nowe wyzwania i możliwości, Lublin, 28-29.06.2022

19) C. Wardak*, **K. Pietrzak**, N. Krstulović, S. Malinowski, *Właściwości potasowach elektrod jonoselektywnych ze stałym kontaktem otrzymanym z nanocząstek tlenku cynku*, 64. Zjazd PTChem, Lublin, 11-16.09.2022r.

Udział w konferencjach międzynarodowych:

Komunikaty ustne:

1) **K. Pietrzak***, C. Wardak, *Uranyl ion-selective electrode with solid contact*, 16th International Students Conference 'Modern Analytical Chemistry', Prague, Czech Republic, 17-18.09.2020

2) **K. Pietrzak***, N. Krstulović, C. Wardak, S. Malinowski, *Metal oxides nanoparticles as solid contact in ion-selective electrodes*, ElecNano9, Paris, France Online, 23-24.11.2020

3) **K. Pietrzak***, N. Krstulović, C. Wardak, S. Malinowski, *Solid state ion-selective electrode based on silver nanoparticles*, 17th International Students Conference 'Modern Analytical Chemistry', Prague, Czech Republic, 16-17.09.2021

4) **K. Pietrzak***, C. Wardak, S. Malinowski, M. Golonka, *The use of polyaniline nanofibers for the construction of ion-selective electrodes with solid contact*, 12th International Conference on "Instrumental Methods of Analysis" (IMA-2021) online, Thessaloniki, Grecja, 20-23.09.2021

5) **K. Pietrzak***, C. Wardak, S. Malinowski, *Influence of the doped ion on the properties of polyaniline nanofibers and the parameters of solid contact ion-selective electrodes based on them*, 1st IMYAC International Meeting for Young Analytical Chemists, Kraków online, 27-28.09.2021

6) **K. Pietrzak***, C. Wardak, S. Malinowski, *New nitrate and potassium electrodes useful for the analysis of agricultural samples*, XLV Międzynarodowe Seminarium Naukowo Techniczne „Chemistry for Agriculture", Karpacz, 21-24.11.2021

7) C. Wardak*, **K. Pietrzak**, *Nitrate-ion selective electrode based on ionic liquid carbon nanotubes nanocomposite – new cheap electrochemical device for monitoring of nitrate in water and plants*, XLIII Międzynarodowe Seminarium Naukowo-Techniczne „Chemistry for Agriculture", Karpacz, Poland, 25-28.11.2018

8) C. Wardak*, **K. Pietrzak**, *All solid state ion-selective electrode for lead monitoring in the environment*, "Current Environmental Issues-2019", Białystok, Poland, 24-26.09.2019

9) C. Wardak*, **K. Pietrzak**, Wykład pt.: *Simple and cheap electrochemical sensor for control of lead content in low level*, XLIV Międzynarodowe Seminarium Naukowo-Techniczne „Chemistry for Agriculture", Karpacz, Poland, 24-27.11.2019

10) S. Malinowski*, C. Wardak, **K. Pietrzak**, *The effect of multiwalled carbon nanotubes on analytical parameters of laccase-based biosensors constructed using Soft Plasma Polymerization technique*, ElecNano9, Paris, France Online, 23-24.11.2020

11) C. Wardak*, **K. Pietrzak**, Wykład pt.: *Nitrate ion-selective electrodes - new constructions and applications in the monitoring of nitrate ions in environmental samples*, XVI International Interdisciplinary Conference „Current Environmental Issues 2021", Białystok online, 22-23.09.2021

12) C. Wardak*, **K. Pietrzak**, Invited lecture pt.: *Recent achievements in all solid state ion-selective electrodes*, 3rd International Conference on Analytical and Bioanalytical Methods, ABC-2021 (online), Boston (USA) 18-20.10.2021

13) C. Wardak*, **K. Pietrzak**, S. Malinowski, Invited lecture pt.: *New materials used in the construction of all solid state ion-selective electrodes*, 3rd International Conference on Materials Science and Engineering (online), Boston (USA) 18-22.04.2022

14) C. Wardak*, **K. Pietrzak**, S. Malinowski, Invited lecture pt.: *Simple and cheap potentiometric sensor for chloride monitoring in water samples*, 4th International Conference on Analytical and Bioanalytical Methods, ABC-2022 (online), Los Angeles (USA) 17-19.10.2022

15) C. Wardak*, **K. Pietrzak**, S. Malinowski, Lecture pt.: *Cheap and easy to use electrochemical sensor for nitrate monitoring in environmental samples*, XLVI Międzynarodowe Seminarium Naukowo-Techniczne „Chemistry for Agriculture", Karpacz, Poland, 20-23.11.2022

Postery:

1) **K. Pietrzak***, C. Wardak, R. Łyszczek, *Solid contact nitrate ion-selective electrode based on cobalt(II) complex with 4,7-diphenyl-1,10-phenanthroline*, Matrafured'19 International Conference of Chemical Sensors, Visegrad, Hungary, 16-21.06.2019

2) **K. Pietrzak***, C. Wardak, *Effect of kind of internal electrode and its modification on the properties of ion-selective electrodes with solid contact*, Matrafured'19 International Conference of Chemical Sensors, Visegrad, Hungary, 16-21.06.2019

3) **K. Pietrzak***, C. Wardak, S. Malinowski, A. Czaplicka, *Multi-walled carbon nanotubes supported by copper(II) oxide nanoparticles in the construction of ion-selective electrodes*, 35th Conference of the European Colloid and Interface Society (ECIS), Ateny, Grecja, 05-10.09.2021

4) **K. Pietrzak***, C. Wardak, *Study of the influence of MWCNTs addition to the ion-selective membrane on the analytical parameters of electrodes sensitive to nitrates*, 12th International Conference on "Instrumental Methods of Analysis" (IMA-2021) online, Thessaloniki, Grecja, 20-23.09.2021

5) **K. Pietrzak***, C. Wardak, A. Czaplicka, *The use of copper oxide nanoparticles for the construction of ion-selective electrodes with solid contact for the determination of copper ions in water*, XVI International Interdisciplinary Conference „Current Environmental Issues 2021", Białystok online, 22-23.09.2021

6) **K. Pietrzak***, C. Wardak, N. Krstulović, S. Malinowski, *Nanomaterials used as solid contact in ion-selective electrodes sensitive to potassium and nitrate ions*, XLV Międzynarodowe Seminarium Naukowo Techniczne „Chemistry for Agriculture", Karpacz, 21-24.11.2021

7) **K. Pietrzak***, C. Wardak, N. Krstulović, *The use of silver nanoparticles in the construction of ion-selective electrodes with solid contact*, XLV Międzynarodowe Seminarium Naukowo Techniczne „Chemistry for Agriculture", Karpacz, 21-24.11.2021

8) **K. Pietrzak***, C. Wardak, *The nitrate SCISEs based on cobalt(II) complex with 4,7-diphenyl-1,10-phenanthroline*, 1st International PhD Student's Conference at the

University of Life Sciences in Lublin, Poland: Environment-Plant-Animal-Product (ICDSUPL), 26.04.2022

9) **K. Pietrzak***, C. Wardak, S. Malinowski, M. Grabarczyk, *Chloride SCISEs based on a nanocomposite of polyaniline nanofibers and multiwalled carbon nanotubes (PANINFs-Cl:MWCNTs)*, 36th European Colloid & Interface Society Conference, Creete, Greece 4-9.09.2022

10) **K. Pietrzak***, C. Wardak, *Testing water samples for the content of nitrate ions using ion-selective electrodes with solid contact*, 36th European Colloid & Interface Society Conference, Creete, Greece 4-9.09.2022

11) C. Wardak*, **K. Pietrzak**, J. Reszko-Zygmunt, *Effect of ionic liquid on potentiometric response of copper ion-selective electrode with solid contact*, XLIII Międzynarodowe Seminarium Naukowo-Techniczne „Chemistry for Agriculture", Karpacz, Poland, 25-28.11.2018

12) C. Wardak*, S. Malinowski, J. Jaroszyńska-Wolińska, **K. Pietrzak**, *Electrochemical biosensor based on laccase and carbon nanotubes for rutin detection*, 6th International Conference and Workshop 'Plant –the source of research material', Nałęczów, Poland, 10-13.09.2019

13) C. Wardak*, **K. Pietrzak**, M. Grabarczyk, R. Łyszczek, *Application of nitrate ion-selective electrode with solid contact based on cobalt(II) complex with 4,7-diphenyl-1,10-phenanthroline for nitrate determination in plants*, 6th International Conference and Workshop 'Plant –the source of research material', Nałęczów, Poland, 10-13.09.2019

14) C. Wardak*, S. Malinowski, J. Jaroszyńska-Wolińska, **K. Pietrzak**, *New strategy for determination of rutin in real samples*, XLIV Międzynarodowe Seminarium Naukowo-Techniczne „Chemistry for Agriculture", Karpacz, Poland, 24-27.11.2019

15) C. Wardak*, **K. Pietrzak**, M. Grabarczyk, J. Lenik, *New electrochemical sensor for nitrate determination in ground waters*, XLIV Międzynarodowe Seminarium Naukowo-Techniczne „Chemistry for Agriculture", Karpacz, Poland, 24-27.11.2019

16) C. Wardak*, **K. Pietrzak**, M. Grabarczyk, *Nitrate Monitoring in Natural Waters Using Solid Contact Ion-selective Electrode Based on Carbon Nanotubes and Ionic Liquid Nanocomposite*, The PortASAP meeting, 18-19.06,2020 - Web conference

17) C. Wardak*, **K. Pietrzak**, M. Grabarczyk, *New miniature ion-selective electrode based on gold microelectrode array*, The PortASAP meeting, 18-19.06,2020 - Web conference

18) C. Wardak*, **K. Pietrzak**, N. Krstulović, M. Grabarczyk, *K^+_ISEs based on metal oxide nanoparticles*, PortASAP Conference 2021 in Rome, 10-11.02.2021

19) C. Wardak*, **K. Pietrzak**, N. Krstulović, M. Grabarczyk, *Copper-sensitive ion-selective electrode with solid contact based on copper oxide nanoparticles- multiwalled carbon nanotubes-nanopomposite*, 10th International Conference "Nanotechnologies and Nanomaterials" NANO-2022, Lviv, Ukraine, 25-27.08.2022

20) C. Wardak*, **K. Pietrzak**, K. Morawska, *Ion-selective electrode with solid contact for potassium determination in agriculture samples*, XLVI Międzynarodowe Seminarium Naukowo-Techniczne „Chemistry for Agriculture", Karpacz, Poland, 20-23.11.2022

21) C. Wardak*, **K. Pietrzak**, K. Morawska, S. Malinowski, *Construction, properties and analytical application of chloride ion selective electrode with solid contact*, XLVI Międzynarodowe Seminarium Naukowo-Techniczne „Chemistry for Agriculture", Karpacz, Poland, 20-23.11.2022

*osoba prezentująca

Łączna ilość osobiście wygłoszonych komunikatów ustnych: 14, w tym 8 (konferencje krajowe) i 6 (konferencje międzynarodowe).

Łączna ilość posterów naukowych (jako autor prezentujący i współautor): 38, w tym 19 (konferencje krajowe) i 21 (konferencje międzynarodowe).

Staże i wyjazdy naukowe:

1) Zagraniczna szkoła letnia MSC w Lyon (Francja) „*Measurement Science in Chemistry*", (07.07. – 20.07.2019).

2) Naukowy wyjazd zagraniczny w Thessaloniki (Grecja) w ramach organizacji COST (European Cooperation in Science & Technology) – „*A PortASAP Training School on Low Cost Air Quality Sensors*" (02.09. – 06.09.2019).

3) Zagraniczny staż naukowy na Uniwersytecie w Zagrzebiu (Chorwacja) w ramach projektu: „CIII-HR-1108-03-1920-M-132094 (CEEPUS) – „*Colloids and Nanomaterials in Education and Research*" (03.02. - 23.02.2020), opiekun stażu: prof. Davor Kovacevic.

4) Zagraniczny staż naukowy w Instytucie Fizyki w Zagrzebiu (Chorwacja) w ramach projektu nr POWR.03.02.00-00.I005/16 „*Międzynarodowe Studia Doktoranckie z Chemii*", (01.03. – 28.08.2020), opiekun stażu: Niksa Krstulović.

5) Międzynarodowa szkoła letnia na UMCS w Lublinie (Polska), „*Modern Research Techniques for Physicochemical Characterization of the Potential Application Systems*", (18.05. – 20.05.2022). W ramach spotkania przedstawiono dodatkowo wystąpienie ustne pt." Application of nanomaterials as a solid contact in ion-selective electrodes" oraz poster naukowy pt. "*Influence of the structure of the nanocomposite used for membrane preparation on the parameters of nitrate selective electrodes*".

Inne osiągnięcia:

1) Stypendium projakościowe w latach: 2018/19, 2020/21, 2021/22 i 2022/23.

2) II miejsce w konkursie na najlepszy poster na IX Ogólnopolskim Sympozjum „Nauka i przemysł – lubelskie spotkania studenckie", Lublin, 28.06.2021.

3) Nagroda Rektora za „oryginalne i twórcze osiągnięcia naukowe związane z opracowaniem nowych czujników elektrochemicznych dedykowanych do oznaczania wybranych jonów metali oraz jonów azotanowych(V) z wykorzystaniem nowych materiałów funkcjonalnych", Lublin, 21.10.2022.